Spring 2007

Adsorption of Lead (II) Ions by Organosilicate Nanoporous Materials

Larry Keith Isaacs
Old Dominion University

ADSORPTION OF LEAD (II) IONS BY

ORGANOSILICATE NANOPOROUS MATERIALS

by

Larry Keith Isaacs
B.S. May 1972, University of New Mexico
M.S. May 2003, Christopher Newport University

A Dissertation Submitted to the Faculty of
Old Dominion University in Partial Fulfillment of the
Requirement for the Degree of

DOCTOR OF PHILOSOPHY

ENVIRONMENTAL ENGINEERING

OLD DOMINION UNIVERSITY
May 2007

Approved by:

Muide Erten-Unal (Director)

Gary C. Schafran (Member)

Resit Unal (Member)

Tarek M. Abdel-Fattah (Member)

ABSTRACT

ADSORPTION OF LEAD (II) IONS
BY ORGANOSILICATE NANOPOROUS MATERIALS

Larry Keith Isaacs
Old Dominion University, 2007
Director: Dr. Mujde Erten-Unal

As-synthesized organosilicate nanoporous (OSNP) materials HMS (hexagonal mesoporous structure) and MCM-41 were used as adsorbents for removal of lead (II) ions in laboratory batch and column studies. Mesoporous organosilicates were prepared from tetraethylorthosilicate (TEOS) and either an ionic (cetyltrimethyl-ammonium) or neutral (dodecylamine) surfactant. Batch reaction distribution coefficients for MCM-41 were K_D = 51.5 L/g (SD = 26.3) at 24 h and K_D = 73.7 L/g (SD = 40.5) at 7 d. OSNP lead (II) ion adsorption increased from pH = 3 until pH ca. 7.5 after which a sharp decrease in adsorption was noted. OSNP materials reflected a dependence on ionic strength consistent with an outer-sphere complexation and electrostatic bonding mechanism. Lead (II) ion adsorption behavior in seven matrix batch solutions was not effective possibly due to soluble complexes that were formed that prevented adsorption and precipitation. There was no difference in the batch adsorption performance of MCM-41 and HMS. Column designs were optimized by response surface methods. OSNP material/sand media head loss at a superficial velocity = 0.49 m/h increased 28.1% compared with sand only media. At column break through, defined as Ce/Co = 0.5, MCM-41/sand media K_D = 46.2 L/g and sand only K_D = 0.04 L/g. There was significant evidence to warrant rejection of the claim that the variances in K_D were equal ($P < 0.001$, n = 12). Adsorption capacity in columns with synthetic adsorbates at Ce/Co = 0.50 were HMS = 0.013 mmol/g (2.74 mg/g) at 0.6 m^3/m^2 h and MCM-41 = 0.071 mmol/g (14.63

mg/g) at 2.1 m^3/m^2 h. For a stormwater treated by single pass column filtration, MCM-41 lead (II) ion adsorption at Ce/Co = 0.50 was 0.028 mmol/g (5.88 mg/g) and sand only = 2.83E-05 mmol/g (0.01 mg/g). Water molecule ionization by metal cations decreased influent pH, combined with deprotonation of MCM-41 during adsorption of lead (II) ions, caused a decrease in pH sufficient to change column adsorption performance. The declining rate sand filtration cost for a 100 m^2 unit in 2007 dollars was estimated at $31,600, however this did not include the cost for MCM-41 adsorbent materials, which are not available commercially. Adsorbent life cycle was calculated at 2.6 years.

This dissertation is dedicated to my wife Marsha who has been forever patient and to our children for their constant encouragement.

ACKNOWLEDGMENTS

There are many people who have contributed to the successful completion of this dissertation. I wish to extend sincere thanks to all my professors and teachers who have encouraged me throughout the conduct of this research. To the dissertation committee Drs. Mujde Erten-Unal, Gary C. Schafran, Resit Unal, and Tarek M. Abdel-Fattah for their collective and individual inquiry that significantly improved my research.

Drs. Schafran, Yoon and Erten-Unal all conducted rigorous graduate course work in wastewater treatment, water treatment, aquatic chemistry, water modeling, and water quality management. Their thought provoking lectures and exams challenged me to study hard and really understand the material.

A very special thanks is extended to Dr. Tarek M. Abdel-Fattah who provided the synthesis method for the nanoporous materials, access to the CNU laboratory, and for the time he spent discussing options, ideas, and concepts of nanotechnology. His extensive knowledge of physical chemistry and his constant mentoring helped me extensively.

Gratefully I thank my graduate advisor, Dr. Mujde Erten-Unal, who from the first day we met in class provided clear timely guidance. Her constant encouragement and suggestions to help me circumnavigate the doctoral process kept me on track and successful. Her cheerful countenance made the process manageable and possible.

Special thanks to my supervisors Ms. Patricia M. Ogorzaly and Mr. Robert C. Barrett who generously allowed me to take leave whenever I needed time to meet school tasks. With their steady and generous support I was able to complete my studies while working full time.

TABLE OF CONTENTS

Page

LIST OF TABLES

LIST OF FIGURES

LIST OF EQUATIONS

1. INTRODUCTION

Soil and water become contaminated with elevated metal concentrations from various anthropogenic processes. Nationwide superfund sites have been documented with elevated concentrations levels of metals (U.S. EPA 1997). Since metals do not readily degrade naturally, immobilization, stabilization and removal techniques have been continually explored for improved remediation solutions (Babel and Kurniawan 2003; Kostal et al. 2005; Lanouette 1977). Recent development of nanotechnologies has offered novel adsorption possibilities for metals in aqueous conditions (Dionysiou and Wiesner 2007; Savage and Diallo 2005). This research focuses on the application of one type of nanoporous materials, with at least one dimension in the nanometer size; explores its ability to remove lead (II) cations discharged from shooting ranges in stormwaters, and considers an application method in a dual-media declining rate sand filtration system.

1.1 Organosilicate Nanoporous Materials

Discovery in 1992 of the family of mesoporous molecular sieve MCM-41 by scientist at Mobil Research and Development Corporation, Paulsboro, NJ (Kresge et al. 1992) and similar breakthroughs by Inagaki et al. (1993), inaugurated a new technology that has generated significant scientific interest and study of synthesized meso-structures (Amato 1993; Feng et al. 1997). These molecular sieves are characterized by an ordered uniformed cylindrical mesoporous structure with at least one dimension in the nanometer range. Physically they fit between ordinary crystalline and amorphous solids (Rao and Cheetham 2001). They are uniquely different from zeolites, with a purely tetrahedral

The model for this dissertation is the *Journal of Environmental Engineering*

structure that display a uniform honeycomb-like non-intersecting tubular channel framework (Schumacher et al. 2000).

Like zeolite synthesis, MCM-41 materials are prepared using a surfactant (organic molecule) and silica or silica-alumina (silicate) at sufficient concentrations to self-assemble into the organosilicate nanoporous (OSNP) structures used in this research (Zhao et al. 1996). Others have demonstrated the MCM-41 family may be synthesized from a variety of temperatures, pH, reaction time and from at least four different gel reaction synthesis routes (Huo et al. 1994, Tanev et al 1995). The large surface area (> 1100 m^2/g) and ordered pore diameters 15 and 100 Å (Beck et al. 1992) make the material uniquely qualified as a special class of meso structures. Per IUPAC, materials with pore diameters of 20 to 500 Å are called mesoporous. The mesostructure can be controlled by a choice of template surfactants, by adding organic moieties, and by changing reaction parameters (temperature, pH, reaction time, and concentrations). The materials also have large metal ion/aqueous distribution coefficients, K_D = 340,000 (Yoshitake et al. 2003, Sayari et al. 2005). This adsorption behavior suggests there may be many industrial, environmental, and medical application possibilities (Feng et al. 1997).

This research focuses on the application of the M41S family of silicate mesoporous molecular sieves with 5 – 50 Å uniform pore structures (Kresge et al. 1992; Vartuli et al. 2001) as lead (II) ion adsorbents in a field condition competitive ion aqueous environment. The setting of this research has basis in two areas. The first is the recurring predominance of particulate-associated and dissolved lead (II) ions in wastewaters and stormwaters in an urban and industrial, namely shoot range context.

The second area is the synthesis of the silicate porous materials, which show promise as an adsorbent with tunable porosities and behavior that may have unique application for the removal of metal ions in solution. Both areas of interest are addressed. The goal of this research was to develop an approach to lead (II) ion adsorption using OSNP material in a low-maintenance passive field application.

1.2 Background of the Problem

Lead is a toxic heavy metal that is nonfunctional biologically, that is, it is not a required macro or micronutrient for flora and fauna. Lead has four valence states. A valence of zero in the elemental form, monovalent, divalent and tetravalent. In the environment lead exist in the divalent form and oxidizes to the tetravalent form only in the presence of very strong oxidizing agents and then is not stable. In aqueous forms it can be found dissolved as a free ion, hydroxide and carbonate forms. It may also exist as particulate bound. The most common dissolved compounds include lead sulfate, lead chloride, lead hydroxide, and lead carbonate (Eisler, 1988). It can be easily adsorbed in plant roots and transported by the xylem throughout the plant interfering with photosynthesis, germination, mitosis and cell division (Baghour et al. 2001).

Lead is a noted source of lead exposure to children through ingestion, respiratory, and dermal uptake. It is also an accumulative biotoxin that is not metabolized and excreted by mammalians. Similarly, fauna are detrimentally affected by exposure to lead (Hettiarachchi et al. 2000). Mitigating transport, accumulation and migration of lead in the environment is desired. Trace to moderate levels of heavy metals naturally occur in soils. A survey of surface horizons pedons of NAD (no known anthropogenic addition) soils across the United States by Burt (2003) found trace amounts of toxic and

micronutrient heavy metals (Table 1). The research reported the physical and chemical properties of soil highly variable. The most important soil factors that determined the amount and distribution of trace metals were parent material, pedogenesis, and anthropogenic contributions. From this study the concentration of metals in NAD soils sources are approximated and provide a basis for initial estimates of background conditions.

The results in Table 1 depict generally higher values in the NAD soils than anthropogenic pedons. Burt et al. (2003) do not offer any detailed explanation for the higher NAD pedon metal concentrations for Cr and Co, but did contend the elevated

Table 1. NAD and Anthropogenic Trace Metals in Pedons Across the U.S.
Soil samples were taken from benchmark soils or soils considered extensive, important, and unique in the soil classification system. As such these soils are more important than other soil types. The studied pedons had a pH range from 2.1 to 9.9. All values are in mg/kg and show the arithmetic mean ± standard deviation. NAD = no known anthropogenic addition.

Metal	NAD Pedons (n = 312)	Anthropogenic Pedons (n = 392)	Percent difference
Pb	12.2 ± 14.1	102.9 ± 156.2	+ 743.4
Cd	0.20 ± 0.18	0.80 ± 3.3	+300.0
Cu	24.7 ± 27.7	74.8 ± 189.3	+ 202.8
Mn	588.9 ± 507.3	589.0 ± 629.8	- 0.02
Zn	162.6 ± 27.2	148.6 ± 491.6	- 8.6
Ni	59.5 ± 279.2	41.3 ± 95.3	-30.6
Co	13.4 ± 30.4	7.9 ± 7.1	- 41.0
Cr	88.7 ± 360.4	29.3 ± 33.5	- 67.0

anthropogenic Pb is most likely from leaded gasoline and lead-based paints. For the purposes of this research the Burt et al. (2003) study provides a point of demarcation for lead and copper in soils. Significant departures from these averages can provide a basis for evaluating the impact of an activity or process on the environment. The next section

discusses how these impacts manifest themselves in waste and stormwaters, which have originated from NAD and anthropogenic soil sources.

Heavy metal ions in urban wastewaters are generated from various industrial and domestic sources. Industrial processes like metal plating, tanneries, mining operations, and car washes discharge metal constituents into the wastewater collection system (Bulut and Baysal 2006). Metals found frequently in domestic wastewaters include cadmium (Cd), chromium (Cr), copper (Cu), iron (Fe), lead (Pb), manganese (Mn), mercury (Hg), nickel (Ni), and zinc (Zn) (Cajuste et al. 1991; Chipasa 2003; Moriyama et al. 1989; Rule et al. 2006; Sorme and Lagerkvist 2002; Tchobanoglous et al. 2003; Wang et al. 2006). Most particulate bound metals are removed in the wastewater treatment processes (Ekster and Jenkins 1996), however dissolved metals (metal in solution after passing through a < 0.45 μm filter) may be discharged in treated wastewaters (Buzier et al. 2006; Gagnon and Saulnier 2003).

Oxidation, complexation, precipitation, and dissolution of metals from natural and anthropogenic sources result in trace metal concentrations in urban wastewaters. Wastewater treatment plant influent metal concentrations from four countries have been reported (Table 2). Feces account for 60-70% of the Cd, Cu, Ni and Zn in domestic wastewater and more than 20% of the mixed wastewater from domestic and industrial processes. Other sources of metals in domestic wastewater are from body care products, pharmaceuticals, cleaning materials and liquid waste. Copper and lead originate from piping depending on the aggressive nature of water (Thornton et al. 2001).

The concentration of lead in urban stormwater has also been the interest of many researchers. The elevated amounts found are concerning, but not surprising considering

Table 2. Average Wastewater Influent Total Metal Concentrations

Metal	Average Daily (µg/L)				
As	NA	NA	NA	NA	2.6
Cd	20	40	30	0.38	<1
Cr	2	20	18	2.8	31
Cu	62	30	75	189	77
Pb	26	80	43	7.4	68
Hg	4	NA	NA	0.57	NA
Ni	17	10	50	6.7	14.3
Zn	28	50	49	160	346
Location	France	Norway	United Kingdom	United Kingdom	Melbourne, Australia
Reference	(Thornton et al. 2001)	(Thornton et al. 2001)	(Thornton et al. 2001)	(Rule et al. 2006)	(Wilkie et al. 1996)

NA = Not Analyzed

the many anthropogenic uses and applications of lead. Lead in urban stormwaters within the continental United States have been reported at 15.5 times background (Murray et al. 2004). One investigator studied the sources of lead in the urban environment and found the highest concentrations in synthetic rain waters leached from painted wood building siding, and found other contributions to the lead urban deposition from roofs, brake dust, automobile tires, automobile oil and concrete. The investigators total annual urban loading estimate for all lead sources was 0.069 kg Pb/ha-yr (Davis et al. 2001). Boller (1997) estimated 50 – 80% of metals in stormwater run-off come from roofs and streets. While these wet weather contributions are significant, a six-year study in California found 33% of lead in surface run-off waters came from dry weather flows, indicating a pervasive and constant anthropogenic urban source (McPherson et al. 2005). Other elevated urban sources include Sweden street sediments (Viklander 1998), and roadsides (Backstrom et al., 2004) which contained elevated lead, and Washington D.C. with trace

elements of lead along roadways (Wigington et al., 1986). A nationwide urban study by the U.S. EPA (1983) reported average stormwater total lead concentrations at 140 μg/L.

The distribution of lead manufactured in the United States includes 72% for storage batteries, 13% in gasoline additives and other chemicals, 2% in solder and 9% for other uses (Yu et al. 2001). The remaining 4% is used as ammunition (shot and bullets). The U.S. Environmental Protection Agency (EPA) estimates the 4% translates into 72,575 metric tons, which is used as ammunition at military and private shooting ranges. This translates into about 7.26×10^7 kg of lead introduced into the environment by this process (U.S.EPA 2001). Lead is heavily accumulated in soils within shooting range boundaries (Astrup et al. 1999; Basunia and Landsberger 2001; Bruell et al. 1999; Cao et al. 2003; Dermatas et al. 2003; Hardison et al. 2004; Vantelon et al. 2005). Lead contamination within shooting ranges have been documented at concentrations to 400,000 mg/kg (Astrup et al. 1999). Shotgun pellets and expended bullets in soils have also been found to transform into lead complexes through weathering in the soil environment (Cao et al. 2003; Jorgensen and Willems 1987). Lead complexes formed by weathering may be more mobile in the environment than thought to occur.

In a 2004 study of 12 Air Force installations by the U. S. Air Force, Headquarters Air Combat Command, Langley Air Force Base (AFB), Virginia, and directed by this researcher, lead in soils outside, but less than 10 m from shooting range boundaries, had dissolved lead concentrations of 194 μg/L suggesting some lead may be migrating off range (Isaacs 2003; Isaacs et al. 2005) (Figure 1).

Stormwater run-off samples were also collected and analyzed for total and dissolved lead. Dissolved lead results are depicted in Figure 2. In other studies, Ma et

al., (2002) found dissolved lead in surface waters near outdoor shooting ranges in Florida from non-detect to 234 μg/L and total lead from non-detect to 694 μg/L. The elevated lead in stormwaters and the proximity of a small river to the shooting ranges, motivated

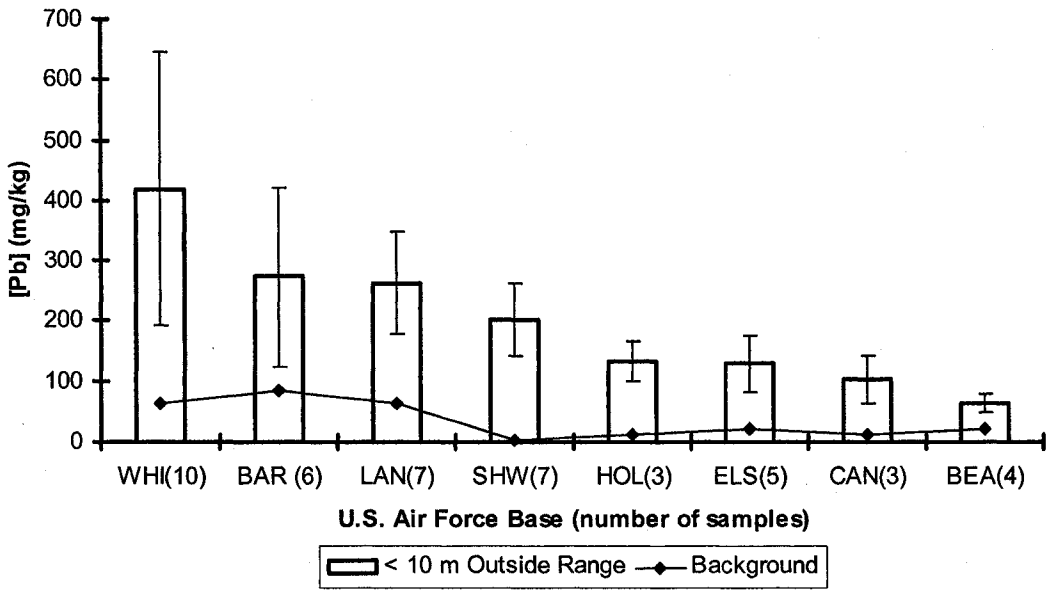

Fig. 1. Average Soil Lead Concentrations Outside Shooting Range Boundaries
Total lead in soils collected in top 10 cm and located outside, but less than 10 m of the defined boundary of the shooting range. Background levels are the 95% upper confidence limit. Error bars depict standard error of averages. U.S. Air Force Base (AFB) abbreviations are WHI – Whiteman AFB, MO; BAR – Barksdale AFB, LA; LAN – Langley AFB, VA; SHW – Shaw AFB, SC; HOL – Holloman AFB, NM; ELS – Ellsworth AFB, SD; CAN – Cannon AFB, NM; and BEA – Beale AFB, CA. Compare also with nationwide Pb in NAD and anthropogenic pedons.

the Louisiana state environmental regulatory department to amend the Barksdale AFB multi-sector stormwater discharge permit limit to 150 μg/L total lead at the outfall nearest the shooting range. Other permit limits have reported total lead for shipyard stormwater outfalls in California, Hawaii, and Virginia, at 335, 140, and 100 μg/L, respectively

(Burgos 1997). All of these amounts are elevated contrasted with stormwater lead (II) concentrations reported by Barrett (2003) who used an EMC for dissolved lead (II) ions in stormwater = 2.1 μg/L and Sansalone (1999) 21.7 μg/L for a Cincinnati, Ohio urban site. The presence of elevated concentrations of lead (II) ions in stormwaters is evident and requires remediation management.

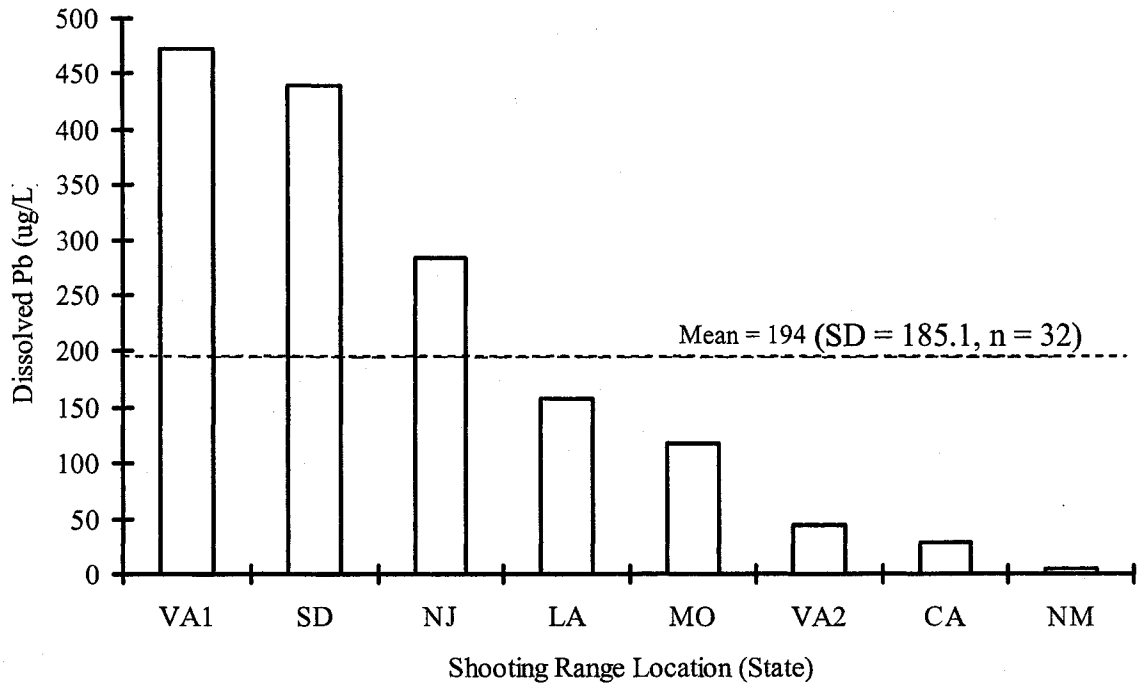

Fig. 2. Dissolved Lead in Stormwaters
Dissolved lead analyzed after filtration through Whatman 0.45 μm filter paper. Samples were analyzed following EPA Method SW-846. Average National Urban survey = 55 μg/L and municipal solid waste = 433 μg/L. U.S. EPA Criteria Continuous Concentration (CCC) for protection of aquatic life and human health in surface water is 1.3 to 7.7 μg/L, and the Criteria Maximum Concentration (CMC) is 34 to 200 μg/L.

1.3 Research Objective

The purpose of this study is to evaluate the adsorption behavior of as-synthesized organosilicate nanoporous material MCM-41 and HMS in batch and column lead (II) ion spiked synthetic solutions. Additionally, the study investigates the adsorption performance of MCM-41 in a 13 cation synthetic and natural stormwater solution via batch and column adsorption studies. The study also considers the implications of headloss, optimization, and concept of operations, to evaluate the practical applications of this evolving technology.

1.4 Research Approach

The specific approach to this research was to evaluate how an in-situ dual media declining rate gravity sand filtration system could be optimized using OSNP materials as media adsorbents to remove dissolved lead (II) ions from a selected ion competitive aqueous solution. The technical approach used OSNP materials in conjunction with sand as a combined media, and sand also acting as a pre-filtration mechanism to remove large particulates. The sequence of accomplishment as executed was as follows:

1. As synthesized OSNP materials were evaluated in screening batch reactions in a single lead (II) ion contaminant environment to determine the best adsorbent.
2. Using the best three performing OSNP materials from the batch reaction, a column study was completed to evaluate breakthrough curves and nominal adsorption capacities
3. Hydraulic studies were completed to evaluate applicability and headloss
4. Stormwaters were collected from a small arms firing range and analyzed for Ca^{2+}, Cr^{2+}, Cu^{2+}, Fe^{2+}, Mg^{2+}, Mn^{2+}, Mo^{2+}, Na^{+}, Ni^{2+}, Sb^{3+}, Sn^{2+} and Zn^{2+} ions using

ICP-MS. The results of collected stormwater data were used to prepare a synthetic stormwater matrix for the column study.

5. Synthesized OSNP materials MCM-41 and HMS were prepared and. characterized by X-ray diffraction, transmission electron microscopy (TEM), scanning electron microscopy (SEM), and Fourier transform infrared spectroscopy (FTIR).
6. Response Surface Methods were applied to select the optimum operating parameters (filtration rate, percent OSNP material, and bed depth) and conducted the experiments using these conditions.
7. Introduced competing ions Ca^{2+}, Cr^{2+}, Cu^{2+}, Fe^{2+}, Mg^{2+}, Mn^{2+}, Mo^{2+}, Na^{+}, Ni^{2+}, Sb^{3+}, Sn^{2+} and Zn^{2+} ions in groups for batch reactions. Evaluated specific ion competition implications for lead (II) ion adsorption.
8. Developed a concept of design for application of the results. Estimated the amount of OSNP materials required and life cycle for the declining rate dual media filtration system.
9. Opportunities and challenges were noted. Areas for further research were identified.

2. LITERATURE REVIEW

This research requires the review of literature in three areas: 1) the synthesis, preparation, characterization and application of OSNP materials, with a specific focus on their use as heavy metal adsorbents, 2) the character of Pb^{2+} ions in the soil and stormwater, along with the current knowledge of the function of filtration and adsorption technologies for control of heavy metals in stormwaters, with a special focus on literature of shooting range applications, and 3) the theoretical considerations applicable to adsorption by powders and porous solids. An examination of each of these areas should identify the literature applicable to the proposed area of study.

2.1 Organosilicate Nanoporous Materials

Since the discovery in 1992 of the synthesis mechanism for ordered mesoporous materials researches have systematically studied and engineered nanoporous materials with a variety of functionalizations, patterned nanostructures, and pore diameters (Rao and Cheetham 2001; Yang and Chao 2002; Zhao et al. 1996). Mixing organic surfactants and a silica or silica alumina source creates the self-assembled nanoporous MCM-41 material. The surfactant molecules possess the typical hydrophobic hydrocarbon tail with polar heads, which self-align to form hexagonal honeycombs. This honeycomb structure then serves as the template upon which an inorganic molecule can bond electrostatically, covalently, or ionically to form the desired molecular sieve. If desired, the surfactant can be removed by calcination or by solvents to reveal large open pore structures. The length of the hydrocarbon chain controls the pore diameter.

Researchers have also prepared other than honeycomb structures like cubic and lamellar or stacked sheet forms (Amato 1993). The mixture molar ratios are adjusted to prepare a supersaturated solution usually in a temperature range of 70 to 150 °C and reacted for varying reaction times. There are at least five routes to achieve the desired self-assembly mesostructure as summarized in Table 3. The synthesis research has generally been motivated to create larger pore diameters, increased wall thickness, easier assembly pathways, more hydrothermally stable, reactive moieties, ionic charge or to generate acidity in polymers.

To date, nanoporous materials have been used in sporting goods, tires, strain-resistant clothing, optics, material strengthening, catalysis, sunscreens, solar cells, cosmetics, and electronics (Rao and Cheetham 2001). Prospects continue to explode as researchers explore potential drug delivery mechanisms, diagnostic tools for medicinal purposes, environmental remediation, toxic metal sensors and aerospace uses (Tao 2003). It is anticipated nanotechnology will generate $1 trillion per year in services and new technologies business by 2015 (Roco 2003).

However, the fate and transport of nanosized particles in the environment is currently not well understood. Many of the nanomaterials developed consist of nonbiodegradable inorganic chemicals and there is little data to enable meaningful conclusions on the biodegradation (U.S. EPA 2007). There are studies in progress to evaluate the processes that control transport and removal of nanoparticles in water and wastewater (Moore 2006, Wiesner et al. 2006) along with the recently published white paper by the U.S. EPA (2007). The complexation of nanoporous materials and metals may have unintended long term consequences which must carefully studied and

understood before they are universally applied. This investigation proposes a field application of nanoporous materials, which the author suggests has potential for environmental remediation after appropriate fate and transport answers are developed.

2.2 Synthesis and Material Preparations

A variety of procedures and methods have been developed to prepare mesoporous structures, where surfactants function as templates for the formation of organic-inorganic OSNP materials (Yang and Chao 2002). As the surfactant/silica molar ratio (SSMR) increases, the silica products self-assemble into one of three phases: Phase 1) SSMR < 1.0: hexagonal phase designated HMS (Figure 3) and MCM-41 (Figure 4), Phase 2), SSMR = 1.0 to 1.5: cubic phase or MCM-48, and Phase 3) SSMR = 1.2 – 2.0: thermally unstable materials. The pore diameter (2 to 10 nm) of OSNP materials is controlled by varying the chain length of the alkyl groups from 8 to 22 carbon atoms of surfactants, by adding solvents to dissolve the hydrophobic chain lengths, or by varying the aging conditions like time or temperature (Zhao et al. 1996). Figures 3 and 4 demonstrate the HMS and MCM-41 chemical structure used in this study. The attractive forces between the surfactant and inorganic molecules are illustrated in the figures.

Thicker material walls have been realized after long crystallization times and the addition of silicate and surfactant materials from "seed" crystalline materials (Mokaya 1999). The thicker walls theoretically could impart more hydrothermally stable materials. Pore diameter, wall thickness, and morphological symmetry is controlled by the choice of surfactant (Berggren et al. 2005). The pore diameter may also be influenced for MCM-41 by temperature, pH, alkalinity and crystallization time

Table 3. MCM-41 Synthesis Pathways

Pathway†	Self-Assembly Mechanism	Unique Characteristic	Morphologic Phase	Reference
I (S^+I^-)	Self-assembled cationic template directs self-assembly of anionic inorganic molecule	Regular arrays of uniform channels with controllable pore diameters from 16 to 100 Å or more. 40% by wt. of original surfactant retained after calcination	Hexagonal	(Beck et al. 1992; Kresge et al. 1992)
II (S^-I^+)	Anionic template directs self-assembly of cationic inorganic species	Electrostatic attractive forces interact with solutes	Hexagonal	(Huo et al. 1994)
III ($S^+X^-I^+$)	Counterion Cl^- or Br^- controls self-assembly of organic and inorganic species of similar charge	Positively charged molecule	Hexagonal and Lamellar	(Huo et al. 1994)
IV ($S^-M^+I^-$)	Counterion Na^+ or K^+ controls self-assembly of organic and inorganic species of similar charge	Negative charged molecule	Hexagonal and Lamellar	No reference found, but mechanism is referred to by Tanev and Pinnavaia (1995)
V (S^0I^0)	Hydrogen bonding and self-assembly of organic and inorganic species	Neutral molecule with larger wall thickness, small scattering domain size, and complementary meso-porosities to pathways I and III.	Hexagonal	(Tanev and Pinnavaia 1995)

† S^+ = surfactant organic ions; I^- = anionic inorganic ions (Note: silica is not an anionic molecule, but acquires a negative charge in the synthesis process); X^- = anionic halides; M^+ = cationic alkaline ions

(Zhao et al. 1996).

The original MCM-41 mesoporous molecular sieve, for example, was synthesized in an alkaline condition (Kresge et al. 1992). OSNP materials in this study were synthesized through self-assembly of an inorganic silica precursor (tetraethyl-orthosilicate) and an organic template of either an ionic (cetyltrimethylammonium) or neutral (dodecylamine) surfactant, and used as synthesized.

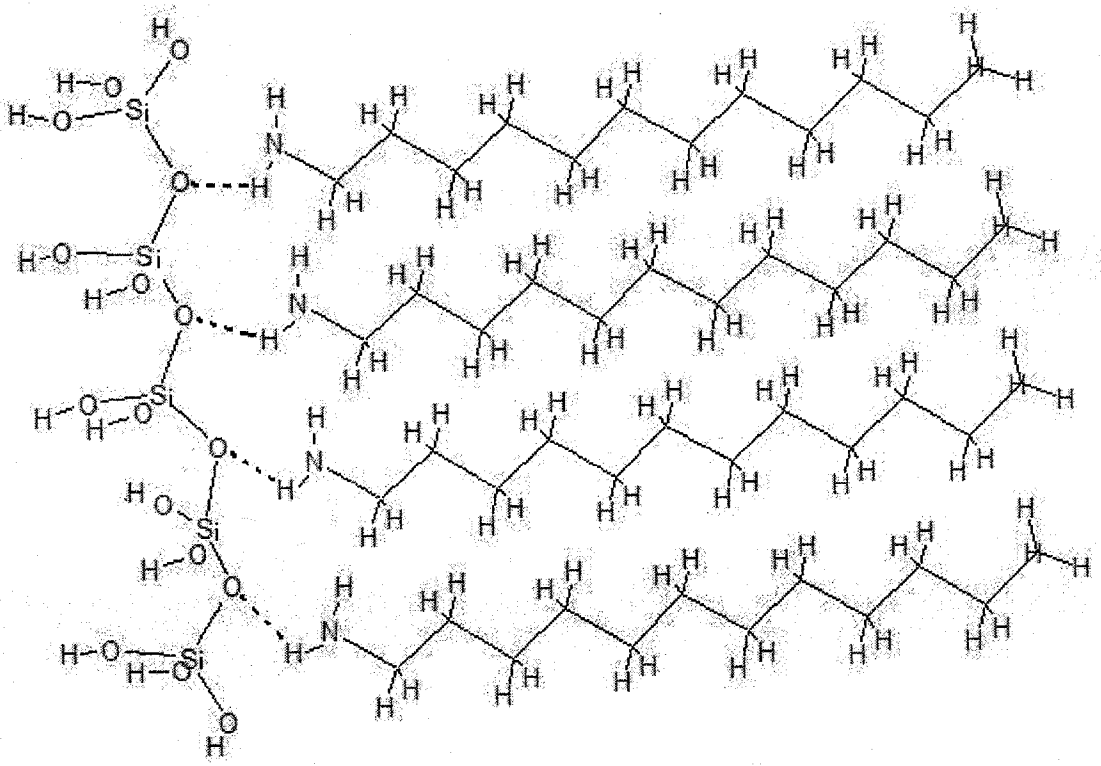

Fig. 3. Chemical Structure of HMS
HMS synthesis is a neutral (S^0I^0) template route that yields a hexagonal mesoporous molecular sieve with physical and catalytic properties substantially different from MCM-41. Hydrogen bonding is the attractive force as depicted by dotted lines.

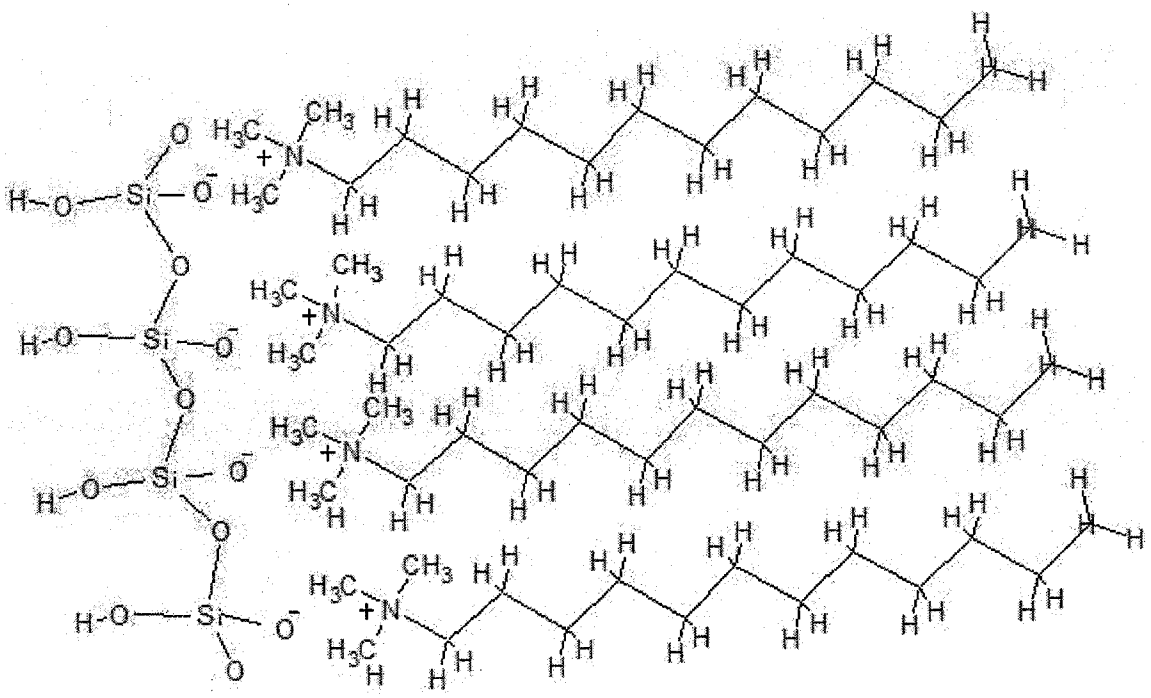

Fig. 4. Chemical Structure of MCM-41
MCM-41 is prepared by an electrostatic assembly pathway. The direct S^+I^- charge matching between cationic quaternary ammonium ion surfactants (S^+) and the anionic silicate precursors (I^-) causes a self-assemblage of long-range hexagonal structures under hydrothermal synthesis conditions at 100 °C. The long range order is greatly reduced when the synthesis is conducted at ambient temperature. Bonding is an electrostatically attractive force between electronegative oxygen and electropositive nitrogen alkyl head group as shown. The electrostatic negative charge may also be the primary attractive force for Pb^{2+} cations in solution.

There are three recognized methods for functionalization of the mesophase structure (Figure 5). The first is by grafting and attaching functional molecules to the surface of the mesoporous silica. For example, grafting to the mesoporous silica internal channels with alkylamines, alkylthiols, alkenes, alkyl halides and epoxides create reactive

moieties within the structure. The second method for surface functionalization

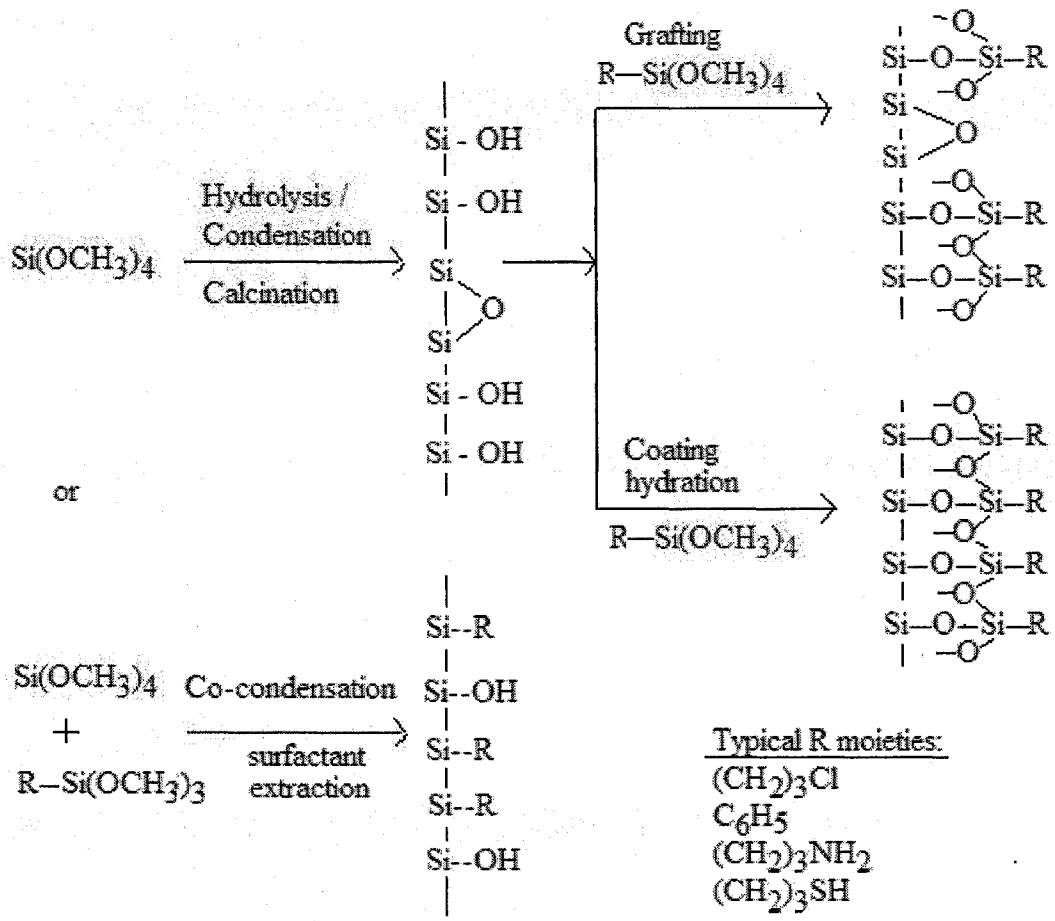

Fig. 5. Surface Functionalization of Mesoporous Materials
Illustration of three functionalization methods: grafting, coating and co-condensation. (modified after Yang and Chao, 2002)

of mesoporous materials is by coating reactions. A "coating" of ligand complexes is achieved by employing enough water to form a monolayer on the pore surface (Zhao et al. 2003) . The third functionalization method is co-condensation. Co-condensation of tetraalkoxysilane and organoalkoxysilanes with Si-C bonds has been used to produce inorganic-organic hybrid moieties.

The surfactant-template synthesis yields van der Waals bonded structures that may leach surfactants in flow-through adsorption designs (Pinnavaia 2006). Whereas creation of covalently bonded mesoporous materials inorganic-organic networks in the pore walls should yield more stability because of stronger bonds. For this study, the latter synthesis method, if achievable, may be more desirable.

2.3 Characterization of Mesoporous Materials

Researchers have characterized mesoporous materials by X-ray powder diffraction (XRD), transmission electron microscopy (TEM), scanning electron microscopy (SEM), nitrogen adsorption-desorption usually following the Brunauer-Emmett-Teller (BET) characterization, Fourier Transform Infrared Spectroscopy (FTIR) reflectance spectra and others. The relationship between the surfactant hydrocarbon chain length the pore diameter has been developed. Pore volumes and the surface area have also been found to increase with the surfactant template concentration. Typical BET surface areas, pore volumes and pore diameters for selected surfactants and functionalization are provided in Table 4.

2.4 Nanoporous Material Applications

The explosive growth of the new technology may best be illustrated by the published literature on OSNP materials. By observing the publications in Science Direct, a respected scientific database operated by the Elsevier Limited Publishing Company, one can find in 1993, one year after the publication of the MCM-41 synthesis in Science, three articles published on synthesis and applications of MCM-41. Five years later in 1999 there were 78, and in 2005, 243 articles, and in 2006, 271 articles were published

Table 4. Representative Functionalized Mesoporous Sieves

Functionalization	Surfactant Template	BET Surface Area (m^2/g)	Pore Volume (cm^3/g)	Pore Diameter (nm)	Reference
Organosilicate Nanocomposite: HMS					
3-aminopropyl--, 2-cyanoethyl--	n-dodecyl-amine	1358		2.9	(Macquarrie 1996)
3-chloroprophyl--	n-dodecyl-amine	597		3.9	(Macquarrie 1996)
3-mercaptopropyl--	n-dodecyl-amine	858 - 1225	0.27 – 0.47	2.2 – 4.1	(Richer 1998)
3-mercaptopropyl--	n-dodecyl-amine	640 - 722	0.27 - 0.55	1.5 – 2.7	(Mercier and Pinnavaia 1998)
vinyl--	n-dodecyl-amine	1520		30	(Burkett et al. 1996)
Organosilicate Nanocomposite: MCM-41					
3-aminopropyl--	CTABr			4.0 – 4.5	(Fowler et al. 1997)
3-aminopropyl--	CTABr	87 - 428	0.16 – 0.76	3.4 – 7.3	(Walcarius et al. 2003)
phenyl-	CTABr	1060 - 1386		18 - 24	(Burkett et al. 1996)
$CH_3HN(CH_2)_{3}$--, $(CH_3)_2N(CH_2)_{3}$--, $H_2N(CH_2)_2NH(CH_2)_{3}$--	CTABr	1110 - 1190	0.96 - 1.06	4.3 – 4.6	(VanDerVoort et al. 1998)
tetramethyl--	CTABr	880	0.87	3.3 – 3.9	(Mokaya 1999)
3-mercaptopropyl--	CTABr	792	0.47	1.4	(Lim et al. 1998)
3-mecaptopropyl--	CTABr	1061	0.44	2.0	(Mercier and Pinnavaia 1998)
3-mercaptopropyl--	CTABr	162 - 818	0.19 – 1.24	3.4 – 7.3	(Walcarius et al. 2003)
Activated Carbon Comparison					
FeO	Not Applicable	625	1.04	5.8	(Reed et al. 2000)

CTABr = $CH_3(CH_2)_{15}N(CH_3)_3Br$

with MCM-41 in the keywords, abstract or title of peered reviewed journals. The process of discovery continues and has led to the concept of self-assembled microstructure, which can serve as structure-directing agents with controllable pore sizes with many applications in a variety of disciplines (Zhao et al. 1996). The remarkable nature of the MCM-41 structure is the construction of surface areas in excess of 1100 m^2/g with, in some cases, pore walls no more than two oxygen atoms thick (Rouquerol et al. 1999). Hence, there are potentially significant opportunities for the chemical modification of OSNP materials with organic and organometallic ligands that are selective to specific metal ions (Olkhovyk et al. 2005). For example, mercury selectivity over copper, cadmium, lead and zinc for thioether functionalized MCM-41 has been demonstrated. In fact, Hg^{2+} adsorption capacities increased directly in proportion to the concentration of the thioether content in the MCM-41 material (Zhang et al. 2003). Similarly, selective adsorption of gold over copper and nickel has been observed using organic amine grafted groups to MCM-41 (Lam et al. 2006). This phenomenon may be the result of the stereo-coordination chemistry between MCM-41 with Hg^{2+}, N and Au^{2+}, and the larger effective charge of Cu and Ni (Zhang et al. 2003).

Table 5 presents a synopsis of adsorption performance for MCM-41 mesoporous silica for various adsorbates. Adsorption capacities of OSNP materials show great promise, particularly for lead (II) ion adsorption to be evaluated in this study. As a general comparison, Swiatkowski et al. (2004) has reported the activated carbon adsorption capacity of lead (II) ions at 0.53 mmol/g from an equilibrium pH = 5.54, 8290 mg/L lead nitrate solution, and Khraisheh et al. (2004) reported a 0.05 mmol/g lead (II) adsorption by diatomite at an equilibrium pH = 4.0, and 1 mg/L lead nitrate solution.

Table 5. MCM-41 Adsorption of Various Adsorbates in Batch Reactions

Adsorbate	Maximum Adsorption Capacity (mmol/g)	BET Surface Area (m^2/g)	Pore Diameter (nm)	MCM-41 synthesis molar ratios	Reference
Au^{3+}	1.4	772-1070	2.79 – 3.09	0.00658 TEOS:1 CTAB:0.292 NH_4-OH: 2.773 H_2O	(Lam et al. 2006)
Benzene	0.18	1160	NA	1 SiO_2:0.64 Na_2O: 0.49 $C1_2H_{25}(CH_3)_3NBr$: 52 H_2O	(Choudhary and Mantri 2000)
Benzene	4.8	1060	3.2	NA	(Zhao et al. 1998)
Ca^{2+}	0.007	1325	3.6	1 TEOS: 0.020 $Ti(OC_4H_9)_4$: 0.36 TMAOH: 110 H_2O: 0.24 (CTMA)Br	(Xu et al. 1999)
Cd^{2+}	0.03	1325	3.6	1 TEOS: 0.020 $Ti(OC_4H_9)_4$: 0.36 TMAOH: 110 H_2O: 0.24 (CTMA)Br	(Xu et al. 1999)
Co^{2+}	0.16 – 0.94	89-1025	3.5 – 11.0	1 SiO_2: 0.28 TMAOH: 0.17 CTAB: 0.17 NH_3: 16.7 H_2O	(Sayari et al. 2005)
Co^{2+}	0.69	580	2.29	1 SiO_2: 6.0 CTMACl: 3 TMAOH: 60 H_2O	(Yoshitake et al. 2003)
Cu^{2+}	0.06 – 1.67	89-1025	3.5 – 11.0	1 SiO_2: 0.28 TMAOH: 0.17 CTAB: 0.17 NH_3: 16.7 H_2O	(Sayari et al. 2005)
Cu^{2+}	0.04	1325	3.6	1 TEOS: 0.020 $Ti(OC_4H_9)_4$: 0.36 TMAOH: 110 H_2O: 0.24 (CTMA)Br	(Xu et al. 1999)
Cu^{2+}	0.36	588	2.32	1 SiO_2: 6.0 CTMACl: 3 TMAOH: 60 H_2O	(Yoshitake et al. 2003)
Fe^{3+}	1.6	310	2.24	1 SiO_2: 6.0 CTMACl: 3 TMAOH: 60 H_2O	(Yoshitake et al. 2003)

Table 5 continued

Adsorbate	Maximum Adsorption Capacity (mmol/g)	BET Surface Area (m^2/g)	Pore Diameter (nm)	MCM-41 synthesis molar ratios	Reference
Hg^{2+}	1.4	854-1264	2.7	1 TEOS: 1 HCl: 0.2 octylamine: 1 TMB: 150 H_2O	(Mercier and Pinnavaia 1998)
Hg^{2+}	5.0	380-1040	3.0 – 4.8	1 SiO_2: 0.28 TMAOH: 0.17 CTAB: 0.17 NH_3: 16.7 H_2O	(Antochshuk et al. 2003)
Hg^{2+}	3.13 – 13.5	242-654	3.13 – 5.02	x TEOS: (0.041 – x)BTESPTS: 0.24 HCl: 8.33 H_2O, where x = 0.041, 0.0402, 0.0385, 0.0376, 0.0368, 0.0354, and 0.0347	(Zhang et al. 2003
Hg^{2+}	0.02	1325	3.6	1 TEOS: 0.020 $Ti(OC_4H_9)_4$: 0.36 TMAOH: 110 H_2O: 0.24 (CTMA)Br	(Xu et al. 1999)
Hg^{2+}	0.07	56	2.9	2.8 SiO_2: 1.0 C_{12}TMABr†	(Olkhovyk and Jaroniec 2005)
Mg^{2+}	0.02	1325	3.6	1 TEOS: 0.020 $Ti(OC_4H_9)_4$: 0.36 TMAOH: 110 H_2O: 0.24 (CTMA)Br	(Xu et al. 1999)
Na^{+}	0.05	1325	3.6	1 TEOS: 0.020 $Ti(OC_4H_9)_4$: 0.36 TMAOH: 110 H_2O: 0.24 (CTMA)Br	(Xu et al. 1999)
Ni^{2+}	0.05 – 0.93	89-1025	3.5 – 11.0	1 SiO_2: 0.28 TMAOH: 0.17 CTAB: 0.17 NH_3: 16.7 H_2O	(Sayari et al. 2005)
Ni^{2+}	0.52	284	2.20	1 SiO_2: 6.0 CTMACl: 3 TMAOH: 60 H_2O	(Yoshitake et al. 2003)
Pb^{2+}	0.02	1325	3.6	1 TEOS: 0.020 $Ti(OC_4H_9)_4$: 0.36 TMAOH: 110 H_2O: 0.24 (CTMA)Br	(Xu et al. 1999)
Pb^{2+}	0.05	NA	3.5	0.0303 TEOS: 0.0036 CTABr: 0.0152 NaOH: 3.939 H_20	(Wright, 2006)
Pb^{2+}	0.19	NA	3.5	0.0303 TEOS: 0.0036 CTABr: 0.0152	(Wright, 2006)

Table 5 continued

Adsorbate	Maximum Adsorption Capacity (mmol/g)	BET Surface Area (m^2/g)	Pore Diameter (nm)	MCM-41 synthesis molar ratios	Reference
				NaOH: 3.939 H_2O	
Zn^{2+}	0.03	1325	3.6	1 TEOS: 0.020 $Ti(OC_4H_9)_4$: 0.36 TMAOH: 110 H_2O: 0.24 (CTMA)Br	(Xu et al. 1999)
Cd^{2+}, Cu^{2+}, Pb^{2+} and Zn^{2+}	Not adsorbed in presence of Hg	242-654	3.13 – 5.02	x TEOS: (0.041 – x)BTESPTS: 0.24 HCl: 8.33 H_2O, where x = 0.041, 0.0402, 0.0385, 0.0376, 0.0368, 0.0354, and 0.0347	(Zhang et al. 2003)
Cu^{2+} and Ni^{2+}	Not adsorbed in presence of Au	772-1070	2.79 – 3.09	0.00658 TEOS:0.001 CTAB:0.292 NH_4-OH: 2.773 H_2O	(Lam et al. 2006)

TEOS = tetraethylorthosilicate; TMB = 1,3,5 trimethylbenzene; TMAOH = tetramethylammonium hydroxide; CTAB = cetyltrimethylammonium bromide; (CTMA)Br = alkyltrimethylammonium bromide = $C_nH_{2n+1}N$-$(CH_3)_3Br$ = C_nTMABr; where n = # carbon atoms

BTESPTS = (1,4)-bis(triethoxysilyl)propane tetrasulfide or $(CH_2CH_2O)3Si(CH_2)_3$-S-S-S-$S(CH_2)_3Si(OCH_2CH_3)_3$

CTMACl = cetyltrimethylammonium chloride; NA = Not Available

As shown, the hydrophobic and hydrophilic character uniquely functionalized MCM-41, presents a tantalizing possibility of options to include the removal of organics, and metals, replacement of hazardous catalysts and potentially separation of gases (Raimondo et al. 1997). Other applications for these OSNP materials include the use as optics (for example, laser-dye doped meso-materials can generate increased emissions or operate as optical wave guides), low dielectric insulators, micro-electronic applications, and other emerging technological applications. The possibility of heavy metal adsorbents is certainly demonstrated and needs further illumination to understand application parameters, controls, and conditions to optimize the performance of these novel materials.

The beneficial properties and application of OSNP materials are dependent upon their structural and chemical composition. The complexion of both of these also affects the thermodynamic properties and with careful selection can "tune" the reactivity of the molecule. Accessibility to the organic groups forms the underlying key to successful complexion of the molecule and which steric formulation can contribute to successful adsorption and kinetics. Although kinetic benefits are important most researchers would consider the overall speed of OSNP adsorption reactions to be fast. There have been some reported improvements to reaction rates when the co-condensation pathway was used (Bibby and Mercier, 2002). As reviewed above, applications of interest include high catalytic activity and selectivity, adsorption of heavy metals, removal of organic compounds, and enhanced activity of sensors (Walcarius et al., 2003).

2.5 Lead in Soils at Outdoor Shooting Ranges

The presence of lead in soils at outdoor shooting ranges is well established in the literature (Astrup et al. 1999; Basunia and Landsberger 2001; Bruell et al. 1999; Chen et al. 2002; Darling and Thomas 2003; Dermatas et al. 2003; Isaacs 2006; John 2002; Lin et al. 1995; Stansley et al. 1992; U.S.EPA 2001). Shooting range soils have elevated concentrations of lead as high as 10 to 100 times background levels (Murray et al. 1997). Lead in the soils of twelve military shooting range soils in the United States were found in concentrations from 10 to 30,610 mg/kg (Isaacs, 2005; Isaacs, 2007). See Appendix B for Isaacs (2007) paper.

Lead was selected as the metal of interest for this study because of the prevalence of lead (II) ions in all shooting range stormwaters evaluated, the addition of total lead to the stormwater permit at one shooting range, and because of its toxicity to aquatic organisms. The presence of lead in these soils is obvious, but there are also elevated particulate and dissolved lead(II) ions in stormwaters from shooting ranges (Bruell et al. 1999; Craig et al. 1999; Isaacs 2006). The quantification of lead in soils from a variety of studies is summarized in Table 6, which highlights the variable nature and range of metal types and concentrations that can be found in shooting range soils. The concentration series (high to low) for selected heavy metals is Pb > Cu > Zn > Sb.

Table 6. Heavy Metals in Outdoor Shooting Range Soils
Values shown are the minimum and maximum values reported in mg/kg Sample locations varied by researcher, however all took samples of impact berms, and many included samples from various locations within the range infield and outfield. Note: AFB = Air Force Base; ND = Non-detect at detection limit = 0.05 mg/kg; blank = data not available.

Location	Cu	Pb	Sb	Zn	Reference
Amarillo, TX	13 - 359	11 - 4675	1 - 517	9 - 136	(Basunia and Landsberger, 2001)
Various, FL		7.3 - 48400			(Cao et al., 2003)
Various, FL		50 - 1142			(Hardison et al., 2004)
South Korea	117 - 192	71 - 184		164 –347	(Lee et al., 2002)
Switzerland, multiple	100 - 4450	1900 - 515800	35 - 17500		(Johnson et al., 2005)
Oberuzwil, Switzerland	20 -2250	110 - 67860	5 - 3020	55 – 1025	(Vantelon et al., 2005)
Barksdale AFB, LA	37 - 369	436 - 4433	<0.05 – 3.27	6.8 – 79	(Isaacs, 2007), see Appendix B
Beale AFB, CA	15.9 - 954	10 - 30610	<0.05 – 5.3	53 –273	"
Cannon AFB, NM	7.1 – 9.3	37 - 102	ND	2.9 – 20.3	"
Ellsworth AFB, SD	56.5 – 148.1	1637 - 7621	ND	3.2 – 93.0	"
Holloman AFB, NM	1.8 – 68.8	10.1 - 2984	<0.05 – 0.20	6.6 – 17.4	"
Langley AFB, VA	13.9 – 40.8	545 - 6320	<0.05 – 7.1	4.0 – 137.3	"
Nellis AFB, NV	32.8 - 48	1137 - 9682	ND	51.8 – 57.5	"
Offutt AFB, NE	27.9 – 106.7	1246 - 2134	<0.05 – 10.08	9.1 – 18.7	"
Shaw AFB, SC	24.0 – 87.6	70.6 - 4355		6.03 – 54.1	"
Whiteman AFB, MO	5.03 – 38.5	384.5 – 764.7	ND	37.7 – 30.7	"

2.6 Complexes of Lead in Soils

Lead in the environment is mostly complexed with organic ligands in natural soils as $PbOH^+$ and $PbHCO_3^+$ (Sposito, 1989). Weathering of elemental lead forms from shooting ranges have also been documented as visible corrosion on lead fragments as crusts of white, gray or brown material, and as hydrocerussite ($Pb(CO_3)_2(OH)_2$), cerussite ($PbCO_3$)and some amounts of anglesite ($PbSO_4$) (Cao et al. 2003; Lin et al. 1995). The bullet abraded residue transforms into hydrocerussite and to a lesser degree cerussite, and massicot (PbO) in as little as one week to 300 years (Cao et al. 2003; Chen et al. 2002; Hardison et al. 2004; Jorgensen and Willems 1987; Vantelon et al. 2005). The lead of weathered bullets exists as particulate or ionic forms and may provide a steady source of potentially labile constituents, which can appear in various soil fractions and in stormwaters. A suggested weathering process was formulated by Ma et al., (2002) and is depicted in Eq. (1a – 1d).

$$2\ Pb(s) + O_2 \leftrightarrow 2\ PbO(s) \quad (1a)$$

$$CO_2 + H_2O \leftrightarrow H^+ + HCO_3^- \quad (1b)$$

$$PbO(s) + HCO_3^- \leftrightarrow PbCO_3(s) + OH^- \quad (1c)$$

$$3\ PbO(s) + 2\ HCO_3^- + H_2O \leftrightarrow Pb_3(CO_3)_2(OH)_2\ (s) + 2\ OH^- \quad (1d)$$

The oxidized lead apparently forms readily when exposed to air and then with carbon dioxide and water exposure forms lead carbonate. The rate of elemental lead dissolution is regulated by both physical and chemical factors. Ma et al., (2002) found for each standard pH reduction, the concentration of lead (II) ions increased about two orders of

magnitude. This is consistent with Eqs. 1c and 1d, which suggest as weathering progresses hydroxyl groups, are formed naturally, raising the soil pH.

Lead is generally non-labile in soil (deMatos et al. 2001). Both aerobic and acidic conditions in soils increase elemental lead dissolution, whereas anaerobic and alkaline conditions decrease it (Scheuhammer and Norris 1995). Lead mobility in soil is driven by redox potential, available anions (e.g. carbonates, phosphates, and sulfates), pH, soil organic matter, and cation exchange capacity (McLean and Bledsoe 1992). Soil organic carbon content has been found to enhance lead adsorption, but dissolved organic carbon improves lead dissolution with decreased soil pH (Sauvé et al. 1998; Strawn and Sparks 2000). Soil colloids have been found to be active participants in transporting lead to groundwater and limiting lead interaction with reactive soil constituents (Citeau et al. 2003). Surface (Abdel-Fattah et al. 2003; Craig et al. 1999) and sub-surface soils (Murray et al. 1997) lead migration has been reported.

For the pH and Eh range of soils found at outdoor ranges lead complexes in the soil and aqueous solutions would be typically found as carbonates and sulfates (Figure 6). Figure 6 depicts the stability of various lead species by Eh-pH relationships for a lead, water and soil system. Metallic lead (Pb^0) is only stable in a very low redox potential environment. Redox potentials for soil water conditions are typically at high levels (McBride et al. 1997). Therefore, it is likely lead will weather (i.e. oxidize) as previously outlined in Equation 1. Lead carbonate would be the expected stable compound between about pH 6 and 8.

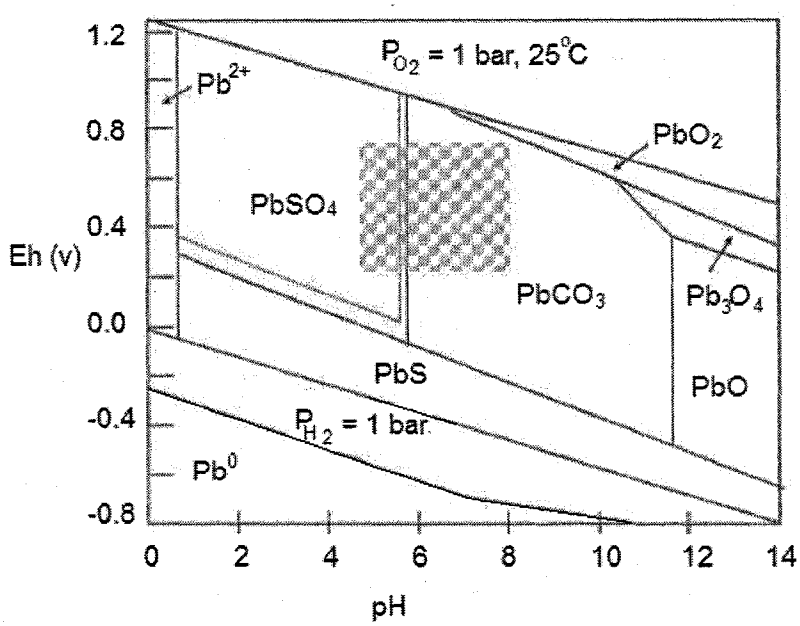

Fig. 6. Eh - pH Stability Diagram for Pb Compounds
Eh-pH stability diagram for activities of dissolved Pb = 10^{-6} M, S = 10^{-3} M and CO_3^{2-} = 10^{-3} M. Shaded area added to illustrate shooting range Eh and pH intersection area. $PbCO_3$ would be the dominant precipitate in the expected pH and Eh range for shooting range stormwaters. Lead(II) ions of interest in this study will be associated as dissolved and particulate attached species. Redrawn after Bradl (2004).

The leachability of metals from soils has been associated with the natural organic matter content. In Table 7 lead leachability was observed in soils from eastern and western location outdoor shooting ranges following a synthetic precipitation leaching procedure protocol. Soils with high pH, and high clay or organic matter content tended to not leach lead cations. However, when lead did leach from soils it was predominantly in particulate form bound to suspended colloids (Isaacs, 2007).

Relevant solubility products for lead minerals and complexes are shown in Table 8. These solubility constants substantiate the general observation that lead compounds in soils are non-labile and transport primarily with soil particulates.

Table 7. Shooting Range Soil and SPLP Lead and Copper Characteristics
Shooting range soil lead and copper concentrations and associated Pb leachate from the synthetic precipitation leaching procedure (SPLP). A more complete review of leaching behavior of lead and copper in soils from outdoor shooting ranges is provided in Appendix B.

Shooting Range Soil						
LOCATION†	CEC ($cmol_c/kg$)	pH	Total Pb (mg/kg)	SPLP Pb (μg/L)	Total Cu (mg/kg)	Ref
East	8.5 – 43.2	5.5 – 6.7	736 – 2720	NA	NA	A
East	4.4 – 17.7	7.7 – 8.1	26 – 3400	837	7 – 0500	B
East	4.82 – 40.6	5.1 – 7.5	7 – 48400	NA	NA	C
West	NA	NA	11 – 4675	NA	13 – 0359	D
West	5.6 – 31.5	6.8 – 8.7	10 - 130000	2 - 2233	3 - 52000	B

† East and West division was arbitrarily set at the Mississippi River
NA = Not Available; SPLP = Synthetic Precipitation Leaching Procedure.
Ref - Reference key:
A - (Cao et al. 2003)
B - (Isaacs, 2007)
C - (Ma et al. 2002)
D - (Basunia and Landsberger 2001)

Table 8. Solubility Products for Selected Lead Minerals and Compounds

Mineral or Compound	Equilibrium Reaction at 25 °C	Log K_{so}†
Hydroxypyromorphite	$Pb_5(PO_4)_3(OH)(s) + 7H^+ \leftrightarrow 5Pb_2+ + 3H_2PO_4^- + H_2O$	-4.14
Lead hydroxide	$Pb(OH)_2(s) \leftrightarrow Pb^{2+} + 2\ OH^-$	-7.71
Anglesite	$PbSO_4(s) \leftrightarrow Pb^{2+} + SO_4^{2-}$	-7.79
Cerrusite	$PbCO_3(s) + 2H^+ \leftrightarrow Pb^{2+} + CO_2(g) + H_2O$	-13.13
Massicot	$PbO(s) + 2H^+ \leftrightarrow Pb^{2+} + H_2O$	-15.09
Chloropyromorphite	$Pb_5(PO_4)_3Cl(s) + 6H^+ \leftrightarrow 5Pb^{2+} + 3H_2PO_4^- + Cl^-$	- 25.05
Galena	$PbS(s) \leftrightarrow Pb^{2+} + 2S^-$	-28.05
Lead phosphate	$Pb_3(PO_4)_2(s) \leftrightarrow 3Pb^{2+} + 2\ PO_4^{3-}$	-44.50
Hydrocerussite	$Pb_3(CO_3)_2(OH)_2(s) + 6H^+ \leftrightarrow 3Pb^{2+} + 2CO_2(g) + 4H_2O$	-45.46

† Solubility constants are from Benjamin (2002).

2.7 Heavy Metal Removal Technologies Overview

Technologies traditionally employed to remove heavy metals from aqueous solutions include chemical precipitation, adsorption (usually carbon adsorption), ion

exchange, and filtration (depth, surface and membrane) processes (Tchobanoglous et al. 2003). The following briefly summarize each of these processes and concludes with a comparative analysis of lead removal performance for each from the literature. Table 9 summarizes the performance characteristics of the traditional removal techniques and highlights their advantages and disadvantages.

Chemical precipitation to form metal hydroxides or sulfides is the most common metals removal method from wastewaters (Tchobanoglous et al. 2003). An example of the stoichiometry for the removal of lead is typical of the chemistry for this process.

$$Pb(OH)_2 \leftrightarrow Pb^{2+} + 2\,OH^- \quad (2a)$$

$$PbS \leftrightarrow Pb^{2+} + S^{2-} \quad (2b)$$

Chemical precipitation is frequently used with or as part of other water treatment processes. For example, chemical coagulation enables the removal of suspended materials from water via precipitation. Softening of water is also a precipitation process when lime or caustic soda is added to precipitate calcium and magnesium.

Adsorption is a physical and chemical process where an adsorbate accumulates at the interphase of a surface or interface. The physical process mechanism is predominantly van der Waals' forces and is a reversible phenomenon. Chemical adsorption is the result of a chemical reaction between the solid and the adsorbate and it is typically not reversible. Adsorption is a proven process for the removal of organics and metals to include water color, odors, taste and residual chlorine. Activated carbon is the most commonly used adsorbent in wastewater treatment technologies. Also, sand has

been used effectively as a metal adsorbents (Muhammad et al. 1998) and its metal adsorption behavior enhanced when sand was coated with an iron oxide (Muhammad et al. 1998; Sansalone 1999). Other adsorbents have been developed using zeolites, clays, organic matter, and certain inorganic media. The difficulty with all these is the low loading capacities and binding energies (Mercier and Pinnavaia 1998).

Ion exchange is a reversible process where ions of a solid and a liquid are exchanged. Ion exchange may be defined as an adsorption process as the exchange of ions occurs at the surface of the solid and ions are being transferred through an interphase from the liquid to the surface of the solid. Exchange materials can be comprised of resins, membranes, zeolites, and clays. Ion exchange effectiveness can be influenced by presence of more selective anions inhibiting the removal of certain ions. Zeolites have been used to remove > 91% heavy metals in wastewater where the ordered preference was Pb > Cu > Zn ~ Cd (Pitcher et al. 2004).

Filtration is a process of removing particulate matter from water (Droste 1997). Various forms of filtration have been employed for many years using filter medias that have consisted of cloths, sand, charcoal, gravel and others, The basic purpose of these filtering methods have been to remove waterborne particulates, particularly in water treatment processes (Crittenden et al. 2005). Nine principal mechanisms have been identified for removing material within a granular filter. They include: 1) straining, 2) sedimentation, 3) impaction, 4) interception, 5) adhesion, 6) flocculation, 7) chemical adsorption, 8) physical adsorption, and 9) biological growth (Tchobanoglous et al. 2003). Filtration, especially the mechanisms of chemical and physical adsorption, is of particular interest in this study to remove inorganics (i.e. particulate bound heavy metals like lead (II) ions).

Filtration of wastewaters may be classified as depth, surface or membrane Depth filtration pertains to the removal of suspended matter at the surface or within the filter medium. Surface filtration is a mechanism where waterborne particulates are removed by straining through a surface media (e.g., a filter cloth) (Tchobanoglous et al. 2003). Membrane technology, basically a surface filtration process, extends beyond basic surface treatment to separate dissolved solids and colloids from solution. A brief summary of depth, surface and membrane application is presented in the following paragraphs.

Depth filtration may be further sub-divided into slow and rapid media systems. Typically the media of choice is sand because of is ready availability and low cost. The grain size of the media is carefully selected for each application as grain size directly impacts headloss and particulate removal efficiency. Researchers have sought methods to enhance or augment the sorption behavior of sand for inorganics (i.e. relative to this study, lead (II) ions) in sand filtration.

Sand has long been used as an effective media to remove particulate-bound contaminants (Yao et al. 1971). While particulate-bound inorganics may be effectively removed, dissolved species may readily pass through a sand-only filter. To enhance the sorption capability Sansalone (1999) coated sand with an iron oxide to increase its surface area and amphoteric surface charge. In column studies Sansalone (1999) reported lead (II) ion removal at Ce/Co = 0.9 for iron oxide coated sand (OCS) = 506 pore volumes (PV) compared to un-coated sand = 20 PV (PV = 2.79 L; influent lead concentration = 5 mg/L; pH = 6.5). Important to note for the OCS, 340 PVs were dissolved lead (II) ions versus 166 PVs particulate bound. Although not mentioned, it was assumed the 20 PV removed by sand was predominantly particulate-bound.

Other media have also been used with sand filtration to enhance particulate and sorption performance. Some of these media include anthracite, garnet, ilmenite ($FeTiO_3$, typically found in beach sand), activated carbon and others (Tchobanoglous et al. 2003). The selection of the appropriate media is site specific and most often determined by the specific objectives of each application. The flow rate of water through the filter is also a critical factor in media selection. Slow sand filters typically operate at 1 to 8 m^3/m^2 d versus rapid sand filters that may operate 100 to 475 m^3/m^2 d (Droste, 1997). Therefore, slow sand filtration would most likely be the preferred filtration strategy to meet the requirements for a stormwater filter system at a shooting range (i.e. contact time, operation by gravity flow, and semi-continuous to intermittent operations).

Surface filtration includes those sorption processes that use diatomaceous earth and cloth/screen filtration. Surface filtration is the method most often encountered for removal of suspended particles used in swimming pools. Surface filters may consist of a matrix of constructed glass or polymeric microfibers, or may use diatomaceous earth (a porous medium) to trap particulates. Surface filtration can have sorption properties similar to depth and membrane filtration. They have been used to remove suspended materials from secondary effluents and from ponds used to receive waters for sedimentary control. Surface filters can remove contaminants that are predominantly particulate bound and be used to enhance or augment other sorption methods.

For membrane technology, water is forced through a membrane, usually by an external force, where particulates larger than the membrane pore openings are trapped. The membrane technologies are characterized by pore sizes and includes microfiltration (> 50 nm), ultrafiltration (2-50 nm), nanofiltration (< 2nm), reverse osmosis (< 2 nm), dialysis (2-50 nm), and electrodialysis (< 2 nm) (Tchobanoglous et al. 2003).

Membranes are used for desalination and have been used for filtration, the removal of microorganisms, and nanofiltration for the recovery of precious metals. Electrodialysis is a specialized membrane process where an electric current is passed through a solution causing the migrations of cations to the cathode and anions to the anode. Alternate spacing of cation and anion permeable membranes causes concentration of dilute salts to form between membrane layers, effectively demineralizing the wastewater.

The selection of a heavy metal removal technology depends on many factors, which collective and simultaneously must be satisfied for each unique situation. For this study, a treatment technology was needed where the dominant factors were contact time, particulate and dissolved lead (II) ion removal effectiveness, low maintenance, low capital cost, and minimal operator skills. A gravity declining rate depth slow sand filtration system was selected based on these criteria and because OSNP materials could be easily added as co-adsorbent media. Other technologies failed in one or more of the selection criteria factors.

Table 9. Traditional Heavy Metal Removal Technologies
Wastewater technologies applicable to heavy metal removal (Crittenden et al. 2005; Tchobanoglous et al. 2003).

Technology	Mechanism	Application Principles	Advantages	Disadvantages
Chemical Precipitation	Chemical reaction of soluble metal compound with precipitating reagent	Alum; Aluminum chloride; Calcium hydroxide; Ferric chloride; Ferric sulfate	Fast reacting; strong chemical bonds; Creates precipitates which enhances sedimentation	Precipitation chemicals dependent on influent quality; sludge disposal; not reversible
Adsorption	Mass transfer; diffusion; physical and chemical adsorption; Electrostatic	Zeolites; synthetic polymers; activated carbon, granular and powdered; Surface area and pore size important factors	Physical adsorption reversible	Chemical adsorption typically not reversible; OSNP materials not been used in wastewater application; pH and ionic strength dependent
Ion Exchange	Ionic bonding	Zeolites; anion resins; cation resins; chelating resins, microbes; plant biomass	High selectivity for the target metal; Efficiency is high	Fluctuating metal conc. hard to design for; pH dependent; Particulates/solvents affect performance; regen. costs
Depth Filtration (slow sand and rapid)	Straining; interception; diffusion; inertial forces; gravitational forces; attachment	Typically sand or anthracite is used; Can be single, dual or multi-media;	Naturally occurring granular minerals effective adsorbent media; microbial development remove organics and minimize head loss build up; Effective TSS removal; Particle removal independent of filtration rate	Efficiency highly dependent upon media effective size, density, shape, hardness, bed porosity, and bed specific surface area; Head loss increases with use; Dissolved species may pass through filter
Surface Filtration	Mechanical sieving	Woven metal fabrics; cloth and synthetic materials	Ease of use/backwash; Effective TSS removal; Can operate intermittently	Disposal of residual solids; Not effective for dissolved constituents
Membrane Filtration	Sieving; Diffusion	Nanofiltration and Reverse Osmosis	Applicable to high dissolved solid constituents and saltwater; No chemicals required	Expensive; Energy Demand; Scale formation; Declining flux rate with use; Difficult to monitor; Filter membrane must be replaced; Brine disposal; propensity to foul

2.8 Mass Transfer Adsorption Theory

Adsorption is the process where a solute is accumulated at the surface liquid interface. Specifically as related to this work, it is the free or dissolved metal ion, adsorbate, in the liquid phase that is adsorbed to the solid phase, adsorbent. The transfer of adsorbate mass to the adsorbent surface constitutes the principle known as adsorption. It could be described in three phases: macrotransport (mass transport by advection and diffusion), microtransport (mass transport by diffusion), and sorption (attachment to the adsorbent). The adsorption mechanism represents an equilibrium relationship between dissolved and adsorbed solutes. The solid-water surface chemistry is important to the application of adsorption processes in natural waters.

Stumm (1992) explains solids can be generalized as inorganic or organic polymers with surfaces bearing functional moieties such as solute ligands –OH, -SH, -SS, and -COOH. These functional moieties may form coordination bonds in one of three possible mechanisms, 1) outer-sphere complex, 2) inner-sphere complexes, and 3) surface precipitates. It is assumed these same coordination bonds can represent the adsorption mechanism on OSNP materials. Several models of this complexation have been developed to represent the metal and ligand adsorption reaction. Two models presented are the site-binding and phase transfer models (Benjamin 2002). The site-binding model assumes surface ligands are attached to specific sites on the adsorbent surface. The second model, the phase transfer model, treats the interfacial region as a phase separate from the solution considering adsorption as a phase transfer reaction. Both adsorption models are reviewed in the following paragraphs.

number of surface sites is quantified by expressing the number of sites per unit mass of solid times the concentration of solid in the system. This provides a representation of the adsorption similar to moles/liter. A surface complexation of a soluble adsorbate can be represented grammatically as simply: the soluble adsorbate A(*aq*) plus hydrated surface site equals adsorbed A plus H_2O. The stoichiometric relationship is shown in Equation 3, where the formation of a complex between a metal ion M^{n+} and a ligand L results in a coordination compound MLn. The model depicted assumes a coordination sphere of six water molecules surrounding the metal.

$$M(H_2O)_6^{2+} + L \leftrightarrow M(H_2O)_5L^{2+} + H_2O \qquad (3a)$$

Therefore, the equilibrium or first formation constant for adsorption is:

$$K_1 = [ML^{2+}] / [M^{2+}][L] \qquad (3b)$$

The second formation constant would then be:

$$K_2 = [ML_2^{2+}] / [ML^{2+}][L] \qquad (3c)$$

The size of the formation constant explains how much of metal will be coordinated with the ligand and how much will be present as a hydrated M^{2+} complex. Assuming the solution is infinitely diluted the activities can be assumed to be the molar concentration of each species. As this model tends to represent the adsorption of hydrophilic species to the adsorbent, and would seem to logically extend to ionic and electrostatic attraction representations.

The Phase Transfer Model. In this model the adsorbed species are not considered

bound to a specific site on the adsorbent, but is thought to move around the surface in response to chemical or electrical forces. Theoretically, there is no limit on the amount of adsorbate that can be bound to the surface of the adsorbent. This interphase representation then can be modeled thus:

$$A(aq) \leftrightarrow \equiv A(\text{interphase}) \quad (4a)$$

$$K_D = \equiv A(\text{interphase}) \ / \ A(aq) \quad (4b)$$

where K_D is called the distribution or partition coefficient. The distribution coefficient represents the equilibrium condition for the surface adsorption complexation reaction and has units L/kg. The distribution coefficient is very valuable to examine sorption behavior of lead (II) ions on OSNP materials because it responds independent of the concentration of suspended solids in water (Stumm 1992). Therefore, using K_D and the phase transfer model to evaluate the complex competitive reactions of ions in stormwater may prove useful to understand the fraction of metal ions in solution.

Adsorption isotherms relate the quantity of adsorbate adsorbed to the quantity of adsorbent in solution at equilibrium. When the isotherm is expressed in mg per gram ratio it provides a relative comparison mechanism to judge performance between various materials. The isotherm models assume various phases or methods of the adsorption reaction. For example, the Langmuir isotherm follows the site-binding model theory where the adsorbate attaches to sites on the surface of the solid adsorbent. It is generally expressed as (Equation 5):

$$q_e = X_m \cdot K_L \cdot C_e / (1 + K_L \cdot C_e) \quad (5a)$$

$$q_e = [(C_o - C_e) * V] / M \quad (5b)$$

where:
q_e = mg of adsorbate per g of adsorbent at equilibrium
X_m = mg of solute adsorbed per g of adsorbent
K_L = the Langmuir constant equal to liter of adsorbent per mg of adsorbate
C_e = equilibrium concentration of adsorbate in solution (mg L^{-1})
C_o = adsorbate initial or original concentration (mg L^{-1})
V = volume of solution (L)
M = Amount of adsorbent used (mg)

The linear form (Equation 6) is expressed by rearranging Equation 5 to the following:

$$C_e / q_e = 1 / (X_m \cdot K_L) + (1 / X_m) \cdot C_e \quad (6)$$

The adsorption capacities of various adsorbents are typically calculated using the Langmuir isotherm. Then the amount of metal retained mg/g can be estimated as:

$$qe = (Co - Ce) * V / M \quad (7)$$

The solid water interface distribution ratios of metals can also be estimated as:

$$K_D = [(Co - Ce) / Ce] \times [V/M] \quad \text{(Stumm, 1992)} \quad (8)$$

The Langmuir isotherm is frequently used, but assumes monolayer adsorption, surface homogeneity, no lateral interaction between adsorbate molecules, and adsorbate molecules are localized, that is they do not diffuse to other binding sites after first attachment.

The Freundlich model assumes no association or dissociation of the molecules after they are adsorbed and there is no chemisorption, and the surface is heterogeneous. At low concentrations the Freundlich equation tends to not reduce to the linear isotherm, but has been shown by experiments of others the van der Waals' adsorption is adequately represented in the mid-concentration ranges (Noll et al. 1992). The Freundlich equation takes the form:

$$x / m = K_f C_e^{1/n} \quad (9)$$

where x/m = mass of adsorbate adsorbed per unit mass of adsorbent (mg/g)
K_f = Freundlich capacity factor (mg adsorbate/g adsorbent)(L H_2O/mg adsorbate)$^{1/n}$
C_e = equilibrium concentration of adsorbate (mg/L)
1/n = Freundlich intensity parameter

The linear form of the equation (Equation 10) can be obtained by taking the log of both sides of the equation.

$$\log (x/m) = \log K_f + (1/n) \log C_e \quad (10)$$

Isotherms have been reported for MCM-41 of the general Type IV, which exhibits a hysteresis, but has been shown to be eliminated by increasing the operating temperatures (Branton et al. 1995). The absence of hysteresis has been confirmed by some for certain grades of MCM-41 (Rouquerol et al. 1999). The dependence of the isotherm shape relative to pore size of MCM-41 has been investigated. Pore sizes 2.5 to 4 nm displayed very steep and reversible pore filling isotherm risers, but at 4.5 nm the Type IV with hysteresis loop occurred. MCM-41 pore diameters used in this study are 3.5 nm and may not encounter the hysteresis loop mentioned.

Adsorption on OSNP materials occurs as either outer-sphere, inner-sphere and in rare instances as surface precipitates. The intermolecular interactions between solute and any solid phase would include surface complexation reactions, electrostatic interactions, hydrophobic, adsorption of surfactants and adsorption of polymers (Stumm, 1992).

All inorganic particles have a charge in aqueous environments and for silica, this occurs because Si-OH loses a proton resulting in the attraction of counter-ions. Therefore for silica, positive ions will collect at the solid – solute interface. Due to the radius of influence of the ions, the adsorbed counter ions will not completely neutralize the charge, causing another layer of counter ions to adsorb to the solid. This process continues until at some distance from the solid surface a charge balance will be reached. It is at this point and beyond there will be a balance of positive and negative ions in the bulk solution. This is the double layer. The boundary of the double layer depends on the initial charge of the solid phase and its potential is difficult to measure directly. The zeta potential is not the surface charge potential, but is used as a representative potential proportional to the surface charge. It represents the potential difference between the adsorbate bulk phase and the plane of shear (Stumm, 1992). The magnitude of the zeta potential helps explain the OSNP material stability. This potential or surface charge can be altered by the addition of surfactants to the adsorbent or solid phase material. Surfactants operate in three forms: as steric hindrance occupying the adsorption sites on the surface of the particle, by electrostatic surface charge changes, and by a combination of both of these processes. OSNP materials attractive forces have been described predominantly as electrostatic, and specifically van der Waals forces (Pinnavaia 2006). Electrostatic attraction or covalent bonds with functional groups is determined by ionic

strength, pH and the type of cation (Strawn and Sparks, 1999). The surface charge is not directly measurable, but can be represented by the zeta potential.

An important factor effecting zeta potential in aqueous systems is pH. The isoelectric point for OSNP materials is pH 2, which reflects the dominant structural moiety of silica (Iler 1979; Kisler et al. 2001). Hence, virgin OSNP materials will be negatively charged under typical solution conditions and exhibit attractive electrostatic forces to cations in the bulk solution. However, zeta potential will also be affected by changing the concentration of cations and the type (valence) of cations in solution. For example Mg^{2+} ion will cancel out more surface charge on OSNP materials than Na^{+} (Vralstad 2005). The implications of multivalent cations are they will have quicker and larger impact to surface charge and subsequent OSNP material adsorption performance. In this study, multivalent cations Ca^{2+}, Cr^{2+}, Cu^{2+}, Fe^{2+}, Mg^{2+}, Mn^{2+}, Mo^{2+}, Ni^{2+}, Pb^{2+}, Sb^{3+}, Sn^{2+} and Zn^{2+} ions were found in shooting range stormwaters. Theoretically then, adsorption performance of OSNP materials may drop significantly in increasing ionic strength conditions.

2.9 Aquatic Chemistry of Lead (II) Ions

The speciation of lead (II) in solution is of interest because some forms, *viz.* species which have lost one organic group form the neutral, fully saturated organo-metallic, are more toxic to aquatic organisms than others (Mester et al. 2000). Further, some species that are soluble (e.g. $Pb(NO_3)_2$) or insoluble (e.g. $PbCl_2$ and $Pb(OH)_2$), which condition is of importance to identify appropriate complexion, precipitation, or ionic exchange treatment processes. An element's speciation is regulated by many factors including other species in solution (i.e. ionic strength), pH and redox conditions.

The need for better speciation of metal complexes is desired to understand the biologically available forms that may be harmful to the environment and anthropogenic interactions (Sanz-Medel 1998). The charge on species can also display different attractive properties to negatively charged colloids in stormwaters. These various charges can regulate how species will react in the aqueous environment. It could be overwhelming to tackle all potential speciation of lead (II) that might be encountered within the current endeavor, it would be prudent to at least examine the expected

Table 10. Hydrolysis Equilibria Lead (II) Speciation in Natural Waters
K = Equilibrium constant at 25 °C

Equilibrium Equation	K	pK	Reference
$Pb^{2+} + H_2O \Leftrightarrow PbOH^+ + H^+$	k_1	7.9	(Xu et al. 1999)
$Pb(OH)^+ + H_2O \Leftrightarrow Pb(OH)_2 + H^+$	k_2	8.3	(Xu et al. 1999)
$Pb(OH)_2 + H_2O \Leftrightarrow Pb(OH)_3^- + H^+$	k_3	11.5	(Xu et al. 1999)
$Pb(OH)_3^- + H_2O \Leftrightarrow Pb(OH)_4^{2-} + H^+$	k_4	13.1	(Xu et al. 1999)
$Pb(OH)_2(s) \Leftrightarrow Pb^{2+} + 2OH^-$	$K_{sp,OH}$	16.1	(Xu et al. 1999)
$Pb^{2+} + CO_3^{2-} \Leftrightarrow PbCO_3$	k_5	7.24	(Benjamin 2002)
$Pb^{2+} + 2CO_3^{2-} \Leftrightarrow Pb(CO_3)_2^{2-}$	k_6	10.64	(Benjamin 2002)
$Pb^{2+} + CO_3^{2-} + H^+ \Leftrightarrow PbHCO_3^+$	k_7	13.2	(Benjamin 2002)
$PbCO_3(s) \Leftrightarrow Pb^{2+} + CO_3^{2-}$	$K_{sp,CO3}$	13.13	(Benjamin 2002)
$Pb^{2+} + Cl^- \Leftrightarrow PbCl^+$	k_8	1.6	(Stumm and Morgan 1996)
$Pb^{2+} + 2Cl^- \Leftrightarrow PbCl_2$	k_9	1.8	(Stumm and Morgan 1996)
$Pb^{2+} + 3Cl^- \Leftrightarrow PbCl_3^-$	k_{10}	1.7	(Stumm and Morgan 1996)
$PbCl_2(s) \Leftrightarrow Pb^{2+} + 2Cl^-$	K_{spCl}	4.77	(Stumm and Morgan 1996)
$SOH_x + nPb^{2+} \Leftrightarrow SOPb_n^{(2n-1)+} + x\,H^+$			(Stumm and Morgan 1996)

Note: The formation of lead nitrate and sulfate were not included as these species should be much less than the hydroxide and carbonate species at the redox potential, ligand concentration and pH of stormwaters from small arms shooting ranges (See Figure 6). SOPb represents the sorption of lead ions to a surface edge SO and is an illustration for OSNP material adsorption.

speciation. The expected hydrated forms of lead (II) in water are Pb^{2+}, $Pb(OH)^+$, $Pb(OH)_2$, $Pb(OH)_3^-$, and $Pb(OH)_4^{2-}$. The carbonate species would include $Pb(CO_3)$ or cerussite or the hydrated form $Pb(OH)_2(CO_3)_2$, hydrocerrusite. Hydrocerrusite is the usually found to be the most stable solid form in natural waters (Bilinski and Schindler

1982). In an estuary environment or otherwise high chloride water, $PbCl^+$ or $PbCl_2$ could be observed. The lead (II) equilibrium relationships are depicted in Table 10. With these equilibrium relationships a distribution of species of lead (II) as a function of pH may be estimated. From the relationship the solid phase that controls solubility may be determined and the species expected for the specific stormwater conditions of interest

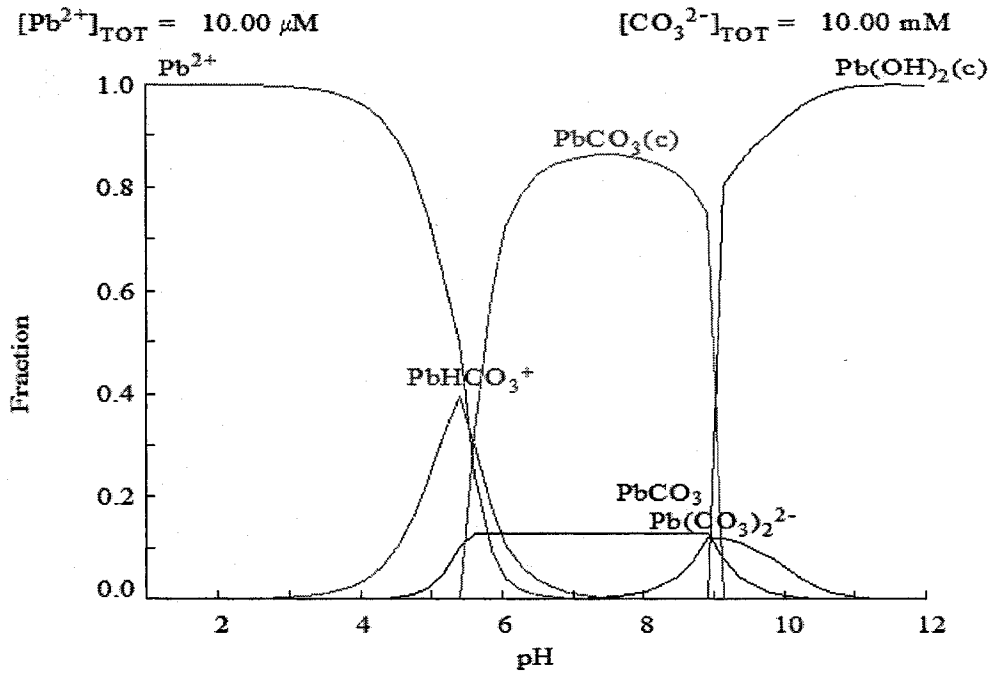

Fig. 7. Speciation of Pb Hydroxide and Carbonate Species
Concentrations approximate anticipated stormwater run-off from small arms shooting ranges. For shooting range stormwater pH range = 5.2 to 7.8 (see Table 14). $PbCO_3(c)$ will likely be the solid phase that controls solubility. Chart was drawn using software developed by the Royal Institute of Technology (Puigdomenech 2004). (c) = crystalline or solid species

may be speculated. For this study of $[Pb^{2+}] \approx 10$ μmol, $[CO_3^{2-}] \approx 10$ mmol and utilizing the equilibrium relationships of Table 10, Figure 7 can be developed. The carbonate was intentionally set high to represent calcareous soil run-off conditions.

The following provides a review of how Figure 7 was constructed. The principal hydrolysis forms of lead (II) ions in water solution are shown in Table 10. Their molar fractions α_0, α_1, α_2, α_3, and α_4 may be estimated in terms of pH and their respective equilibrium constants. With the following equations the distribution of each hydrolysis species and carbonate complexes can be calculated, and represented on a fraction plot as shown in Figure 7.

$$\alpha_0 = [1 + k_1/(H^+) + k_1k_2/(H^+)^2 + k_1k_2k_3 / (H^+)^3 + k_1k_2k_3k_4/(H^+)^4]^{-1} \quad (11a)$$

$$\alpha_1 = \alpha_0 * k_1/(H^+) \quad (11b)$$

$$\alpha_2 = \alpha_0 * k_1k_2/(H^+)^2 \quad (11c)$$

$$\alpha_3 = \alpha_0 * k_1k_2k_3/(H^+)^3 \quad (11d)$$

$$\alpha_4 = \alpha_0 * k_1k_2k_3k_4/(H^+)^4 \quad (11e)$$

The interpretation of the figure is based on the total Pb^{2+} and CO_3^{2-} that specifies the resultant graphs as shown in Figure 7. For the chosen concentrations some dissolved Pb^{2+} species would be expected for pH < 6, and for 6 < pH < 9, $PbCO_3$ would be the expected dominate solid controlling lead (II) ion solubility.

Similarly, for conditions of this study at $[Pb^{2+}]$ = 10 μmol and $[Cl^-]$ = 1.0 mmol then Figure 8 can be developed to evaluate the contribution of chloride may have on the speciation of lead (II) hydroxide complexes. Figure 8 is constructed using the molar fractional amounts Equations 11a through 11c, along with the same hydrolysis complexes for lead (II) ions. In this controlled analysis free lead (II) ions would exist in large fractions and $PbCl^+$ = 0.3 molar fraction until ca. pH = 7, at which point the hydroxide precipitate would dominant the aqueous environment.

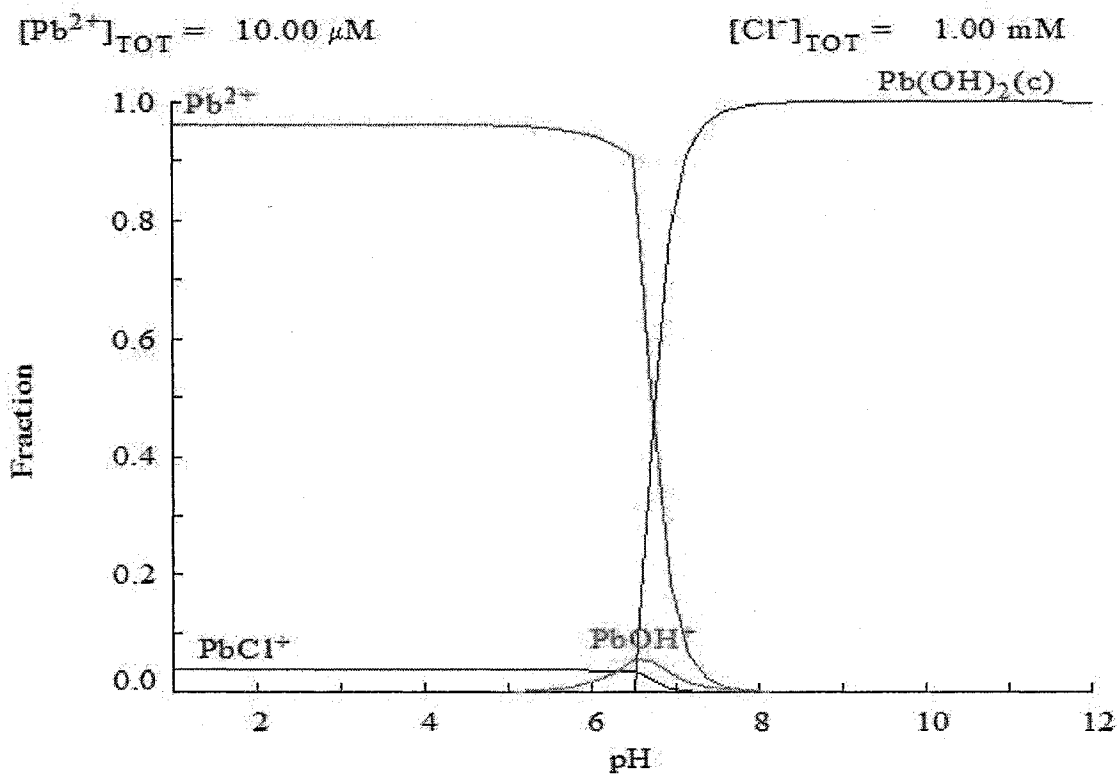

Fig. 8. Speciation of Pb Hydroxide and Chloride Species
Fractions of lead and chloride ions anticipated in stormwater run-off from small arms shooting ranges. For shooting range stormwater pH range = 5.2 to 7.8 (see Table 14). Free lead (II) ions and $Pb(OH)_2(c)$ will dominate this pH range. (c) = crystalline or solid species

2.10 Optimization Using Response Surface Methodology

RSM is an experimental design process of mathematical and statistical methods applicable with broad application to many disciplines. The response is typically measured on a continuous scale and is the chosen variable that most likely influences the response curve. The purpose of use is to enable exploration of the response surface with equal precision, in any direction. It is fundamentally about analyzing the results of experiments to ensure valid and objective conclusions are obtained (Montgomery 2005).

Optimization of any experiment has at least one objective - alter controlled variables to maximize or minimize the output of a process. In relation to this research it is possible to vary parameters (media depth, filtration rate, percent OSNP material used, and possibly others) to maximum the adsorption efficiency. In theory a starting point is selected, typically an educated guess, and the media depth, for example, is varied to the most optimum benefit. Then at this optimum media depth the filtration rate is varied until again the optimum performance is realized. Other parameters may also be adjusted similarly. This type of approach is called a one-factor-at-a-time strategy, however it misses one critical part of the analysis; the interaction between the factors. The correction to this is to conduct a factorial experiment and vary the controlling variables or parameters of interest together.

RSM has been used to optimize processes in manufacturing, engineering structural optimizations, campaign and voting results, Department of Defense budgets and many others (Montgomery 2005). In one study RSM was used to analyze clinical enzyme assays varying three parameters simultaneously (London et al. 1982). The method is well established and has become a basis for design and analysis of experiments.

The fundamental concept is, by educated selection, dependent and independent factors are chosen that are theorized to have the dominant influence on the outcome of the process. A simple two-factor analysis is illustrative of the RSM concept. For a sand filtration system, two factors might be filtration rate and media depth. If these two parameters were set at a range of values that represent the reasonable expectation of the process, then the interaction of these two full ranges would represent all the combination of the two factors at two levels, high and low (Fig. 9).

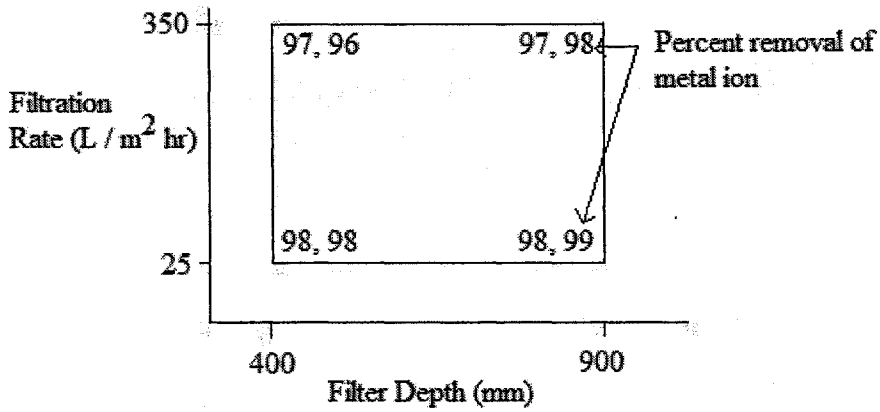

Filter Depth Effect = (97+98+98+99)/4 - (97+96+98+98)/4 = 0.75

Filtration Rate Effect = (97+96+97+98)/4 - (98+98+98+98)/4 = -1.25

Interaction Effect = (97+98+98+98)/4 - (98+99+97+96)/4 = 0.25

Fig. 9. 2^2 Factorial RSM Pb^{2+} Adsorption by Granular Filtration
Adapted from Montgomery (2005)

The results of this illustration in Fig. 9 demonstrates the filtration rate has larger effect on the adsorption of lead (II) ions and the negative sign would suggest an inverse relationship exists, that is a slower filtration rate would enhance metal adsorption. The combination of each factor, that is, the 2^3 and 2^4 factorial designs, will create 8 and 16 runs, respectively. If there were n factors each at two levels there would be 2^n runs necessary. To keep the optimization process simple, with reduced run times, and lower costs, fewer levels and factors are selected.

One way to address this numerical problem is to do what is called a fractional factorial experiment. A subset of the runs are used, but selected to represent the major

points of maximum, minimum and interaction. This process can be as informative about the effects of the factors considered. The objective is always the same, determine which process variable affects the response the most. A logical follow-on to this analysis then is to evaluate variations to optimize the response. Iterative runs of this process will create responses that will plot as contours on traditional charts, and in the previous example contours of percent metal removal efficiencies. The resultant is a surface or to use the terminology of this process, a response surface. To locate the optimum it will be necessary to continue the 2^2 factorial experiment varying filtration rate and filter depth together. Once a region of optimum performance is found a new round of experiments are formulated to attempt to improve the previous operational set points. The end result should enable the development of an empirical model of the process. This process is known as response surface methodology. Response surface methodology (RSM) is then a mathematical representation of the problem and allows statistical analysis of the problem from which an optimum operating location can be determined. If the response can be represented by a linear function of the independent variables then the approximate function can be represented as shown.

$$y = \beta_o + \beta_1 x_1 + \beta_2 x_2 + \cdots + \beta_k x_k + \varepsilon \qquad (12)$$

If there is non-linearity in the process then a polynomial of higher degree must be used. The second order function would be of the following form (Equation 13):

$$y = \beta_o + \sum_{i=1}^{k} \beta_i x_i + \sum_{i=1}^{k} \beta_{ii} x_i^2 + \sum\sum_{i<j} \beta_{ij} x_i x_j + \varepsilon \qquad (13)$$

It is assumed the response in this research will be linear in nature. Linearity was validated by setting the operational column at mid-points of the model and comparing results with predicted values. This method of least squares evaluation estimates the precision of the model. Since the model proved linearity at a 90% confidence level the second order model at Equation 13 was not used.

3. METHODS AND MATERIALS

Screening batch and column experiments using various functionalizations (i.e. thiol, ether, hydroxyl, amine, phosphate) of OSNP materials (Table 11) were conducted, followed by the selection of the OSNP material from this group that most effectively removed lead (II) ions. Using the selected OSNP material, batch reaction experiments with lead (II) ions in DI water were completed, followed by batch reactions with a matrix solution of 13 cations. Column experiments were optimized for media depth, filtration rate and percent mass of OSNP (w/w) material following procedures for Response Surface Methods. Column studies were completed using a 13-cation matrix solution in tap water and with stormwater collected from a Virginia shooting range.

3.1 Synthesis and Characterization of OSNP Materials

Two formulations were used for the OSNP materials. Their specific formulations are described in the following paragraphs after which descriptions of the analytical methods for qualitative characterization are discussed.

3.1.1. HMS Synthesis.

The surfactant template was prepared by first adding 10 mL EtOH, then 87 mL DI H_2O to 1.2424g n-dodecylamine ($C_{12}H_{27}N$, MW 185.36) and stirred. The silicate was prepared by adding 12 ml EtOH to 6.8280 g tetraethylorthosilicate (TEOS, $Si(OC_2H_5)_4$, MW 208.33). Both solutions were stirred to homogeneity and then the silicate added to the surfactant template solution. Molar ratios of the final mixture were 217 mmol C_{12} amine: 6.74 mmol TEOS: 217 mmol EtOH: 4833 mmol H_2O. The solution was stirred overnight at ambient temperature. Afterwards, the material was dried for 4 d then rinsed

with DI H_20 and EtOH through Whatman No. 3 filter paper. Collected materials were air dried for 3 d and bottled.

3.1.2. MCM-41 Synthesis

The surfactant template was prepared by first adding 71 mL DI H_20 to 1.3286 g n-hexa-decyltrimethylammonium bromide (CTABr, $CH_3(CH_2)_{15}N(CH_3)_3Br$, MW 364.46), and then stirred. To this mixture 6.3228 g TEOS was added, stirred into the mixture, and NaOH added drop wise until pH 12. Final mixture molar ratios were 3.636 mmol CTABr: 30.3 mmol TEOS: 15.15 mmol NaOH: 3939 mmol H_20. After approximately 30 min of stirring the solution was added to Parr Instrument Company, Moline, IL stainless steel reactors and set in a pre-heated 110 °C oven for 3 d. After cooling the resultant mixture was filtered through Whatman No. 3 filter paper using DI H_20 and EtOH. Collected materials were then air dried for 3 d and bottled.

3.1.3. Characterization of OSNP Materials

Qualitative analysis for the meso-structural order was determined by X-ray powder diffraction (XRD) patterns on a Rigaku Corporation diffractometer Miniflex, number 2005. The diffractometer was equipped with a rotating anode and Cu-Kα X-radiation source (wavelength λ=0.15418 nm). Scanning speed was one-half degree per minute and 1,000 cps with a goniometer radius = 150 mm. Slit opening angle was 2.5°, divergence slit 1°, scatter slit 1° and receiving slit 0.3 mm. All measurements were started ca. 10 degrees and peaks identified to 0 degrees. Results were compared to nanoporous material species spectra as published in the literature. Identification was based on position of the lines in diffraction pattern and their relative intensities

Table 11. OSNP Batch Reaction Materials
The first 6 OSNP materials were of the general formula $[SiO_2]_{1-x}$ $[SiO_{1.5}((CH_2)_3\ SH)]_x$

Reference	OSNP Material Structure Description
1	Thiol functionalized, wormhole structure, powdered, x = 0.15
2	Thiol functionalized, wormhole structure, powdered, x = 0.30
3	Thiol functionalized, wormhole structure, powdered, x = 0.50
4	Thiol functionalized, foam framework, powdered, x = 0.15
5	Thiol functionalized, foam framework, powdered, x = 0.30
6	Thiol functionalized, wormhole structure, 1-10 μm, x = -0.50
7	Phosphate functionalized
8	40% ether functionalized
9	15% thiol functionalized
10	16% thiol functionalized
11	10% amine functionalized
12	40% amine functionalized
13	17% amine functionalized
14	Hydroxide functionalized
15	Hydroxide functionalized
16	Hydroxide functionalized
17	Amine functionalized
18	Amine functionalized
19	Amine functionalized
20	Amine functionalized
21	Hydroxide functionalized
Control	1000 mg/L $Pb(NO_3)_2$ in DI H_2O

The diffraction angle 2θ generated by the diffractometer was used to determine the spacing between the planes of the molecular structure. Then applying the Bragg equation (Eq.14), the distance between the planes was calculated from the known

$$n\lambda = 2\,d\sin\theta \qquad (14)$$

where n = is an integer; λ = wavelength (Å); d = inter-planar distance (Å); θ = angle of incidence and constructive interference. See Figure 10.

wavelength of the source and the measured angle. The line intensities reflect the number and kind of atomic reflection centers in each set of planes resulting from scattering that

occurs as a consequence of interaction of the radiation with atoms in the molecule. It was expected from the literature MCM-41 would have a very strong peak at the d100 reflection line and three weaker peaks at d110, d200 and d210 (Kresge et al. 1992; Vartuli et al. 2001; Zhou et al. 2001).

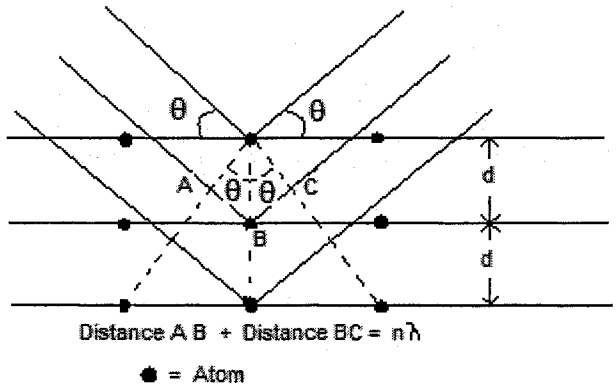

Fig. 10. Bragg's Law Diffraction Nomenclature

Infrared absorption spectrometry reflectance (FTIR – Fourier Transform Infrared) was obtained to evaluate molecular vibrations, either stretching or bending. Typically heavier atoms will vibrate slower than lighter ones, and stronger bonds will vibrate faster than weaker bonds. The character of the metal adsorption bond and other molecular bonds to and within the OSNP materials may be elucidated this way (Skoog et al. 1998).

Transmission Electron microscopy (TEM) was used to identify and to elucidate the morphology of the material. Pore diameters were qualitatively determined by TEM. Quantitative metal concentrations were obtained using a Spectra AA 220 Graphite Furnace Atomic Adsorption (GFAA) spectrometer with a Varian Graphite Tube Analyzer (GTA) 110 located at the Applied Research Center (ARC), Christopher Newport University Laboratory, and the Isotope and Trace Element Research (LITER) inductively

coupled plasma mass spectroscopy (ICP-MS) located at Old Dominion University. The ICP-MS used in this study was a Finnigan ELEMENT 2 double focusing sector field (SF)-ICP-MS (Bremen, Germany). The magnetic and electric sector mass analyzers were in reversed Nier-Johnson geometry. Sample introduction was achieved using a self-aspirated Perfluoroalkyoxy (PFA) microflow nebulizer (50 μL/min). Scanning electron microscopy (SEM) explored morphology and formula weights using a Jeol JSM-820 scanning electron microscope with an accelerating voltage of 4.5 kV to 15.0 kV and magnification from x500 to x3300. Samples were mounted using a doubled sided conductive carbon double-sided sticky tape.

3.2 Screening OSNP Materials by Batch and Straw Columns

The objective of the screening experimentation was to identify best performing candidates adsorbent materials to be used in column and competitive ion studies. Batch reactions were prepared of 21 OSNP materials of various silica-based templates. The first group of silica OSNP materials had wormhole and foam framework structures with the formula $[SiO_2]_{1-x}$ $[SiO_{1.5}((CH_2)_3\ SH)]_x$ with x between 0.05 and 0.50. These were all thiol-functionalized OSNP materials; reference materials 1 – 6 in Table 11. Additional OSNP materials with various functional groups, phosphate, ether, thiol, amine and hydroxide, were also prepared; reference material numbers 7 – 21 in Table 11. Control for the experiment was 1000 mg/L lead (II) standard as $Pb(NO_3)_2$ in DI H_2O.

A flatbed shaker was used to suspend materials throughout the batch mixing phase. All materials were run in triplicate with 5 mg OSNP material in 100 mL of DI H_2O in polypropylene wide-mouth bottles at 23 ± 1 °C. Lead standard was lead nitrate and measured at 1913 ±37 mg/L. Fifty mL of DI H2O was used to pre-wet each sample

for preservative prior to analysis. Equilibrium was verified by allowing samples 7 through 21 to react an additional 6 d. All samples were centrifuged and a second aliquot filtered through a 0.45 micron syringe filter for dissolved analysis. Each sample was preserved with nitric acid and analyzed by ICP-MS. Sources of error include pipettes used in multiple dilutions of the samples, balances, and standard concentrations. The error associated with the dilutions was anticipated to be approximately 2-3% due to the large dilutions (1000-fold dilution or more) needed to bring the sample concentrations within the instrument calibrated linear range. Quality control measurements were completed to include measurements of standards, blanks, and three laboratory controls prepared by adding 50 mL of DI H_2O and 40 mL of the $Pb(NO_3)_2$ solution. The resulting relative percent deviation for the control samples averaged 6.9%. Distribution coefficients (K_D) were computed for each material.

Straw column studies were completed of three OSNP materials to evaluate approximate loading capacities. A standard solution of 5 mg/mL Pb^{2+} as $Pb(NO_3)_2$ from Environmental Express, NC was passed through a EiChrom 2.54 cm diameter column containing 0.100 g of OSNP material. The effluent for each aliquot was collected separately and tested for Pb by means of Plumbtesmo® test paper. The test paper is sensitive to 0.05 μg/L Pb^{2+} and was used to detect column break through as a qualitative determination. Loading capacities were calculated as number of aliquots x 0.200 mL/aliquot x metal concentration (mg/mL) divided by mass (g) of OSNP material used. Results were tabulated as mg adsorbate / g adsorbent. Equivalent molar quantities adsorbed in mmoles/g were also computed.

3.3 Screening OSNP Materials in Column Studies

In this portion of the study a qualitative screen in small diameter straw columns was completed to evaluate approximate break-through, and to estimate loading capacity. The primary objective was to validate the type of OSNP material to use in the full column and sand filtration development.

The first column study used 7 mm inside diameter by 60 mm borosilicate columns with a polyethylene frit in the bottom to support the adsorbent materials. Approximately 0.1 g of OSNP material was placed into the column and 10 drops of isopropyl alcohol and 2 mL of DI H2O added for wetting. A polyethylene frit was added to the top of the media to disperse the liquid and create plug flow. Contaminant solution was 5,000 mg/L as $Pb(NO_3)_2$ and added in 200 μL portions. Qualitative breakthrough was determined using Plumbotesmo® test paper sensitive to 5 μg/L total Pb. Breakthrough fraction was computed as the number of 200 μL aliquots that produced a positive test paper results.

The loading capacity column study were completed of the OSNP materials using 2.54 cm x 150 cm EiChrom borosilicate columns fritted at bottom of adsorbent as support. To each of three columns 5.0 g of OSNP material was added with only light hand tamping. The volume was measured and the pore volume of the material assumed to be ca. 45%. This assumed porosity is what can be expected from non-compacted fine-grained aggregate (Freeze and Cherry, 1979). Influent water was as-provided tap water spiked with 500 mg/L of Pb^{2+} as $Pb(NO_3)_2$. Contaminated water was added in either 50 mL or 100 mL aliquots and allowed to filter by gravity through the OSNP adsorbent media.

Effluent was collected in 160 mL nalgene beakers and tested each morning using semi-quantitative indicator test papers for total Pb. These papers were calibrated on the

standard solutions so that a positive test indicated > 5 μg/L for total Pb. These results provided indications of break-through after which the solutions were decanted into centrifuge tubes and analyzed by ICP-MS. Loading capacity was then estimated by multiplying the number of aliquots x aliquot liter x metal concentration / mass of test material x 100. Result provided the mg/g loading capacity. The equivalent molar capacity in mmol/g was also computed by dividing the mg/g metal loading capacity by the atomic weight of the metal of interest.

3.4 Hydraulic Evaluation

Water headloss through a filter bed was modeled considering particle shape (ϕ = particle shape factor, typically set as 1.0 for spheres, 0.82 for rounded sand, 0.75 for average sand, and 0.73 for crushed coal and angular sand), depth of the filter bed, superficial filtration velocity (m/s), porosity (the ratio of the particles voids to total volume), acceleration due to gravity (9.81 m/s^2), coefficient of drag, and geometric mean diameter between sieve sizes. There have been a number of models developed by Kozeny, Carman, Hazen, Rose, and others. For the initial screening processes the headloss formula developed by Carmen (1937) and Kozeny (1927) was used as shown in Equation 15. The computation for this study was based on the superficial velocity measured in the laboratory for similar 600 mm media depth columns to maintain a constant head.

To evaluate headloss due to the addition of OSNP materials to a sand filter, a simple experimental design consisting of a 5.08 cm diameter polyvinylchloride schedule 40 pipe capped with a Whatman No. 3 paper filter (particle retention 6 μm) and plastic end cap with 14 – 4.8 mm holes was prepared. The drilled holes provided about 50%

porosity in the end cap to minimize headloss and support the paper filter. In the first column commercial sand with d_{10} = 0.21 mm and UC = 2.55 sieve was filled to the 600 mm depth. To this column tap water was added via a Control Company model 3386 mini-variable speed peristaltic pump to maintain a specific head in the column. To a second column of the same size as the first, 7.9 cm of 5% by volume amine functionalized powdered OSNP material and sand were added to the bottom 100 mm. To the remainder of the column sand was added to the 600 mm depth. To this second column tap water was added via Control Company model 3386 peristaltic pump to maintain the same head as in the first column. The implications to hydraulics of the filtration system were evaluated due to the addition of powdered OSNP materials and headloss estimated.

$$h = \frac{k * \mu * (1 - \varepsilon)^2 * A * \upsilon * L}{g * \rho * \varepsilon^3 * V} \tag{15}$$

Where:	Input Values:		
h = head loss in filter depth L (m)	k =	5	
k = dimensionless Kozeny constant, 5 or 6	g =	9.81 m/s^2	
g = acceleration of gravity, 9.81 m/s^2	μ / ρ =	1.13E-06 m^2/s	
μ = absolute viscosity of water, N s/m^2	ε =	0.40	
ρ = density of water, kg/m^3	d =	0.00021 m	
μ / ρ = kinematic viscosity of water; at 15 C	Ψ =	0.85	
ε = porosity, dimensionless	υ =	1.67E-04 m/s =	0.60 m/h
A / V = grain surface area per unit volume of grain	L =	0.6 m	
= specific surface S (or shape factor = 6.0 - 7.7)	h =	0.3664 m =	36.6 cm
= 6/d for spheres; d = mean size of media			
= 6 / (Y * deq) for irregular grains			
Y = grain sphericity or shape factor			
deq = grain diameter of spheres of equal volume			
υ = filtration (superficial) velocity (m/s)			
L = depth of filter, m			

0.5 m Sand only			0.1 m Sand and 5% OSNP		
Input Values:			Input Values:		
k =	5		k =	5	
g =	9.81 m/s^2		g =	9.81 m/s^2	
μ / ρ =	1.13E-06 m^2/s		μ / ρ =	1.13E-06 m^2/s	
ε =	0.40		ε =	0.40	
d =	0.00021 m		d =	0.00010 m	
Ψ =	0.85		Ψ =	0.85	
υ =	1.36E-04 m/s =	0.49 m/h	υ =	1.36E-04 m/s =	0.49 m/h
L =	0.5 m		L =	0.1 m	
h =	0.2491 m =	24.9 cm	h =	0.2197 m =	22.0 cm

Estimated dual media headloss = 46.9 cm

3.5 Leachability of OSNP Materials from Sand Filter

Leaching characteristics of OSNP and sand media were evaluated in 9.525 mm ID vinyl tubing 230 mm long with Whatman No. 3 paper filter end caps. The Whatman filter has a porous membrane with an average particle retention size of 6 μm. To one column

14.07 g of sand and 0.45 g of HMS material were thoroughly mixed and added, and 14.05 g sand and 0.50 g of MCM-41 material were thoroughly mixed and added to a second column. Mass OSNP material to sand ratios were 3.1% and 3.4% for HMS and MCM-41, respectively. Tap water was added at an average of 12 mL/min (SD = 5.6, n = 45) from 9 Dec 06 to 26 Jan 07. Influent and effluent turbidity, pH, temperature and conductivity were measured at irregular intervals throughout the period. Flow rates were measured at each sample collection time. Control samples were prepared using 0.0 to 0.0210 g MCM-41, and 0.0 to 0.0293g HMS in tap water. Control turbidity, pH, and conductivity were measured at various times throughout the 48 d. Analytical equipment included Mettler Toledo Model PR5002, balance d = 0.01 g (Switzerland) and Labpro Data Logger using a TI-86 interface and Vernier software (Beaverton, OR). Turbidity calibration was completed prior to all measurements using 890 nm LED with 0.25 NTU resolution and ± 5% accuracy for readings above 25 NTU. Conductivity and pH were calibrated as needed. Turbidity and conductivity of effluent were compared to influent by single factor analysis of variance.

3.6 Synthetic Stormwater Characteristics

Stormwaters were collected 6 Oct 06 from the Langley AFB small arms firing range and analyzed by ICP-MS following methods explained in section 3.1.3, Characterization of OSNP Materials. The results are summarized in Figure **11**. Based on the concentration of elements from this analysis and from metal leachate studies conducted (see Appendix B) a synthetic formulation was devised as presented in Table 12. A more complete description of the source of the soils, the edaphic characteristics, and mineral content of the shooting range soils is provided in a paper by this author

published in the *Journal of Hazardous Substance Research.* A copy of the article as published is at Appendix B. While each of these metals could be selected as metals of interest for this adsorption study, lead (II) ions were the preferred metal ion because of the elevated dominance in the studies, its known toxicity and for the following additional reasons:

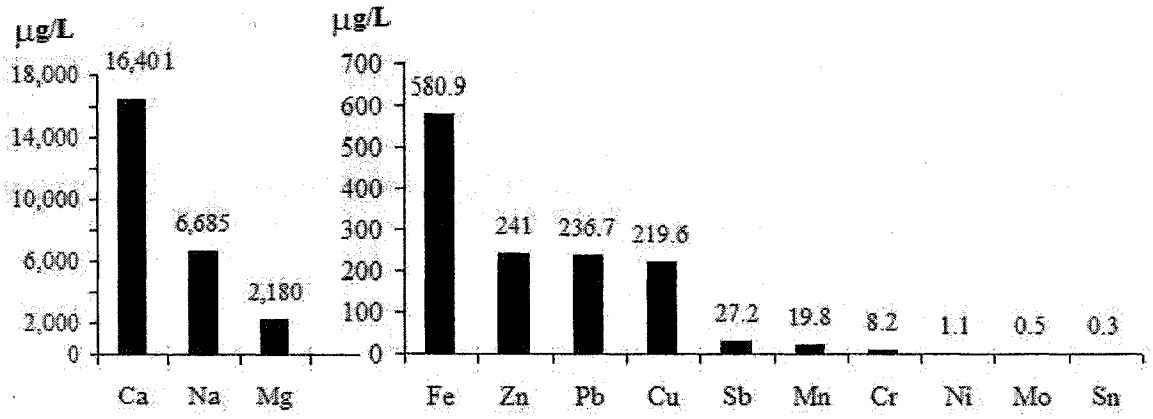

Fig. 11. Metals in Stormwaters Collected from Small Arms Firing Ranges
Time collected: 12:15 pm in light to heavy rain. Ambient T = 17.2 C; Dewpoint = 16.1 C; barometric pressure = 30.06 in (1018.0 mb); wind NE23G33 (mph), visibility 1.63 mi, clouds FEW005, BKN018, OVC039, Collected ca. 19L from Outfall. pH = 7.43. Samples were analyzed in triplicate by ICP-MS with RSD <10%.

- The amine OSNP materials have been shown to be effective adsorbents of the divalent lead ion (Xu et al., 1999). Lead in shooting range stormwaters have been found in waters with pH range of 5.5 to 8.5, and therefore will most likely be in a 2^+ oxidation state in carbonate or sulfate form as shown in 6 (Bradl 2004; Weng 2004) or as free ions or attached to suspended particulates.

- One shooting range in the twelve range study had a National Pollution Discharge Elimination System (NPDES) permit limit = 0.15 mg/L total lead. The point of compliance is at the shooting range stormwater outfall.

- Manganese (Mn) and iron (Fe) are secondary Safe Drinking Water Act (SDWA) constituents of concern for color, taste, and odor purposes. They are not typically regulated in stormwater discharge permits and as such do not pose a regulatory concern. They have toxicity at elevated levels, but are essential nutrients for biological organisms, and are abundant in soils and ground water. Manganese exists naturally in both divalent and quadravalent forms typically as oxides, carbonates, and hydroxides that are only slightly soluble. Iron exists also in two forms, as divalent and trivalent, ferrous and ferric, respectively. It is not uncommon for surface waters to contain iron constituents. Since neither ionic form poses a regulatory or health related concern they are not isolated for this study. However, their ionic lead (II) adsorption interference within the synthetic water matrix will be considered as lead sorbs readily to manganese hydroxides over iron oxides by a factor of 40, potentially restricting the mobilization of lead (Hettiarachchi et al. 2000).

- The inorganics Cu and Zn will be used as competing ions in the synthetic stormwaters prepared. MCM-41 has been shown to be an effective adsorbent of Cu (Algarra et al., 2005). Sb has been found by others in shooting range soils (Johnson et al. 2005) and may also be of interest as a competitive ion.

- Improving the quality of urban stormwaters prior to discharge to receiving waters is desired. The pathway for lead exposure to the general population, to include

children, is by ingestion in drinking waters (Royce et al. 2000). Further, depending on the hardness of water the toxicity of lead in stormwaters can exceed acute aquatic life criteria (Burton and Pitt 2001; Engstrom 2004; Paulson and Amy 1993).

Based on these results and the leachate analysis described previously, 13 cations, namely Ca^{2+}, Cr^{2+}, Cu^{2+}, Fe^{2+}, Mg^{2+}, Mn^{2+}, Mo^{2+}, Na^{+}, Ni^{2+}, Pb^{2+}, Sb^{3+}, Sn^{2+} and Zn^{2+}

Table 12. Cation Analysis of Stormwater and Synthetic Solutions
Stormwater was collected 6 Oct 2006 approximately 6 h after the onset of heavy rain fall at Langley AFB, VA small arms range. 24 h rainfall = 2.03 in. The stormwater concentration data is the tabulated data of Figure 11. Tungsten and Arsenic have been reported at some ranges, but were not present in stormwaters collected at the Langley AFB small arms firing range. Batch solutions were prepared using deionized water. The column adsorbate concentrations are for laboratory tap water, except for the additional spiking of lead (II) ions as $Pb(NO_3)_2$. Batch and column solution were analyzed by ICP-MS with instrument detection limits from 0.1 to 3.6 μg/L.

Element	Stormwater (μg/L)	Batch Adsorbate (μg/L)	Column Adsorbate (μg/L)
Ca	16,401	65,002	31,063
Na	6,685	3,439	23,973
Mg	2,180	576	1,680
Fe	580.9	674	46
Cu	219.6	113	467
Pb	236.7	1,017	1,060[†]
Zn	241	5,342	2,127
Sb	27.2	152	0.7
Mn	19.8	319	9.4
Cr	8.2	72	4.5
Mo	0.5	26	0.2
Ni	1.1	28	4.7
Sn	0.3	479	0.1

[†] Lead (II) ion concentration was spiked to this concentration

ions were selected to constitute the synthetic solutions as shown in Table 12. This phase of this research was to evaluate performance of OSNP material as adsorbents in a controlled matrix high ionic strength solution and with natural stormwaters.

OSNP materials have had limited field application (Algarra et al. 2005) and most synthesized mesoporous sieve research has been used for applications in controlled environments and with limited to no ionic competition (Abdel-Fattah and Bishop 2004; Antochshuk et al. 2003; Huo et al. 1995; Juang et al. 2006; Mercier and Pinnavaia 1998; Xu et al. 1999; Yokoi et al. 2004; Yoshitake et al. 2003). This study proposed to improve the understanding of OSNP materials application in selected constituent synthetic stormwaters. Actual stormwater from a small arms firing range in Virginia were also used.

Urban stormwaters are highly variable and often contain a large range (1 μm to 10,000 μm) of particulates (Sansalone et al. 1998), elevated concentrations of dissolved solids (e.g. ~120 mg/L $CaCl_2$), metals (Cu & Pb ~ 0.08 mg/L, Zn ~ 0.6 mg/L), and nutrients (NO_3^- ~ 2 mg N/L and P ~ 0.6 mg/L) (Davis et al. 2001; Wigington et al. 1986). These amounts are typically uniquely characteristic of each urban environment (Engstrom 2004; Vaze and Chiew 2004).

A summary of pH, TSS and lead (II) and copper (II) in shooting range and urban stormwater conditions are provided in Table 13. The average dissolved lead concentration in eight shooting range stormwaters was 91.5 μg/L (SD=22.3, n=34), which was significantly higher than urban stormwater at 1.2 μg/L (SD=0.4, n=34) ($F = 16.35$, $F_{crit} = 3.99$, $P = 0.0001$, $n = 68$). Also, total and dissolved stormwater lead concentrations at shooting ranges had a larger range and greater maximums than urban stormwaters. These differences in concentrations and conditions would suggest shooting

range stormwaters provide a rich "target" for remediation, immobilization and removal research. Developing control methods will be increasingly important to range managers as lead migration in stormwaters persist effecting receiving streams.

3.7 RSM Optimization Experimental Set-up

Prior to conducting the column studies with matrix solutions a response surface was developed to optimize column performance. A 2^3 factorial experimental design was selected for ease of execution (only 8 runs were required). A fractional experiment of 2^3 requires two levels be established for three parameters. The objective of RSM is to fit a model to the data to create a response surface from which optimum performance can be

Table 13. Stormwater Characteristics

LOCATION[†]	pH	TSS (mg/L)	Total Pb (µg/L)	Dissolved Pb (µg/L)	Dissolved Cu (µg/L)	Reference
Shooting Range Stormwater						
East	NA	NA	600 - 1600	22 -160	17 - 29	(Isaacs, 2007)
East	6.4 – 6.6	NA	840 - 5655	42 - 283	NA	(Stansley et al. 1997)
East	5.2 – 6.5	NA	NA	11.7 – 473	NA	(Craig et al., 1999)
West	NA	NA	5.2 - 26000	4.2 - 450	1.7 - 160	(Isaacs, 2007)
Urban Stormwater						
NURP	NA	101	144	NA	NA	(U.S.EPA 1983)
West	NA	62 - 192	< 100	< 100	< 100	(Characklis and Wiesner 1997)
West	6.3 – 7.8	4 - 236	1.8 - 59	0.28 – 14.2	1.8 – 28.1	(Engstrom 2004)
Langley AFB SAFR Water Quality Parameters						
LOCATION[†]	pH	TSS (SD) (mg/L)	Total Pb (µg/L)	TDS (SD) (mg/L)	Turbidity (NTU)	Date Collected
Outfall	7.16	61([††])	594	151.5 (26.3)	34	17 Apr 06
Outfall	7.19	43(3.2)	1442	66.6 (11.6)	24	22 Apr 06
Impact Berm	7.22	1204([††])	NM	36.0 (6.2)	670	3 Jun 06
Outfall	7.42	52.2([††])	237	114.3([††])	33	6 Oct 06

[†] East and West division was arbitrarily set at the Mississippi River; NURP = National Urban Runoff Program; AFB = Air Force Base; SAFR = Small Arms Firing Range; SD = standard deviation; NM = not measured

[††] Only one measurement taken

selected. Experiments typically vary a factor over its range with other factors held constant. With RSM all variables are varied simultaneously show interaction effects are observed and documented (Montgomery 2005). For a filtration system, effluent quality is an important response variable and was selected as the key response variable for this study. The fractional design of experiment for the study selected the amount of OSNP material used, bed depth and filtration rate as key parameters (Crittenden et al. 2005). These parameters were selected based on their obvious interest (e.g. OSNP material) and impact to effluent quality. Influent quality, TSS, particle size and distribution were all controlled, while porosity, density, type and shape media were held constant. Selected RSM coded factor levels were selected to encompass the expected range of operations of the in-situ filtration system.

Table 14. RSM Coded Factor Levels

Coded Factor	Low (-1)	High (+1)
A. OSNP Material w/w (%)	2.0	10.0
B. Filter Depth (mm)	200	400
C. Filtration Rate (mL/min)	2	20

Eight columns 12.7 mm in diameter were prepared and configured for each possible combination of levels. That is, one column setting was prepared for all parameters set at the low level, a second for all high levels, and so forth. Influent was lead (II) spiked tap water using diluted 1,000 ± 3 μg/mL lead nitrate manufactured by Environmental Express, catalogue number 100028-1 (Mt. Pleasant, SC). Flow rate was

regulated by a Control Company model 3386 variable flow peristaltic mini-pump (Friendswood, TX). Effluents were collected at various intervals from 5 to 3300 min or 2 to 379 bed volumes (BV). Samples were analyzed by graphite furnace atomic absorption (GFAA) spectroscopy, Varian Spectra AA model 220FS (Mulgrave, Australia) with ultra hollow cathode lamps 5-point smoothing, with 3 to 4 replicates in a 9-step ramp process culminating in measurements with ionized sample at 2100 C. Chemical modifier 800 mg/L palladium was used as recommended by the manufacturer. Instrument detection limit was calculated following Kaiser (1970) and Long and Winefordner (1983) as 3 standard deviations from eight background measurements of blank samples. For these and all other experiments in this study the calculated detection limit of total lead by GFAA was ±1 μg/L. Samples were acidified with one to two drops of 70% analytical grade HNO_3 prior to analysis.

3.8 Adsorption Isotherm of Lead (II) Ions by MCM-41 and HMS

Batch reactions were conducted to evaluate isotherms with 22.5 to 27.1 mg OSNP materials in 5 to 80 mL adsorbate (Table 12) with 1,017 μg/L lead (II) ion as $Pb(NO_3)_2$. Bottles were vigorously shaken for 30 s and equilibrated at 48 h at 20 ± 3 °C. Samples were allowed to equilibrate for 24 h, supernatant withdrawn, acidified, filtered through spun glass and analyzed by GFAA as previously described in Section 3.7. Only the top 5 mm of supernatant was withdrawn by pipette for analysis. Langmuir and Freundlich isotherm coefficients and adsorption capacities were determined. Comparisons were made to literature values.

3.9 Influence of pH on Batch Reaction Adsorption

The effects of pH were examined using 25 mg of OSNP material added to 25 mL of adsorbate (Table 12) with 1,017 μg/L lead (II) ion as $Pb(NO_3)_2$. Hydrogen ion concentrations were prepared by adding analytical grade NaOH and HNO_3 drop wise to DI water to prepare solutions at pH of 2, 4, 5, 8, 10 and 12. Once OSNP materials were added they were vigorously shaken for 30 s and equilibrated for 48 h at 20 ± 3 °C. The supernatant was collected, acidified with nitric acid, then filtered through spun glass and analyzed by GFAA as previously described in Section 3.7. Similar procedures were followed for batch matrix solutions (See Table 15 in the next section) using 25 mg OSNP material in 25 mL of adsorbate solution. Solution pH varied from 2 to 11.

3.10 Adsorption Interference by Competitive Ions

The effects of competitive ions were examined in step-wise fashion grouped as shown in Table 15. The concentration of each cation was as described previously in Table 12. All metals were from nitrate salts by Environmental Express (Mt Pleasant, SC) at 1,000 ± 3 μg/mL in 1 to 5% HNO_3. Antimony solution also contained 0.1% HF. Serial dilutions were prepared at target solution concentrations and analyzed

Table 15. Matrix Solution Constituents
Concentration of each metal is shown as batch synthetic values in Table 12.

Matrix	Elements
1	Pb, Mo, Ni, and Sn
2	Matrix 1 plus Sb, Mn, Cr
3	Matrix 2 plus Cu, Zn
4	Matrix 3 plus Fe
5	Matrix 4 plus Mg
6	Matrix 5 plus Na
7	Matrix 6 plus Ca

by GFAA as described in Section 3.7. Approximately 25 mg of MCM-41 and HMS were added to 25 mL of each matrix solution and vigorously shaken for 30 s. Samples were equilibrated for 48 h at 20 ± 3 °C. The supernatant was collected, acidified with nitric acid, then filtered through spun glass and analyzed by GFAA as previously described in Section 3.7. Distribution coefficients were calculated for comparative purposes.

3.11 Column Study

Column experimental set-up was as prescribed by the response surface optimization which was 216 mm media depth, 11 mL/min flow rate and OSNP 3 percent w/w sand mixture. Flow was adjusted initially to the RSM optimized rate and with time (ca. 20 hours) reduced to gravity flow rate. Gravity flow operations were conducted to simulate actual operating conditions that were expected for the field filtration unit. Influent lead (II) ion concentrations varied from 500 to 1,000 μg/L. Matrix solutions contained nitrate salts of 13 cations as described in Table 12. Bed volume (BV) was 27.4 mL for all columns evaluated. The column operated in a down-flow mode. Flow rate was monitored throughout the sample period and adjusted periodically as needed, except for gravity flow processes. Flow rate was not continuous and stopped for 7 d to simulate anticipated start – stop field conditions for an in-situ sand filtration system. All sorption experiments were carried out at a room temperature of 20 ± 3 C with an influent pH = 6.87 (n = 18, SD = 0.36). Influent and effluent samples were collected at irregular intervals from initial to ca. 1,400 BVs, then analyzed for pH, turbidity, conductivity, temperature and lead (II) ion concentration using methods previously described. The amount of lead (II) ion adsorption was calculated using Equation 15.

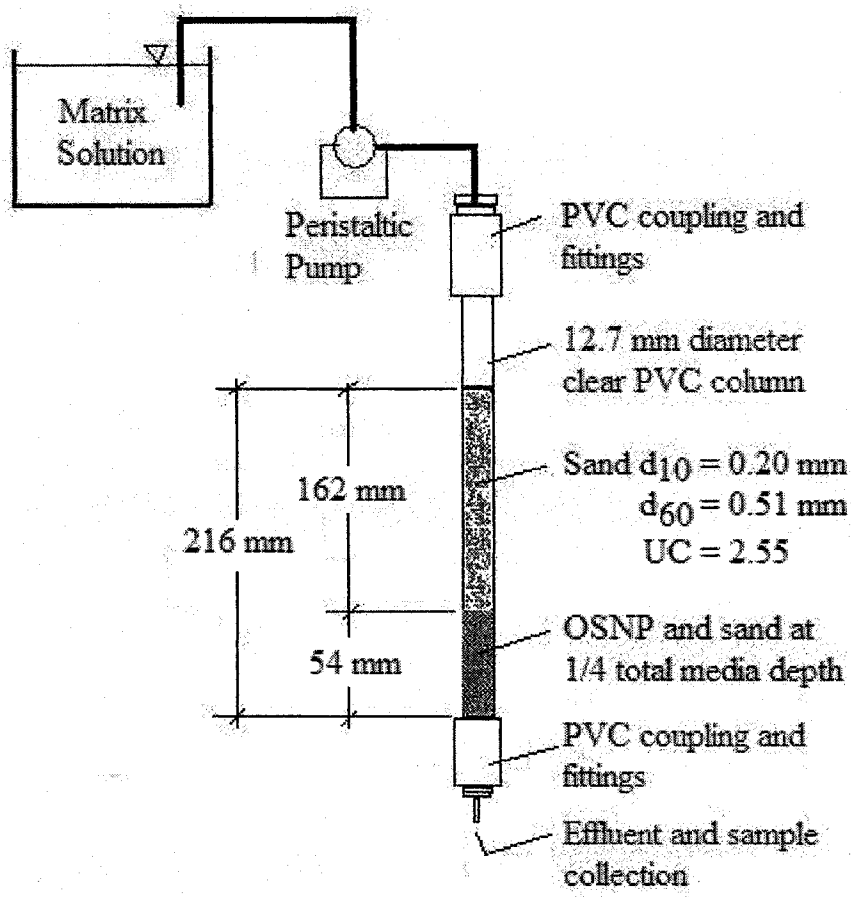

Fig. 12. Column Study Experimental Set-up
Optimized column configuration was based on Response Surface Method media depth, filtration rate and percent w/w OSNP and sand. UC = uniformity coefficient.

$$qe\ (mg/g) = (Co - Ce) * V / W \quad (16)$$

where:
qe = Amount of equilibrium adsorption of metal
Co = Influent concentration
Ce = Effluent concentration
W = Dry mass of adsorbent

The percent of metal removed is calculated by the ratio of the difference in metal concentration before and after adsorption (Co – Ce) and the initial concentration of lead (II) ions in the aqueous solution (Co).

$$\text{Percent Removed} = (Co - Ce) * 100 / Co \quad (17)$$

Specific break-through concentrations were identified for each column. Break-through BVs were determined when the effluent reached 50% of the feed concentration. Breakthrough curves were plotted and break through capacities estimated following the method developed by Treybal (1980).

To evaluate recycle efficiency an optimized column of 0.38 g of MCM-41 mixed with 15.02 g sand (same sand used through-out this study) was placed in a 12.7 mm ID PVC column from 0 to 54 mm, and then from 54 to 216 mm 44.10 g of sand was placed. Feed stock was the discharge from a previous column of the same design parameters. Columns were operated only to 50 bed volumes to expedite the evaluation.

3.12 Sand Filtration Concept Design

Stormwater declining rate sand filtration sizing and design followed procedures developed by Urbonas (2002) in policy guidance developed for the urban drainage and flood control district of Denver, Colorado. The design procedure began by determining the average event mean concentration of TSS using published USGS datasets, followed by calculating the average annual TSS load in stormwater runoff, and next determining the required drain time to determine filter size. The estimates for the reduction in TSS were from literature and removal filtration rates were based on results of data in this

study. The design concepts were developed based on work published by Logsdon et al. (2002), Urbonas (2003), El-Taweel and Ali (2000), and Sansalone (1999).

Biological action is important in the proper function of the design of slow sand filtration (Logsdon et al. 2002). Therefore, no chemical pretreatment was suggested in the concept design. Sand effective size (d_{10}) for this experiment was 0.20 mm and uniformity coefficient 2.55, which met accepted design practices for sand filtration (Visscher 1990). Filtration rate was determined at a minimum necessary to evacuate a 25-year storm within 12 hr.

4. RESULTS AND DISCUSSION

4.1 OSNP Material Characterization

X-ray diffraction patterns for MCM-41 had one strong well resolved peak at approximately 2 degree 2θ, two moderate peaks at 4.5 and 5.3 degrees 2 θ, and two very shallow resolved reflections between 6 and 8 degrees 2θ (Figure 13). Typically only the

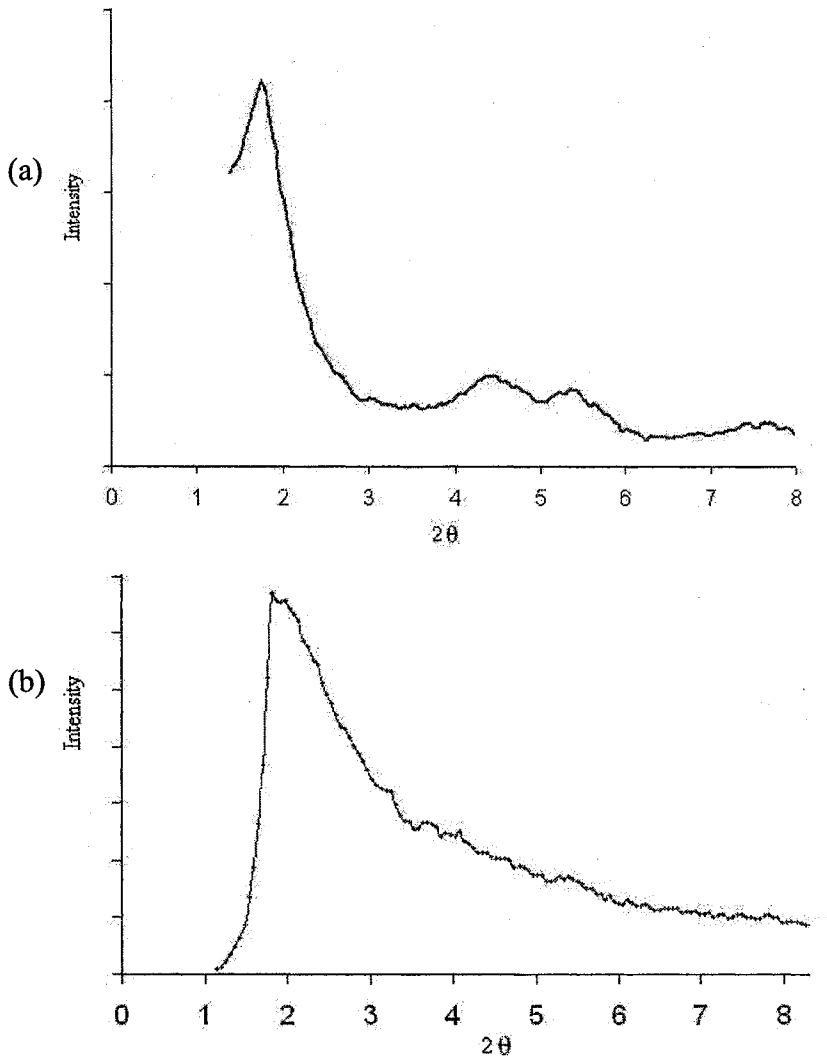

Fig. 13. XRD Diffraction Patterns
As-synthesized (a) MCM-41 and (b) HMS diffraction patterns were similar to literature values, with a sharp d_{100} reflection at ca. 2°.

ca. 2° 2θ can be observed in most cases and the others are virtually absent (Zhao et al. 1996). XRD patterns of all as synthesized forms of mesoporous molecular sieves show five reflections at very low angles and as expected, slightly shifted left of calcined materials (Fenelonov et al. 1999).

The HMS molecular form has one intensive reflection at 2° 2θ that closely resembled literature XRD patterns (Zhang et al. 1997). Both OSNP material diffraction patterns showed lower ordered reflections and agreed with as synthesized reports by Zhao et al. (1998), Jaroniec et al. (2001), and Yokoi et al. (2004). Using Bragge (Equation 14) for the sharp d_{100} reflection for both OSNP materials a pore spacing of ca. 43 Å can be calculated (Figure 14). This is typical spacing compared to literature values.

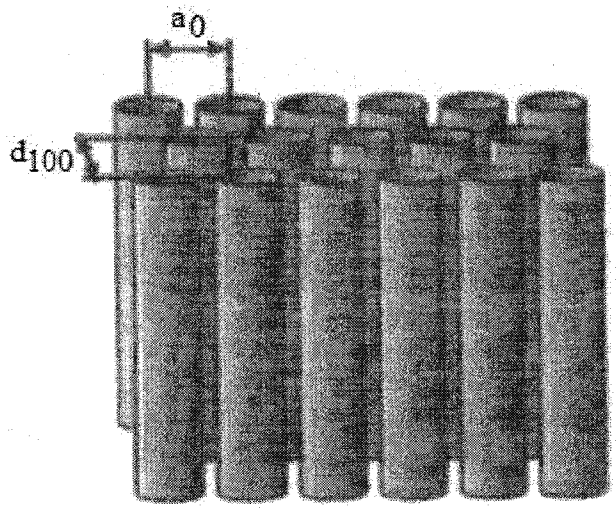

Fig. 14. Schematic Representation of OSNP Material Structure
Internal structure of OSNP materials consist of ordered arrays of cylindrical mesopores. The d_{100} pore spacing ca. 38 Å and a_0 hexagonal unit cell spacing ca. 43 Å for a reflection at 2° 2θ. Cartoon from Fenelonov et al. (1999).

As synthesized materials retain the surfactant organic chain, which have been shown to be strong micelle expanders (Sayari and Yang 1999). Fenelonov et al. (1999) estimated

Si OSNP materials prepared by methods published by Beck et al. (1992) and, Feuston and Higgins (1994) had a pore wall thickness (PWT) from 5.5 to 8.4 Å. Using a nominal value for PWT = 7.0 Å, the pore size (PS) for the OSNP materials of this study may be estimated by PS = a_0 – PWT = 43 – 7.0 = 36 Å. The XRD patterns for MCM-41 d_{100} reflection, with additional 110, 200 and 210 reflections, indicate a long-range ordered hexagonal framework.

Transmission electron microscopy (TEM) of both materials are depicted in Figure 15. HMS structure is hexagonal with "worm" irregular pore openings and MCM-41 shows hexagonal arrays of uniform honeycomb openings. The micrographs

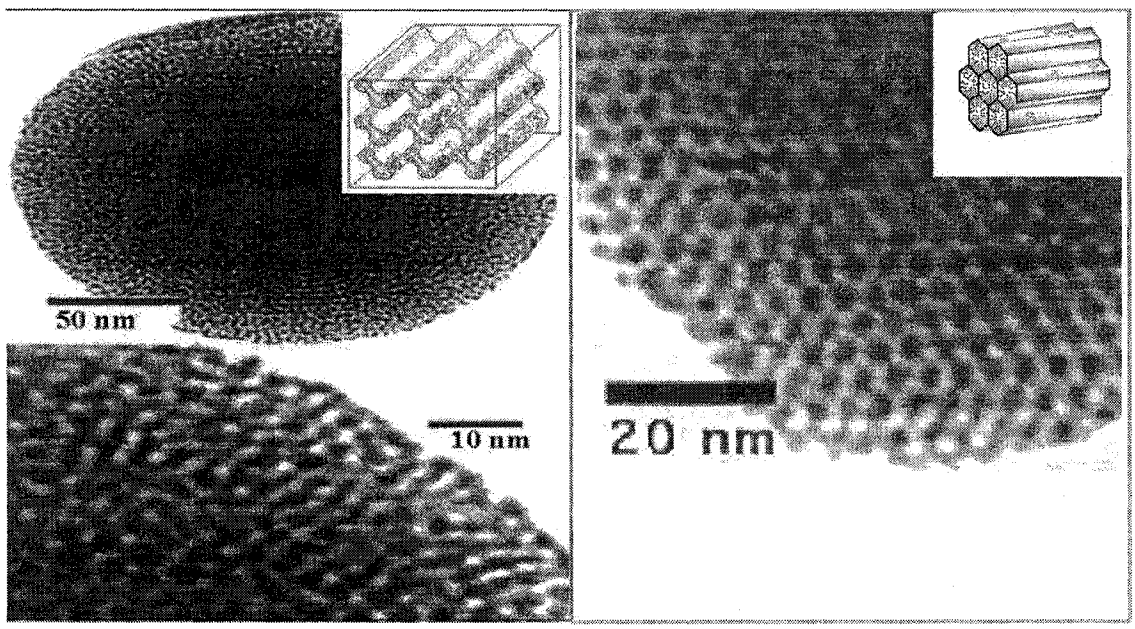

Fig. 15. Transmission Electron Micrographs
(a) HMS and (b) MCM-41 with estimated pore openings of 39 Å and 36 Å, respectively. MCM-41 TEM was similar to Jaroniec et al. (2001).

clearly show a 35 to 39 Å pore opening. The morphology of HMS depicts a repeating worm hole and MCM-41 a honeycomb hexagonal porous structure as reported in the

literature (Mokaya et al. 2000; Muroyama et al. 2006; Pauwels et al. 2001; Yokoi et al. 2004).

SEM morphology reflected a crystalline structure with expected formula weights. For example, MCM-41 was for C – 23%, O – 15%, N – 19% and Si – 43%. Magnification at x2700 provided some observable morphological characteristics although the focus could not be optimized (Figure 16). These morphological characteristics were similar to SEM results reported by Huang (2000) and Mokaya et al. (2000), who reported sub-micrometer sized free standing agglomerates of curved hexagonal rods with dimensions 5 to 15 μm.

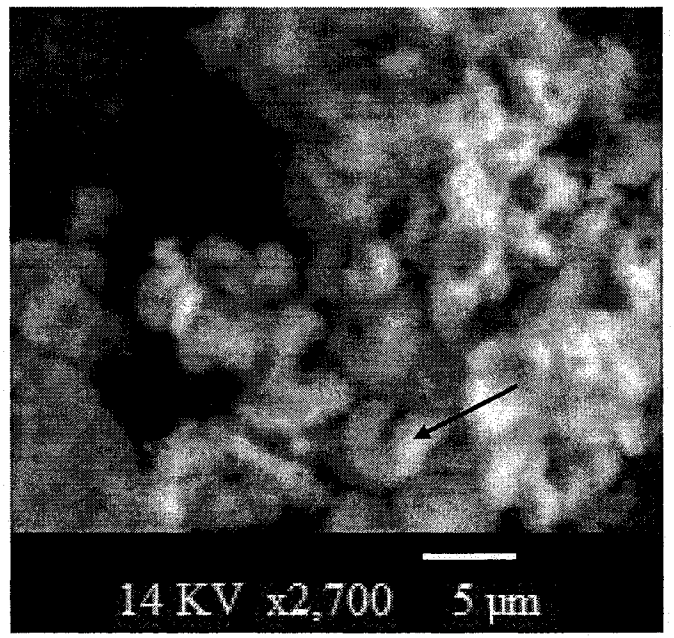

Fig. 16. SEM Micrographs MCM-41
The arrow points to a curved hexagonal rod approximately 7 μm in length.

Fourier transform infrared spectroscopy (FTIR) was used to evaluate vibration frequency shifts in the functional moieties. Fundamental frequency peaks for OSNP materials before and after exposure to lead (II) ions are illustrated in Table 16. Peaks had

minor shifts in wave numbers after lead sorption. Most likely this phenomenon was due to the interaction between lead ions and other functional groups. However, these band shifts may reflect the effect of the heavier lead ions on vibration frequencies, and the fact stronger bonds usually vibrate faster than weaker bonds (Skoog et al, 1998). The adsorbed lead ions interacted more strongly within HMS than MCM-41. This could imply lead ions in HMS are more closely associated with the external OSNP material structure than MCM-41, and may explain a reduced performance at high ionic strength.

Table 16. FTIR Frequency of HMS and MCM-41 OSNP Materials
Frequency units = cm^{-1}; s = strong peak, m = moderate peak, and w = weak peak.

Functional Moiety	Vibration Characteristic	HMS	HMS w/ Pb^{2+}	MCM-41	MCM-41 w/ Pb^{2+}
CH_2	Asymmetric stretch	2912 s	2897 s	2911 s	2906 s
CH_2	Symmetric stretch	2843 m	2833 m	2840 m	2838 m
C—N C—CH_2	Scissor bending	1457 m	1441 m	1458 m	1468 m
C—N	Stretch	1221 s	1206 s	1194 s	1199 s
Si–O—Si	Asymmetric stretch	1049 s	1048 s	1025 s	1023 s
CH_2	Rocking	773 w	766 w	764 w	758 w

4.2 OSNP Material Selection

Batch reactions of 21 OSNP materials of various silica-based templates were screened to select the most effective lead (II) ion adsorbent to use in the column studies. The phosphorus and amine functionalized OSNP materials were the best adsorbents in batch reactions (Figure 17). Thiol functionalization has been found effective mercury (II) ion selective adsorbents, but not for lead (II) ions (Brown et al. 1999). Mercier and

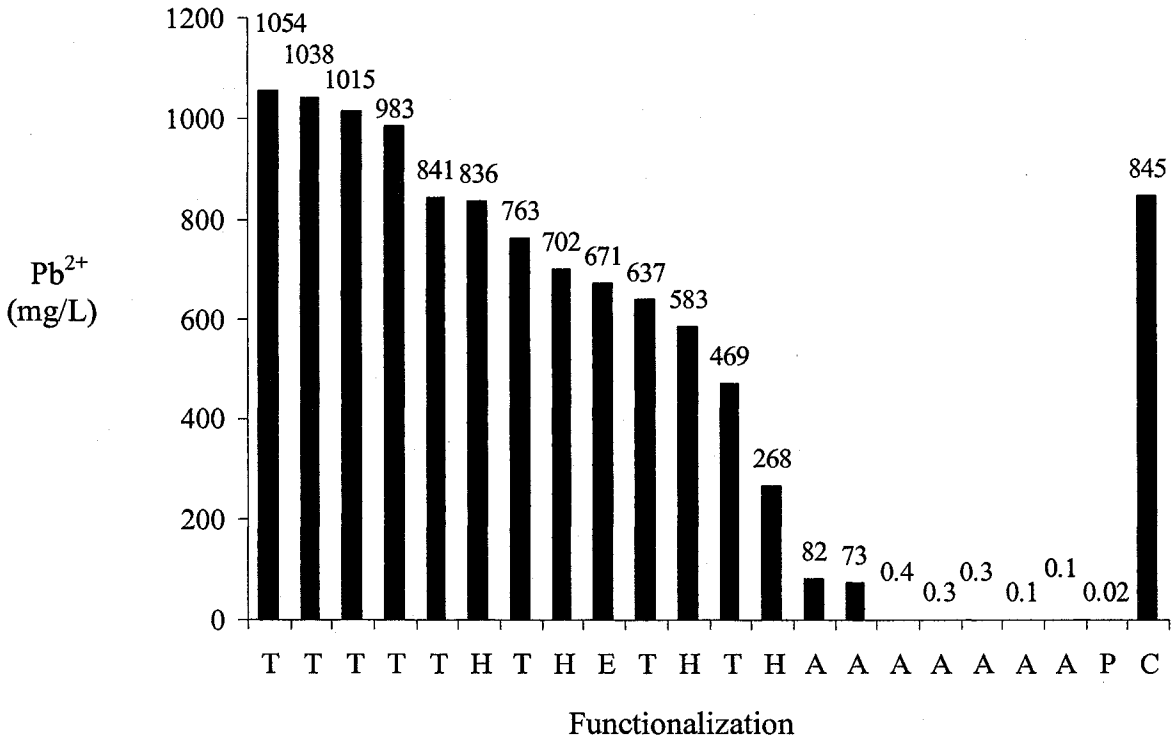

Fig. 17. OSNP Adsorption by Functionalization
Functionalization is T = thiol; H = R-OH; E = R-O-R; A = R-NH_2 and P = phosphorus. C was control using $Pb(NO_3)_2$.as lead (II) ion adsorbate.

Pinnavaia (1998) found hydroxyl sites could be congested increasing steric hindrance, and reducing pore diameter and volumes that resulted in poor heavy metal sorbance. The ether functionalization has also been reported as not effective for lead (II) adsorption (Zhang et al. 2003). Phosphorus functionalized OSNP lead (II) adsorption was excellent, however because of potential release of this nutrient to discharge streams adverse impacts to water quality could develop. Therefore, phosphorus functionalization was not selected for further study. Additionally, the 40% amine functionalization performed nearly as well as the phosphorus moiety. The amine functionalized material removed above 90% of lead (II) ion and in 5 of 7 amine formulations > 99% lead (II) ion was removed.

The distribution coefficient (K_D) was used as a comparative tool to evaluate sorption of materials following the method by Stumm (1992). Table 17 depicts the 24 h and 7 d K_D of the five amine-functionalized materials. The distribution coefficient ratio K_D = Cs / Cw (L/g); where Cs = concentration of the adsorbate adsorbed per unit mass of solid (mg/g) and Cw is the concentration of the adsorbate remaining in solution at equilibrium (mg/mL). The distribution coefficient is only valid for the particular

Table 17. Distribution Coefficients for Amine Functionalized Materials
Reference number is same as Table 11. 5 g OSNP materials were added to 50 mL of adsorbate at $[Pb^{2+}]$ = 1,000 mg/L resulting in concentrations shown at 24 h and 7 d. 24 h average K_D = 51.5 L/g (SD = 26.3) and 7 d average K_D = 73.7 L/g (SD = 40.5)

Sample ID (Reference no.)	$[Pb^{2+}]$ (µg/L) (24 h)	$[Pb^{2+}]$ (µg/L) (7 d)	K_D (L/g) (24 h)	K_D (L/g) (7 d)
A (19)	255	79	39.2	126.6
B (20)	125	109	80.0	91.7
C (17)	126	119	79.4	84.0
D (12)	284	260	35.2	38.4
E (18)	417	358	24.0	28.0

reaction computed and only for that temperature and conditions. In simple terms the distribution coefficient calculated herein is the ratio of the sorbed species to the dissolved species and is most valuable for comparison within this study, but these results may not be of value to compare with other studies with different parameters. While this computation does not respond directly to variations in pH, ionic strength or temperature, it does provide an indirect qualitative measurement of the effects of these parameters.

The distribution coefficient calculation for the material reference item 20 at 24 h was as follows:

$$Cs = \{ [(1{,}000 - 0.125)\ mg\ /\ L] \}^{*}\ 0.05\ L / 5\ g = 10\ mg / g$$

$$Cw = 0.125\ mg/L\ ^{*}\ L / 1000\ mL = 0.000125\ mg/mL$$

$$K_D = Cs / Cw = 10\ mg/g\ / 0.000125\ mg/mL = 79{,}990\ mL / g = 80.0\ L/g$$

Table 17 values appear typical and similar to values reported by Toshiyuki et al. (2003) who computed K_D valued for amine functionalized MCM-41 adsorption of iron and copper. Based on these data, amine functionalized material 19 was selected to use in the column loading capacity study and to evaluate for application in the proposed in-situ sand filtration unit.

4.3 Screening Breakthrough and Loading Capacity

Only the amine functionalized materials (reference material 19 and 20, (Table 17) were used for the column break-through and loading capacity evaluations. For this study break-through was defined as Ce / Co = 0.5, where Co is the influent concentration and Ce is the effluent or equilibrium concentration. Once break-through occurred then the adsorption or loading capacity of the material was estimated at that bed volume.

The process used a standard solution of 5 mg Pb/mL in 0.200 mL aliquots with 0.100 g adsorbent. Plumbtesmo® test paper was used to ascertain breakthrough at 50 mg Pb/L. Material reference number 19 lead (II) ion capacity = 39 mg/g (0.19 mmol Pb /g) and material number 20 = 10 mg/g (0.05 mmol Pb/g). These adsorption amounts are comparable to values reported by Xu et al. (1999) and Wright (2006) (See Table 5). The screening procedure adequately justified the use of as synthesized amine-functionalized material for study in the column applications.

4.4 Headloss

The headloss in the 216 mm media depth column, at a superficial velocity = 0.49 m/h, using sand only, was 36.6 cm, but with sand and OSNP material in the bottom third of the column, headloss was 46.9 cm. This 28.1% increase, while significant, occurred at superficial velocity that is greater than the shooting range application 0.21 m/h minimum needed to evacuate a 25-year stormwater volume within 12 h.

Decreasing flow rate occurred over time for all columns as a result of increased silica packing and reduced particle pore space. Gravity flow rate for the MCM-41 and sand column changed from an initial 31.0 mL/min to 1.75 mL/min in 22.1 h. The d_{10} = 0.20, d_{50} = 0.46, d_{60} = 0.51 mm and UC = 2.55 sand used in this experiment was within recommended slow sand filtration size (Crittenden et al. 2005). Pelletizing the OSNP materials would improve hydraulics, however the OSNP in this experiment represented less than 3% of media adsorbent by mass.

4.5 Leachability of OSNP Materials in Sand Filtration

There was no difference in the tap water influent and effluent turbidity of HMS ($F = 0.07$, $P = 0.79$, $n = 24$) and MCM-41 ($F = 0.14$, $P = 0.71$, $n = 24$) materials during a 48

d leachate evaluation period. The turbidity results were not statistically significant for either material because of excessive variation within groups. This may have occurred from fluctuations due to measurements at instrument detection limit.

There was a statistically significant difference in the conductivity of tap water influent compared with HMS effluent ($F = 9.85$, $P = 0.005$, $n = 24$). There was no difference in the MCM-41 effluent conductivity compared with the influent tap water used, but this result was not statistically significant indicating the result may have simply occurred by chance ($F = 1.84$, $P = 0.19$, $n = 24$). Figure 18 demonstrates graphically the difference and similarity of conductivity results for HMS and MCM-41, respectively.

Pinnavaia (2006) reported to this author the amine moiety leached in controlled experiments when operated at ca. 45 psi. Although a very low pressure (< 5 psi) was applied in this study, much less than 45 psi (flow rates were from 1 to 29 mL/min), additional research is needed to validate the leaching characteristics. Since HMS did demonstrate some leaching characteristics, development of a polymeric binder may be appropriate to agglomerate the materials into porous particles that would have less leaching tendencies. Pelletization by Hartmann and Bischof (1999) was accomplished by pressing OSNP materials in a steel die of 40 mm diameter, using a hand operated press for 30 min. Pressures from 20 to 600 N/mm were applied to create disk that were crushed and sieved to pellets of 0.2 to 0.3 mm.

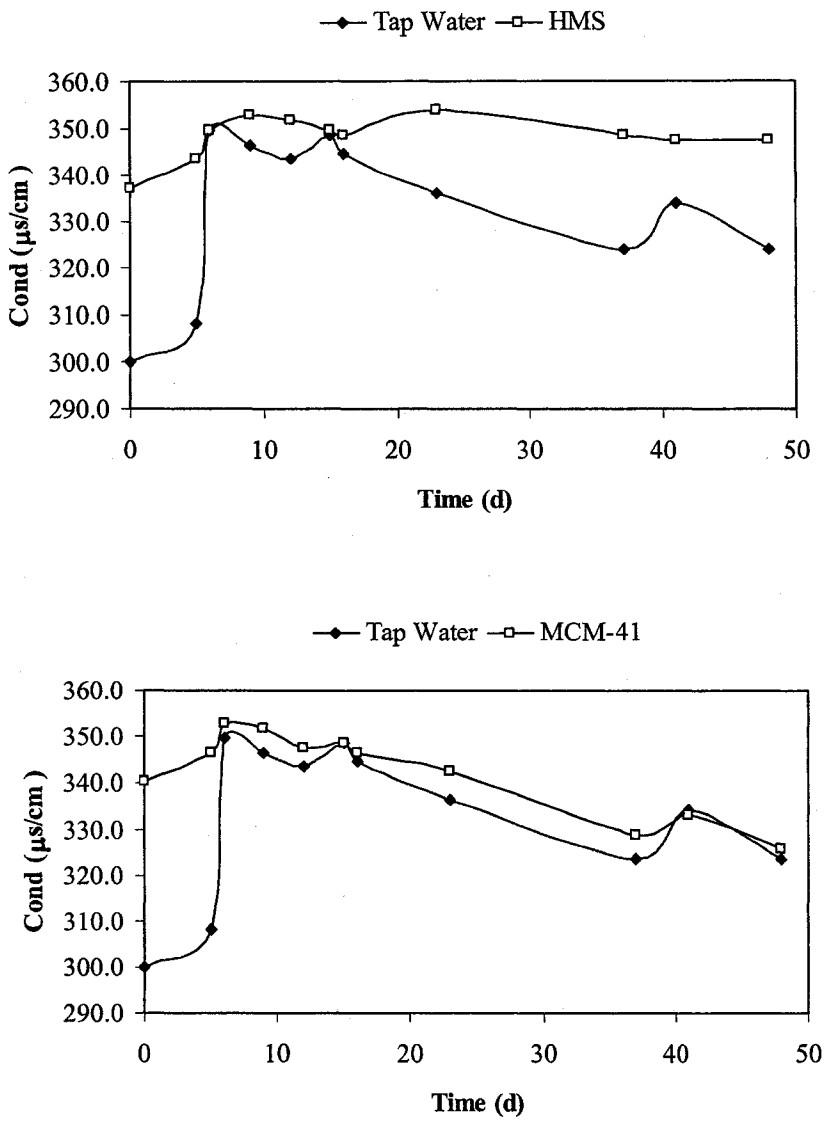

Fig. 18. Effluent Conductivity Values Versus Influent Tap Water

4.6 Column Optimization By Response Surface Methods

Before column studies were conducted operating conditions were optimized. This approach ensures enhanced sorption performance while conducting the experiment. Results of RSM analysis 2^3 fractional factorial runs are depicted in Table 18. The coded

factors are the minimum and maximum range operating conditions of the experiments and quantities explained in the Methods section (Table 14). The method published by Montgomery (2005) was used to calculate the main and interaction effects. Computation details follow with an explanation of the development of the optimization column parameters.

Table 18. Design Matrix in Geometric Notation

Sixteen columns were prepared to provide a replicate for each run. Factor A = OSNP Material Amount: 2 – 10 % (w/w); Factor B = Media Bed Depth : 200 - 400 mm, and Factor C = Filtration Rate: 2 - 20 mL/min. Replicate 1 sample was collected at BV = 2 to 24 and replicate 2 was collected at BV = 8 to 61.

Run	Code Factor A	Code Factor B	Code Factor C	Replicate 1 ($[Pb^{2+}]$ (μg/L)	Replicate 2 ($[Pb^{2+}]$ (μg/L)
1	-1	-1	-1	26.08	51.80
2	+1	-1	-1	22.06	28.98
3	-1	+1	-1	84.91	65.01
4	+1	+1	-1	24.66	33.60
5	-1	-1	+1	82.38	43.94
6	+1	-1	+1	70.31	163.95
7	-1	+1	+1	77.92	88.44
8	+1	+1	+1	88.15	83.44

By convention the labels, main effects, two-factor and three-factor interactions are evaluated to ascertain the parameter that has the most influence on performance. From Table 18, replicate 1 and 2 are summed to provide totals to examine the treatment combinations. For model run 1 the replicate total = 26.08 + 51.80 = 77.88 μg/L. Table 19 reflects the results with labels and Figure 19 the labeling convention in 3-dimensional geometric cube format. Totals were computed for each condition, a sum of the averages or grand average calculated, and reference numbers assigned using common terminology

Table 19. Adsorption Treatment Combinations and RSM Labels

Run	Replicate Total (μg/L)	Labels
1	77.88	(1)
2	51.04	a
3	149.92	b
4	58.26	ab
5	126.32	c
6	234.26	ac
7	166.36	bc
8	171.59	abc

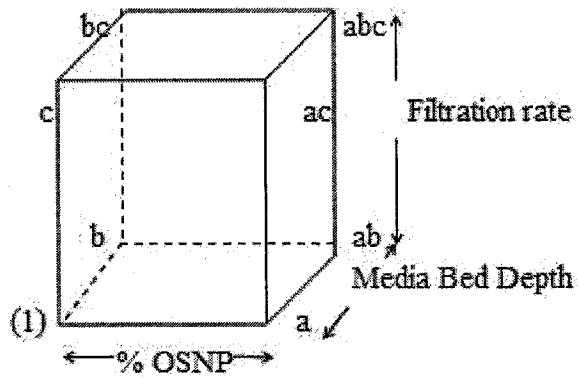

Fig. 19. 2^3 Factorial Design Labels

and assignment conventions for design of experiment RSM. Next, the factor affects were estimated, the sum of the squares computed, total sum of the squares, and the percentage contribution of each model term to the total sum of the squares. Finally the regression model was estimated following the generalized formula:

$$y = \beta_0 + \beta_i x_i + \beta_j x_j + \beta_{ij} x_i x_j \quad (18)$$

Where β_0 = Regression coefficient for grand average / number of replicates
β_i = Regression coefficient for parameter causing maximum factor affect / 2 (2 is for 2 levels)
β_j = Regression coefficient for parameter causing second largest factor affect / 2
β_{ij} = Regression coefficient for interaction parameter causing the largest factor affect / 2
x_i = Coded variable for parameter with maximum affect
x_j = Coded variable for parameter with second largest maximum affect
y = Model output; for this study; concentration of total lead (II) ions

This model includes only the first three factors causing the maximum affect and assumes the first two are primary factors and the third is an interaction parameter. The model was

expanded to other factor interactions to represent the significant contributions of all main and interaction effects as necessary.

The sum of the squares is computed for each parameter and parameter interaction to enable evaluation of the deterministic variables. This was done by taking the square of the contrast between the high and low levels divided by four times the number of replicates. The contrast is computed for each parameter and each parameters interaction with each other parameter. For example, to compute the factor effects and influence of parameter A the high and low values are contrasted and divided by 8 (4 items x 2 replicates) as follows: $A = (1 / 4*n)* [(a + ac + abc + ab) – (c + bc + (1) + b)] = (1 / 8)* [(a + ac + abc + ab) – (c + bc + (1) + b)]$. The effects of other parameters were estimated similarly followed by computation of the sums of squares. The results are shown below.

Table 20. Factor Effect Summary
Summary of the effects of A – Percent OSNP, B – media depth, and C – filtration rate on lead (II) ion adsorption performance.

Factor	Effect Estimate	Sum of Squares	Percent Contribution
A	39.14	3678.60	7.78
B	-26.79	1722.43	3.64
C	68.06	11120.43	23.52
AB	-57.70	7992.44	16.91
AC	58.26	8150.05	17.24
BC	-44.94	4848.19	10.26
ABC	-40.72	3981.02	8.42
Error		5782.14	12.23

The total sum of the squares is: $SS_T = \sum y_{ij}^2 – [(\sum y_{ij})^2 / 8n]$; $i = 1 – 8$; $j = 1 – 2$ resulting in $SS_T = 47275.30$; and the error sum is computed as: $SS_E = SS_T - SS_A - SS_B - SS_C - SS_{AB} - SS_{AC} - SS_{BC} - SS_{ABC}$. Substituting values: $SS_E = 47275.30 – 3678.60 –$

1722.43 – 11120.43 – 7992.44 – 8150.05 – 4848.19 – 3981.02 = 5782.14. The summarized results are provided in the following table with estimated P-values.

Table 21. Analysis of Variance Summary for Dual-Media Filter
The model explained 87.8% of the variation in the results with a 91% confidence this result did not occur by chance. The filter bed depth was not statistically significant, however this parameter had the least affect on the model.

Item	Sum of Squares	DF	Mean Square	F_0	~P-value
Model	14213.85	7	2030.55	2.81	0.0856
A Percent OSNP	3678.60	1	3678.60	5.09	0.0541
B Filter Bed Depth	1722.43	1	1722.43	2.38	0.1612
C Filtration Rate	11120.43	1	11120.43	15.39	0.0044
AB interaction	7992.44	1	7992.44	11.06	0.0105
AC interaction	8150.05	1	8150.05	11.28	0.0100
BC interaction	4848.19	1	4848.19	6.71	0.0321
ABC interaction	3981.02	1	3981.02	5.51	0.0469
Error	5782.14	8	722.77		
Total	47275.30	15			

The ANOVA suggests C – filtration rate, was the dominant process explaining 23.52% (100* 11120.43 / 47275.30) of the variation, followed by the interaction between AC (percent OSNP and filtration rate) and then the interaction between AB – percent OSNP and filter depth. Therefore, using the factor effect values from Table 20 the regression model and response surface can be represented by Equation 18.

The regression coefficients were adjusted by one-half since the regression coefficient measures the effect of a unit change in x on the mean of y and the effect estimate is based on a two-unit change (from – 1 to +1). In the equation, x_1 represents the variable for parameter A or percent OSNP, x_2 represents the parameter B or media depth, x_3 represents the variable for parameter C or filtration rate, and variable x_1x_3 represents the parameter interaction AC or percent OSNP and filtration rate. Taking into

consideration filtration rate (C), and the interaction between AC, AB, and BC from 20, the regression model (Equation 18) takes the following form.

$$y = \text{Grand Average} + (A/2)*x_1 + (A*C/2)*x_1 x_3 + (A*B/2)*x_1x_2 + (B*C/2)*x_2x_3 \qquad (19)$$

The ANOVA yielded coefficients for coded variables for A = -0.3325, B = 3.5393 and C = 22.5894. These values represent the direction of steepest descent in terms of coded variables or more precisely the direction of the vector:

$$\partial Y / \partial A\,, \quad \partial Y / \partial B\,, \quad \partial Y / \partial C$$

The increment for each coded variable was then calculated by the proportional partial differentials:

$$\Delta A = \Delta C * (\partial Y / \partial A) / (\partial Y / \partial C) \qquad \Delta B = \Delta C * (\partial Y / \partial B) / (\partial Y / \partial C) \qquad (20)$$

The increment for each coded variable was calculated as: $\Delta A = +1 * -0.333 / 22.589 = -0.0147$ and $\Delta B = +1 * 3.539 / 22.589 = 0.1568$. The coded variables were then translated into actual values for each parameter as follows:

Percent OSNP = [(max – min) / 2] * ΔA = [(10 - 3)/2]*-0.01472 = -0.05 %;

Media Bed Depth = [(max – min) / 2] * ΔB = [(400-200)/2]*0.024 = +15.7 mm; and

Filtration Rate = [(max – min) / 2] * ΔC = [(20 - 2)/2]* 1.0 = 9.0 mL/min.

These new operating conditions were established as the incremental adjustments necessary, and the experiment was run again. The revised parameter conditions provided a new set of results. Using the next increment, a new column was built at the new

parameters and the experiment run again. This process continued until there was no further improvement (decrease) in removal of lead (II) ion. The next to last experiment represents when the theoretical optimization has been achieved.

Following the above described procedure the experiment was conducted to optimize the model. This was accomplished and the results are in Table 22. Run #2 represented the optimum reduction for lead (II) ion in the effluent, therefore these parameters became the optimized column design parameters. The experiment was conducted at the optimized parameters for 2.95% w/w OSNP material, 216 mm media bed depth and 11.0 mL/min filtration rate.

Table 22. Optimized Operating Column Parameters
The first run was selected on the response surface to begin the process. The second run was the incremental adjustment as calculated to optimize the parameters. The third run was the second increment of adjustments and found an increase in output. Run number 2 best represented the optimized operating parameters.

Run #	Percent OSNP (w/w)	Filter Depth (mm)	Filtration Rate (mL/min)	$[Pb^{2+}]$ (μg/L)
1	3	200.0	2.0	37.9
2	2.95	215.7	11.0	20.4
3	2.90	231.4	20.0	37.0

To improve the statistical significance of the model a natural log transformation was completed. The transformed sum of the squares values are depicted in Table 23 and normal probability and residual plots at Figures 20 and 21.

Table 23. Log Normal Transformed ANOVA
The Model F-value of 5.21 implies the model is significant. There is only a 1.67% chance that a "Model F-Value" this large could occur due to noise. P values < 0.0500 indicate model terms are significant. In this case C, AB, AC, BC, ABC are significant model terms. P values > 0.1000 indicate the model terms are not significant.

Factors	Sum of Squares	df	Mean Square	F value	p-value
Model	4.23	7	0.60	5.21	0.0167
A-OSNP Material	0.52	1	0.52	4.46	0.0678
B-Bed Depth	0.20	1	0.20	1.75	0.2220
C-Filtration Rate	3.05	1	3.05	26.28	0.0009
AB	1.79	1	1.79	15.44	0.0044
AC	2.15	1	2.15	18.52	0.0026
BC	1.16	1	1.16	10.02	0.0133
ABC	0.84	1	0.84	7.21	0.0277
Pure Error	0.93	8	0.12		
Cor Total	5.16	15			

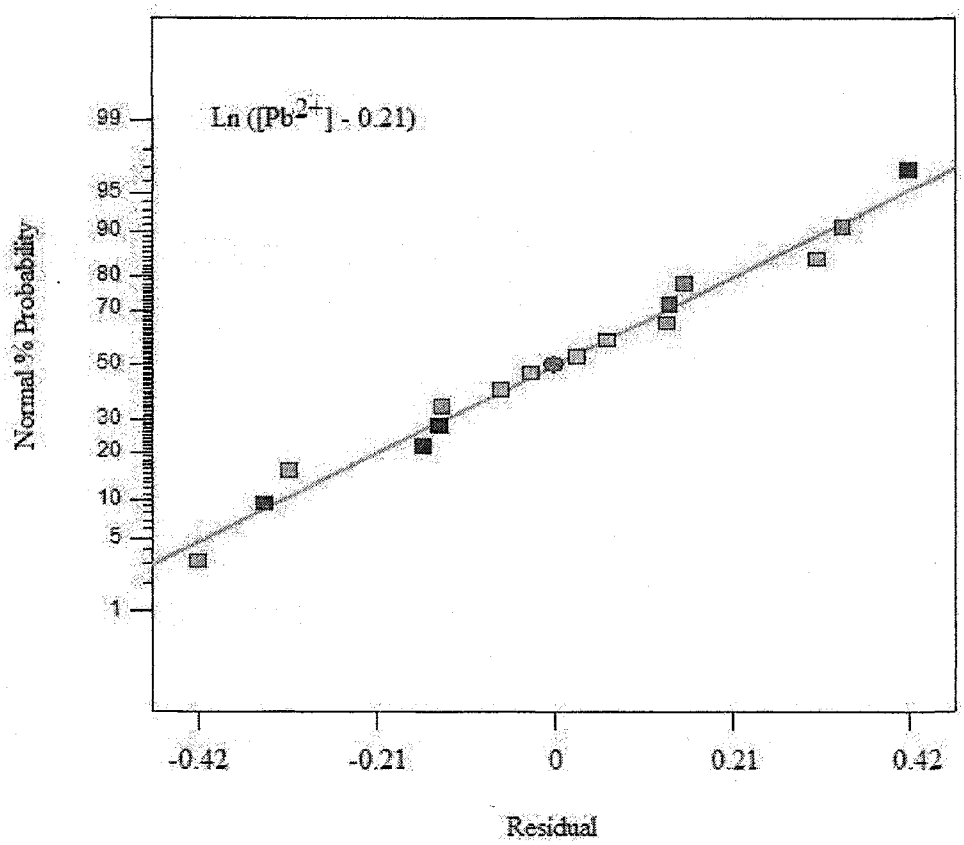

Fig. 20. Model Normal Percent Probability Plot

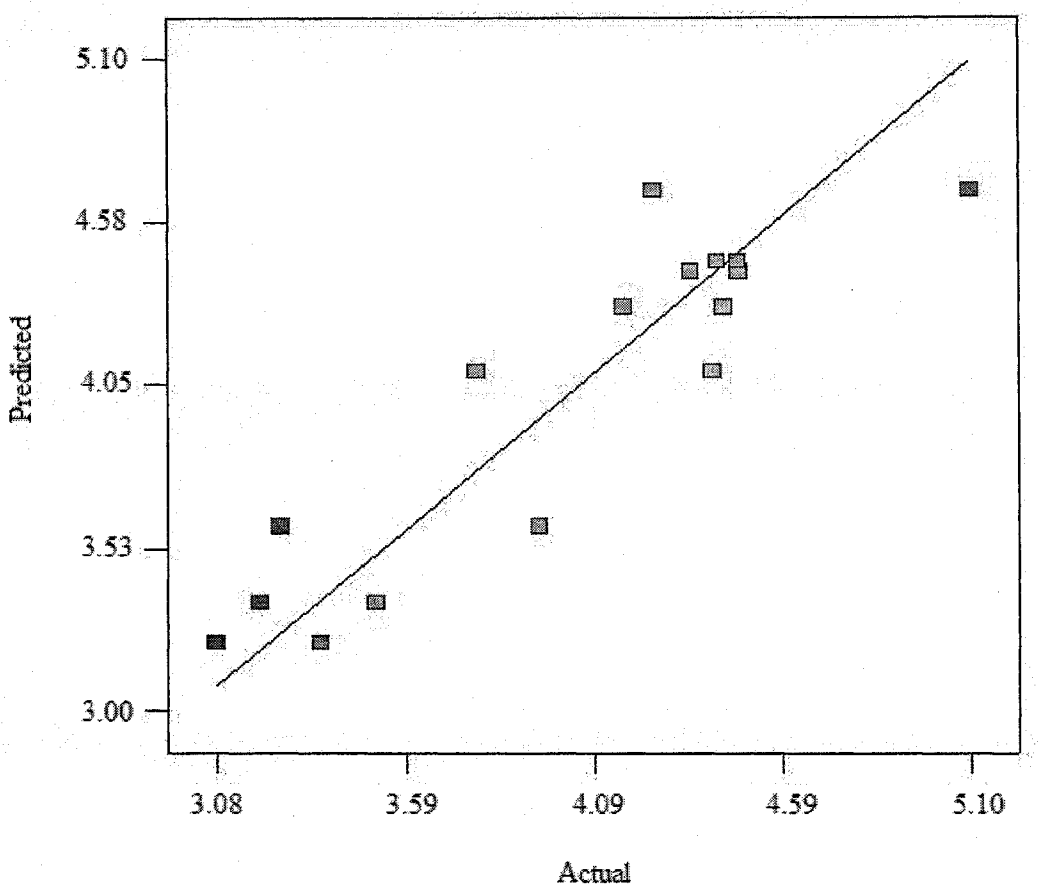

Fig. 21. Model Predicted Versus Actual Plot

The final transformed equation in terms of coded factors became:

$Ln([Pb^{2+}]-0.21 = 4.3088442 + 0.232131 * A - 0.145615 * B + 0.6960257 * C - 0.432103 * A * B + 0.582931 * A * C - 0.429786 * B * C - 0.364659 * A* B * C$

The final transformed equation in terms of actual factors was:

$Ln([Pb^{2+}]-0.21 = 3.3618175 - 0.17981 *$ OSNP Material $+ 0.0033873 *$ Bed Depth $- 0.1611629 *$ Filtration Rate $+ 0.000105 *$ OSNP Material $*$ Bed Depth $+ 0.0685008 *$ OSNP Material $*$ Filtration Rate $+ 0.0003535 *$ Bed Depth $*$ Filtration Rate $- 0.000149 *$ OSNP Material $*$ Bed Depth $*$ Filtration Rate. With the regression model developed the

performance of the proposed filtration was used to develop a 3-dimensional representation of the response surface (Figure 22).

To evaluate the linearity of the model various points of the three factors were selected and compared to model predicted values from the response surface. An OSNP percent w/w of 13.5%, a filtration rate of 11.0 mL/min and media depth of 300 mm were selected to validate the linearity of the response surface. A 13.5% OSNP material percentage was intentionally selected to evaluate whether the model prediction would be correct considering the apparent outlier at 10% OSNP material and 200 mm media depth. The column was operated until approximately 100 BV and predicted versus measured values compared. The 5-sample points average was within 0.6 relative percent difference to the predicted value indicating a linear model could apply to the surface (Table 24).

Table 24. Mid-Point RMS Model Linearity Validation
Linearity check set percent OSNP material = 13.5%, filtration rate = 11.0 mL/min and media depth = 300 mm. Metal analysis was by GFAA with RSD < 2.4 for all samples.

Bed Volume	Predicted $[Pb^{2+}]$ (µg/L)	Measured $[Pb^{2+}]$ (µg/L)	Residual	Relative Percent Difference
27	309	127	-182	83.2
43	309	405	96	26.9
45	309	355	46	13.8
69	309	243	-66	24.1
74	309	407	98	27.2
Average	309	307	-2	0.6

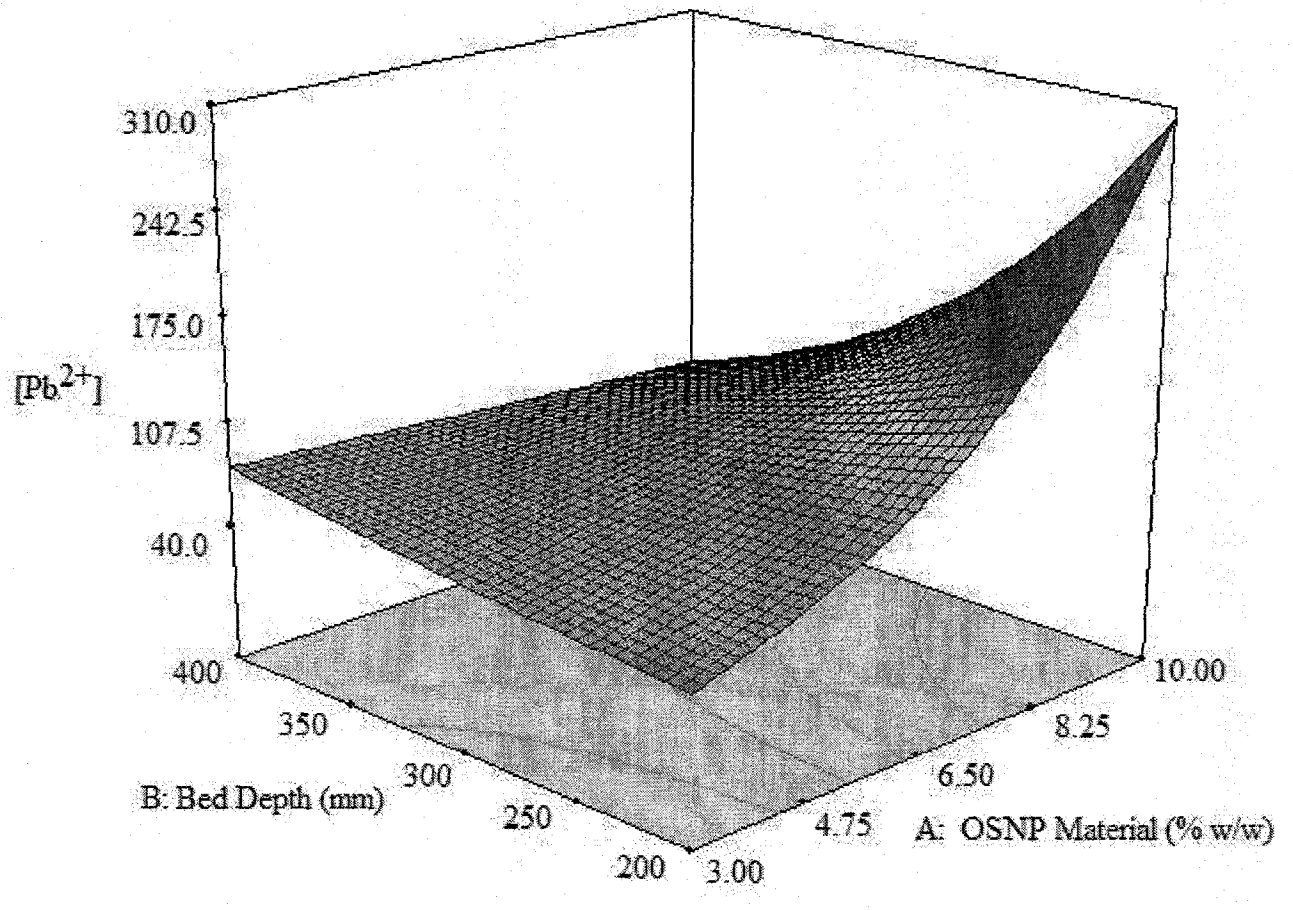

Fig. 22. Response Surface Model
Transformed RSM representing 3 parameter variables: filtration rate, bed depth and percent OSNP material (w/w). Filtration rate set at 11.0 mL/min for this model surface. Apparent outlier result at 10 % OSNP Material and 200 mm was included in the model.

With the model developed various operating condition scenarios to evaluate operational effects were performed. With a constant percent mass OSNP material amendment and by varying the filtration rate and media depth a series of points were predicted for the sand filtration system (Figure 23).

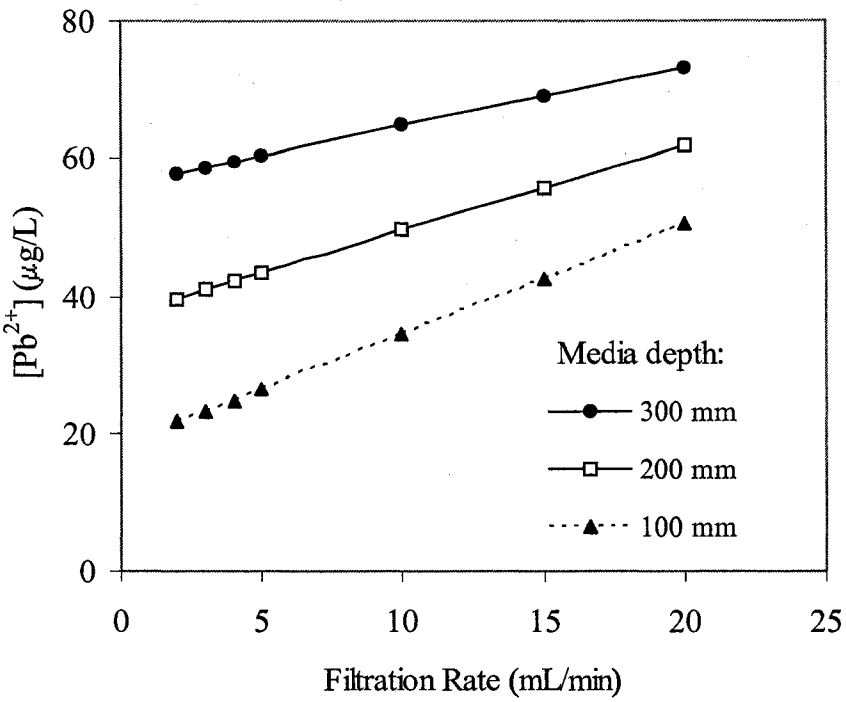

Fig. 23. RSM Model Predictions at Constant OSNP Material Amendment
OSNP material set at 3.0 % w/w amendment to filter. All computed values are within model linear range.

From Figure 23 with a maximum operational filtration rate of 10 mL/min or 4.74 m^3/m^2 h loading rate for the test column, and at 300 mm, the predicted total lead (II) ion concentration at discharge would be ca. 65 µg/L. This provides a 57% safety factor for the shooting range that has a stormwater permit limit of 150 µg/L total lead (II). The model predicts the intuitive conclusion that operation at a lower filtration rate, i.e.

increased adsorbent and adsorbate contact time, should yield better results. Hence, operation of the system by gravity flow would be appropriate. Further experiments were conducted at optimized flow rates (11.0 mL/min) and at gravity flow rates. Section 4.8 below discusses the scale up plan for the full size filtration unit.

4.7 Isotherms, Influence of pH and Competitive Ions

4.7.1. Adsorption Isotherm

Freundlich and Langmuir coefficients for batch reactions for HMS and MCM-41 materials are shown in Table 25. The Freundlich coefficient K_F and Langmuir coefficient X_m expresses the adsorption capacity of the adsorbent. Xu et al. (1999) has reported 3.18 mg (0.02 mmol/g) lead (II)/g maximum adsorption of Ti-MCM-41 with lead (II) removal efficiencies of 63.6% for 1:500 g/mL ratio of Ti-MCM-41 to adsorbate. By comparison Reed et al. (2000) has reported X_m = 3.06 mg/g (0.015 mmol/g) for virgin GAC and 4.35 mg/g (0.021 mmol/g) Fe-GAC in batch reactions with 1 mg/L $Pb(NO_3)_2$ adsorbate.

Table 25. Freundlich and Langmuir Parameters
Equations for batch reaction isotherms were presented in Section 2.8, Mass Transfer Adsorption Theory. All reactions were conducted at pH range of 5.8 to 7.1 and T = 20 ± 3C. Adsorbate solution = 1017 μg Pb^{2+}/L (RSD = 3.1, n=6).

OSNP Material	Langmuir (Fig. 24 and Fig. 25)			Freundlich (Fig. 26)		
	X_m (mg/g)	K_L (L/mg)	r^2	K_F (mg/g)	1/n	r^2
HMS	1.28	1.56	0.94	0.94	0.17	0.99
MCM-41	1.29	0.29	0.98	1.14	0.14	0.99

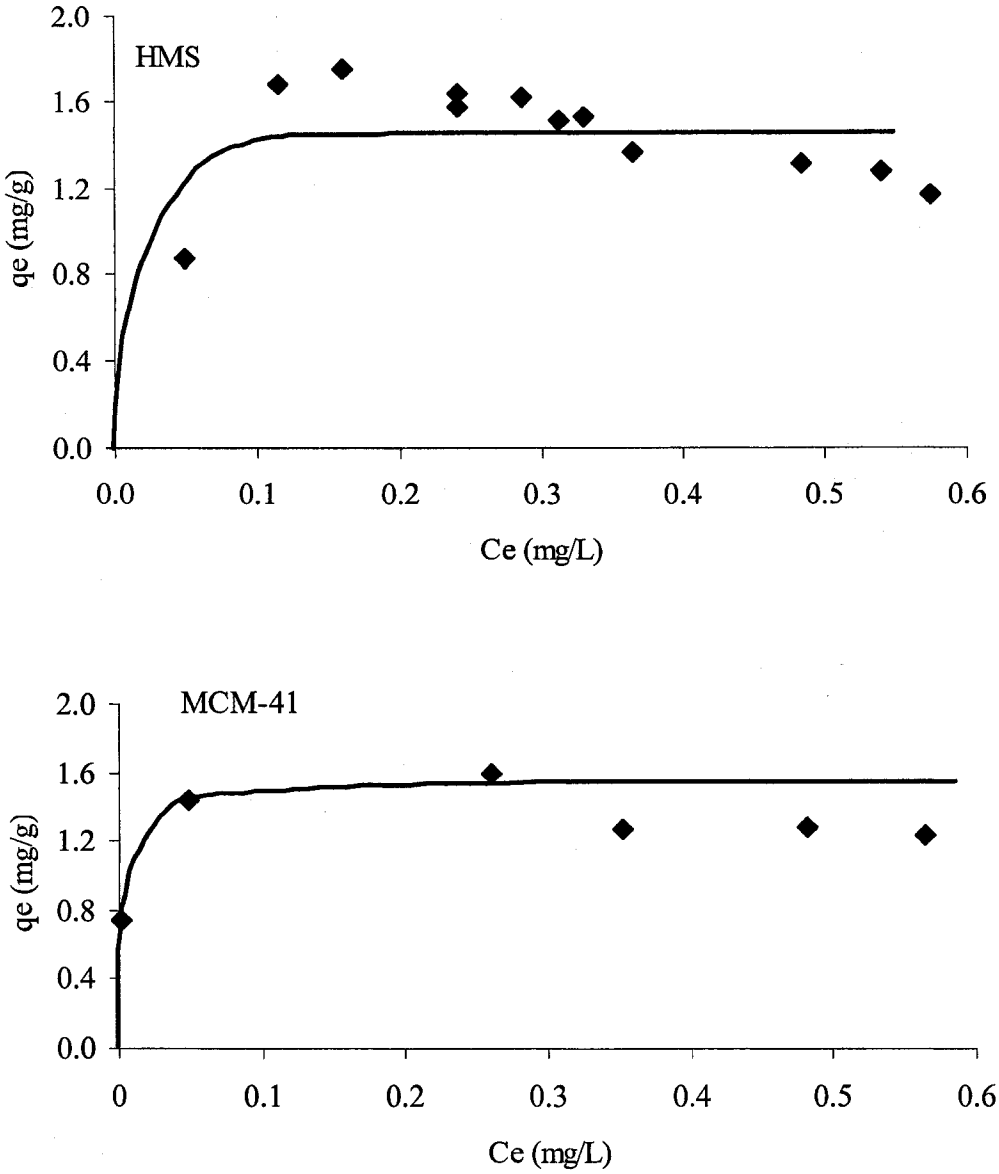

Fig. 24. Adsorption Isotherm Lead (II) Ions on OSNP Materials
Lines were hand drawn to represent Langmuir isotherms.

There was moderate agreement between the Freundlich and Langmuir models for MCM-41 (RPD = 12.3 %), but not for HMS (RPD = 30.6%). There are differences between the two models as discussed earlier. The Langmuir isotherm assumes

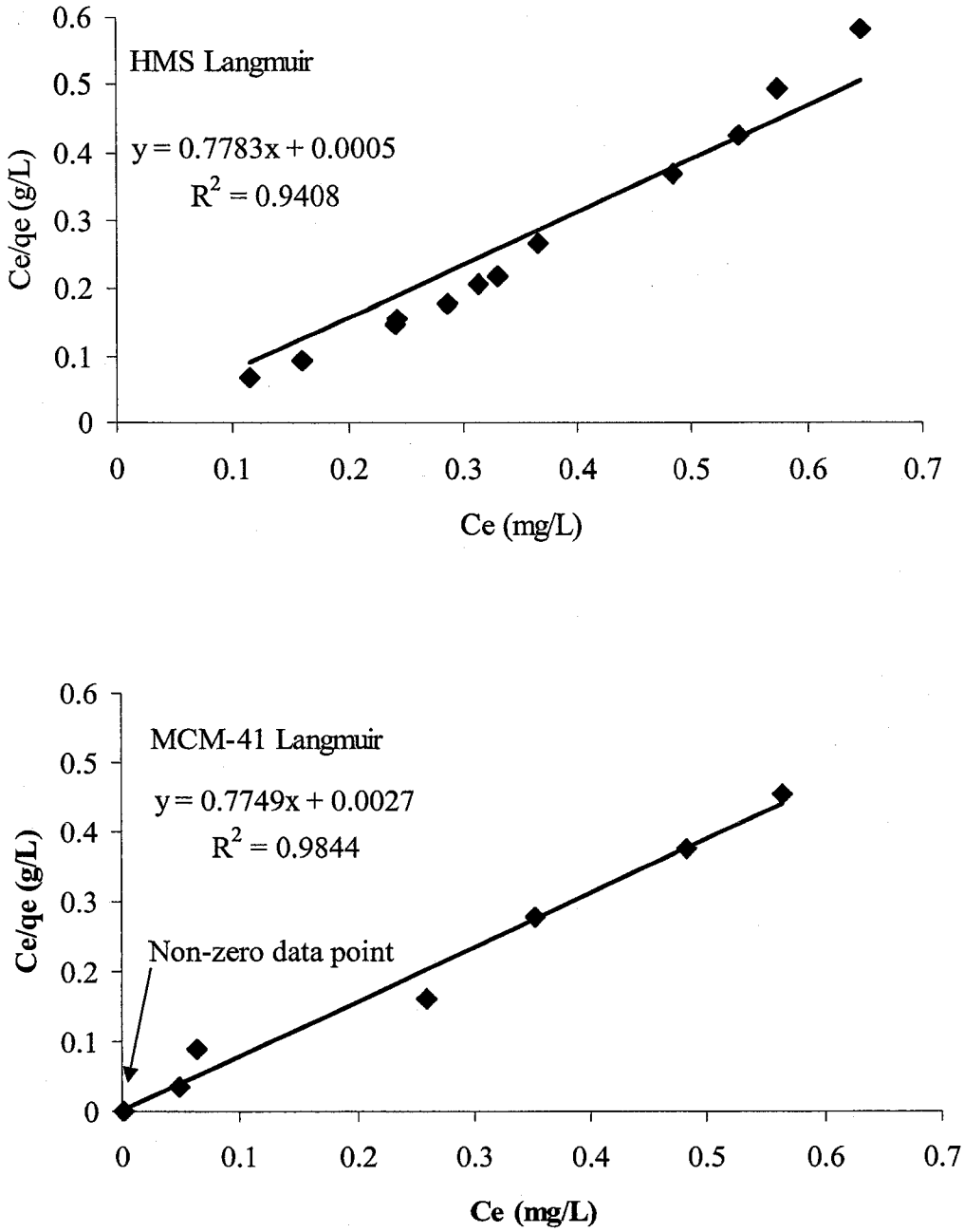

Fig. 25. Langmuir Adsorption Isotherm Coefficients Plots

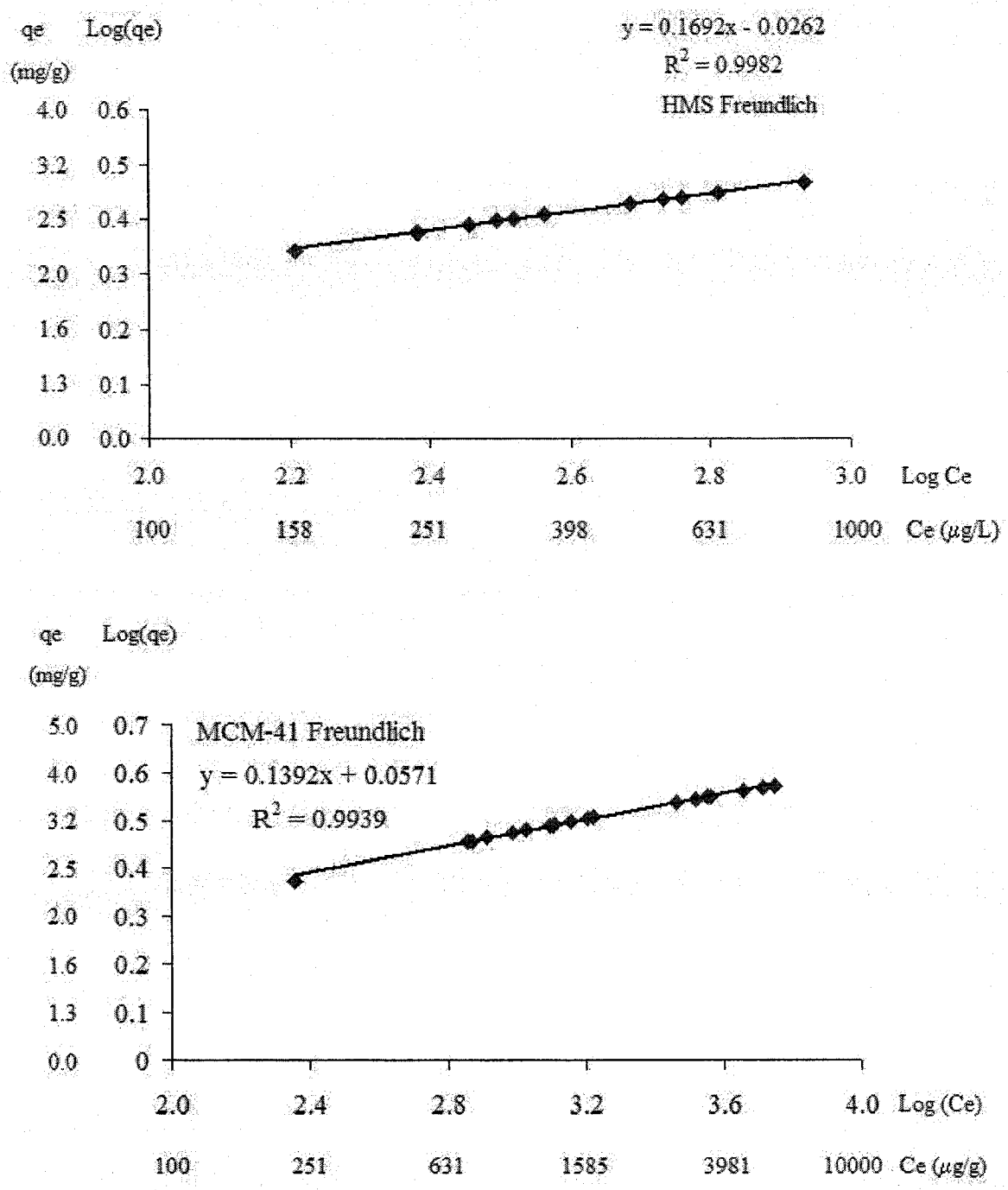

Fig. 26. Freundlich Adsorption Isotherm Coefficient Plots

monolayer adsorption, surface homogeneity, no lateral interaction between adsorbate molecules, and adsorbate molecules do not diffuse to other binding sites after first attachment. The Freundlich equation is an empirical model designed to represent a heterogeneous system.

The Langmuir constant K_L relates the affinity or strength of attraction between the adsorbate and adsorbent. The Freundlich coefficients also relate to capacity and adsorption intensity. A Freundlich value $1/n < 1$ indicates a favorable adsorption and increasing capacity (Juang et al. 2006). MCM-41 adsorption maximum had favorable adsorption and comparable Freundlich 1/n values to Wright (2006), Xu et al. (1999) and Zhang (2003). HMS had more favorable strength of attraction to lead (II) ions in the competing ion environment. A qualitative discussion of this response behavior follows in section 4.7.3.

4.7.2. Influence of pH

The effects of pH are depicted in Figure 27. Lead (II) ion removal increased to ca. pH = 6, after which a sharp drop in adsorption began at ca. pH > 7.5. An explanation for the decreased adsorption at higher pH ca. 6 may simply be the availability of hydrolysis products. Hydrolysis products, such as $Pb(OH)^+$, $Pb(OH)_2$, $Pb(OH)_3^-$, and $Pb(OH)_4^{2-}$ would have increased at higher pH, but these complexes with negative charges are difficult to adsorb by negatively charged OSNP material edges. Further, as illustrated at Fig. 7 and Fig 8, as the pH increases above ca 6.5 the concentration of free lead (II) ions available to adsorb is decreased, and the amount of lead (II) ions that could be precipitated would be more. This same phenomenon was reported by Xu et al. (1999) who experienced a similar pH response curve to lead (II) ion adsorption on Ti-MCM-41.

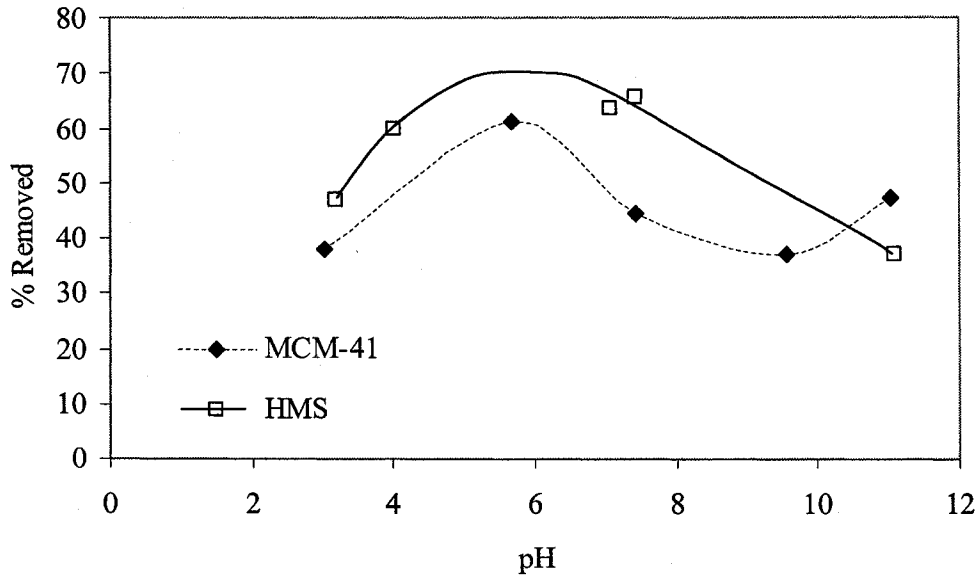

Fig. 27. Effect of pH on Lead (II) Ions Removed in Matrix Solution
Matrix solution 7 with cations used for batch reactions. Initial $[Pb^{2+}]$ = 1017.3 µg/L (RSD = 3.1, n = 4). Average mass of MCM-41 = 26.8 mg (SD = 1.65, n = 7) and HMS = 26.3 mg (SD = 1.05, n = 5). Conductivity of adsorbate solutions was 2721.6 to 905.1 µs/cm at pH 2.36 to 7.43, respectively. Results are average of triplicate analysis by GFAA with RSD < 5.0.

Lead (II) adsorption capacity at each pH value is summarized in Table 26. HMS seemed to be less impacted by competing ions than MCM-41, and adsorbed more lead (II) ions at all, but pH = 11.03, but this was not statistically significant (P = 0.22, n = 15). MCM-41 with the tri-methyl amine moiety would have 3 times the proton exchange sites than HMS, assuming equal alkyl chain lengths. Therefore, MCM-41 would be more susceptible to the presence of competing ions or increased solution ionic strength. The maximum adsorption capacity occurs at a pH range of ca. 7, which is within shooting range storm waters pH of 5.1 to 8.7 (See Table 7).

Table 26. Adsorption Capacity at Specific pH
MCM-41 adsorbent = 0.025 mg (SD = 123, n = 5) and HMS = 0.025 mg (SD = 123, n = 5) in 25 mL of $[Pb^{2+}]$ = 1017.3 µg/L (RSD = 3.1, n = 4) with concentrations of twelve other cations in solution as in Table 12, see the column labeled, "Batch Adsorbate." Optimum adsorption was at pH = 5.7 to 7.4.

MCM-41		HMS	
pH	Adsorption (mg/g)	pH	Adsorption (mg/g)
3.03	0.43	3.18	0.51
5.67	0.56	4.02	0.60
7.08	0.27	7.08	0.69
7.43	0.60	7.43	0.83
11.03	0.50	11.08	0.40

4.7.3. Influence of Competitive Ions

To evaluate the effect of competitive ions, 7 matrix solutions were prepared with increasing numbers of cations added at concentrations anticipated in shooting range outfall stormwaters (Table 15). The cation concentrations were added to reflect the expected field concentrations. This approach, while realistic, made the evaluation of specific cation interference less obvious because cation concentrations were not equal. Characteristics of matrix adsorbate solutions are found in Table 27. The following two paragraphs provide a summary of the results, followed by a more thorough qualitative discussion of results observed using hard soft acid base principles.

Distribution coefficients (K_D) for each matrix solution were calculated by Equation 8. Figure 28 shows MCM-41 was not an effective adsorbent of lead (II) ion in adsorbate solution until matrix 6. Matrix 1 through 4 cations Mo, Ni, Sn, Sb, Mn, Cr, Cu, Zn, and Fe, may complex with solution species preferentially excluding lead (II) ion adsorption on MCM-41 surfaces. However, with the addition of Na at Matrix 6, sodium hydroxyl and other complexions were more likely formed at MCM-41 surface sites,

et al. (2005) who reported Na cations did not interfere with Ni adsorption on amino-functionalized MCM-41, unless Cu or Co were present at which

Table 27. Batch Matrix Solution Characteristics
All solutions were prepared using DI H_2O and Environmental Express 1,000 ± 3 µg/mL in 2% HNO_3 standard solutions (Mt Pleasant, SC). Metal analysis was by GFAA. pH adjustments were made with 0.2M NaOH. All values are averages of triplicates with RSD <10%. Batch reactions were completed using solutions with final pH as shown.

Matrix	Initial pH	Cond. at initial pH (µs/cm)	Reaction pH	Cond. at Final pH (µs/cm)	$[Pb^{2+}]$ (µgL)
1	5.53	10.3	7.54	33.1	590
2	5.18	11.4	7.30	32.1	696
3	5.08	15.5	7.67	30.0	659
4	3.81	48.6	7.43	69.3	736
5	3.19	277.2	7.44	144.8	778
6	2.82	792.4	7.03	337.2	780
7	2.36	2721.6	7.43	905.1	911

Cond. = Conductivity

MCM-41 adsorption efficiency was decreased. Any analyte in the matrix with a higher formation constant would be retained preferentially.

When a significant concentration of Ca^{2+} ions were added at matrix 7, the MCM-41 lead (II) adsorption decreased. Calcium may have preferentially formed covalent bonds with hydroxyl ions and would tend to increase solution pH. Fewer surface sites were available for lead (II) ion adsorption. Lead precipitate complexes likely formed (e.g. $Pb(OH)_2$) further reducing available lead (II) ion adsorption by OSNP materials A strong dependence on competing ions would suggest an outer-sphere complexation and electrostatic bonding (Stumm, 1992).

HMS performed better in the competing ion condition than MCM-41, but also experienced a similar adsorption decline when the Ca cation was added. This difference in performance may be understood by noting the 1:3 ratio of HMS protons to MCM-41

protons in the OSNP material amine head group (Figure 3 and Figure 4). Fewer available protons would mean HMS is less influenced by competing ion hydrolysis and cation complexations. The Ca cation is more electropositive and may have preferential protone exchange reaction than other cations, contributing to the decrease in adsorption performance by OSNP materials. This preference for protons and hydroxyl formations simply out compete the metal cations in solution for OSNP material adsorbent surface sites.

Hohl and Stumm (1976), Davis and Leckie. (1978) and Xu et al. (1999) measured the number of protons released when lead (II) ions bind to heavy metals. Xu et al. (1999) reported when Ti-MCM-41 adsorbed lead (II) ions, 1.5 to 1.7 protons were released, on average.

From Figure 28 HMS materials were less impacted by competing ions than MCM-41. In addition to the argument presented above, this may be rationalized by observing the structure of aminopropyl functionalized HMS material (Figure 29). HMS is significantly different structurally to MCM-41. Zhang et al. (1997) has shown that the textural mesoporosity of HMS, which can be controlled by the choice of synthesis solvent, greatly facilitates access to the framework mesopores. Steric hindrance and

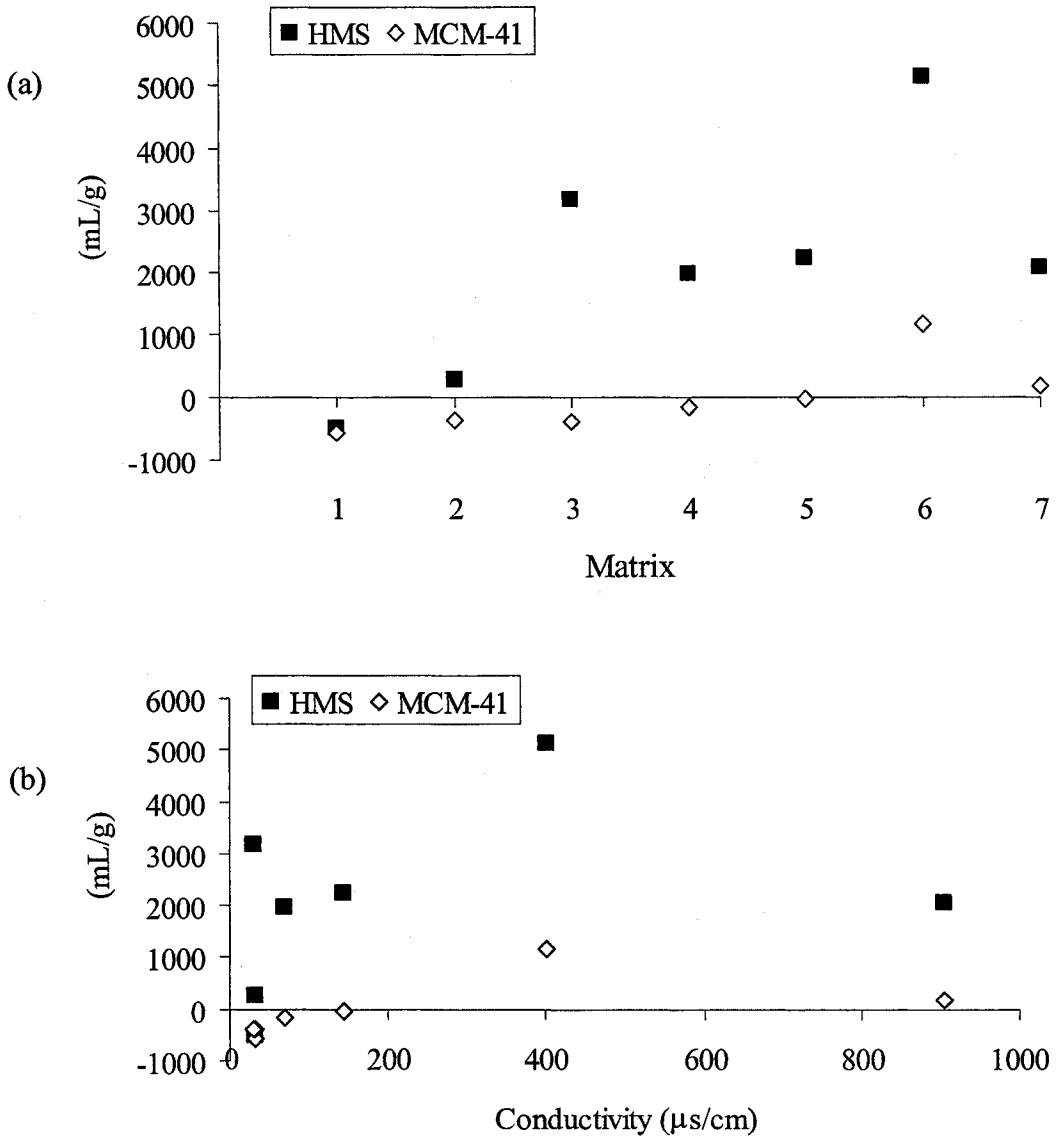

Fig. 28. Lead (II) Distribution Coefficients in Batch Reactions
Average pH for all matrix batch solutions = 7.32 (SD = 0.24, n = 7) in 25 mL of 748.2 µg Pb^{2+}/L (SD = 125.7, n = 7) using an average 0.0257 g MCM-41 (SD = 0.0031, n = 7) and 0.0251 g HMS (SD = 0.0007, n = 7) of OSNP adsorbate. Matrix constituents and concentrations are in Table 12 and Table 15. Chart (a) is by matrix category and chart (b) by conductivity. All samples were analyzed in triplicate by GFAA with RSD < 5.0.

electrostatic interference is avoided through a decreased head group size that leads to an increase radius of curvature and to larger micelle size. In contrast MCM-41 with the trimethyl-head-group or increased head-group size, leads to a decrease in the radius of curvature and to a reduction in micelle size, and less electrostatic access (Figure 29).

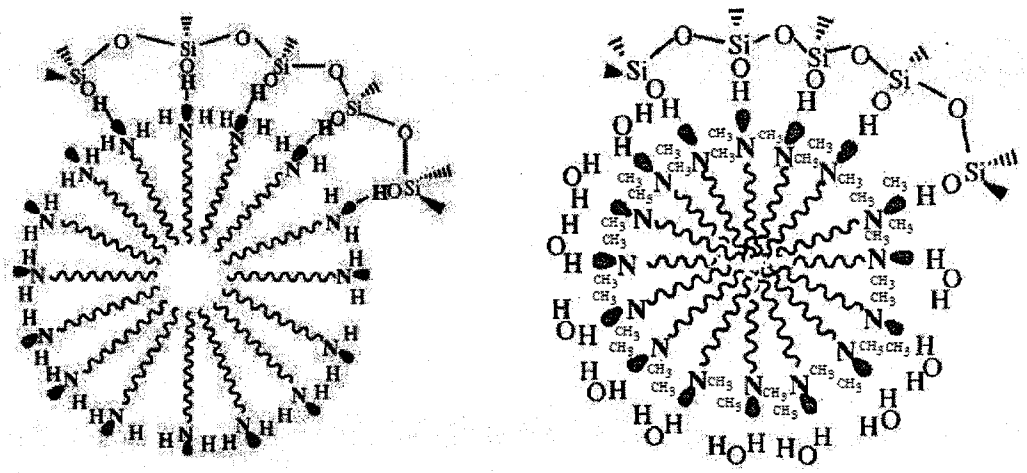

(a) (b)

Fig. 29. Silicate Surfactant Mesostructure
Nanoporous hexagonal mesoporous structure Lewis structure after Zhang et al. (1997) and Tanev and Pinnavaia (1996). (a) HMS. (b) MCM-41; Not all methyl groups are shown. The darkened tear drops are surfactant amine head group unpaired lone electrons that participate in hydrogen bonding with the silicate moiety.

MCM-41 possesses both hydrophobic and hydrophilic properties, but a greater tendency to hydrophobic characteristics. This allows hydrolysis to be the primary sorption phase in its meso-pores in competitive ionic solutions. This reaction phenomenon suggests the adsorption of lead (II) ions includes bidentate surface complexing and surface hydrolysis with hydroxyl moieties. Isomorphous substitution by other metals (e.g. Al) MCM-41 can improve the hydrophilic characteristic (Zhao et al. 1996).

4.7.4. Qualitative Discussion On OSNP Adsorption in Batch Reactions

The following provides a qualitative argument, in addition to the previous discussion, for the response pattern observed in Figure 28. Hard soft acid base (HSAB) principles would suggest there is a preference or order that an individual cation bonds with a particular ligand before another. This order of stability is determined primarily by electrostatic forces and offers some interpretation of the adsorption behavior of OSNP materials in batch reactions.

HSAB would predict the formation constant for a metal M^{3+} to be greater than a M^{2+} due its larger charge density. Said a different way, the formation constant is basically determined by the charge of the metal ion. In a generalization of the HSAB chemistry, cations have a preferred bonding order between ligands. The stability or formation constant, as presented in Equation 3, then hints at the stability of the complex.

Pearson (1963) organized Lewis acids and bases into hard, borderline or soft following the premise that hard Lewis acids prefer to bind to hard Lewis bases and soft Lewis acids prefer to bind to soft Lewis bases. For the 13 cations of this study, Pb^{2+}, Fe^{2+}, Ni^{2+}, Cu^{2+}, Zn^{2+}. Sn^{2+} and Sb^{3+} cations are considered borerline Lewis acids, whereas Na^{+}, Mg^{2+}, Ca^{2+}, Mo^{3+}, Mn^{2+}, and Cr^{3+} are considered hard Lewis acids. Although not previously listed Fe^{3+} and Sn^{4+} are hard Lewis acids and could exist in the batch solutions as follows. Ferric iron would be generated in the presence of oxygen according to the reaction $4\ Fe^{2+} + O_2 + 4\ H^{+} \rightarrow 4\ Fe^{3+} + 2\ H_2O$, which would react with hydroxyl anions to produce the very insoluble $Fe(OH)_3$ ($K_{sp}= 2.6 \times 10^{-39}$). Similarly, tin could likely exist as $SnCl_4$ or $Sn(OH)_6^{2-}$. Typically the +4 oxidation state complexes are covalent and the +2 mostly ionic.

Consider matrix 1 response (Figure 28). Neither HMS or MCM-41 adsorbed lead (II) ions. Matrix 1 cations included the nitrate salts of Pb^{2+}, Mo^{2+}, Ni^{2+} and Sn^{2+} at concentrations of 4.9, 27, 47, and 4 μM, respectively (Table 12). Using the formation constants from Appendix C the fraction diagram at Figure 30 can be drawn. At the

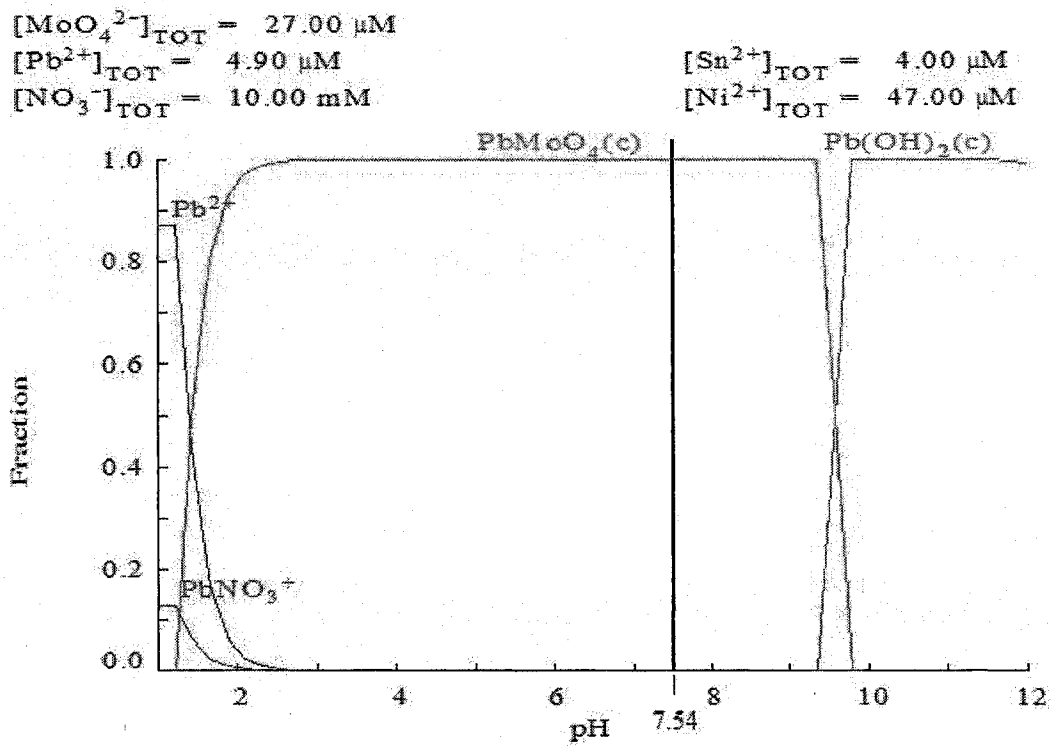

Fig. 30. Fraction of Lead (II) Ions in Matrix 1
Matrix 1 solution reaction pH = 7.54 is shown by vertical bar. Chart was made using the software application MEDUSA.

matrix reaction pH lead (II) ions would exist predominantly as the PbMoO4 precipitate. If there were any free lead (II) ions they would have been preferentially bound to CO_3^{2-}, and Mo per HSAB (See equilibrium equations with formation constants = 17.46, 13.229, and 15.62 for example). Therefore, the poor performance at matrix 1 may have been due to precipitation. For analysis, although only supernatant was withdrawn from the top 5-

10 mm of an equilibrated and settle 48 h solution, suspended precipitate was undoubtedly collected. The analytical result of no lead (II) ion removal was possibly due to soluble complexes that were formed that prevented adsorption and precipitation.

For matrix 2 a similar analysis was completed. The following figure reflects the addition of Sb^{2+}, Mn^{2+} and Cr^{2+} ions to the adsorbate. The same result occurred, again due to precipitation of $PbMoO_4$ (See Appendix C formation constant = 15.62).

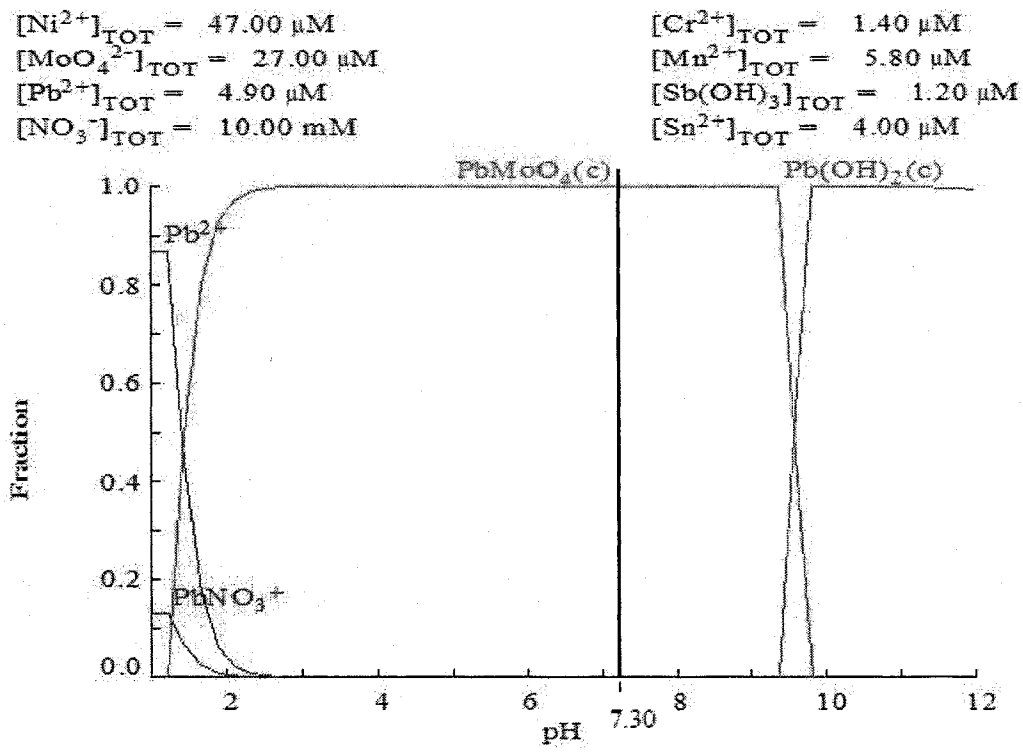

Fig. 31. Fraction of Lead (II) Ions in Matrix 2
Matrix 2 solution reaction pH = 7.30 is shown by vertical bar. Chart was made using the software application MEDUSA.

Matrix 3 lead (II) ion fractions were similar to Matrix 2 with PbMoO4 controlling lead solubility for much of the pH range of interest (Figure 32). Figure 28 did show

significant removal for HMS, but remained ineffective for MCM-41. With a primary amine surfactant, HMS has less steric hindrance than MCM-41 (See Figure 29), and may

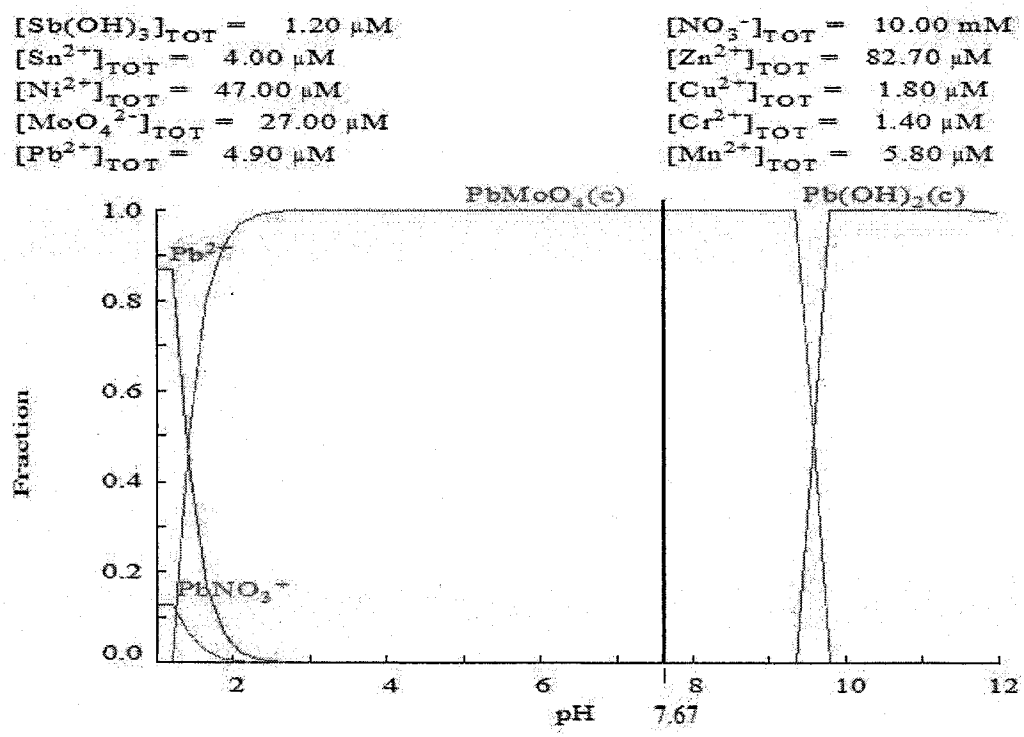

Fig. 32. Fraction of Lead (II) Ions in Matrix 3
Matrix 3 solution reaction pH = 7.67 is shown by vertical bar. Chart was made using the software application MEDUSA.

have allowed easier access to the lone pair electrons on the surfactant N. This would allow some lead (II) complexations represented in Appendix C equilibrium constants, such as Log K_{NH3} = 1.5 and Log K_{NO3} = 1.4. Matrix 4, 5, 6 and 7 looked very similar to Matrix 3. The addition of Fe^{2+} (Matrix 4) and Mg^{2+} (Matrix 5) had no apparent effect to MCM-41 adsorption, and HMS lead (II) ion adsorption was only slightly less effective than matrix 3. The species controlling lead solubility was consistently PbMoO4.

Lead molybdate is a poisonous white powder. During the experiment a residue of white powder was observed at the bottom of all batch reactions. Since the OSNP materials are also a white powder it was not apparent that this precipitate was interfering with the experiment. The precipitation of PbMoO4 likely clogged the pores of MCM-41, which are closely packed with surfactant (Figure 29). HMS was less susceptible to this blocking interference with only a primary aminated surfactant, and therefore able to remove some lead(II) ions that found their way into the more open pores of HMS.

For Matrix 7 the adsorption performance of HMS and MCM-41 drastically declined. This phenomenon may be explained by noting that Ca^{2+} and $CO3^{2-}$ complexes with Mg^{2+} (Log K = 29.968, 17.09, -19.894, -30.272, - 68.543) and Mo^{2+} (Log K = 7.95). All of these complexes are precipitates and would interfere by coating the OSNP materials to prohibit access by lead (II) ions. Calcium was added at 64 times the lead (II) ion concentration to simulate calcareous soil stormwater runoff. In this instance however, at pH 7.43, the Ca^{2+}, Mg^{2+}, and Mo^{2+} complexes coated the nanoporous materials and rendered them ineffective.

The batch isotherm and pH reactions did not suffer from the PbMoO4 precipitation problem as they were prepared with at an earlier time and used a different matrix 7 batch. The initial batch reaction [Mo] = 0.1 μg/L = 0.001 μM versus the subsequent matrix 7 batch, which had [Mo] = 26 μg/L = 27 μM. The quantity of Mo in the lower amount was 4-orders less than the competitive ion batches and was low enough to not influence lead (II) ion solubility.

4.8 Lead (II) Ion Adsorption Performance in Columns

Column studies were conducted to resemble the proposed application of OSNP materials in stormwater treatment to include start and stop flow regimes. Unlike batch reactions where adsorbents stay in contact with the adsorbate until equilibrium is achieved, in a dynamic column, the adsorbate is constantly flowing such that absolute equilibrium is never achieved. However, the dynamic equilibrium at certain milestones on the isotherm curve can provide quantifiable positions for comparison between adsorbents or other design parameters. The sorption of metals capacity (mg/g) was calculated using Equation 7 and column breakthrough capacities following Treybal (1980). The distribution coefficient (L/g) was computed using Equation 8. The column break-through point Ce/Co = 0.5 was used for comparative purposes for breakthrough maximum adsorption capacity and K_D.

4.8.1. Column Break Through Curves

MCM-41 break through occurred at 250 BV (13.5 h, influent pH = 6.86, flow rate 2.1 m^3/m^2 h). The HMS and columns were at flow rates of 0.6 m^3/m^2 h (reduced flow to simulate gravity flow), and broke through with Ce/Co = 0.5 ca. at 30 BVs (83.6 h, influent pH = 6.86), and 15 BV (0.5 h, influent pH = 7.19) (Fig. 33). The Treybal (1980) method was used to determine column capacities at breakthrough, but modified to use break through bed volumes in lieu of break-through time. Equation 21, BTc = Breakthrough capacity, is the modified form to estimate adsorption capacity and the results are provided in Table 28.

BTc = break through BV x feed concentration / mass of adsorbent in bed (21)

MCM-41 break-through was much later than the HMS and sand column (Figure 33). While the sand column results showed a traditional break-through curve, the MCM-41 and HMS responses were unique and nonlinear. For MCM-41 at ca. 24 BVs, Ce/Co = 0.49 and 0.68, and for HMS at from 4 – 40 BV, Ce/Co ranged from 0.43 to 0.71. For HMS this appeared to be a break-through point and the Ce/Co = 0.5 value was used to compute the adsorption capacity. MCM-41 had good sorption to ca. BV = 250 BVs where Ce/Co = 0.5. The two earlier values for MCM-41 at 0.49 and 0.68 may have resulted from channeling and by-pass. They are otherwise not explainable.

Breakthrough capacities were computed for each adsorbent and are listed in Table 28. Comparison to studies by Goel et al. (2005) and Sansalone (1999) suggest the OSNP materials are of comparable adsorption capacity accepting the fact that both studies used had lead influent concentrations at 5 and 6 times the influent concentration of this study.

Table 28. Lead (II) Ion Adsorption Capacity for MCM-41, HMS and Sand Columns Cation concentrations are listed in Table 12 as column adsorbate. The bottom of columns to 54 mm bed height was sand (d_{10} = 0.20 mm) and OSNP material. Sand was placed from 54 mm to 216 mm bed height for each column. All columns were 12.7 mm inside diameter clear polyvinyl chloride pipe (See Fig 12). BV = 27.4 mL. Btc = Breakthrough capacity

Adsorbent	Influent lead (II) (µg/L)	Break through Ce/Co = 0.5	Hydraulic Loading Rate (m^3/m^2 h)	Bed Height (mm)	BTc (mg/g)	Reference
MCM-41	1060	250	2.1	216	14.627	This study
HMS	1060	30	0.6	216	2.735	This study
Sand	1060	15	0.6	216	0.003	This study
Act. Carbon	6000	19	7.5	400	2.89	(Goel et al. 2005)
Sand w/ iron coated oxide	5000	7†	2.6†	612	0.004†	(Sansalone 1999)

† Calculated from data in referenced literaturefor comparative purposes.

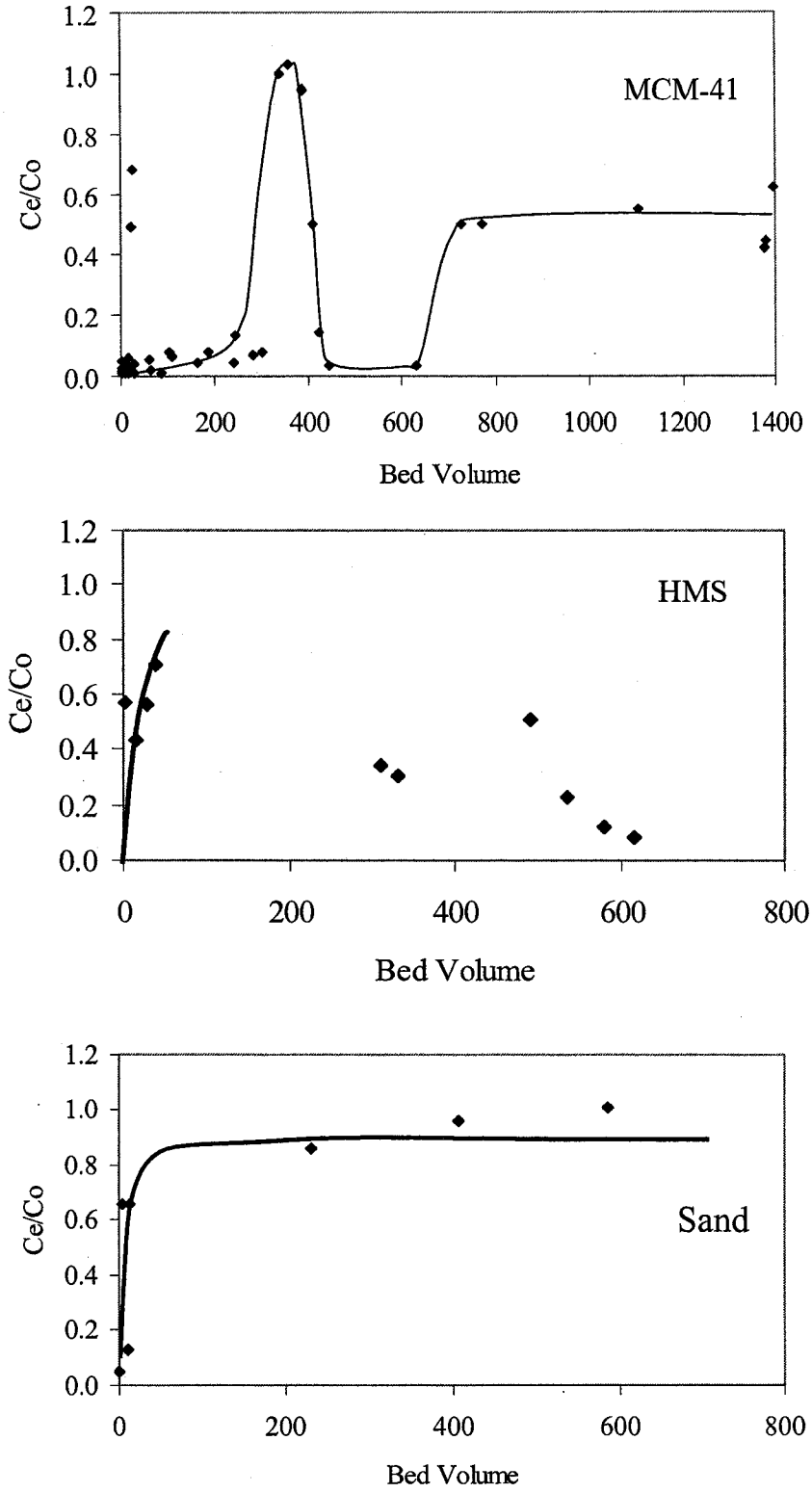

Fig. 33. Column Breakthrough Curves for Lead (II) Ions
Break through curves for (a) MCM-41 and (b) HMS and (c) sand only media at constant bed height = 216 mm. Hydraulic loading rate = 2.1 m^3/m^2 h for MCM-41 and for HMS and sand = 0.6 m^3/m^2 h for sand. Influent $[Pb^{2+}]$ = 1060 µg/L (SD = 505.2, n = 11).

4.8.2. Discussion of Atypical Adsorption Isotherm for MCM-41

The nonlinear response isotherm for MCM-41 material requires further explanation. There are three distinct areas of response and they are shown in Figure 34. These specialized areas of response were referred to as zone 1, 2 and 3. A qualitative discussion by response zones follows.

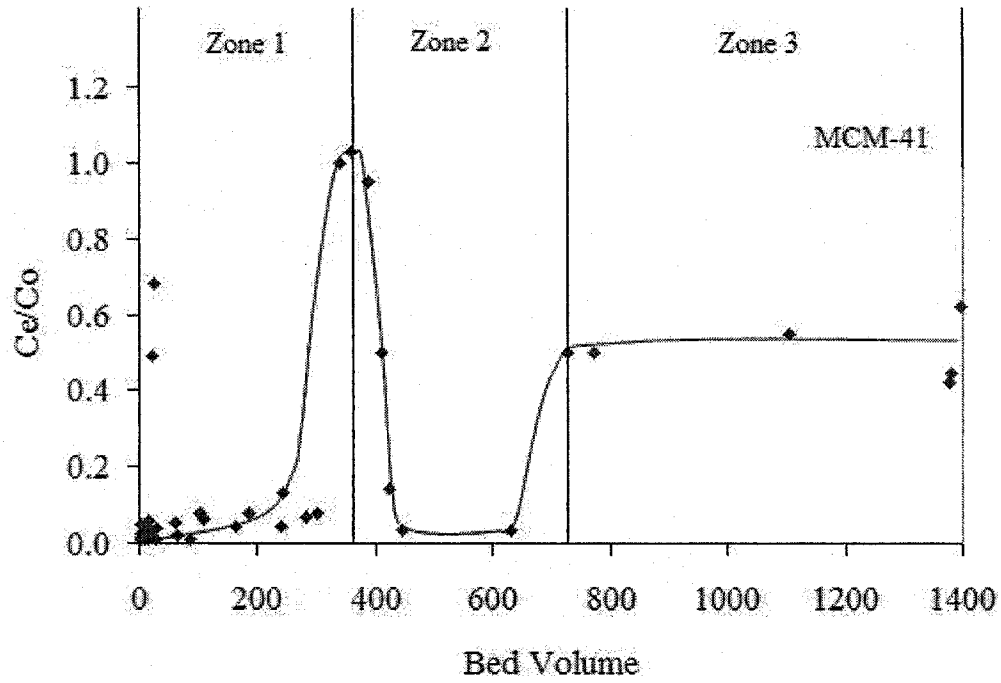

Fig. 34. MCM-41 Adsorption Isotherm by Reference Zones

Zone 1. In this zone the response adsorption is typical for MCM-41 sorption of heavy metals and has been reported by others. Yoshitake et al. (2002) has reported adsorption isotherms of arsenate and chromate on functionalized MCM-41. A very steep slope characterizes the initial curve until saturation where saturation was found to not be significantly dependent on the silanol functional groups. In fact, Yoshitake et al. (2002) suggest the different frameworks (i.e. silicate amino group ratio) may influence the

accessibility or utility of the amino groups causing adsorption sites to congregate on parts of the MCM-41 surface while other parts remain unused. Walcarius et al. (2003) found a similar relationships between mesoporous solids with pore sizes ~35Å (i.e. similar to pore size of MCM-41 materials in this study) that were crowded with aminopropyl groups. This directly affected both accessibility to the active sites and diffusion rates. Walcarius et al. (2003), but also reported very fast reaction rates sorbing Cu and Hg, with significant reduction the rate of adsorption once about 40% of the total capacity of the material had been reached. Both researchers hypothesized the metal cations are unable to reach deep into the material once the pore entrance sites had been populated.

From this review the response curve in zone 1 (Figure 34) represents fast adsorption because of the large, uniform, and easily accessible pore channels. According to HSAB (Hard Soft Acid Base) principles, the aminopropyl groups on MCM-41 are hard bases. The cationic adsorption mechanism of MCM-41 for heavy metals ions such as, lead (II) ions and cadmium (II) ions would interact according to HSAB chemistry (Perez-Quintanilla et al. 2006). By frontier molecular orbital theory a hard Lewis acid and a hard Lewis base would yield an ionic bound complex. Similarly, a soft Lewis acid and a soft Lewis base would yield a covalently bound complex. Specifically in this study, lead (II) ions are considered a borderline Lewis acid and the surfactant head group moiety RNH_2, a hard Lewis base, and therefore, their interaction characteristics are intermediary between a covalent and ionic bonding. Therefore, the lead (II) ion adsorption on OSNP material would generally be less stable then a hard-hard and soft-soft complex.

As a hard Lewis base (RNH_2), OSNP material adsorptive properties would prefer hard Lewis acids, like H^+, Na^+, K^+, Mg^{2+}, Ca^{2+}, Mn^{2+}, Al^{3+}, and Fe^{3+}. The Irving-Williams stability series (Irving and Williams 1953) contains 7 of the cations included in

this study and provides the expected stability of metal ion complexes for this study as follows: $Ca^{2+} < Mg^{2+} < Mn^{2+} < Fe^{2+} < Ni^{2+} < Cu^{2+} < Zn^{2+}$. Presumably, the electrostatic nature of complexation would also predict the stability constants for metals with 3+ charge to be greater than those for metals with a 2+ charge.

Zone 2. To examine more closely the behavior that drives the change in zone 2 a plot of the pH, flow, and turbidity are provided in Figures 35, 36 and 37.

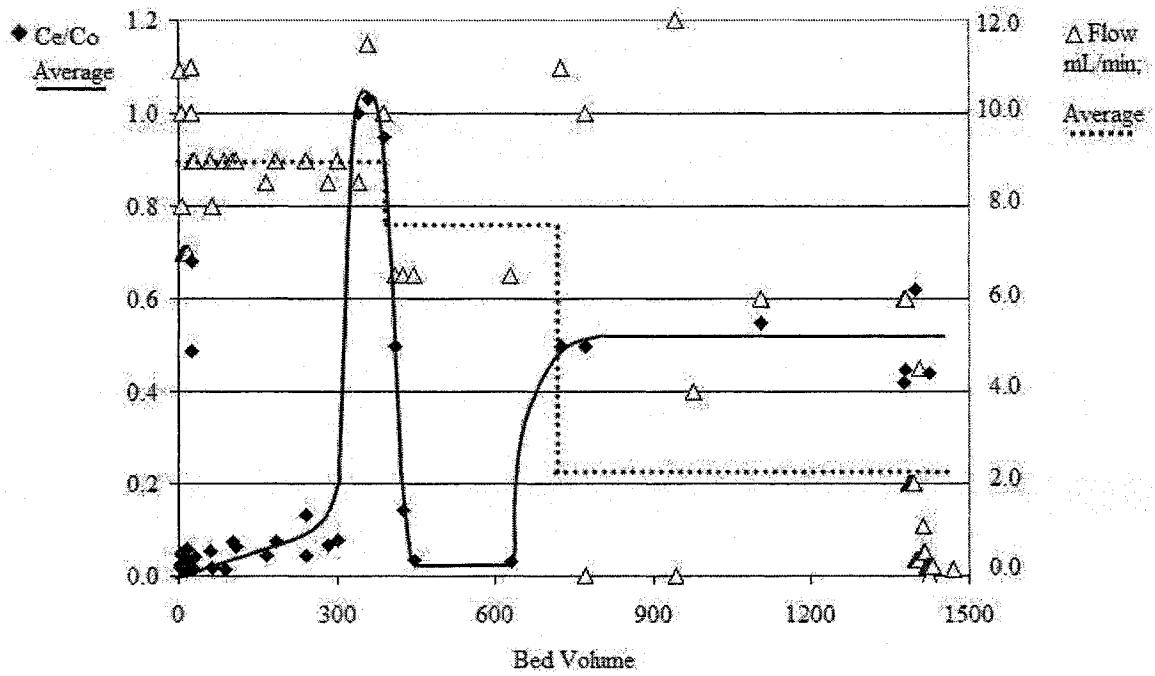

Fig. 35. MCM-41 Adsorption and Flow Rate

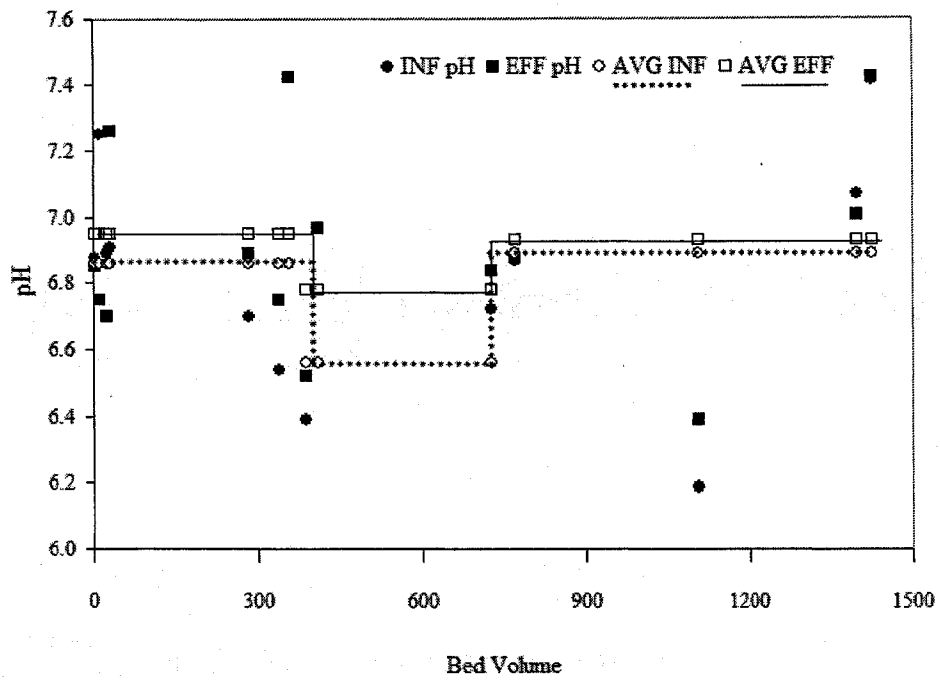

Fig. 36. MCM-41 Bed Volume vs Effluent pH

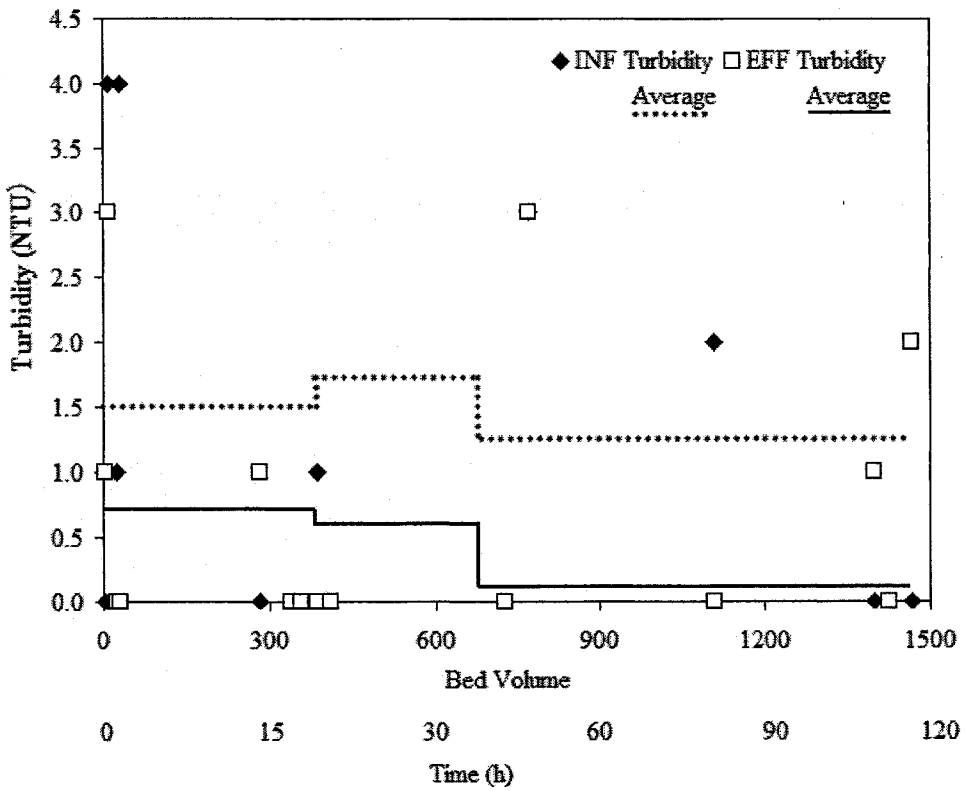

Fig. 37. MCM-41 Turbidity vs Bed Volume and Elapsed Time

From Figures 35 to 37 for zone 2, there is a noteworthy decrease in adsorbate influent flow (-9.3%), a decrease in influent pH (-4.4%) and an increase in influent turbidity (+13%). Noting in Figure 8 the fractional species of lead (II) ions versus pH, it is obvious the initial average pH = 6.86 the $Pb(OH)_2$ is controlling solubility, but as soon as the average pH dropped to 6.56 much of the precipitate would have been available as free lead (II) ions. The influent pH decreased by hydrolysis by the various cations according to the general relationship of a metal cation coordination with water: $[M(H_2O)n)^{z+} + H_2O <==> [M(H_2O)_{n-1}(OH)]^{(z-1)+} + H_3O^+$. This reaction decreased the pH with increased contact time in the adsorbate supply tank. The hydronium ion production was described by Rutgers and Hendrikx (1962) who developed a relationship that pKa is proportional to the charge squared divided by the atom bonding radius.

MCM-41 also contributed to effluent pH decrease. Researchers have documented the release of hydrogen ions during the adsorption of metal cations by MCM-41 materials. Xu et al. (1999) measured the release of protons during adsorption of lead (II) ion in 0.20 L solution of 0.40 g Ti-MCM-41 at pH 7.0. They noted protons were released during the adsorption reaction. They titrated with 0.1469 M carbonate-free NaOH to maintain pH (± 0.10 unit) for 2 h, after which the pH remained stable. The quantity of base added was used as a direct measure of proton release. They suggest this phenomenon is explained by the formation of surface complexes with two deprotonated sites or simultaneous adsorption and hydrolysis. There were 1.5 – 1.7 protons released on average per lead (II) ion adsorbed suggesting a bidentate surface complexing and surface hydrolysis with surface hydroxyl groups.

For this experiment, zone 2 lead (II) ions availability increased as the pH decreased, which then, in turn, were adsorbed by the MCM-41 material. Interestingly, as

the lead (II) ions were adsorbed, protons were again released lowering the pH, which at zone 3, $Pb(OH)_2$ precipitated, starting the cycle over. The dissolved portions of precipitates easily passed through the column, which caused the overall lead (II) ion adsorption to decrease. Presumably, if the column experiment had continued the cycle of deprotonation of the silanol, i.e. drop in pH, adsorption by MCM-41, and then precipitation would have continued indefinitely.

4.8.3. Column Break-Through Using Recycled Adsorbate

Since both OSNP materials had removal of ca. 30% to 50%, for HMS and MCM-41, respectively, the effluent of one column was collected and used as feed for a new "recycled" column. The objective of this portion of the experiment was to validate whether a tandem or series filtration system would significantly reduce discharge lead (II) ions. An optimized column of 0.38 g of MCM-41 mixed with 15.02 g sand (same sand used through-out this study) was placed in a 12.7 mm ID PVC column from 0 to 54 mm, and then from 54 to 216 mm 44.10 g of sand was placed. Feed stock was the discharge from a previous column. Columns were operated only to 50 bed volumes to expedite the evaluation. Column effluent concentrations due to recycling are depicted in Table 29.

Table 29. Effect of Recycling on Adsorption Performance
All lead (II) concentrations were measured within first 50 BVs of each column. Solute average flow rate = 2.1 m^3/m^2 h = 4.5 mL/min; influent pH = 6.74. Both columns were configured with the identical media amounts.

Column Description	$[Pb^{2+}]$ (μg/L)	Std Dev	n
Column 1 Influent	2811	2416	3
Column 1 Effluent and Column 2 Influent	472	58	2
Column 2 Effluent	260	169	10

An additional 44.7% reduction in effluent lead (II) concentration was achieved with a total removal of ca 93% in the tandem filtration test. The use of filtration in series is not a new practice and stormwater systems often use roughing filters, which contain coarse media followed by another filter unit with finer media. In some instances an additional filter bed with even finer media is appropriate (Logsdon et al. 2002).

4.8.4. Column Break Through; An Abbreviated Validation Check

A column was prepared simply to attempt to duplicate the response previously observed with MCM-41 materials. The results were again similar to those previously reported above, showing an immediate break through, followed by a restored adsorption behavior when free lead (II) ions were available (Figure 34). After initial start up break through with Ce/Co computed for < 0.2 to 130 BVs, the high initial adsorption slope was observed at about 10 BVs. The adsorption isotherm appeared to duplicate what had already been seen in Figure 33 for MCM-41. This phenomenon replicated the same pattern as observed in the initial adsorption column study and suggest initial adsorption is good until protons begin to be released by OSNP materials adsorbing cations. As shown in Figure 34, after initial breakthrough, the column filter began the cycle of precipitation, adsorption, and precipitation previously observed.

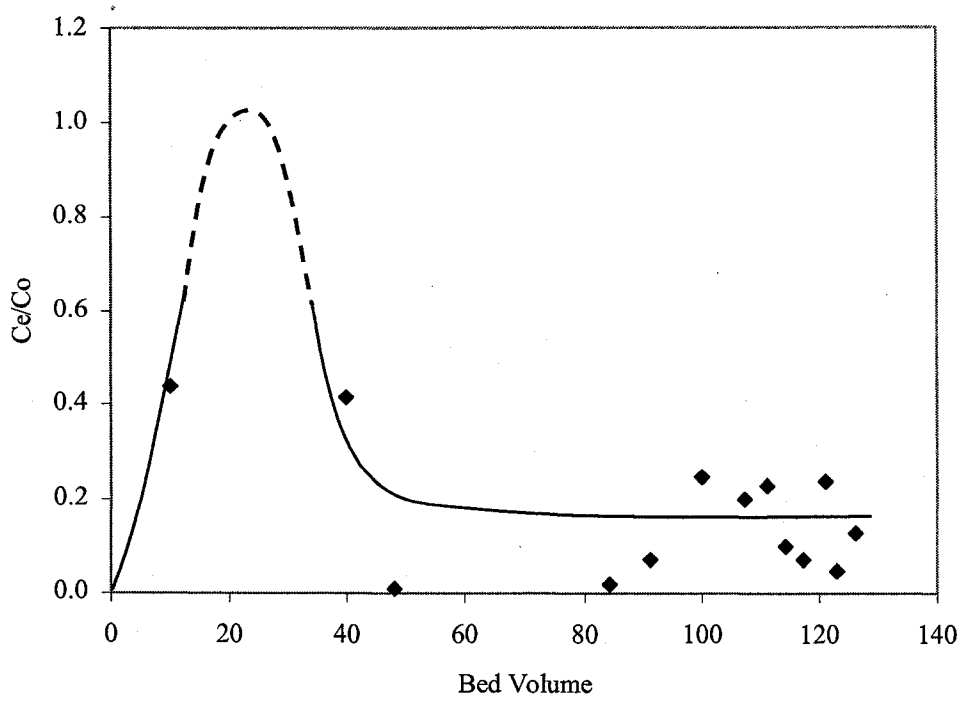

Fig. 38. Column Adsorption of Matrix Solute
Adsorption behavior mirrored that seen in Fig. 33. Average flow = 4.5 mL/min. Influent pH for BV 0 to 25 = 7.35 and pH for BV 25 – 123 = 6.48. Effluent pH for BV 0 to 25 = 6.64 and pH for BV 25-123 = 6.55. The Ce/Co response at 10 and 40 BVs are similar to MCM-41 response in Figure 33. The dotted plot represents expected response for the area without data points from ca. 15 to 35 BVs based on previous MCM-41 response. Total elapsed time was 20 BV = 1.5 h.

4.8.5. OSNP Material Performance Using Stormwater

Approximately 19 L (ca. 694 BV for columns used in this study) of stormwater was collected from a military shooting range in Virginia on 6 Oct 2006. Twenty-four hour precipitation on the day of collection was 2.03 in (51.56 mm). Collection was made at 12:15 pm and 0.58 in (14.73 mm) precipitation had fallen in the previous 12 hr. The sample was collected from a well-established outfall during moderate rainfall with wind NE 23 G 33. The outfall collects drainage from ca. 1.8 acres (0.73 ha) consisting of a

single rifle and handgun firing range with 5 yr and 40 yr aged impact berms. The 5 yr berm had been constructed in front of the older 40 yr aged impact berm.

Both berms had significant accumulations of lead fragments in the soils (See Appendix B for a more complete description; reference range VA1 and VA2). Lead (II) concentrations at this outfall from February 1998 to October 2006 were: dissolved = 192.7 μg/L (SD = 239.6, n = 22) and total = 601.0 μg/L (SD = 536, n = 14). Key parameters of stormwater when used in columns for this study, not when collected, were pH = 6.06, turbidity = 14 NTU, conductivity = 171.2 μs/cm and temperature 20 ± 3° C. Cations measured by ICP-MS for this stormwater are shown in Table 30 (Same as shown in Table 12, but repeated here to add RSD and instrument detection limit for each element). Cation and anion charge balance are shown in Table 31.

Table 30. Total Cations in Shooting Range Stormwater
RSD is relative standard deviation and DL is instrument detection limit. All measurements were by ICP-MS.

Element	μg/L	RSD	IDL	Element	μg/L	RSD	IDL
Ca	16401	4.2	1.1	Sb	27	0.3	0.0
Na	6685	14.3	1.1	Mn	20	0.3	0.0
Mg	2180	4.8	0.2	Cr	8	4.7	0.0
Fe	581	0.5	0.3	Ni	1	1.0	0.0
Cu	220	0.3	8.4	Mo	0.5	4.3	0.0
Pb	237	1.0	0.0	Sn	0.3	5.1	0.0
Zn	241	0.6	3.6				

Because of the limited stormwater supply the solution was split between three columns. The first and second column was configured with the optimized 216 mm media depth with the bottom 54 mm containing MCM-41 and sand (d_{10} = 0.20 mm). In the third column 216 mm of sand only was placed. The first 50 BVs for the MCM-41

amended and the sand only media columns found there was significant evidence to warrant rejection of the claim that the K_D variances are equal ($F = 20{,}965$, $P << 0.001$, $n = 12$). Average K_D values for MCM-41/sand and sand only media columns were 2.1 L/g (SD = 2.6, n = 6) and 0.02 L/g (SD = 1.9, n = 11), respectively.

Table 31. Stormwater Charge Balance
Stormwater collected 6 Oct 06 from Langley AFB VA small arms range outfall. DOC (Dissolved Organic Carbon) was estimated at 0.5 x TDS. Bromide and Fluoride were not analyzed. Sulfate was assumed < 5 mg/L. Bicarbonate data is an estimate. Typically bicarbonate in rainwater < 10 mg/L and < 200 mg/L in surface streams (Crittenden et al. 2005). The bicarbonate value used here is within this range and would be expected to be very low for this shooting range as measured soil carbonates averaged 43 mg/kg and were < 0.05 mg/kg in one berm (See VA1 and VA2 in Table 35).

		Eq/L	
Parameter	mg/L	Cations	Anions
Ammonia-N	0.059	4.21E-06	-
Antimony	0.0272	6.70E-07	
Bromide	0	-	0.00E+00
Bicarbonate	31.5	-	6.30E-04
Calcium	16.401	8.18E-04	-
Chlorides	0.001	-	2.82E-08
Copper	0.2196	6.91E-06	
Chrome	0.0082	3.15E-07	
DOC	85.6	-	8.56E-04
Fluoride	0.0	-	0.00E+00
Iron	0.5809	2.08E-05	-
Lead	0.5157	4.98E-06	
Magnesium	2.180	1.79E-04	-
Manganese	0.0198	7.21E-07	-
Molybdenum	0.0005	1.04E-08	
Nickel	0.0011	3.75E-08	
pH	7.43	3.72E-08	-
Potassium	< 5	6.39E-05	-
Sodium	6.685	2.91E-04	-
Strontium	0.0	0.00E+00	-
Sulfate	<5	-	5.21E-05
Sulfide	nd	-	-
Tin	0.0003	5.05E-09	
Zinc	0.241	7.37E-06	-
	Totals =	0.00140	0.00154
			RPD = 9.4%

The adsorbent media response to stormwater is shown in Figure 39. Distribution coefficient for MCM-41/sand and sand only columns at Ce/Co = 0.5 were 1.1L/g and 0.038 L/g, respectively. All three columns responded similar to previous adsorption profiles including a 0.55 pH drop at ca. BV = 75. MCM-41 began to improve after ca. 60 BV and continued to show decreasing lead (II) ion concentrations until a second Ce/Co = 0.5 was reached at ca. 200 BV and K_D = 46.2 L/g. Adsorption capacity at break through = 5.88 mg/g (0.028 mmol/g).

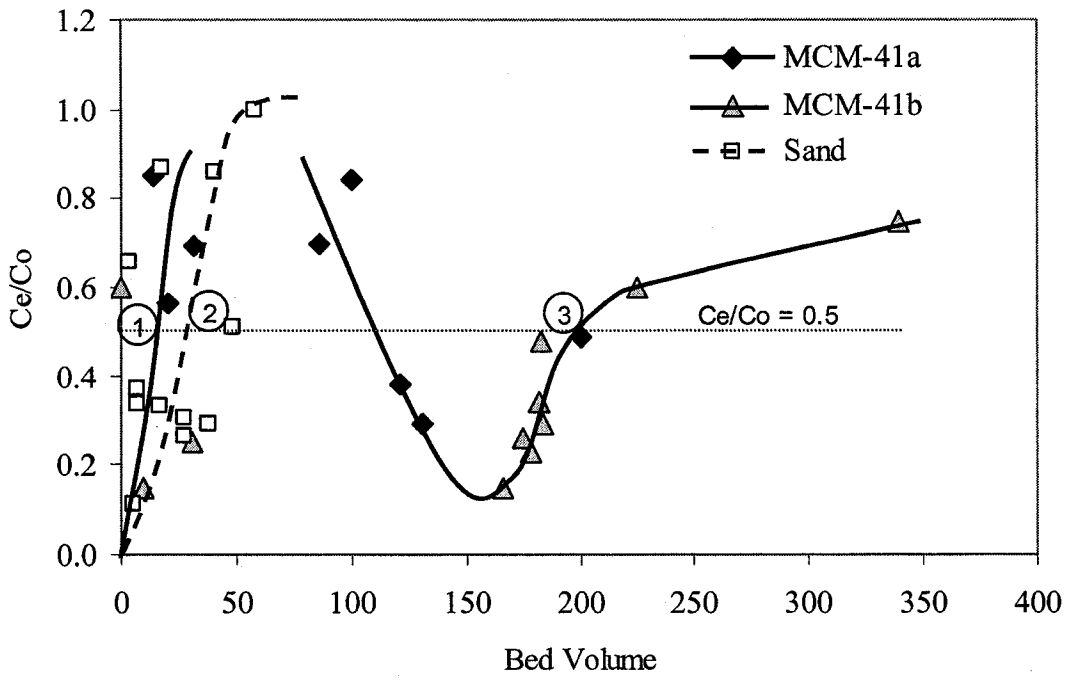

Fig. 39. Column Lead (II) Ion Adsorption of Stormwater
Initial breakthrough for MCM-41/sand (point 1) = 20.0 BV and sand (point 2) = 17.2 BV. MCM-41 breakthrough (point 3) = 200 BV. Average influent pH for BV 0 to 75 = 6.70 and average pH for BV 75 to 200 = 6.55. Average effluent pH for BV 0 to 75 = 6.57 and BV = 75 to 200 = 6.33. Stormwater influent lead (II) concentration = 515.7 µg/L (SD = 214.1, n = 7). Flow rate was by gravity that began at 8.5 mL/min and declined after 24 h to ca. 1.8 mL/min, and then after another 24 h to 0.98 mL/min. Average elapsed time was BV = 3.27 h. Concentrations of other cations and anions in solution are as shown in Table 30. MCM-41 column had 0.39 g OSNP and 15.03 g sand from the bottom of the column to 54 mm, and from 54 mm to 216 mm sand only.

4.9 Sand Filtration Conceptual Design

Sand filtration design may be based on one of three concepts: the Austin, the Washington, D.C. and the Delaware sand filter (U.S. EPA 1999). The main differences between these are: above or below ground, drainage area served, filter surface area, and runoff quantities. The Austin sand filtration system is applicable to large drainage areas and is suited for pervious / impervious surfaces, located at grade, and can be easily adapted to a 0.4-1.2 hectare shooting range (Figure 40). The Austin filter concept

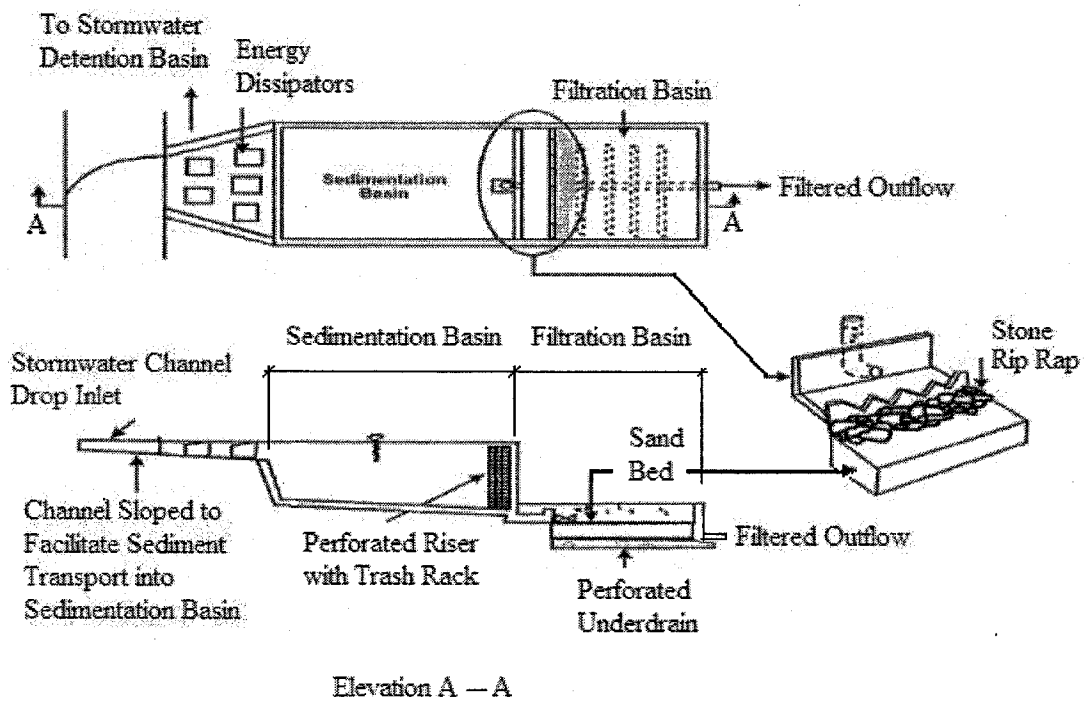

Fig. 40. Austin Sand Filter Design Concept
Modified from combination of designs by Barrett (2003) and Schueler (1992).

was selected and the design parameters developed following the Urban Drainage and Flood Control District, Denver, Colorado guidelines for sizing and operating sand filtration (Urbonas, 2002). Application research by Barrett (2003) University of Texas was also considered in the preparation of the concept design. The filter media was modified from a single media concept to include dual media, sand and OSNP material in accordance with the optimized column test completed in this study.

4.9.1 Conceptual Design Procedure

The selected area for the design was a small arms firing range located at Barksdale Air Force Base, Louisiana where outfall stormwater total lead (II) concentrations were from 5.2 – 490 μg Pb^{2+}/L. Range sizing parameters were as follows.

Table 32. Small Arms Range Filter Sizing Parameters
Concept of operation includes rain striking impact berm and sidewall, then runoff draining by gravity to detention volume catch basin, where large debris is removed as it flows to dual media filtration and then to discharge. SCS = Soil Conservation Service.

Range Parameter	Quantity (English – Metric)
Drainage Area	1.5 acres = 0.607 hectares
TSS Event Mean Concentration, EMC_{TSS}	120 mg/L
Average precipitation storm depth, P_{SD}	1.22 in = 28.19 mm
Range imperviousness, I_a	0.42 for Bermuda grass (*Cynodon dactylon*)
Runoff coefficient, C	0.29
Avg. annual run-off, $P_A = n * P_{SD} * C$	17.4 in = 442 mm
Avg. annual TSS load, L_{TSS}	161.2 lbs = 73.1 kg/y
Rainfall intensity for SCS Type 3 storm	8 in = 203.2 mm
Flow, Q = C*0.9*I*A/16	0.197 cfs = 482 m^3/d
Design Safety Factor	1.5
Detention Capture Volume, V	7,416 ft^3 = 210 m^3
Minimum Filtration Rate for 12 h cycle	0.21 m^3/m^2 h

4.9.2 Design Parameters Calculations

The average event mean concentration (EMC) of TSS for the small arms range catchment area was determined. The U.S. EPA (1983) EMC of TSS for Louisiana was 120 mg/L. From Table 13 this value falls within literature values for Western urban stormwater, and is slightly higher than the shooting range TSS collected for this study (avg = 52.2 mg/L, SD = 9.0, n = 3).

The average annual TSS was estimated using the runoff coefficient, which was calculated as $C = 0.858*I_a^3 - 0.788 * I_a^2 + 0.774 * I_a - 0.04$. A Soil Conservation Service range imperviousness factor for Bermuda grass (*Cynodon dactylon*), $I_a = 0.42$ was used yielding $C = 0.29$. The average storm precipitation was $P_{SD} = 1.11$ in for the area that occurs in 54 annual storm events. Annual average run-off from the range was therefore: $P_A = n * P_{SD} * C = 54*1.11*0.29 = 17.4$ in. The TSS load for the range catchment was estimated as $L_{TSS} = ac * 43{,}560.17 * (P_A/12) * (EMC * 10^{-6} * 62.4)$. Then for this design TSS load was $L_{TSS} = 73.1$ kg/y. Barrett (2003) has reported clogging of the filtration system when loads were between 5 and 7.5 kg/m^2 of the filter area. For this concept design a 100 m^2 filter would suggest a filter life = 7.0 y.

The time to fully discharge the captured volume was estimated based on historical storm event periodicities for Louisiana. Based on the concept design and proposed detention volume a conservative 12 h capture and discharge cycle would satisfy the 25-year storm event cycle. Barrett (2003) used a 24 h discharge cycle and Urbonas (2002) has recommended a preferred drainage time of 12 to 24 hours.

The proposed construction includes a detention filtration basin directly upstream and structurally connected to the filtration area. The total TSS in the basin would theoretically be captured by the filter, excluding any by-pass. The TSS concentration

leaving the filter may be expressed as TSS (Leaving) = EMC * R_T, where R_T = total system's average removal rate of TSS. Urbonas (2002) suggested removal rate for a 12 h drain time = 0.50. Therefore the TSS (Leaving) = 120*0.50 = 60 mg/L. The estimate for the average annual TSS load removed by the filter is then: Total average removed TSS = (60 mg/L / 120 mg/L) * 73.1 kg = 36.6 kg. The filter's maintenance frequency was assumed to be twice per year. Barrett (2003) has reported ca. 49 h/y maintenance was required to inspect, dewater, and structurally repair 5 Austin filters constructed in California.

The water capture volume for the range area was estimated as: Vwc = Volume max mean runoff * runoff coefficient (C) * mean storm depth in inches = 1.12 * 0.29 * 2.79 = 0.91 watershed inches. The value = 1.12 is from Urbona's (2002) graph of maximized coefficient versus drain time of captured volume in hours. Gravity drain time was assumed to be 2 in / hr (50.8 mm / hr). The 2.79 in was published by Driscoll et al. (1989) as mean storm depths of precipitation in the United States. This incorporates an additional safety factor since the Barksdale AFB area average precipitation is 1.22 in (28.19 mm). The calculation is then V_{WC} = (0.91 in * ft / 12 in) * 1.5 ac * 43,560 ft^2 / ac = 4,955 ft^3 = 140 m^3.

The sand filter area was estimated as total removed TSS / (TSS average/area * number of times filter is cleaned per year) = 36.6 kg / (0.18 kg/m^2 * 2) = 102 m^2. A second method uses the flow-through rate of the filter to estimate the sand filter area and was computed as: Area filter = (Capture volume) / (flow * time for capture volume to drain through filter in hours) = (140 m^3) / (0.115 m/h * 12 h) = 2,152 ft^2 = 101 m^2. The results obtained by the two methods are compared (102 m^2 vs. 101 m^2), and the flow rate

through the filter is adjusted until both results agreed. The filtration design area needed for this sand filtration unit = 100 m^2 (Figure 41).

From the above an in-situ sand filtration unit of 100 m^2 surface area was required based on a superficial flow rate of 0.11 m/h. Laboratory gravity stormwater flow rate through 216 mm of MCM-41/sand column after 24 h was 1.75 mL/min or 0.71 m/h. The lead (II) ion removal rates were ca. 60 to 80 %, hence a tandem or second filtration system may be required to further reduce effluent concentrations. The first filtration unit would be located inside the range berms and discharge via piping to a second filtration unit located outside the berm area, but prior to discharge to the permitted outfall

4.9.3 Filtration Unit Concept Design

The filtration unit could be constructed as shown in Figure 41 as an open-air filter with a separate sedimentation basin. Since the shooting range complex does not typically have trees within the range complex liter accumulation should be minimal and allow the construction of an open-air filtration unit. This will facilitate maintenance access, which has been identified as a critical issue for Austin filters.

The in-ground filtration unit must have a minimum of 1 m inlet to outlet vertical height to operate hydraulically (Barrett 2003). This study used d_{50} = 0.46 mm sand, but it may be appropriate to consider a greater d_{50} sand along with pelletization of the nanoporous materials, which as synthesized have powder fractions. To facilitate maintenance monitoring, automatic samplers similar to Sigma 900 Max series and flow meters similar to Sigma 950 series should be part of the construction.

Barrett (2003) reported 1999 costs for 5 Austin concrete cast-in place filters constructed in Los Angeles (3 ea) and San Diego (2 ea) at an average cost per unit = $257,375 or $2,009 / m^3 of water quality volume. These costs included recycle pumps

for some units because there was inadequate elevation for the required hydraulic head to operate the systems by gravity flow. Further, some of the filter units were part of larger California highway projects. Assuming these factors and adjusting for an annual inflation of 2% per year, 2007 construction cost would be approximately $225,000 to

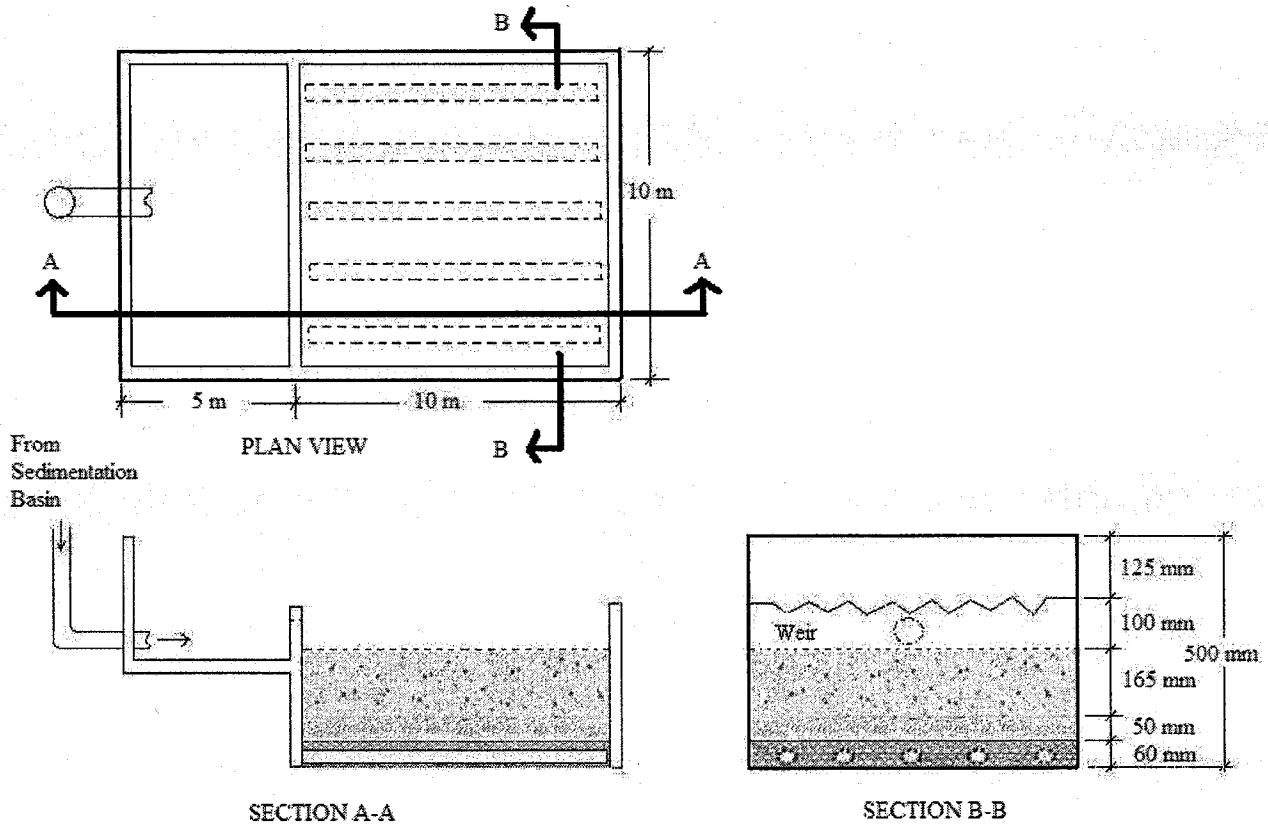

Fig. 41. In-Situ Sand Bed Filtration Design Concept
Under drain consist of PVC pipe 10 – 15 cm in diameter with 1 cm perforations. Filter fabric is wrapped around each under drain pipe to prevent sand and particulates from discharging. The system is designed to collect and treat the first 1.3 cm (0.5 in) of runoff.

$250,000 range. This may be considered the "high end" design due to type of construction (in conjunction with state highway projects) and the location (Los Angeles and San Diego, California). In separate studies by the U.S. EPA (1999) the estimate for

an Austin sand filter to support a 0.4 ha (1 ac) drainage area was estimated at $18,500 in 1997. For 0.61 ha (1.5 ac) initial costs would increase by 40% to ca. $25,900. Inflating to 2007 dollars at inflation, i = 2% for n = 10 y, the estimated Austin filter costs = $P(1 + i)^n = 25900 * (1 + .02)^{10} =$ $31,572.

The costs for nanoporous materials were not estimated, as they are not commercially available for wholesale purpose for this intended purpose. However, the life cycle of the filter media can be estimated as follows. The design concept from this study would require 2.95% or say 3.00% w/w, nanoporous material in the first 54 mm of the 100 m^2 sand filtration unit. The required filtration unit volume for the OSNP material & sand mixture = 10 m x 10 m x 0.054 m = 5.4 m^3. OSNP materials optimized in this study requires 3.0% w/w, therefore assuming 1,602 kg dry sand/m^3 x 5.4 m^3 x 0.03 = 259.52 kg MCM-41 needed. Based on this column study adsorption capacity = 14.627 mg/g. Then the total lead (II) ion capacity of the filtration unit would be = 259.52 kg x 14.627 mg/g = 3,796 g lead (II) ion. Assuming average lead (II) ion concentration in stormwater = 194 μg/L and the capture volume per storm event =140 m^3, for 54 storm events per year for Barksdale AFB, the total life cycle for the MCM-41 adsorbent would be 2.58 y. This is a conservative estimate, as it assumes no removal by the sand above the OSNP material and sand mixture.

5. SUMMARY AND CONCLUSION

Field analysis and laboratory experiments were conducted to evaluate the lead (II) ion adsorptive properties by organosilicate nanoporous materials. OSNP materials were used as amendments to sand filtration for lead (II) ion removal from synthetic and shooting range stormwaters. Series order by functionalization of silica-based mesostructure templates for removal of lead (II) ions in batch reactions was phosphorus > amine > hydroxyl > ether > thiol. Amine functionalization was selected for further batch and column studies; the phosphate functionalization was not used because of the potential contribution to eutrophication in receiving streams. The HMS and MCM-41 materials were characterized by a variety of techniques, which reflected literature mesoporous structure and pore size.

Batch competitive ion adsorption studies found a strong dependence on ionic strength that implies an outer-sphere complexation and electrostatic bonding metal attraction. Outer-sphere complexation indicates a bonding mechanism that is less stable and highly susceptible to pH variations. Stumm (1992) found there is a 1 to 2 pH unit range where sorption will rise from near zero to almost 100%. The affect of pH on OSNP material adsorption showed maximum adsorptive properties in the 5.5 to 6.5 pH range.

Column designs were optimized using a 2^3 factorial design response surface. The three factors used were percent by w/w of OSNP materials, media depth and filtration rate. A linear response surface was developed with optimized column parameters of ca. 2.95 % OSNP material (w/w), 216 mm media depth and 11.0 mL/min filtration rate, which were then used for subsequent column studies. Some experiments were operated by gravity flow and were stopped for extended periods to simulate operational conditions

expected in the field application. OSNP materials had 28.1 % increase in headloss compared to sand only columns. HMS showed leaching characteristics in a 48 d study (P = 0.005), but the MCM-41 material did not show a similar response (P = 0.19).

The fraction of metal species in solution was directly influenced by pH, and competing ions (i.e. ionic strength). The unique characteristic of OSNP materials to release protons while adsorbing metal cations (i.e. basically an ionic exchange process) would predict a need to explore carefully the application of this material before a field application could be considered. For the pH range < 6.7 free lead (II) ions are available for adsorption. pH > 6.7 $Pb(OH)_2$ precipitate is the dominant controlling species. In the presence of other cations like Mo, PbMoO4(s) controlled solubility and this would be an important consideration for the application of this material.

The objective of the current work was to examine the adsorptive properties of the amine-containing mesoporous silica HMS and MCM-41 toward lead (II) ions in non-competing and competing ion aqueous solution. MCM-41 media and sand columns were also operated using stormwater collected from a shooting range. OSNP materials fit both Langmuir and Freundlich isotherm models in batch reactions and the Freundlich model most closely represented the adsorption performance of both materials (r^2 = 0.99). HMS had a lead (II) ion adsorption capacity of 1.28 mg/g in batch reactions and MCM-41 had 10.75 mg/g (0.052 mmol/g). In column studies, lead (II) ion adsorption for spiked tap water in single pass filtration at break through (Ce/Co = 0.5) was for HMS = 2.74 mg/g (0.013 mmol/g) and MCM-41 = 14.627 mg/g (0.071 mmol/g). Stormwater lead (II) ion adsorption in single pass filtration for MCM-41 = 5.84 mg/g (0.028 mmol/g).

An Austin single pass sand filtration unit was proposed with estimated costs starting ca. $31,572 to a high-end cost of ca. $250,000 was presented. Adsorbent life

cycle based on 140 m^3 capture volume per storm event at 194 µg/L total lead would take 2.6 y before the MCM-41 adsorbent material would reach capacity. Discharge to a second filtration unit did reduce lead (II) ion concentrations by 44.7% and may be necessary to achieve desired end concentrations. Recycling of wastewater may be yet another consideration. Adjustment to media size used in this study (d_{50} = 0.51 mm) could also be considered to improve hydraulics, although the sand used was well within typical values used by others, namely Barrett (2003) and Sansalone (1999) who used 0.6 mm and 0.5 mm sand, respectively in single pass through sand filtration units.

In the current work OSNP materials in combination with sand media did improve lead (II) ion adsorption performance and capacity. The hydrophilic channels in OSNP materials allow the transport of water-soluble species such as metallic cations into the meso pores. This further allows increased opportunities for contact with amino-surfactants. Hence, further improvements to the OSNP materials performance may be obtained by increasing the surface area and pore volume during synthesis as proposed by Xu et al. (1999), Walcarius et al. (2003), Sayari et al. (2005) and others.

The MCM-41 mesoporous structures have well defined hexagonal ordered pore structure that can be controlled by the choice of surfactants and reaction parameters. In this study it was shown OSNP materials might be used in conjunction with traditional sand media be used to enhance lead (II) ion adsorption, however high ionic strength solution of primary metal cations, plus the deprotonation behavior of OSNP materials adsorbing cations lowers pH and influence OSNP adsorption effectiveness. The OSNP material has a large BET surface area (typically > 1,000 m^2/g) with hydrophobic and hydrophilic properties that can also be modified. The OSNP material showed promise as

an innovative molecular sieve for lead (II) ion adsorption for in-situ sand filtration applications.

5.1 Perspectives on Future Work

There were many questions and additional areas of study identified during the course of this study. If time and money had allowed, each should have been pursued to more fully elucidate the potential and condition of application of OSNP materials. The following provides a summary of perspectives on future work that is needed.

The OSNP materials have at least one dimension in the nanometer size and as such may reduce media porosity. While the straining is typically the primary mechanism for particulate removal in filtration, the increase in head loss in field applications with OSNP materials could limit their applications. Pelletization of OSNP materials would agglomerate the materials into larger media diameters and allow the less hindered flow of solutions through the porous medium. Pelletization by Hartmann and Bischof (1999) have demonstrated the possibility as previously discussed.

The batch reactions in the current study were hampered by lack of access to ICP-MS analysis such that the implications and preference of cations by OSNP materials were not completely explored. Additional work is needed to better understand the selective surface chemistry of organosilicate materials and how they can be "tuned" to specific cations. Sayari et al. (2005) has reported MCM-41 amine functionalized materials sorption affinity for three cations as Cu > Co > Ni. The structure, porosity, density of organic groups, reaction type, and analyte size all affect the adsorption characteristics. For example, Walcarius et al. (2003) reported that increasing the amount of grafted moieties in the mesopores caused reduced mass-transfer rates because of greater steric

hindrance. The subtleties in design of these mesoporous materials are sensitive and require further research and development.

The current work chose a starting range of amendment amounts, which were optimized within the chosen range. Additional work for amendment amounts in a different range should be completed. The performance in conjunction with other proven medias like zeolites, activated carbon, anthracite, etc. is needed to optimize the results. In theory this optimization could design target analytes for removal while excluding others. In the earlier part of this study HMS had a very selective adsorption response in batch reactions to a solute with various nitrate salts of metals. Lam et al. (2006) showed that SH-MCM-41 had selective adsorption of silver (I) over copper (II) ions, and the behavior was not influenced by metal concentration, anion, or pH. They proposed the HSAB principle could be a useful guide in the development of selective adsorbents. Brown et al. (1999) reported thiol functionalized silicas were selective for mercury (II) ions over cadmium (II), lead (II), zinc (II), cobalt (II) iron (II) copper (II) and nickel (II). The selective and enhanced performance of the OSNP material may be exploited in conjunction with other adsorptive media.

Desorption of the media needs further study. Procedures to remove the analyte while retaining the mesoporous structure must be developed. Most researchers have used acids to desorb and regenerate adsorbents. Wright (2006) used vinegar as a desorbent with some success, while Ganjali et al. (2004) used 3 M HOAc, 3 M HNO_3, 3 M HBr and 3M HCl. The use of mild acids is desired to avoid creating a hazardous waste stream as defined by the Resource Conservation and Recovery Act regulations for corrosiveness.

In some batch and column reactions effluent amounts exceeded available influent lead (II) ion concentrations. This phenomenon may be understood when MCM-41 is

mixed in aqueous solutions the polar water molecules fills the entire length of the pores without voids or hollow spaces (Tun and Mason 2002). Initially this may concentrate metal ions in the equilibria or column effluents. In surface complexation these surface hydroxyl groups exchange with other ligands and is in fact the main mechanism of ligand adsorption (Stumm, 1992). While initial effluent lead (II) ion concentrations were high ligand exchanges with the adsorbate dropped these amounts. Additional work to more fully characterize this attribute should be undertaken to accommodate this in the design of OSNP material applications.

5.2 Conclusion

This study used OSNP materials MCM-41 and HMS as novel adsorbents for the removal of lead (II) ions from aqueous and natural stormwaters. The empirical data and analysis completed suggests the following conclusions may be proposed.

1. Amine functionalized MCM-41 and HMS mesoporous materials were more effective as lead (II) ion adsorbents than thiol, hydroxyl or ether functionalizations.

2. OSNP materials and sand media in a declining rate single pass filtration increase headloss, which must be appropriately considered in application designs.

3. Batch and column reactions of OSNP materials can be effectively modeled with Langmuir and Freundlich isotherms. The OSNP materials adsorption behavior was characteristic of outer-sphere complexation and electrostatic attractive forces (i.e. van der Waals).

4. As for most adsorption process pH is the "master variable." The application of OSNP materials has a specific pH range (5.0 – 6.5) where lead (II) ion adsorption is optimized. This pH range is typical of shooting range stormwater run-off. Above pH = 6.7 lead precipitates will control solubility. If Mo is in solution with Pb, PbMoO4 can

precipitate at ca. pH = 2.5 to 9.6 controlling solubility. Lead molybdate can interfere with OSNP material adsorption.

5. MCM-41 was more susceptible to the presence of competing ions than HMS.

6. For the shooting range conditions of this study, like rainfall, and lead (II) ion concentration in stormwater run-off, the MCM-41 / sand media could operate 2.6 y before Ce/Co = 0.5 breakthrough.

REFERENCES

Abdel-Fattah, T. M., and Bishop, B. (2004). "Organo-silicate nanocompostes for the removal of chlorinated phenols from aqueous media: Kinetics and environmental stability." *Journal of Environmental Science and Health, Part A*, A39(11-12), 2855-2866.

Abdel-Fattah, T. M., Isaacs, L. K., and Payne, K. B. (2003). "Small Arms Range Lead Management Issues: Activated Carbon Molecular Sieves (5A and 13X), and Naturally Occurring Zeolites as Lead Adsorbents." *Federal Facilities Environmental Journal*, 14(2), 113-126.

Algarra, M., Jimenez, M. V., Rodriguez-Castellon, E., Jimenez-Lopez, A., and Jimenes-Jimenez, J. (2005). "Heavy metals removal from electroplating wastewater aminopropyl-Si MCM-41." *Chemosphere*, 59, 779-786.

Amato, I. (1993). "Chemists work their way from pores to riches." *Science*, 259(5097), 891.

Antochshuk, V., Olkhovyk, O., Jaroniec, M., Park, I.-S., and Ryoo, R. (2003). "Benzoylthiourea-modified mesoporous silica for mercury(II) removal." *Langmuir*, 19, 3031-3034.

Astrup, T., Boddum, J. K., and Christensen, T. H. (1999). "Lead Distribution and Mobility in a Soil Embankment Used as a Bullet Stop at a Shooting Range." *Journal of Soil Contamination*, 8(6), 653-665.

Babel, S., and Kurniawan, T. A. (2003). "Low-cost Adsorbents for Heavy Metals Uptake from Contaminated Water: A Review." B97, 219-243.

Barrett, M. E. (2003). "Performance, cost, and maintenance requirements of Austin sand filters." *Journal Water Resource Planning and Management*, 129(3), 243-242.

Basunia, S., and Landsberger, S. (2001). "Contents and leachability of heavy metals (Pb, Cu, Sb, Zn, As) in soil at the Pantex firing range, Amarillo, Texas." *Journal of the Air & Waste Management Association*, 51(10), 1428-1435.

Beck, J. S., Vartuli, C., Roth, W. J., Leonowicz, M. E., Kresge, C. T., Schmitt, K. D., Chu, C. T.-W., Olson, D. H., Sheppard, E. W., McCullen, S. B., Higgins, J. B., and Schlenker, J. L. (1992). "A new family of mesoporous molecular sieves prepared with liquid crystal templates." *J. Am. Chem. Soc.*, 114, 10834-10843.

Benjamin, M. M. (2002). *Water Chemistry*, McGraw-Hill Companies, New York, NY.

Berggren, A., Palmqvist, A. E. C., and Holmberg, K. (2005). "Surfactant-templated mesostructured materials from inorganic silica." *Soft Matter*, 1, 219-226.

Bilinski, H., and Schindler, P. (1982). "Solubility and equilibrium constants of lead in carbonate solutions (25oC, I = 0.3 mol dm-3)." *Geochimica et Cosmochimica Acta*, 46(6), 921-928.

Boller, M. (1997). "Tracking heavy metals reveals sustainability deficits of urban drainage systems." *Water Science and Technology*, 35(9), 77-87.

Bradl, H. B. (2004). "Adsorption of heavy metal ions on soils and soils constituents." *Journal of Colloid and Interface Science*, 277, 1-18.

Branton, P. J., Hall, P. G., and Sing, K. S. W. (1995). "Physisorption of alcohols and water vapour by MCM-41, a model mesoporous adsorbent." *Adsorption*, 1(1), 77-82.

Brown, J., Mercier, L., and Pinnavaia, T. J. (1999). "Selective adsorption of Hg2+ by thiol-functionalized nanoporous silica." *Chemical Communications*, 1999, 69-70.

Bruell, R., Nikolaidis, N. P., and Long, R. P. (1999). "Evaluation of remedial alternatives of lead from shooting range soil." *Environmental Engineering Science*, 16(5), 403-414.

Bulut, Y., and Baysal, Z. (2006). "Removal of Pb(II) from wastewater using wheat bran." *Journal of Environmental Management*, 78, 107-113.

Burgos, W. D. (1997). "Heavy Metal Adsorbents for Stormwater Pollution Prevention." U.S. Navy Report NSRP 0514, San Diego, CA.

Burkett, S. L., Sims, S. D., and Mann, S. (1996). "Synthesis of hybrid inorganic-organic mesoporous silica by co-condensation of siloxane and organosiloxane precursors." *Chemical Communications*, 11, 1367-1368.

Burton, G. A., and Pitt, R. (2001). *Stormwater effects handbook: A toolbox for watershed managers, scientists, and engineers*, Lewis Publishers, Boca Raton, FL.

Buzier, R., Tusseau-Vuillemin, M.-H., and Mouchel, J.-M. (2006). "Evaluation of DGT as a metal speciation tool in wastewater." *Science of the Total Environment*, 358(1-3), 277-285.

Cajuste, L. J., Carrillo, R. G., Cota, E. G., and Laird, R. J. (1991). "The distribution of metals from wastewater in the Mexican valley of Mezquital." *Water, Air, & Soil Pollution*, 57-58(1), 763-771.

Cao, X., Ma, L. Q., Chen, M., Hardison, D. W., and Harris, W. G. (2003). "Lead transformation and distribution in the soils of shooting ranges in Florida, USA." *Science of the Total Environment*, 307, 179-189.

Cao, X., Ma, L. Q., Chen, M., Hardison, D. W., and Harrisa, W. G. (2003). "Weathering of Lead Bullets and Their Environmental Effects at Outdoor Shooting Ranges." *Journal of Environmental Quality*, 32, 526-534.

Characklis, G. W., and Wiesner, M. R. (1997). "Particles, metals, and water quality in runoff from large urban watershed." *Journal of Environmental Engineering*, 123(8), 753-759.

Chen, M., Daroub, H., Ma, L. Q., Harris, G., and Cao, X. (2002). "Characterization of Lead in Soils of a Rifle/Pistol Shooting Range in Central Florida, USA." *Soil & Sediment Contamination*, 11(1), 1-17.

Chipasa, K. B. (2003). "Accumulation and fate of selected heavy metals in a biological wastewater treatment system." *Waste Management*, 23(2), 135-143.

Choudhary, V. R., and Mantri, K. (2000). "Adsorption of aromatic hydrocarbons on highly siliceous MCM-41." *Langmuir*, 16, 7031-7037.

Citeau, L., Lamy, I., vanOort, F., and Elsass, F. (2003). "Colloidal facilitated transfer of metals in soils under different land use." *Colloids and Surfaces A: Physicochem. Eng. Aspects*, 217, 11-19.

Craig, J. R., Rimstidt, J. D., Bonnaffon, C. A., Collins, T. K., and Scanlon, P. F. (1999). "Surface Water Transport of Lead at a Shooting Range." *Bulletin of Environmental Contamination and Toxicology*, 63(3), 312-319.

Crittenden, J. C., Trussell, R. R., Hand, D. W., Howe, K. J., and Tchobanoglous, G. (2005). *Water treatment: Principles and Design*, 2nd, John Wiley & Sons, Inc., Hoboken, NJ.

Darling, C. T. R., and Thomas, V. G. (2003). "The distribution of outdoor shooting ranges in Ontario and the potential for lead pollution of soil and water." *Science of the Total Environment*, 313, 235-243.

Davis, A. P., Shokouhian, M., and Ni, S. (2001). "Loading estimates of lead, copper, cadmium, and zinc in urban runoff from specific sources." *Chemosphere*, 44(5), 997-1009.

Davis, A. P., Shokouhian, M., Sharma, H., and Minami, C. (2001). "Laboratory study of biological retention for urban stormwater management." *Water Environ. Research*, 73(1), 5-14.

Davis, J. A., and Leckie, J. O. (1978). "Surface ionization and complexation at the oxide/water interface II. Surface properties of amorphous iron oxyhydroxide and adsorption of metal ions." *Journal of Colloid and Interface Science*, 67(1), 90-107.

deMatos, A. D., Fontes, M. P. F., Costa, L. M. D., and Martinez, M. A. (2001). "Mobility of heavy metals as related to soil chemical and mineralogical characteristics of Brazilian soils." *Environmental Pollution*, 111(3), 429-435.

Dermatas, D., Menounou, N., Dutko, P., Dadachov, M., Arienti, P., and Tsaneva, V. (2003). "Lead and Copper Contamination in Small Arms Firing Ranges." *Proceedings of the 8th International Conference on Environmental Science and Technology*, Lemnos Island, Greece, 134-141.

Dionysiou, D. D. D., and Wiesner, M. (2007). "Environmental Nanotechnology." *Environmental Engineering Science*, 24(1), 1.

Droste, R. L. (1997). *Theory and practice of water and wastewater treatment*, John Wiley & Sons, Inc., New York, NY.

Ekster, A., and Jenkins, D. (1996). "Nickel and copper removal at the San Jose/Santa Clara water pollution control plant." *Waster Environment Research*, 68, 1172-1178.

El-Taweel, G. E., and Ali, G. H. (2000). "Evaluation of roughing and slow sand filters for water treatment." *Water, Air, & Soil Pollution*, 120, 21-28.

Engstrom, A. (2004). "Characterizing water quality of urban runoff: Interactions of heavy metals and solids in Seattle residential catchments," University of Washington, Seattle.

Fenelonov, V. B., Romannikov, V. N., and Derevyankin, A. Y. (1999). "Mesopore Size and Surface Area Calculations for Hexagonal Mesophases (types MCM-41, FSM-16, etc.) Using Low-angle XRD and Adsorption Data." *Microporous and Mesoporous Materials*, 28, 57-72.

Feuston, B. P., and Higgins, J. B. (1994). "Physical sorption of argon, nitrogen and oxygen by MCM-41, a model mesoporous adsorbent." *Journal of Physical Chemistry*, 98(16), 4459-4462.

Fowler, C. E., Burkett, S. L., and Mann, S. (1997). "Synthesis and characterization of ordered organo-silica-surfactant mesophases with functionalized MCM-41-type architecture." *Chemical Communications*, 18, 1769-1770.

Gagnon, C., and Saulnier, I. (2003). "Distribution and fate of metals in the dispersion plume of a major municipal effluent." *Environmental Pollution*, 124, 47-55.

Ganjali, M. R., Babaei, L. H., Badiei, A., Ziarani, G. M., and tarlani, A. (2004). "Novel method for the fast preconcentration and monitoring of a ppt level of lead and copper with a modified hexagonal mesoporous silica compound and inductively coupled plasma atomic emission spectrometry." *Analytical Sciences*, 20, 725-729.

Goel, J., Kadirvelu, K., Rajagopal, C., and Garg, V. K. (2005). "Removal of lead(II) by adsorption using treated granular activated carbon: Batch and column studies." *Journal of Hazardous Materials*, 125(1-3), 211-220.

Hardison, D. W., Ma, L. Q., Luongo, T., and Harris, W. G. (2004). "Lead contamination in shooting range soils from abrasion of lead bullets and subsequent weathering." *Science of the Total Environment*, 328, 175-183.

Hartmann, M., and Bischof, C. (1999). "Mechanical stability of mesoporous molecular sieve MCM-48 studied by adsorption of benzene, n-heptane, and cyclohexane." *Journal of Physical Chemistry*, 103(30), 6230-6235.

Hettiarachchi, G. M., Pierzynski, G. M., and Ransom, M. D. (2000). "In situ stabilization of soil lead using phosphorus and manganese oxide." *Environmental Science & Technology*, 34(21), 4614-4619.

Hohl, H., and Stumm, W. (1976). "Interaction of Pb^{2+} with hydrous α-Al_2O_3." *Journal of Colloid and Interface Science*, 55(2), 281-288.

Huang, L., Guo, W., Deng, P., Xue, Z., and Li, Q. (2000). "Investigation of synthesizing MCM-41/ZSM-5 composites." *Journal Physical Chemistry*, 104, 2817-2823.

Huo, Q., Leon, R., Petroff, P. M., and D.Stucky, G. (1995). "Mesostructure design with gemini surfactants: Supercage formation in a three-dimensional hexagonal array." *Science*, 268(5215), 1324-1327.

Huo, Q., Margolese, D. L., Ciesla, U., Feng, P., Gier, T. E., Sieger, P., Leon, R., Retroff, P. M., Schuth, F., and Stucky, G. D. (1994). "Generalized synthesis of periodic surfactant/inorganic composite materials." *Nature*, 368, 317-321.

Iler, R. K. (1979). *The chemistry of silica*, John Wiley & Sons, NY, NY.

Irving, H., and Williams, R. J. P. (1953). *Journal of Chemical Society*, 3192-3210.

Isaacs, L. (2007). "Lead leaching from soils and in storm waters at twelve military shooting ranges." *Journal of Hazardous Substance Research*, VI, 1-30.

Isaacs, L. K. (2003). "Lead Immobilization in Soil and Stormwater from a Small Arms Range Using Phosphate, Sedimentation, Filtration, and Organo-silicate Nanocomposite Adsorption Treatments," Report, Christopher Newport University, Newport News, VA.

Isaacs, L. K., Kull, R., and Montalvo, M. (2005). "Small Arms Range Lead Migration in Stormwater Run-off." *U.S. Air Force Environmental Training Symposium*, Louisville, KY, 525-535.

Jaroniec, M., Kruk, M., Shin, H. J., Ryoo, R., Sakamoto, Y., and Terasaki, O. (2001). "Comprehensive characterization of highly ordered MCM-41 silicas using nitrogen adsorption, thermogravimetry, X-ray diffraction and transmission electron microscopy." *Microporous and Mesoporous Materials*, 48, 127-134.

John, P. C. (2002). "Pollution hazards from sporting shooting ranges: Environmental and economic considerations illustrated from a proposal at Bodalla state forest Australia." Australian National University.

Johnson, C. A., Moench, H., Wersin, P., Kugler, P., and Wenger, C. (2005). "Solubility of antimony and other elements in samples taken from shooting ranges." *Journal Environmental Quality*, 34, 248-254.

Jorgensen, S. S., and Willems, M. (1987). "The Fate of Lead in Soils: The Transformation of Lead Pellets in Shooting-Range Soils." *Ambio: A Journal of the Human Environment*, 16(1), 11-15.

Juang, L.-C., Wang, C.-C., and Lee, C.-K. (2006). "Adsorption of basic dyes onto MCM-41." *Chemosphere*, 64(11), 1920-1928.

Kaiser, H. (1970). "Report for analytical chemists. II. Quantitation in elemental analysis." *Analytical Chemistry*, 42(4), 26A-59A.

Kisler, J. M., Stevens, G. W., and O'Connor, A. J. (2001). "Adsorption of proteins on mesoporous molecular sieves." *Mater. Phys. Mech.*, 4, 89-93.

Kostal, J., Prabhukumar, G., Lao, U. L., Chen, A., Matsumoto, M., Mulchandani, A., and Chen, W. (2005). "Customizable biopolymers for heavy metal remediation." *Journal of Nanoparticle Research*, 7, 517-523.

Kresge, C. T., Leonowica, M. E., Roth, W. J., Vartuli, J. C., and Beck, J. S. (1992). "Ordered mesoporous molecular sieves synthesized by a liquid-crystal template mechanism." *Nature*, 359, 710.

Lam, K. F., Yeung, K. L., and McKay, G. (2006). "An investigation of gold adsorption from a binary mixture with selective mesoporous silica adsorbents." *Journal of Physical Chemistry*, 110, 2187-2194.

Lam, K. F., Yeung, K. L., and McKay, G. (2006). "A rational approach in the design of selective mesoporous adsorbents." *Langmuir*, 22(23), 9632-9641.

Lanouette, K. H. (1977). "Heavy Metals Removal." Chemical Engineering Deskbook, 73-80.

Lim, M. H., Blanford, C. F., and Stein, A. (1998). "Synthesis of ordered microporous silicates with organosulfur surface groups and their applications as solid acid catalysts." *Chemical Materials*, 10, 467-470.

Lin, Z., Comet, B., Qvarfort, U., and Herbert, R. (1995). "The chemical and mineralogical behaviour of Pb in shooting range soils from central Sweden." *Environmental Pollution*, 89(3), 303-309.

Logsdon, G. S., Kohne, R., Abel, S., and LaBonde, S. (2002). "Slow sand filtration for small water systems." *Journal of Environmental Engineering and Science*, 1(5), 339-348.

London, J. W., Shaw, L. M., Theodorsen, L., and Stromme, J. H. (1982). "Application of response surface methodology to the assay of gamma-glutamyltransferase." *Clinical Chemistry*, 28, 1140-1143.

Long, G. L., and Winefordner, J. D. (1983). "Limit of detection. A closer look at the IUPAC definition." *Analytical Chemistry*, 55(7), 712A-724A.

Ma, L. Q., Cao, R. X., Hardison, D., Chen, M., Harris, W. G., and Sartain, J. (2002). "Environmental impacts of lead pellets at shooting ranges and arsenical herbicides on golf courses in Florida." Florida Center for Solid and Hazardous Waste Management, University of Florida, Report No. 02-01.

Macquarrie, D. J. (1996). "Direct preparation of organically modified MCM-type materials. Preparation and characterisation of aminopropyl-MCM and 2-cyanoethyl-MCM." *Chemical Communications*, 16, 1961-1962.

McBride, M. B., Richards, B., Steenhuis, T., Russo, J. J., and Suave, S. (1997). "Mobility and solubility of toxic metals and nutrients in soils fifteen years after sludge application." *Soil Science*, 162, 487-496.

McLean, J. E., and Bledsoe, B. E. (1992). "Behavior of metals in soils." *EPA/540/S-92/018*, Environmental Protection Agency.

McPherson, T. N., Burian, S. J., Stenstrom, M. K., Turin, H. J., Brown, M. J., and Suffet, I. H. (2005). "Trace Metal Pollutant Load in Urban Runoff from a Southern California Watershed." *Journal of Environmental Engineering*, 131(7), 1073-1080.

Mercier, L., and Pinnavaia, T. J. (1998). "A Functionalized Porous Clay Heterostructure for Heavy Metal Ion (Hg2+) Trapping." *Microporous and Mesoporous Materials*, 20, 101-106.

Mercier, L., and Pinnavaia, T. J. (1998). "Heavy metal ion adsorbents formed by the grafting of a thiol functionality to mesoporous silica molecular sieves: Factors affecting Hg(II) uptake." *Environmental Science & Technology*, 32(18), 2749-2754.

Mokaya, R. (1999). "Improving the stability of mesoporous MCM-41 silica via thicker more highly condensed pore walls." *Journal Physical Chemistry*, 103(46), 10204-10208.

Mokaya, R., Zhou, W., and Jones, W. (2000). "Restructuring of mesoporous silica: high quality large crystal MCM-41 *via* a seeded a recrystallisation route." *Journal of Materials Chemistry*, 10, 1139-1145.

Montgomery, D. C. (2005). *Design and analysis of experiments*, John Wiley & Sons, Inc., Hoboken, NJ.

Moriyama, K., Mori, T., Arayaskiki, H., Saito, A., and Chino, M. (1989). "The amount of heavy metals derived from domestic sources." *Water Science and Technology*, 21, 1913-1916.

Muhammad, N., Parr, J., Smith, M. D., and Wheatley, A. D. (1998). "Adsorption of Heavy Metals in Slow Sand Filters." *24th WEDC Conference*, Islamabad, Pakistan, 346-349.

Muroyama, N., Ohsuna, T., Ryoo, R., Kubota, Y., and Terasaki, O. (2006). "An analytical approach to determine the pore shape and size of MCM-41 materials from X-ray diffraction data." *Journal Physical Chemistry*, 110(22), 10630-10635.

Murray, K., Bazzi, A., Carter, C., Ehlert, A., Harris, A., Kopec, M., Richardson, J., and Sokol, H. (1997). "Distribution and mobility of lead in soils at an outdoor shooting range." *Journal of Soil Contamination*, 6, 79-93.

Murray, K. S., Rogers, D. T., and Kaufman, M. M. (2004). "Heavy Metals in an Urban Watershed in Southeastern Michigan." *Journal of Environmental Quality*, 33, 163-172.

Noll, K. E., Gounaris, V., and Hou, W.-S. (1992). *Adsorption Technology for Air and Water Pollution Control*, Lewis Publishers, Inc., Chelsea, MI.

Olkhovyk, O., Antochshuk, V., and Jaroniec, M. (2005). "Thermogravimetric studies of benzoylthiourea-modified MCM-41 after adsorption of mercury ions from aqueous solutions." *Chemical Communications*, 130(104-108).

Olkhovyk, O., and Jaroniec, M. (2005). "Ordered mesoporous silicas with 2.5-dimercapto-1,3,4-Thiadiazole ligand: High capacity adsorbents for mercury ions." *Adsorption*, 11(3-4), 205-214.

Paulson, C., and Amy, G. (1993). "Regulating metal toxicity in stormwater." *Water Environment & Technology*, 5(7), 44-49.

Pauwels, B., Tendeloo, G. V., Thoden, C., Rhizn, W. V., and Jacobs, P. A. (2001). "Structure determination of spherical MCM-41 particles." *Advanced Materials*, 13(17), 1317-1320.

Perez-Quintanilla, D., Hierro, I. d., Fajardo, M., and Sierra, I. (2006). "Adsorption of cadmium(II) from aqueous media onto a mesoporous silica chemically modified with 2-mercaptopyrimidine." *Journal of Materials Chemistry*, Advance Article.

Pinnavaia, T. J. (2006). "Leaching behavior of mesoporous material surfactants in flow through systems." Personal Communication to L. K. Isaacs, Yorktown, VA, 25 Apr 06.

Pitcher, S. K., Slade, R. C. T., and Ward, N. I. (2004). "Heavy metal removal from motorway stormwater using zeolites." *Science of the Total Environment*, 334-335, 161-166.

Puigdomenech, I. (2004). "MEDUSA, Make Equilibrium Diagrams Using Sophisticated Algorithms and HYDRA, Hydro Chemical Equilibrium - Constant Database." Downloaded 3 Apr 2006, http:/www.kemi.kth.se/medusa.

Raimondo, M., Perez, G., Sinibaldi, M., DeStefanis, A., and Tomlinson, A. A. G. (1997). "Mesoporous M41S materials in capillary gas chromatography." *Chemical Communications*, 15, 1343-1344.

Rao, C. N. R., and Cheetham, A. K. (2001). "Science and technology of nanomaterials: current status and future prospects." *J of Materials Chemistry*, 11, 2887-2894.

Reed, B. E., Vaughan, R., and Jiang, L. (2000). "As(III), As(V), Hg, and Pb removal by Fe-oxide impregnated activated carbon." *Journal of Environmental Engineering*, 126(9), 869-873.

Richer, R. (1998). "Direct synthesis of functionalized mesoporous silica by non-ionic alkylpolyethyleneoxide surfactant assembly." *Chem. Comm*, 16, 1775-1777.

Roco, M. C. (2003). "National nanotechnology initiative: Overview and environmental aspects." National nanotechnolgoy coordinating office (NNCO) interagency research Meeting/workshop- Nanotechnology and the environment: Applications and Implications, Washington D.C.

Rouquerol, F., Rouquerol, J., and Sing, K. (1999). *Adsorption by Powders and Porous Solids*, Academic Press, London, UK.

Royce, S. E., Nastoff, T., Rush, V., Tucker, P., and Wigington, P. S. (2000). "Lead Toxicity." Agency for Toxic Substances and Disease Registry, U.S. Department of Health and Human Services, 56p.

Rutgers, A.T. and Hendrikx, Y. (1962). *Trans. Faraday Soc.*, 58, 2184-2196.

Rule, K. L., Comber, S. D. W., Ross, D., Thornton, A., Makropoulos, C. K., and Rautiu, R. (2006). "Diffuse sources of heavy metals entering an urban wastewater catchment." *Chemosphere*, 63, 64-72.

Sansalone, J. J. (1999). "Adsorptive infiltration of metals in urban drainage - media characteristics." *Science of the Total Environment*, 235(1), 179-188.

Sansalone, J. J., Koran, J. M., Smithson, J. A., and Buchberger, S. G. (1998). "Physical Characteristics of Urban Roadway Solids Transported during Rain Events." *Journal of Environmental Engineering*, 124(5), 427-440.

Sanz-Medel, A. (1998). "Toxic trace metal speciation: Importance and tools for environmental and biological analysis." *Pure and Applied Chemistry*, 70(12), 2281-2285.

Sauvé, S., McBride, M., and Hendershot, W. (1998). "Soil solution speciation of lead(II): Effects of organic matter and pH." *Soil Sci. Soc. Am. J.*, 62, 618-621.

Savage, N., and Diallo, M. S. (2005). "Nanomaterials and water purification: Opportunities and challenges." *Journal of Nanoparticle Research*, 7, 331-342.

Sayari, A., Hamoudi, S., and Yang, Y. (2005). "Applications of pore-expanded mesoporous silica. 1. Removal of heavy metal cations and organic pollutants from wastewater." *Chemical Materials*, 17(1), 212-216.

Sayari, A., and Yang, Y. (1999). "Expanding the pore size of MCM-41 silicas: Use of amines as expanders in direct synthesis and postsynthesis procedures." *Journal of Physical Chemistry*, 103(18), 3651-3658.

Scheuhammer, A. M., and Norris, S. L. (1995). "A review of the environmental impacts of lead shotshell ammunition and lead fishing weights in Canada." Canadian Wildlife Service, 56 pp.

Schueler, T. R. (1992). "A current assessment of urban best management practices." Metropolitan Washington Council of Governments.

Skoog, D. A., Holler, F. J., and Nieman, T. A. (1998). *Principles of Instrumental Analysis*, 5th Ed., Brooks/Cole.

Sorme, L., and Lagerkvist, R. (2002). "Sources of heavy metals in urban wastewater in Stockholm." *The Science of the Total Environment*, 298(1), 131-145.

Stansley, W., Kosenak, M. A., Huffman, J. E., and Roscoe, D. E. (1997). "Effects of lead-contaminated surface water from a trap and skeet range on frog hatching and development." *Environmental Pollution*, 96(1), 69-74.

Stansley, W., Widjeskog, L., and Roscoe, D. E. (1992). "Lead contamination and mobility in surface water at trap and skeet ranges." *Bulletin of Environmental Contamination and Toxicology*, 49(5), 640-647.

Strawn, D. G., and Sparks, D. L. (2000). "Effects of Soil Organic Matter on the Kinetics and Mechanisms of Pb(II) Sorption and Desorption in Soil." *Soil Science Society Am J*, 64, 144-156.

Stumm, W. (1992). *Chemistry of the Solid-Water Interface*, John Wiley & Sons, Inc., New York, NY.

Stumm, W., and Morgan, J. J. (1996). *Aquatic chemistry, Chemical equilibria and rates in natural waters*, 3rd, John Wiley & Sons, Inc., New York, NY.

Tanev, P. T., and Pinnavaia, T. J. (1995). "A neutral templating route to mesoporous molecular sieves." *Science*, 267(5199), 865-867.

Tao, N. J. (2003). "Detection of heavy metal ions using polymer nanojunctions." National nanotechnolgoy coordinating office (NNCO) interagency research Meeting/workshop- Nanotechnology and the environment: Applications and Implications, Washington D.C.

Tchobanoglous, G., Burton, F. L., and Stensel, H. D. (2003). *Wastewater Engineering Treatment and Reuse*, 4th Ed., McGraw Hill, Boston, MA.

Thornton, L., Butler, D., Docx, P., Hession, M., Makropoulos, C., McMullen, M., Nieuwenhuijsen, M., Pitman, A., Rautiu, R., Sawyer, R., Smith, S., and White, D. (2001). "Pollutants in urban waste water and sewage sludge." European Commission, ISBN 92-894-1735-8, 273pp.

Toshiyuki, Y., Takashi, T., and Hideaki, Y. (2003). "Selective selenate adsorption on cationated amino-functionalized MCM-41." *Bulleting of the Chemical Society of Japan*, 76(11), 2225-2232.

Treybal, R. E. (1980). *Mass transfer operations*, third ed., McGraw Hill, New York, NY.

Tun, Z., and Mason, P. C. (2002). "Observation of adsorption of water in MCM-41 with neutron diffraction." *Langmuir*, 18, 975-977.

U.S.EPA. (1983). "Results of the Nationwide Urban Runoff Program." 200 p.

U.S.EPA. (2001). "Best Management Practices for Lead at Outdoor Shooting Ranges." EPA-902-B-01-001, 86 pp.

Urbonas, B. R. (2002). "Stormwater sand filter sizing and design: A unit operations approach." Urban Drainage and Flood Control District, Denver, CO, 19p.

VanDerVoort, P., Mathieu, M., Mees, F., and Vansant, E. F. (1998). "Synthesis of high-quality MCM-48 and MCM-41 by means of the GEMINI surfactant method." *Journal Physical Chemistry*, 102, 8847-8851.

Vantelon, D., Lanzirotti, A., Scheinost, A. S., and Kretzschmar, R. (2005). "Spatial distribution and speciation of lead around corroding bullets in a shooting range soil studied by Micro-x-ray fluorescence and absorption spectroscopy." *Environmental Science & Technology*, 39(13), 4808-4815.

Vartuli, J. S., Malek, A., Rloth, W. J., Kresge, C. T., and McCullen, S. B. (2001). "The sorption properties of as-synthesized and calcined MCM-41 and MCM-48." *Microporous and Mesoporous Materials*, 44-45, 691-695.

Vaze, J., and Chiew, F. (2004). "Nutrient loads associated with different sediment sizes in urban stormwater and surface pollutants." *Journal of Environmental Engineering*, 130(4), 391-396.

Viklander, M. (1998). "Particle Size Distribution and Metal Content in Street Sediments." *Journal of Environmental Engineering*, 124(8), 761-766.

Vralstad, T. (2005). "Synthesis and characterization of cobalt-containing mesoporous model catalysts," Dissertation, Norwegian University of Science and technology.

Walcarius, A., Etienne, M., and Lebeau, B. (2003). "Rate of access to the binding sites in organically modified silicates. 2. Ordered mesoporous silicas grafted with amine or thiol groups." *Chemical Materials*, 15(11), 2161-2173.

Wang, J., Huang, C. P., and Allen, H. E. (2006). "Predicting metals partitioning in wastewater treatment plant influents." *Water Research*, 40, 1333-1340.

Weng, C.-H. (2004). "Modeling Pb(II) Adsorption Onto Sandy Loam Soil." *Journal of Colloid and Interface Science*, 272, 262-270.

Wigington, P. J. J., Randall, C. W., and Grizzard, T. J. (1986). "Accumulation of selected trace metals in soils of urban runoff swale drains." *Water Resource Bulletin*, 22(1), 73-79.

Wilkie, P. J., Hatzimihalis, G., Koutoufides, P., and Connor, M. A. (1996). "The contribution of domestic sources to levels of key organic and inorganic pollutants in sewage: The case of Melbourne, Australia." *Water Science Technology*, 34(3-4), 63-70.

Xu, Y.-M., Wang, R.-S., and Wu, F. (1999). "Surface Characters and Adsorption Behavior of Pb(II) onto a Mesoporous Titanosilicate Molecular Sieve." *Journal of Colloid and Interface Science*, 209, 380-385.

Yang, C.-M., and Chao, K.-J. (2002). "Functionalization of molecularly templated mesoporous silica." *Journal of the Chinese Chemical Society*, 49, 883-893.

Yao, K.-M., Habibian, M. T., and O'Melia, C. R. (1971). "Water and wastewater filtration: Concepts and applications." *Environmental Science & Technology*, 5(11), 1105-1112.

Yokoi, T., Yoshitake, H., and Tatsumi, T. (2004). "Synthesis of amino-functionalized MCM-41 via direct co-condensation and post-synthesis grafting methods using mono-, di= and tri-amino-organoalkoxysilznes." *Chemical Communications*, 14.

Yoshitake, H., Yokoi, T., and Tatsumi, T. (2002). "Adsorption of chromate and arsenate by amino-functionalized MCM-41 and SBA-1." *Chemical Materials*, 14(11), 4603-4610.

Yoshitake, H., Yokoi, T., and Tatsumi, T. (2003). "Adsorption behavior of arsenate at transition metal cations captured by amino-functionalized mesoporous silicas." *Chemical Materials*, 15(8), 1713-1721.

Yu, B., Zhang, Y., Shukla, A., Shukla, S. S., and Dorris, K. L. (2001). "The Removal of Heavy Metals from Aqueous Solutions by Sawdust Adsorption - Removal of

Lead and Comparison of its Adsorption with Copper." *Journal of Hazardous Materials*, B84, 83-94.

Zhang, L., Zhang, W., Shi, J., Hua, Z., Li, Y., and Yan, J. (2003). "A new thioether functionalized organic-inorganic mesoporous composite as a highly selective and capacious Hg2+ adsorbent." *Chemical Communications*, 210-211.

Zhang, W., Pauly, T. R., and Pinnavaia, T. J. (1997). "Tailoring the framework and textural mesopores of HMS molecular sieves through an electrically neutral (SoIo) assembly pathway." *Chemistry of Materials*, 9(11), 2491-2498.

Zhao, G. X. S., Lee, J. L., and Chia, P. A. (2003). "Unusual Adsorption Properties of Microporous Titanosilicate ETS-10 toward Heavy Metal Lead." *Langmuir*, 19, 1977-1979.

Zhao, X. S., Audsley, F., and Lu, G. Q. (1998). "Irreversible change of pore structure of MCM-41 upon hydration at room temperature." *Journal of Physical Chemistry*, 102(21), 4143-4146.

Zhao, X. S., Lu, G. Q., and Millar, G. J. (1996). "Advances in mesoporous molecular sieve MCM-41." *Industrial Engineering Chemical Research*, 35(7), 2075-2090.

Zhao, X. S., Ma, Q., and Lu, G. Q. (1998). "VOC removal: Comparison of MCM-41 with hydrophobic zeolites and activated carbon." *Energy and Fuels*, 12, 1051-1054.

Zhou, C., Zhang, B., Li, Q., Cai, Y., Chen, Y., and Ge, Z. (2001). "Synthesis and Characterization of Mesoporous Molecular Sieves MCM-41 Modified in Framework by B and Al." *Gaoxiao Huaxue Gongcheng Huebao*, 15(5), 425-428.

APPENDICES

A. ACRONYMS AND DEFINITIONS

AFB	Air Force Base
ARC	Applied Research Center, Jefferson Laboratory, Newport News, Virginia
ANOVA	Analysis of Variation
BV	Bed Volume
Ce / Co	Breakthrough level (ratio of equilibrium to original concentration)
CCC	Criteria Continuous Concentration
CMC	Criteria Maximum Concentration
CTAB	Cetyltrimethylammonium bromide
DI	Deionized, typically used as DI water
EBCT	Empty Bed Contact Time
EMC	Event Mean Concentration
EtOH	Ethanol
ICP-MS	Inductively Coupled Plasma – Mass Spectroscopy
FTIR	Fourier Transform Infrared
GFAA	Graphite Furnace Atomic Adsorption
HSAB	Hard Soft Acid Base
IR	Infrared Spectroscopy
IUPAC	International Union of Pure and Applied Chemistry
K_D	Partition or Distribution Coefficient
K_f	Coefficient of Formation
MEDUSA	Make Equilibrium Diagrams Using Sophisticated Algorithms
MCM-41	Not an acronym, but a designation for a family of synthesized mesoporous materials to include MCM-48, SBA-15, HMS, etc., which differ in synthesis, morphology, structure, porosity, and pore diameters. Amato

	(1993) suggested MCM stands for Mobile Composition of Matter and Rouquerol et al. (1999) describes the materials as Mobil Catalytic Material, number 41. In this paper MCM is used as presented by the original researchers without interpretation to the designation MCM-41.
NAD	No Known Anthropogenic Additive; Used in a soil contamination context
NOM	Natural Organic Matter
NPDES	National Pollutant Discharge Elimination System
NURP	National Urban Runoff Program conducted in 1982 by the U.S. EPA
OSNP	Organosilicate Nanoporous
PSD	Precipitation Storm Depth
PWT	Pore Wall Thickness
RCRA	Resource Conservation and Recovery Act
RSM	Response Surface Methodology
S	Schmidt Number, a dimensionless number used to characterize the ratio of fluid flows momentum diffusivity or viscosity to mass diffusivity.
SBA-15	Hexagonal mesoporous silica structure with thicker walls than MCM-41
SSMR	Surfactant/silica molar ratio
TDS	Total Dissolved Solids
TEM	Transmission Electron Microscopy
TEOS	Tetraethylorthosilicate
TMAOH	Tetramethylammonium hydroxide
TMB	1,3,5 trimethylbenzene
TSS	Total Suspended Solids
UC	Uniformity Coefficient

B. JOURNAL PAPER: LEAD LEACHING FROM SOILS AND IN STORM WATERS AT TWELVE MILITARY SHOOTING RANGES

Manuscript was submitted Mar 27,2006. Review comments were received Jul 25, 2006 and a revised manuscript submitted Aug 17, 2006. The revised manuscript was submitted Aug 25, 2006 and approved for publication on Aug 29, 2006. The paper published Feb 22, 2007

Isaacs, L.K. (2007) Lead leaching from soils and in stormwaters at twelve military shooting ranges, *Journal of Hazardous Substance and Research*, VI, 1-30.

The following is the release authorization from the editor to use the paper in this dissertation:

-----Original Message-----
From: lerick@ksu.edu [mailto:lerick@ksu.edu]
Sent: Tuesday, Nov 21, 2006 8:18 AM
To: Isaacs Larry K Civ ACC/A7VQ
Cc: clovin@ksu.edu; bbruns85@ksu.edu
Subject: Re: Manuscript "Lead Leaching from Soils and in Storm Waters at Twelve Military Ranges"

Dear Mr. Isaacs,

Your request to include this manuscript or any parts of it in your dissertation is approved.

Larry E. Erickson
Editor, Journal of Hazardous Substance Research Professor of Chemical Engineering and Director, Center for Hazardous Substance Research Kansas State University
lerick@ksu.edu
Phone: (785) 532-4313

On Mon, Nov 20, 2006, Isaacs Larry K Civ ACC/A7VQ wrote:

Dear Dr. Erickson,

I would like to request permission to include subject manuscript in my dissertation. The dissertation is planned for publication in May 2007 at Old Dominion University in partial fulfillment of the requirement for the degree of Doctor of Philosophy in Environmental Engineering. Your favorable approval is greatly appreciated.

Respectfully,

Larry K. Isaacs, P.E.

LEAD LEACHING FROM SOILS AND IN STORM WATERS AT TWELVE MILITARY SHOOTING RANGES

L.K. Isaacs

U.S. Air Force, Headquarters Air Combat Command, Environmental Division, Environmental Quality Branch, Langley AFB, Virginia 23665-2769. Phone: (757) 764-9342; Fax: (757) 764-9369.

ABSTRACT

Soils from impact berms at twelve military shooting ranges were evaluated for lead leaching by particle size distribution, sequential extractions, stormwater analysis, batch studies with amendments of crushed apatite (FB) and triple super phosphate (TSP), and column leaching studies with amendments of ashed apatite (FBa) and TSP. Soil particle fractions were determined by ASTM D422-63 and by x-ray diffraction; lead leaching was found by EPA's SPLP and TCLP. Total and dissolved lead in soils and stormwaters were determined by ICP-MS. The residual fraction averaged 79.8% of total mass of lead in all soils. There was significant correlation between TCLP results and lead in the less than 0.075 mm size fraction for all soils in the study ($r^2 = 0.82$, $P << 0.001$, $n = 13$), along with a significant correlation of lead in stormwater and soil Fe ($r^2 = 0.56$, $P = 0.03$, $n = 8$) and Mn ($r^2 = 0.59$, $P = 0.03$, $n = 8$). Average dissolved lead in stormwater = 104 µg/L (SD = 152, n = 17). Batch study of FB 3% and 5% amendments sorbed 85.3% and 88.2% lead, respectively. TSP 3% and 5% amendments created phosphate precipitates that captured 97.6% and 92.7% lead, respectively. In column studies, FBa amended soils had mixed effectiveness as lead adsorbents and TSP amended soils leached more lead than control in all, but Virginia (VA) soils. Control, non-amended soils, did not leach lead for three soil combination types, New Mexico range b (NMb), Nevada (NV) and South Dakota range 2 (SD2). NMb soil had no lead leachate

presumably due to the high organic matter, pH = 8.2 and very high sulfides. In the NV range soil a combination of pH = 8.7, low moisture = 1.2% and mostly fine gravels had no lead leachate. SD2 range had no leachate with pH = 8.2, moderate clay and organic matter content. Both TSP and FBa amendments leachate pH were significantly different than control leachate pH (FBa: $F = 9.47$, $P = 0.003$, $n = 120$; TSP: $F = 115.5$, $P << 0.001$, $n = 135$). Leachate pH dropped an average 3.7 standard units (SD = 0.93, n = 13) in the first week for TSP amended soils. Soil pH was the most significant indicator of soil leaching behavior. While TSP can be an effective lead immobilization mechanism, the reduction of soil pH can have an unintended consequence for lead ions not precipitated as phosphates. Range operators would be prudent to monitor soil pH regularly and to know their soil clay and organic matter content.

Keywords: *Lead Leaching; Column Study; Stormwater Pollutant; Soil Particle Size; Shooting Range*

INTRODUCTION

Shooting range soils have elevated concentrations of elemental lead as high as 10 to 100 times background levels (Murray et al., 1997). Concern for migration of this anthropogenic source has been a focus of research by many (Abdel-Fattah et al., 2003; Bruell et al., 1999; Cao et al., 2003; Craig et al., 1999; Dermatas et al., 2006; Hardison et al., 2004; Jorgensen and Willems, 1987; Lin et al., 1995; Murray et al., 1997; Scheuhammer and Norris, 1995; Stansley et al., 1992; U.S.EPA, 2001). Shooting ranges contain large amounts of lead contaminated soil that may become mobile through two primary pathways: physical abrasion and weathering. The physical abrasion of bullets has been found to be a significant source of lead contamination in the soils (Hardison et al., 2004). The abraded residue transforms into hydrocerussite ($2Pb(CO_3)(OH)_2$) and to a lesser degree cerussite ($PbCO_3$), and massicot (PbO) in as little as one week (Cao et al., 2003; Hardison et al., 2004; Jorgensen and Willems, 1987). Weathering of elemental lead forms from shooting ranges have also been documented as visible corrosion on lead fragments as crusts of white, gray or brown material and as hydrocerussite, cerussite and some amounts of anglesite ($PbSO_4$) (Cao et al., 2003; Lin et al., 1995). The lead of weathered bullets exists as particulate or ionic forms and may provide a steady source of potentially labile constituents, which can appear in various soil fractions and in stormwaters (Cao et al., 2003). These oxidized lead compounds in earthen bullet impact berms provide a constant source of lead in the soil matrix, where the rate of elemental lead dissolution is regulated by both physical and chemical factors.

Lead dissolution

Lead mobility in soil is driven by redox potential, available anions (e.g. carbonates, phosphates, and sulfates), pH, soil organic matter, and cation exchange capacity (Basta et al., 1993; Dragun, 1998; Pickering, 1986). Both aerobic and acidic conditions in soils increase elemental lead dissolution, whereas anaerobic and alkaline conditions decrease it (Scheuhammer and Norris, 1995). Organic carbon has been found to enhance lead adsorption (Basta et al., 1993; Sauve et al., 1998). Soil colloids have been found to be active participants in transporting lead to groundwater and limiting lead interaction with reactive soil constituents (Citeau et al., 2003). Surface and sub-surface soils lead migration has been reported (Abdel-Fattah et al., 2003; Craig et al., 1999; Murray et al., 1997). Dissolution and subsequent migration may require implementation of best management practices (BMPs) to control and immobilize lead complexes.

Lead Immobilization

In-situ immobilization of lead may be accomplished by soil amendments with phosphoric acid (H_3PO_4) (Yang et al., 2001); TSP (triple super phosphate) which in concentrated form is composed of monocalcium phosphate hydrate, $Ca(H_2PO_4)_2 \cdot H_2O$ and generally contains 43-50% P_2O_5 (Budavari, 1989); or apatites ($Ca_{10}(PO_4)_6(OH)_2$) to convert soluble lead to pyromorphite species [$Pb_5(PO4)_3(OH, Cl, F...)$]. Pyromorphite is extremely stable ($K_{SP} = 10^{-80}$) and its precipitate formation an immobilization objective. Pyromorphite can be formed from soil lead compounds like cerrusite ($PbCO_3$), anglesite ($PbSO_4$) and galena (PbS) when exposed to phosphates. Some studies have suggested pyromorphites can also be a natural weathering product in soil (Cotter-Howells et al., 1994; Klein and Hurlburt, 1993). Changing the available lead to less soluble forms using phosphates has been shown effective, (Brown et al., 2005; Fayiga and Ma,

2006; Ownby et al., 2005). TSP amended 3.2% and 1% phosphoric acid soils have been reported the most effective lead treatments to bioavailability reduce in fescue grass (Brown et al., 2005). Hydroxyapatite has also been shown to be an effective calcium phosphate-based [$Ca_5(PO_4)_3(OH)$] lead immobilizing amendment (Ryan et al., 2001). Phosphate sources of various types have been used to include fish hard parts as an effective metal adsorbent (Wright et al., 1995).

Objectives

Researchers, previously mentioned, have studied and reported the distribution of lead contamination at shooting ranges, the distribution and geochemistry of metals in range soils, the effectiveness of different amendments and mechanisms of metal sorption, remediation technologies, and other edaphic topics. These research efforts have advanced our understanding of shooting range environmental knowledge. The challenge to range managers is to translate this information into effective range BMPs. In this study key soil characteristics of shooting range impact berms are identified to assist the range environmental professional to predict the lead leaching behavior of range soils. To clarify lead leaching characteristics of range soils the objectives of this research focused in three areas: 1) Quantification of the physical and mineralogical associations of lead in shooting range impact berm soils; 2) Measurement of the lead concentrations in range stormwaters, and 3) Characterization of the soil lead leaching behavior via laboratory batch and column studies with apatite and TSP amendments. Statistical correlations are presented where appropriate.

Range Site Description

The twelve small arms firing ranges (SAFRs) were located in nine states and are hereafter referred to by the alphanumeric codes: CA: California - one range, LA1, LA2,

and LA3: Louisiana – three ranges at same site, MO: Missouri - one range, NE: Nebraska - one range, NMa: New Mexico – one range and NMb: New Mexico - one range (Note: The two ranges in New Mexico were at two different military installations approximately 350 km apart.), NV: Nevada - one range, SC: South Carolina - one range, SD2: South Dakota - one range (Note: SD2 is used to differentiate from range SD1 at this same site, but SD1 was not included in this paper), and VA1 and VA2: Virginia - one range with two berms, one 5 y aged berm in front of a 40 y aged berm, respectively. Site approximate locations are depicted in Figure 42.

Each range consists of a firing line, a target line, and an impact berm located behind the target line, except the NV range did not have an impact berm. The distance from the firing line to the target line was 25 m to 100 m for pistol ranges, and 100 m to 950 m for rifle ranges. Impact earthen berms varied in height from 1.5 m to 15 m, with an average height of 6 m. Soil volumes in these impact berms ranged from 75 m^3 to 15,000 m^3. In 2003 these small arms training ranges averaged approximately 371,430 rounds of 5.56 mm, 7.62 mm, and 9 mm size fired per range complex per year, adding about 1,960 kg of lead to each range complex annually. Typical operations and maintenance for SAFR berms included periodic sieving soil to remove and recycle lead shot from the berm areas, repairing berm erosion caused by storm events and bullets, and replacement of berm soils to reduce ricochet (ITRC 2004).

MATERIALS and METHODS

Soil characterization

Approximately 25 kg of berm soil from surface depths of 2 to 20 cm was collected at each shooting range using stainless steel shovels and trowels. Soil was

collected across the face of berms equal distance apart, within impact zones, and along a single transect. Aliquots of soil were thoroughly mixed and homogenized. Large, visible organic constituents including roots, twigs or leaves were removed. Berm soils, although likely indigenous to the area, were not necessarily from the immediate location of the shooting ranges. Range operators were not aware of the original source of berm soils. Geotechnical characteristics of soil are shown in Table 33. Soil particle fractions were determined by ASTM D422-63. Lead particle sizes were evaluated using standard sieve sizes 4, 10, 60, and 200. Lead chemical associations were determined by sequential extraction following Ryan et al., 2001. EPA's Synthetic Precipitation Leaching Procedure (SPLP) SW846-1312 and Toxicity Characteristic Leaching Procedure (TCLP) SW846-1311 were completed on each size fraction, and chemical analysis for metals in soils followed SW846-6010B and 3050B (USEPA, 1999). Soil clays and crystalline components were characterized by Perkin Elmer XRD using Cu Kα radiation. Measurements were made using continuous scanning techniques, and XRD patterns were obtained from 2 to 60° 2θ. Triplicate distilled/de-ionized (DDI) blanks, triplicate reverse osmosis water blanks, and triplicate quality control (QC) reagent standards were used for each analysis. The percent standard deviation of the reagent QC standards < 5 percent. Blank values were subtracted from the measured values. Soil crystalline phases are reported in Table 34.

To evaluate lead leaching from operational ranges into stormwater, run-off samples were taken when possible during field visits. Stormwater samples were collected from ranges at CA, LA1, LA3, MO, NMa, SD2, VA1 and VA2. Stormwater samples at the other sites were not collected. Two to four samples were collected with one duplicate sample from surface stormwaters down gradient of berms in natural swales

or constructed drainage, and from 1 to 150 m from range boundaries. Samples were collected in the middle of streams or channels width and stormwater depth. Dissolved samples were filtered using a 0.45 μm hourglass filter. Samples were analyzed for total and dissolved metals following USEPA method SW846-6020.

Batch Study

Batch studies were completed on each soil with and without amendments. Amendments for batch studies were added at 3% and 5% by mass. Crushed apatite II (FB) was used as supplied by PIMS NW Inc., and TSP was as potassium phosphate (KH_2PO_4) and phosphoric acid (H_3PO_4), which generally contains 43-50% P_2O_5 (Budavari, 1989). Soils and amendments were air dried after mixing in the batch test vessel. Amended soils TCLP solutions were added to batch samples and continuously shaken for 24 ± 2hr. Leachates from each batch sample were filtered with a 0.45 μm filter and analyzed using Perkin Elmer Inductively Coupled Plasma Optima 4300 DV.

Columns Set-up

A preliminary screening batch analysis of the VA1 and VA2 soils found the 3% amendment effective and equilibrated at 28 d. Therefore, 150 g of hand mixed soil was added with 3% ashed apatite II (FBa) and 3% triple super phosphate (TSP) to 4 cm inside diameter borosilicate columns that were 30 cm long. Ashed apatite II was utilized to avoid the build-up of biofilm experienced in the preliminary 28 d study with VA soils.

A column of each soil with no amendment was prepared as controls. The soil for the test filled approximately 20 cm of each column. TSP and FBa were supplied as previously referenced, but FBa was further prepared to remove organics by heating in a muffle furnace for 24 h at 450 °C. To each column 35 mL of tap water was added daily Monday through Friday, for 5 weeks (approximately 35 days). Effluent was collected in

Nalgene bottles twice weekly (Mondays and Fridays) and analyzed for total As, Cr, Cu, Fe, Ni, P, Pb, Mn, Mo, Sb, Sn, V, W and Zn by EPA SW846 Method 6010B ICP-MS. Only total lead results are reported in this paper. Effluent pH was recorded ±0.05 and masses within ±0.05 g. Each analytical run included triplicate DDI blanks, triplicate RO water blanks, and triplicate QC reagent standards. Percent standard deviation of the reagent QC standards was typically less than 5 percent. Leachates from columns were analyzed by ICP-MS.

RESULTS and DISCUSSION

Physical soil parameters from berm soils had a CEC average = 15.8 meq/100 mL (SD = 8.1, from 31.5 (SD2) to 4.4 (SC), n =12), pH average = 7.7 (SD = 0.6, from 6.8 (LA1) to 8.7 (NV), n = 12), moisture content average = 15.3% (SD = 8.3, from 1.2% (NV) to 25.8% (LA1), n = 12), and soil texture generally as sand, with some silt and clay elements (Table 33). Berm average age = 33.7 y (SD = 19.8, from 5 y (VA1) to 60 y (LA1, LA3, MO), n = 13) indicating seasoned and well weathered impact earthen berms. Iron and manganese concentrations were within typical soil U.S. nationwide averages. Edaphic lead associations were reviewed and are presented below in three areas: 1) particle size and physical characteristics, 2) crystalline phases as determined by XRD, and 3) metal partitioning by sequential extraction. Results and discussions of field stormwater sampling, batch and column leaching studies are then presented.

Particle size and physical characteristics:

Particle size distributions are depicted in Figures 43 and 44. The order from largest to least percent clay for the first three soils were SD2 > LA3 > MO, which were the same soils as the XRD analysis, but in a slightly different order, LA3 > MO > SD2

(Table 34). Tables 35, 36 and 37 provide the results of the sequential extraction, lead associations by fraction and leaching, and stormwater lead concentrations, respectively. The SD2 and LA3 soils also had small exchangeable lead associations, however, the MO soil had the highest lead associations in the exchangeable fraction of any soil in this study (Table 35). The silt-clay fraction has been shown to be an effective transporting mechanism of heavy metals in stormwaters (King, 1988). Heavy metal associations generally decreased with smaller size fractions (Table 36), contrary to findings by Zhang et al., (2003) who noted heavy metal attachment increased with the smaller aggregate size. This phenomenon may have been due to lead fragments in the larger size fractions as it is well established surface attachment mechanisms have dominant control of the distribution of the heavy metals among the various fragment sizes (Zhang et al., 2003).

Lead in stormwaters with suspended solids seem to corroborate the potential for lead migration. For example, stormwater dissolved lead concentrations for SD2 and MO were 440 and 118 μg/L, respectively (Table 37). The SD2 and MO ranges topography had been graded to direct range surface runoff to stormwater collection basins and ditches where samples for this study were collected. LA3 had a much lower dissolved concentration at 4.2 μg/L, which likely was a result of the application of TSP approximately one year prior to this study, implementation of a stormwater BMP that re-sloped the range infield to reduce stormwater surface velocity, and seeded indigenous Bermuda grass (*Cynodon dactylon*) in the drainage pattern. The high clay content soil of LA3, and prior to the BMP implemented in previous work to this study, found 2001 stormwaters had total lead = 2,350 μg/L and in 2002 = 3,730 μg/L (Abdel-Fattah et al., 2003).

The size and lead association relationship may be further supported in part by the correlation of the smallest soil fractions and the TCLP results. For example, TCLP and lead in the < 0.075 mm fraction was significantly correlated for all soils in the study (r^2 = 0.82, P << 0.001, n = 13). Similarly, but not as strong was the TCLP and lead correlation in the from 0.075 to 0.250 grain size (r^2 = 0.54, P = 0.004, n = 13), and TCLP and lead in the from 0.250 to 2.00 grain size (r^2 = 0.38, P = 0.02, n = 13). Less lead leached with the smaller fractions similar to results by Dermatas et al. (2006).

Stormwater field sample results are in Table 37. Order of largest to smallest dissolved lead concentrations were SD2 > LA1 > MO > VA1 > CA > VA2 > LA3 > NMa. The SD2 and LA1 soils lead associations had 13,623 and 172,800 mg/kg in the from 0.250 to 2.00 mm soil fraction, 5,548 and 2,441 mg/kg lead in the from 0.075 to 2.50 mm fraction and 817 and 11,137 mg/kg in the less than 0.075 mm fraction, respectively (Table 36). Suspended colloids may be contributing to the total and dissolved lead in shooting range stormwaters, however no statistical correlation with stormwater total or dissolved lead and grain size was found. The second soil in the series was LA1, which had stormwater from a combined M-9 (pistol) and M-60 (machine gun) range. The LA3 stormwater was from a M-16 range that had the TSP treatment previously mentioned. This analysis seems to indicate that the LA3 soil treatment may have reduced lead mobility compared with the LA1 soil, with no treatment.

The third soil in the dissolved lead in stormwater series, MO, did not show a tendency to lead leaching in the batch and column studies. The iron content in the MO soil at 18,210 mg/kg was greater than any other soil in this survey (Table 33), and may be inhibiting lead cation exchange with soil micelles, and therefore, contributing to the elevated lead in stormwaters.

The fourth, fifth, and sixth soils in the series were VA1, CA and VA2 soils, respectively had high lead amounts in the <0.075 mm fraction than other soils, 8,294 mg/kg, 18,587 mg/kg and 6,111 mg/kg, respectively, potentially providing a ready source of lead cation surface attached colloids (Table 36). The NMa soil had the least dissolved lead of those measured (Table 37). The NMa soil also had high gypsum content (75%), which decreases the electrical double layer between the clay surface and the soil solution as the double charged calcium ions balance the charge rather than monovalent ions such as sodium (Quirk, 1994). Because the double charge calcium ions are more strongly attracted to clay surfaces, sulfate anions are available to bind with free cations such as Pb^{2+} to form the insoluble lead sulfate salt.

Lead stormwater concentrations were positively correlated with Fe soil concentration ($r^2 = 0.56$, $P = 0.03$, $n = 8$) and Mn soil concentration ($r^2 = 0.59$, $P = 0.03$, $n = 8$), which agree with King (1988). However, this disagrees with findings reported by Amacher et al., (1986) who found a negative correlation. The correlation may be attributable simply to the soil colloidal transport mechanism that can carry metal cations in stormwaters.

Heavy metal contaminants in soils have been reported to interfere with adsorption by apatite. This may have had similar impacts on the natural adsorbent mechanisms in MO soils of this study and contributed to the observed correlation. Seaman et al. (2001) found other metals in the soil can reduce the amount and rate at which PO_4 becomes available for precipitation with the heavy metal of concern, changing the formation of secondary phosphate precipitates. For example, the MO soil with 18,210 mg/kg Fe could form strengite ($FePO_4 \cdot 2H_2O$) inhibiting the formation of the desired Pb phosphate precipitates. Lead also sorbs readily to manganese hydroxides over iron oxides by a

factor of 40 potentially further restricting the mobilization of lead (Hettiarachchi et al., 2000). MO soil was 875 mg/kg Mn, the highest of the range soils studied.

Crystalline phases

Most soils were dominated by sand or crystalline phase quartz (70-85%) (Table 34). Sandy soils are characteristic of soil types used for small arms firing range impact berms to reduce ricochet (ITRC, 2004; US EPA, 2001). There were two soils that were not dominated by quartz; NMa and NV soils had quartz = 5% and 40%, respectively.

The NV soil contained 50% carbonates and 40% quartz, and this range did not have a constructed impact berm. The NV soil was sampled along the firing lane beds of an alluvial fan and had the least amount of clay soil of those surveyed. The NV soil also had the highest gravel content of soil types, which does not readily adsorb heavy metals (Bradl, 2004). NV soil also had a very low exchangeable lead association (Table 35).

Pb(II) metal partitioning

The sequential extraction found in the residual an average 10,114 mg/kg lead (SD = 7,783, from 13 to 44,500 mg/kg, n = 13) representing 79.8% of the total lead mass. This would suggest lead in the earthen berms is mostly in metallic form and not likely bioavailable or tending to dissolution naturally (Tessier et al., 1979). However, research by others has found lead pellets and fragments can transform quickly into lead compounds on the surface of lead fragments and soils (Jorgensen and Willems, 1987). Berm average age = 33.7 y would provide ample time for oxidization of lead to hydrocerussite ($2Pb(CO_3)(OH)_2$), cerussite ($PbCO_3$) and massicot (PbO), the most commonly found Pb(II) forms in range soils (Hardison et al., 2004; Jorgensen and Willems, 1987). The high lead residual association differed from Cao et al., (2003) who

found shooting range soils in Florida primarily associated with the carbonate fraction, and Bruell et al., (1999) found 40% of the total lead at a Connecticut shooting range was in the exchangeable fraction. This difference suggests lead fraction associations will be uniquely defined for each shooting range.

The exchangeable lead fraction averaged 105 kg (SD = 260.8, from non-detect to 797 mg/kg, n = 13) for all soils (Table 35). The two soils with the highest exchangeable amounts were CA = 797 mg/kg and SC = 85.1 mg/kg. Average lead in soils extracted as lead carbonates was 1055 mg/kg (SD = 3,059, from non-detect to 10,270 mg/kg, n = 13), with the highest carbonates CA =10,270 mg/kg, SD2 = 379 mg/kg, and NE = 303.4 mg/kg. The top four OM & sulfide associations in decreasing order were CA = 6,312 mg/kg, SD2 = 1,793 mg/kg, NE = 448 mg/kg and SC = 372.1 mg/kg. Soil organic matter, sulfides and carbonates affect the desorption of lead as observed by Suavé et al. (1998) where soils from pH 6.5 to 8 and with higher OM content contribute to a more labile lead species. There was no correlation between OM & sulfide and lead leachate (less than 0.075 mm fraction) observed probably because these fractions were such low percentages of the total lead in the sample. For example, the SD2 soil for all fractions, excluding the residual, was 0.1% of the lead mass (Table 35).

Total soil lead was negatively correlated with moisture and not statistically significant in this study ($r^2 = 0.24$, $P = 0.10$, $n = 12$). This negative correlation agrees with Lee et al., (2002) who found a significant negative correlation with moisture content ($r^2 = 0.95$, $P \leq 0.001$). There was no correlation found between stormwater lead concentrations and moisture content (Table 37).

Batch Results

The batch test procedure was used to determine the adsorption effectiveness of amended versus not amended soils. Non-amended soils served as control. FB and TSP, as supplied, were both generally effective adsorbents of lead cations with some exceptions (Table 38). Immobilization of lead for all soils by FB 3% and 5% amendments averaged 85.3% (SD = 24.5, from 12.4 to 99.7%, n=13) and 88.3% (SD = 24.3, from 19.5 to 100%, n=13), respectively. TSP 3% and 5% amendments average lead adsorption results were 97.6% (SD = 3.13, from 90.8 to 99.7%, n=13) and 92.7% (SD = 22.7, from 17.3 to 99.8%, n=13), respectively.

CA, NMb, and SD2 soils had less than optimum adsorption performance by both amendments. The CA had 631 mg/L OM & sulfides and pH = 7.2, which combination, OM and near neutral pH, has been shown to preferably form lead OM complexes (Sauvé et al., 1998). NMb and SD2 had high OM compared to other soils in this study at 593 and 179 mg/L, respectively, however soil pH = 8.2 for both. Although a pH = 8.2 is not near neutral, it is still within the less soluble range for lead compounds and would partially contribute to the reduced leachate in the NMb and SD2 soils. Likely, the combination of pH and OM content synergistically operates to sorb metal cations. Increasing OM was likely a significant contributor to the decreased sorption in all three soils (Strawn and Sparks, 2000).

The CA soil also had other significant presence of other metals, which has been shown to inhibit heavy metal immobilization by apatite (Seaman et al., 2001). The CA soil had 12,727 mg/kg iron, and then coupled with the higher CA exchangeable (797 mg/L) and OM & sulfide (6,312 mg/L) lead fractions, this could further explain the low FB sorption of the CA soil. In other soils, total iron for MO soil = 18,210 mg/kg, NMb

soil = 5,833 mg/kg, and SD2 soil = 16,993 mg/kg (Table 33). Each of these three soils, MO, NMb and SD2, also showed reduced FB adsorption.

The TSP 5 % amendment was not effective on the NMa soil (17.3%). The NMa soil had the highest CEC of the soils in this study group (26 meq/100 mL), and uniquely the only soil with 75% gypsum content (Table 34). Gypsum ($CaSO_4$) calcium cations likely dominated the soil colloid exchange sites, and inhibited PO_4^{2-} from reacting with lead cations. TSP 5% amendment for NMa soil performed poorly, and this was the only soil with inhibited TSP lead adsorption. TSP performance may be less effective in soils with high Pb concentrations although no statistical correlation was found in this data set and the control Pb concentration range was significant, from 1.04 to 1,294 mg/L.

The 3% FB amendment had the lowest overall general adsorption performance (85.3% , from 12.4 to 99.7%, SD = 24.5, n = 13) and the 3% TSP the best (97.6%, from 90.8 to 99.7 %, SD = 3.1, n = 13). Brown et al. (2005) also found TSP amended 3.2% acidic soils effective for lead immobilization.

Pb Soil Leaching Behavior in Column Studies

Results of soil column leaching with and without amendments are shown in Figure 45. The FBa amended soils leached less lead than control for LA3, NMa, SC, SD2, VA1, and VA2 soils. The TSP amendment leached less lead than control for the VA1 and VA2 soils likely due to the more porous soil allowing phosphate precipitate compounds to form more readily. All soils leached lead from control soils except NMb, NV and SD2 soils. For NMb the combination of pH = 8.2, low clay content, and high OM/sulfides yielded no lead in leachate during the 5 week period. In the NV soil, a combination of pH = 8.7, very low moisture = 1.2%, and mostly fine gravel, a moderate lead amount in the < 0.075 mm fraction, also resulted in no leaching. The SD2 control

soil did not leach during the 5 week study, but for different reasons than the NMb and NV soils. SD2 had the common denominator of higher pH = 8.2, a higher CEC = 31.5 meq/100 mL, and moderate clay and OM content, which was sufficient to hold metal cations.

The change in leachate pH from control was an important result as depicted Figure 46. For both amendments, leachate pH was significantly different than control leachate pH (FBa: $F = 9.47$, $P = 0.003$, $n = 120$; TSP: $F = 115.5$, $P << 0.001$, $n = 135$). In general, in the first week leachate pH dropped an average of 3.7 (SD = 0.93, n = 13) standard units for the TSP amended soils. The TSP leachate pH gradually increased and approached the control pH by week 5 and did not return to original values except for the NMa soil as gypsum is known to ameliorate soil acidity. The effects of the TSP leachate pH reduction can be illustrated by observing the MO soil. The MO soil pH at week 1 = 4.0, week 2 = 4.6, week 3 = 5.0, week 4 = 5.3, and week 5 = 5.6 (Figure 47). The MO leachate control pH at end of week 1 = 8.5 and by the end of the 5-week study = 8.8. The MO soil at low pH would see orthophosphate ions precipitated or adsorbed by species of Fe(III) and other metal di- and trivalent cations capturing available surface and inter-phase micelle Pb(II) adsorption sites. Then presumably available lead cations were released. The MO soil had the highest iron content of all soils in the study.

An analysis of variance of only the control leachate amounts between the highest 6 clay content soils and the remaining 6 soils as reported above in particle size distribution found a significant difference in the two groups. This held true using either the particle size series sequence or XRD series order ($F = 11.0$, $P = 0.002$, $n = 60$ and $F = 7.5$, $P = 0.007$, $n = 60$, respectively). This observation of clay correlation with lead retention in soils agrees with others (Bradl, 2004; King, 1988; Zhang et al., 2003).

CONCLUSIONS

Soils and stormwaters from impact berms at twelve military shooting ranges were evaluated for lead leaching. The residual fraction accounted for 79.8% of total lead mass in all soils studied. All soils leached lead in excess of the EPA RCRA hazardous waste TCLP limit of 5 mg/L, except the MO soil which had high clay content. Clay content and grain size are factors in the transport of lead in stormwaters. Significant correlation was found between lead in stormwater and total iron and manganese in soils. Total soil lead was negatively correlated with moisture content. FB, FBa and TSP amended soils generally performed as effective lead adsorbents, although ashed apatite may have had impacted performance from a degraded internal structure presumably caused by the high temperature ash process. Column studies found most soils tended to leach lead, except for those soils with high clay (MO) or high pH (NMb and NV). Amendments containing 3% TSP caused a significant decrease in pH. TSP pH changes may have caused increased lead leaching in soils as pH was reduced to less than 5 in the first week of application. The FBa 3% amendment pH generally reflected the control pH for the study period. Apatite and phosphorus can be effective amendment soil treatments.

The twelve range soils were uniquely characteristic, however essential range edaphic data can provide the necessary information to effectively manage and control lead leaching. While no single soil parameter can explicitly predict lead leaching behavior, each range environmental steward should understand the impact on berm soil of pH, particle size distribution, CEC, and soil concentration of iron, manganese, and organic matter. With this minimal information shooting range managers can tailor appropriate BMP responses, minimize soil leaching behavior and estimate the propensity of lead cation migration to stormwater.

ACKNOWLEDGEMENTS

The support provided by the U.S. Air Force for this study and the support of Parsons Inc. staff, Mr. Bob Kull, Mr. John Ledbetter, Ms. Dawn DeMartino, and Mr. Ken Rice who completed the field and analytical work is gratefully acknowledged. Special thanks to Dr. Steven Larson, U.S. Army, Vicksburg, MS for volunteering to complete the soil column study, helped interpret the data, and his corporate expert knowledge of shooting range soil chemistry; and for Ms. Michelle Thompson, U.S. Army, Vicksburg, MS who spent many hours laboring to make sure all the sequential extraction, daily pore volumes, and analysis got done. To Dr. Judith Wright , PIMS NW Inc., whose professional skill, knowledge and advice were greatly appreciated. A grateful thank you to the reviewers who made very useful and constructive improvements to the manuscript. The views expressed in this article are those of the author and do not necessarily reflect the official views of the U.S. Air Force or Department of Defense.

REFERENCES

Abdel-Fattah, T. M., L. K. Isaacs, and K. B. Payne, 2003. Small arms range lead management issues: activated carbon, molecular sieves (5A and 13X), and naturally occurring zeolites as lead adsorbents. Federal Facilities Environ. J., 14(2), 113-126.

Amacher, M. C., J. Kotuby-Amacher, H. M. Selim, and I. K. Iskandar, 1986. Retention and release of metals by soils: evaluation of several models. Geoderma, 38, 131-154.

Basta, N. T., D. J. Pantone, and M. A. Tabatabai, 1993. Path analysis of heavy metal adsorption. Soil Agron. J, 85, 1054-1057.

Bradl, H. B., 2004. Adsorption of heavy metal ions on soils and soils constituents. Journal of Colloid and Interface Science, 277, 1-18.

Brown, S., B. Christensen, E. Lombi, M. McLaughlin, S. McGrath, J. Colpaert, and J. Vangronsveld, 2005. An inter-laboratory study to test the ability of amendments

to reduce the availability of Cd, Pb, and Zn in situ. Environmental Pollution, 138, 34-35.

Bruell, R., N. P. Nikolaidis, and R. P. Long, 1999. Evaluation of remedial alternatives of lead from shooting range soil. Environmental Engineering Science, 16(5), 403-414.

Budavari, S., ed. 1989. Merck Index. Merck & Co., Inc., Rahway, NJ.

Cao, X., L. Q. Ma, M. Chen, D. W. Hardison, and W. G. Harris, 2003. Lead transformation and distribution in the soils of shooting ranges in Florida, USA. Science Total Environ, 307, 179-189.

Citeau, L., I. Lamy, F. vanOort, and F. Elsass, 2003. Colloidal facilitated transfer of metals in soils under different land use. Colloids and Surfaces A: Physicochem. Eng. Aspects, 217, 11-19.

Cotter-Howells, J., P. Champness, J. Charnock, and R. Pattrick, 1994. Identification of pryomorphites in mine-waste contaminated soils by ATEM and EXAFS. Eur. J. Soil Science, 45, 393-402.

Craig, J. R., J. D. Rimstidt, C. A. Bonnaffon, T. K. Collins, and P. F. Scanlon, 1999. Surface Water Transport of Lead at a Shooting Range. Bulletin of Environmental Contamination and Toxicology, 63(3), 312-319.

deMatos, A. D., M. P. F. Fontes, L. M. D. Costa, and M. A. Martinez, 2001. Mobility of heavy metals as related to soil chemical and mineralogical characteristics of Brazilian soils. Environmental Pollution, 111(3), 429-435.

Dermatas, D., N. Menounou, M. Dadachov, P. Dutko, G. Shen, X. Xu, and V. Tsaneva, 2006. Lead leachability in firing range soils. Environmental Engineering Science, 23(1), 88-101.

Dragun, J. 1998. The soil chemistry of hazardous materials, 2nd ed. Amherst Scientific Publishers, Amherst.

Fayiga, A. O., and L. Q. Ma, 2006. Using phosphate rock to immobilize metals in soil and increase arsenic uptake by hyperaccumulator *Pteris vittata*. Science Total Environ, 359(1-3), 17-25.

Hardison, D. W., L. Q. Ma, T. Luongo, and W. G. Harris, 2004. Lead contamination in shooting range soils from abrasion of lead bullets and subsequent weathering. Science of the Total Environment, 328, 175-183.

Hettiarachchi, G. M., G. M. Pierzynski, and M. D. Ransom, 2000. In situ stabilization of soil lead using phosphorus and manganese oxide. Environmental Science & Technology, 34(21), 4614-4619.

ITRC, 2004. Technical Guideline: Environmental Management at Operation Outdoor Small Arms Firing Ranges, Interstate Technology & Regulatory Council, 22-67.

Jorgensen, S. S., and M. Willems, 1987. The Fate of Lead in Soils: The Transformation of Lead Pellets in Shooting-Range Soils. Ambio: A Journal of the Human Environment, 16(1), 11-15.

King, L. D., 1988. Retention of metals by several soils of the Southeastern United States. Journal of Environmental Quality, 17, 239-246.

Klein, C., and C. Hurlburt. 1993. Manual of Mineralogy. John Wiley & Sons, New York.

Lee, I.-S., O. K. Kim, Y.-Y. Chang, B. Bae, H. H. Kim, and H. H. Baek, 2002. Heavy Metal Concentrations and Enzyme Activities in Soil from a Contaminated Korean Shooting Range. Journal of Bioscience and Bioengineering, 94(5), 406-411.

Lin, Z., B. Comet, U. Qvarfort, and R. Herbert, 1995. The chemical and mineralogical behaviour of Pb in shooting range soils from central Sweden. Environ. Pollution, 89(3), 303-309.

Murray, K., A. Bazzi, C. Carter, A. Ehlert, A. Harris, M. Kopec, J. Richardson, and H. Sokol, 1997. Distribution and mobility of lead in soils at an outdoor shooting range. J. Soil Contamination, 6, 79-93.

Ownby, D. R., K. A. Galvan, and M. J. Lydy, 2005. Lead and zinc bioavailability to *Eisenia fetida* after phosphorous amendment to repository soils. Environ. Pollution, 136, 315-321.

Pickering, W. F., 1986. Ore Geol. Rev. 1.83-146. in Rampley, C.G.and Ogden, K.L. 1998. Preliminary studies for removal of lead from surrogate and real soils using a water soluble chelator: adsorption and batch extraction. Environ. Science & Technology, 32(7), 987-993.

Quirk, J.P., 1994. Interparticle forces: A basis for the interpretation of soil physical behaviour. Advances in Agronomy, 53, 121-183.

Ryan, J. A., D. Zhang, D. Hesterberg, J. Chou, and D. E. Sayers, 2001. Formation of chlorophyromorphite in a lead-contaminated soil amended with hydroxyapatite. Environ. Science & Technology, 35(18), 3798-3803.

Sauvé, S., M. McBride, and W. Hendershot, 1998. Soil solution speciation of lead(II): Effects of organic matter and pH. Soil Sci. Soc. Am. J., 62, 618-621.

Scheuhammer, A. M., and S. L. Norris. 1995. A review of the environmental impacts of lead shotshell ammunition and lead fishing weights in Canada, Rep. No. 88. Minister of Environment Canadian Wildlife Service. Ottawa.

Seaman, J. C., J. S. Arey, and P. M. Bertsch, 2001. Immobilization of nickel and other metals in contaminated sediments by hydroxyapatite addition. Journal of Environmental Quality, 30, 460-469.

Sposito, G. 1989. The Chemistry of Soils. Oxford University Press, New York.

Stansley, W., L. Widjeskog, and D. E. Roscoe, 1992. Lead contamination and mobility in surface water at trap and skeet ranges. Bulletin of Environmental Contamination and Toxicology, 49, 640-647.

Strawn, D. G., and D. L. Sparks, 2000. Effects of Soil Organic Matter on the Kinetics and Mechanisms of Pb(II) Sorption and Desorption in Soil. Soil Science Society Am J, 64, 144-156.

Tessier, A., P. G. C. Campbell, and M. Blisson, 1979. Analytical Chemistry, 51, 844-851.

US EPA. 2001. Best Management Practices for Lead at Outdoor Shooting Ranges. EPA-902-B-01-001, 86 pp.

US EPA. 1999. Test methods for evaluating solid waste, physical/chemical methods. Washington, D.C., USEPA/SW-846.

Wright, J., L. M. Peurrung, T. E. Moody, J. L. Conca, X. Chen, P. P. Didzerekis, and E. Wyse. 1995. In situ immobilization of heavy metals in apatite mineral formulations. SERDP Technical Report, Dept. of Defense. 154 p.

Yang, J., D. Mosby, S. Casteel, and R. Blanchar, 2001. Lead immobilization using phosphoric acid in a smelter-contaminated urban soil. Environ. Science & Technology, 35, pp. 3553-3559.

Zhang, M. K., Z. L. He, D. V. Calvert, P. J. Stoffella, X. E. Yang, and Y. C. Li, 2003. Phosphorus and Heavy Metal Attachment and Release in Sandy Soil Aggregate Fractions. Journal of Environmental Quality, 67(4), 1158-1167.

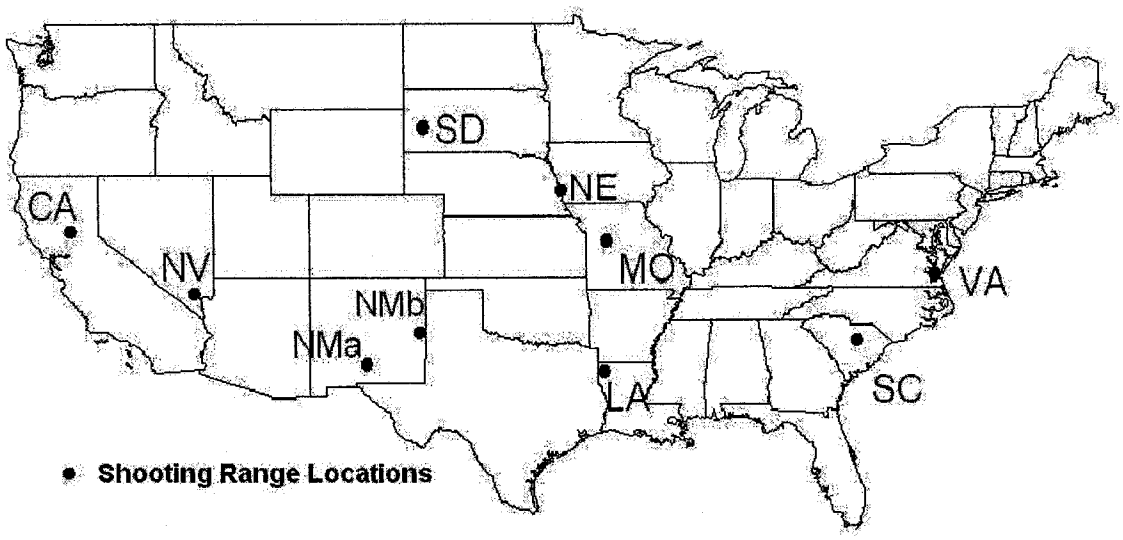

Fig. 42. Locations of Military Small Arms Firing Ranges in Nine States

Table 33. Geotechnical Characteristics of Shooting Range Berm Soils
Soil color followed Munsell method, that is 2.5YR6/8 is hue or measure of chromatic composition – 2.5Yellow-Red, value is degree of lightness or darkness - 6 (black = 0; white = 10) and chroma is strength of spectral color – 8 (neutral = 0; strongest = 8). Berm ages are estimates based on interviews with range operations personnel. Soil texture abbreviations are: Cly-clay, Fn – Fine, Lm – Loam, Slty – Silty, Snd – Sand, Sndy – Sandy. LA2 and SD1 impact berm soils were not analyzed.

Parameter	CA	LA1	LA3	MO	NE	NMa	NMb
Moisture %	2.1	25.8	20.9	18.9	15.4	24	14.4
Bulk Density (g/cm^3)	1.89	1.59	1.58	1.62	1.59	1.36	1.61
Specific Gravity	2.64	2.64	2.71	2.52	2.59	2.94	2.50
pH	7.2	6.8	7.3	7.2	8.1	7.4	8.2
CEC (meq/100 ml)	13.5	5.6	9.4	20.1	15.5	26.0	17.9
Fe (mg/kg)	12727	1656	4237	18210	1312	1068	5834
Mn (mg/kg)	502	37.9	93.9	875	41.5	13.3	155
Soil color	2.5YR6/8	2.5YR3/6	5YR3/4	10YR4/3	7.5YR3/1	5YR6/6	5YR4/6
Soil Texture	Lm	Cly Lm	Slty Cly	Slty Cly	Lm	Sndy Lm	Sndy Cly Lm
Berm Age (yr)	41	60	60	60	34	39	10†

† SAFR was constructed in 1961. In 1994 an earthen berm was constructed 25 m from firing line. Old berm at 100 m was abandoned.
†† There is no impact earthen berm at this range. Sample was taken approximately 350 m on centerline from firing line.
††† SAFR was constructed in 1967, but after a storm in 1986, the berm was pushed back and a new berm constructed.

Table 33 continued

Parameter	NV	SC	SD2	VA1	VA2
Moisture %	1.2	7.9	23.8	11.3	17.7
Bulk Density (g/cm^3)	1.80	1.86	1.47	1.87	1.67
Specific Gravity	2.66	2.54	2.62	2.62	2.60
pH	8.7	8.1	8.2	7.7	7.7
CEC (meq/100 ml)	19.3	4.4	31.5	8.7	17.7
Fe (mg/kg)	6971	2710	16993	653	385
Mn (mg/kg)	185	7.63	914	6.90	5.45
Soil color	10YR6/3	2.5YR4.5/8	10YR4/2	7.5YR4/1	7.5YR2.5/1
Soil Texture	Fn Slty Snd	Sndy Cly Lm	Cly	Sndy Lm	Sndy Lm
Berm Age (yr)	22[††]	18[†††]	15	5	40

[†] SAFR was constructed in 1961. In 1994 an earthen berm was constructed 25 m from firing line. Old berm at 100 m was abandoned.

[††] There is no impact earthen berm at this range. Sample was taken approximately 350 m on centerline from firing line.

[†††] SAFR was constructed in 1967, but after a storm in 1986, the berm was pushed back and a new berm constructed.

Table 34. Percent Soil Crystalline Phases as Determined by XRD
Quartz and cristobalite are forms of SiO_2. Impact berm soil crystalline phases were predominantly sands with some clay. ND = not detected

Crystalline Phases	CA	LA1	LA2	LA3	MO	NE	NMa	NMb	NV	SC	SD2	VA1	VA2
Clay	~12-14	~16-18	~18-20	~25	~20-22	~14-16	~5-7	~13-15	~ 4-6	~12-14	~17-19	~16-18	~10-12
Quartz	~70	~75	~75	~70	~70	~80	~5	~80	~40	~85	~70	~80	~85
Cristobalite	~10	ND	ND	ND	ND	ND	ND	ND	ND	ND	ND	ND	ND
Feldspar	~2-3	~5	~5	~2	~5-7	~5	~2	~5	~2-3	~1-2	~2-3	~2	~2
Carbonates	ND	ND	ND	ND	ND	ND	~10	ND	~50	ND	~10	~1	~1
Gypsum	ND	ND	ND	ND	ND	ND	~75	ND	ND	ND	ND	ND	ND
Iron Oxide	~1-2	<0.5	<0.5	<0.5	ND	~1	ND	ND	<1	ND	ND	ND	ND

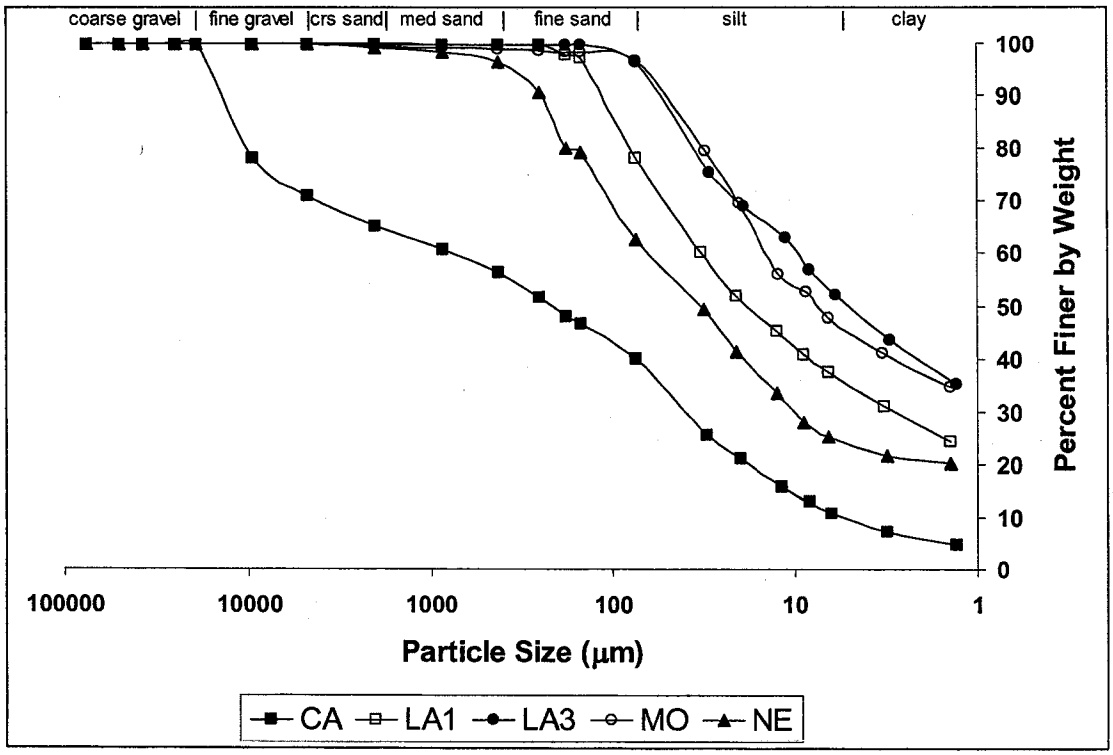

Fig. 43. Particle Size Distribution
Sample LA2 was not analyzed for particle sizes.

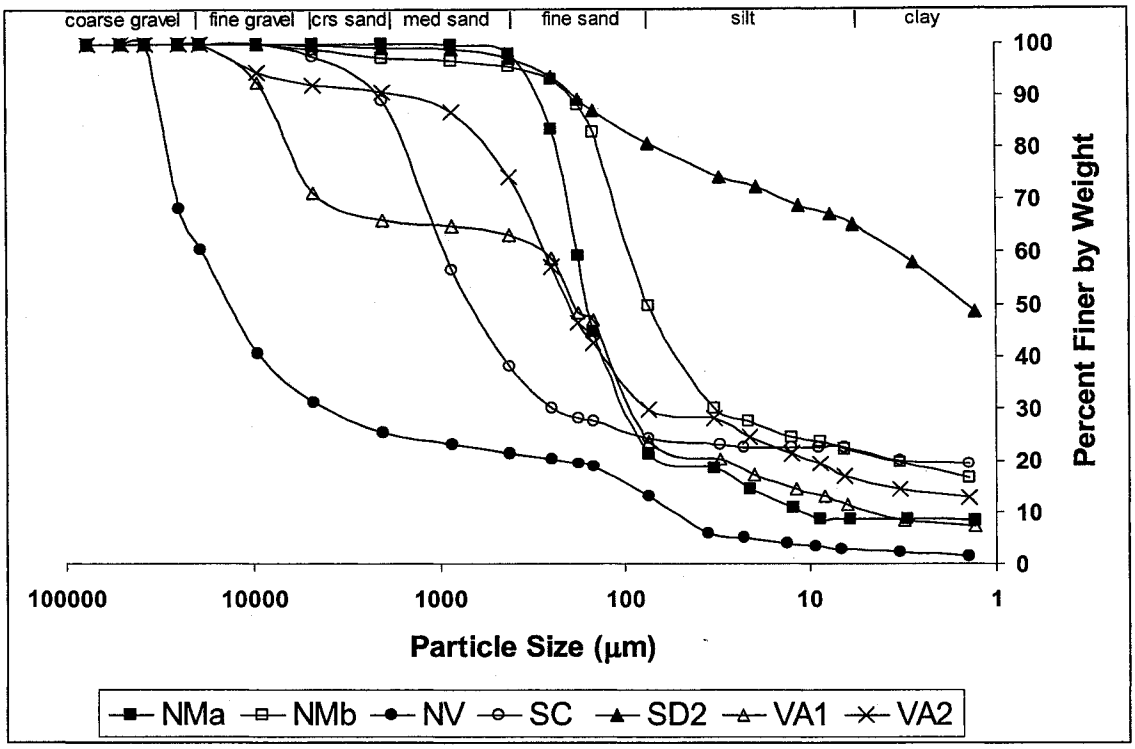

Fig. 44. Particle Size Distribution
NV soil was collected approximately 350 m from the firing line along a perpendicular transecting firing lanes centerline. Sample SD1 was not analyzed for particle sizes.

Table 35. Bulk Soil Sequential Extraction Pb Associations in mg/kg
Values are the average of triplicate samples. Values <0.05 indicate results less than the detection limit of 0.050 mg/L. OM = Organic Matter; SD = Standard Deviation.

Parameter	CA	LA1	LA2	LA3	MO	NE	NMa	NMb	NV	SC	SD2	VA1	VA2
Exchangeable	797.0	<0.05	<0.05	6.1	24.4	10.6	0.1	2.5	<0.05	85.1	6.9	12.3	<0.05
SD	79.8	0.0	0.0	0.4	1.6	0.1	0.0	0.0	0.0	36.9	1.3	21.3	0.0
Percent	1.2	0.0	0.0	0.5	4.3	0.1	0.0	4.6	0.0	2.8	0.1	0.7	0.0
Carbonates	10,270.2	<0.05	98.0	50.6	127.7	303.4	2.2	10.2	39.0	234.4	379.3	86.0	<0.05
SD	2,851.3	0.0	169.8	12.2	34.6	124.0	0.7	1.8	38.1	16.3	40.2	2.8	0.0
Percent	15.0	0.0	2.4	3.8	22.3	2.7	0.0	18.5	0.5	7.6	2.8	4.7	0.0
Fe-Mn	4,673.4	<0.05	61.2	68.6	139.7	127.6	0.8	16.5	33.2	74.6	398.2	<0.05	<0.05
SD	3,957.5	0.0	33.1	24.1	24.7	60.2	0.4	2.9	14.7	22.9	210.6	0.0	0.0
Percent	6.8	0.0	1.5	5.2	24.4	1.1	0.0	30.1	0.5	2.4	3.0	0.0	0.0
OM & sulfides	6,312.0	<0.05	158.2	163.0	72.0	447.8	1.6	13.1	104.0	372.1	1,792.5	<0.05	<0.05
SD	636.2	0.0	23.5	41.8	46.5	57.6	0.4	3.4	83.3	68.3	1,693.1	0.0	0.0
Percent	9.2	0.0	3.8	12.4	12.6	3.9	0.0	23.8	1.5	12.1	13.5	0.0	0.0
Residual	46,466	1,475	3,816	1,030	208	10,491	44,500	12.7	6,925	2,321	10,747	1,736	1,742
SD	35,089	640	5,809	1,123	38	4,834	23,160	0.7	11,417	1,040	17,553	141	326
Percent	67.8	100.0	92.3	78.1	36.4	92.2	100.0	23.1	97.5	75.2	80.7	94.6	100.0
Total	68,519	1,475	4,134	1,319	572.4	11,381	44,504	54	7,102	3,087	13,324	1,834	1,742
Percent	100	100	100	100	100	100	100.	100	100	100	100	100.	100

Table 36. Lead Fractional and Soil Leaching Associations
Totals are in units mg/kg and SPLP and TCLP are in units mg/L. SD = standard deviation. Results are averages of triplicates.

Grain Size (mm)	Analysis	CA[†]	LA1	LA2	LA3	MO	NE	NMa	NMb
> 4.75	Total	-	42523	100903	8462	408	-	3060	-
	SD	-	6476	132868	10192	64.1	-	161	-
2.00 to 4.75	Total	45240	165700	211500	10110	745	33487	3227	176
	SD	401	13811	54784	0	86.1	9497	156	12.2
0.250 to 2.00	Total	68597	172800	86863	114	1377	70690	8955	49.6
	SD	15216	29012	10533	137	50.1	66113	1252	11.5
0.250 to 2.00	SPLP	4.93	24.5	5.17	10.4	5.13	4.19	0.387	0.053
	SD	0.71	2.25	0.578	4.05	2.17	1.37	0.142	0.005
0.250 to 2.00	TCLP	1323	2629	1637	1115	0.304	5786	267	5.13
	SD	13.0	66.7	85.1	210	0.105	7496	24.5	2.17
0.075 to 0.250	Total	22383	2441	1047	<0.05	857	11057	2436	19.6
	SD	382	152	40.1	0	14.5	136	95.6	0.850
0.075 to 0.250	SPLP	3.30	0.326	0.299	0.580	0.794	0.840	0.203	<0.050
	SD	0.23	0.284	0.005	0.186	0.874	0.383	0.134	0.0
0.075 to 0.250	TCLP	970	617	92.2	313	0.237	744	137	0.794
	SD	23.9	54.8	18.8	14.4	0.169	22.3	7.73	0.874
< 0.075	Total	18587	11137	3753	1.36	136	7166	3799	41.3
	SD	2843	297	45.2	0.47	118	488	72.3	5.35
< 0.075	SPLP	1.58	2.11	0.064	0.521	0.121	0.391	0.151	<0.050
	SD	0.13	0.358	0.009	0.034	0.026	0.144	0.023	0.0
< 0.075	TCLP	716	349	106	56.7	0.050	308	333	0.054
	SD	5.69	262	3.24	7.02	0.0	13.2	227	0.007

[†] 2,00 to 4.75 mm SPLP: CA = 0.718 mg/L, SD=-.635; NV = 0.050 mg/L, SD = 0.0 and 0.250 to 2.00 mm TCLP: CA = 967 mg/L, SD = 221 and NV = 0.469 mg/L, SD = 0.030

Table 36 continued

Grain Size (mm)	Analysis	NV†	SC	SD2	VA1	VA2
> 4.75	Total	7685	13297	-	36710	32100
	SD	0.0	172	-	7948	1806
2.00 to 4.75	Total	12111	48883	-	36410	13323
	SD	4877	8274	-	27622	1539
0.250 to 2.00	Total	3534	4.95	13623	3475	7497
	SD	395	1.79	3718	138.2	2893.9
0.250 to 2.00	SPLP	1.01	0.064	-	3.79	2.06
	SD	0.22	0.016	-	0.809	0.816
0.250 to 2.00	TCLP	292	605	96.4	417	727
	SD	224	42.6	34.0	32.09	98.18
0.075 to 0.250	Total	668	2634	5548	1239	1636
	SD	93.7	2287	7017	15.52	112.9
0.075 to 0.250	SPLP	0.212	0.180	0.050	1.21	0.944
	SD	0.020	0.057	0.0	0.287	0.313
0.075 to 0.250	TCLP	32.7	484	6.04	77.4	96.2
	SD	2.54	15.1	0.622	2.32	6.37
< 0.075	Total	907	12530	817	8294	6111
	SD	14.8	244	45.1	198.03	67.55
< 0.075	SPLP	0.156	1.24	0.053	3.31	0.930
	SD	0.051	0.674	0.005	0.698	0.229
< 0.075	TCLP	8.10	727	1.29	11.7	6.54
	SD	2.97	14.2	0.069	5.16	4.63

Table 37. Measured Stormwater Lead Concentrations
Measurements are in □g/L. Average dissolved Pb = 104.0 □g/L (SD = 152, n = 17). At least one field duplicate was taken for each sampling event. NS = not sampled. n = number of samples. Std Dev = standard deviation. Not applicable fields were left blank.

Parameter	CA	LA1	LA2	LA3	MO	NE	NMa	NMb
Total Pb	46.0	490	NS	5.2	26008	NS	27.8	NS
Std Dev	34.3				44163		19.8	
Dissolved Pb	29.2	310	NS	4.2	118	NS	4.1	NS
Std Dev	20.9				99.1		2.7	
n	4	1		1	3		4	

Parameter	NV	SC	SD2	VA1	VA2
Total Pb	NS	NS	9250	600	1600
Std Dev			6718		
Dissolved Pb	NS	NS	440	61	26
Std Dev			14.1		
n			2	1	1

Table 38. Batch Study Results

Amendments with percent adsorbed < 90.3% have been highlighted by bold-lined boxes. Control and adsorbed amounts are in units mg/L. Results are averages of triplicates. FB = Apatite II; TSP = triple super phosphate; SD = Standard Deviation. <0.050 indicates instrument detection limit.

Amendment	CA	LA1	LA2	LA3	MO	NE	NMa	NMb
Control	1294	263	154	839	1.042	703	84.3	153.9
SD	92.1	76.7	59.4	115.8	0.49	91.1	70.3	51.3
3% FB	1134	2.38	3.20	105	0.198	271	0.687	<0.05
SD	95.2	0.89	2.00	164.5	0.03	51.1	0.12	0.0
% Adsorbed	12.4	99.1	97.9	87.5	81.0	61.5	99.2	99.0
5% FB	1042	1.00	0.82	3.70	0.140	6.57	0.675	<0.05
SD	93.0	0.23	0.12	0.88	0.16	4.52	0.12	0.0
% Adsorbed	19.5	99.6	99.5	99.6	86.6	99.1	99.2	99.0
3% TSP	9.04	1.07	0.49	3.98	0.086	2.29	171†	<0.05
SD	0.57	0.19	0.09	1.11	0.20	0.29	35.1	0.0
% Adsorbed	99.3	99.6	99.7	99.5	91.8	99.7	-	99.0
5% TSP	4.87	0.44	0.29	1.79	<0.05	1.86	69.7	2.87
SD	0.35	0.17	0.22	0.72	0.0	0.55	34.1	0.96
% Adsorbed	99.6	99.8	99.8	99.8	95.2	99.7	17.3	98.0

† Mass removed was greater than control.

Table 38 continued

Amendment	NV	SC	SD2	VA1	VA2
Control	44.7	566	15.5	266	311
SD	26.0	55.6	5.0	133.1	91.3
3% FB	1.37	5.35	2.30	1.01	1.05
SD	1.62	4.0	1.6	0.55	0.40
% Adsorbed	97.0	90.3	85.2	99.6	99.7
5% FB	20.7	1.23	1.29	0.110	1.08
SD	23.0	0.18	0.36	0.05	0.25
% Adsorbed	53.7	99.8	91.7	99.9	100.0
3% TSP	0.599	2.37	0.492	8.87	28.6
SD	0.12	0.27	0.13	7.00	16.1
% Adsorbed	98.7	99.6	96.8	96.7	90.8
5% TSP	0.389	1.59	0.248	2.15	3.23
SD	0.82	0.13	0.16	0.66	3.53
% Adsorbed	99.1	99.7	98.4	99.2	99.0

† Mass removed was greater than control.

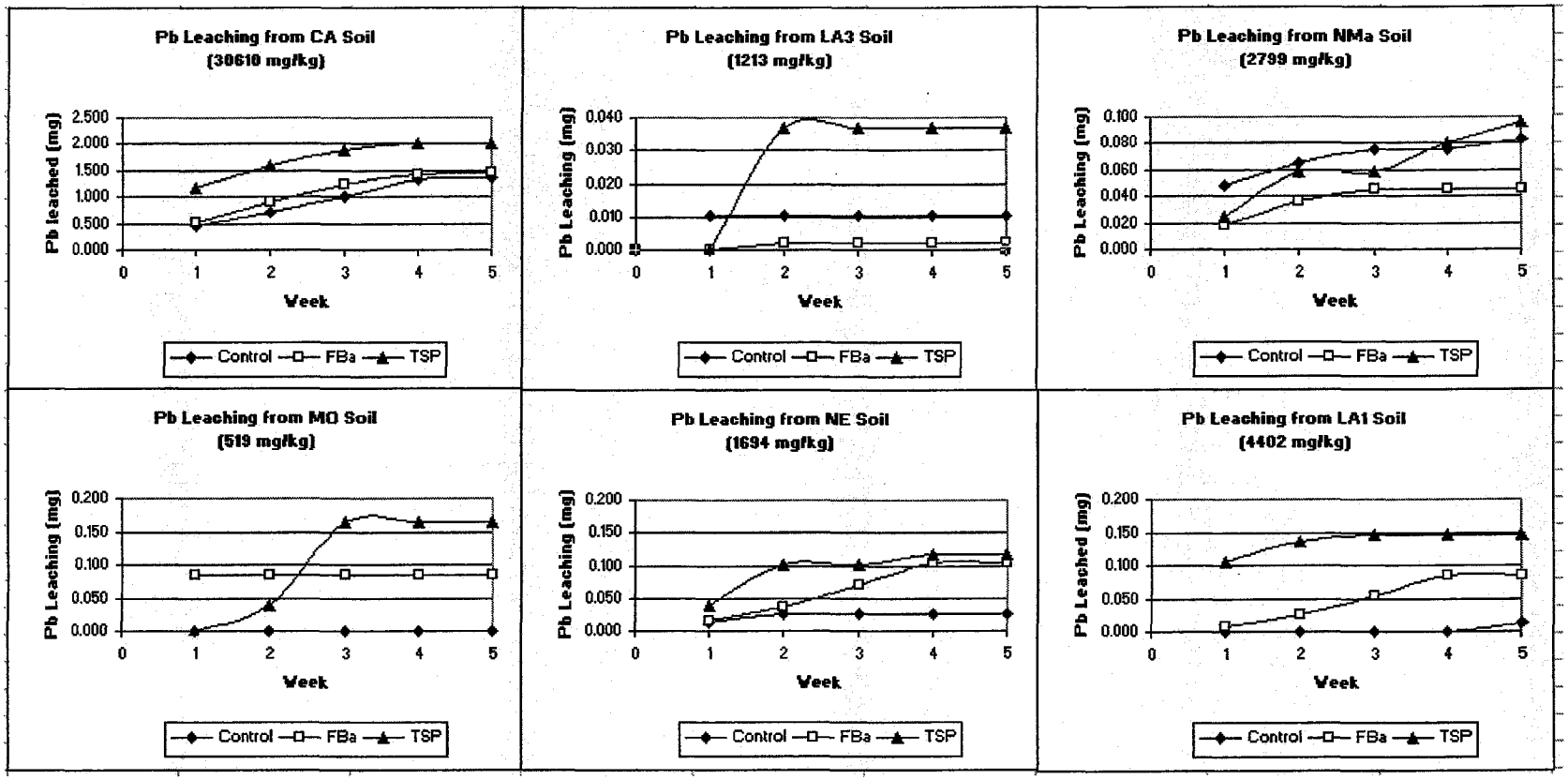

Fig. 45. Lead Leaching Behavior in Soils From Column Studies
Control had no amendments added. Amounts are accumulative over 5 week study period. Original soil lead concentration is shown in parenthesis. Amendment 3% FBa reduced the amount of lead released compared to control for LA3 and NMa soils. Amendment 3% TSP did not reduce the amount of lead released compared to control for any of these soils.

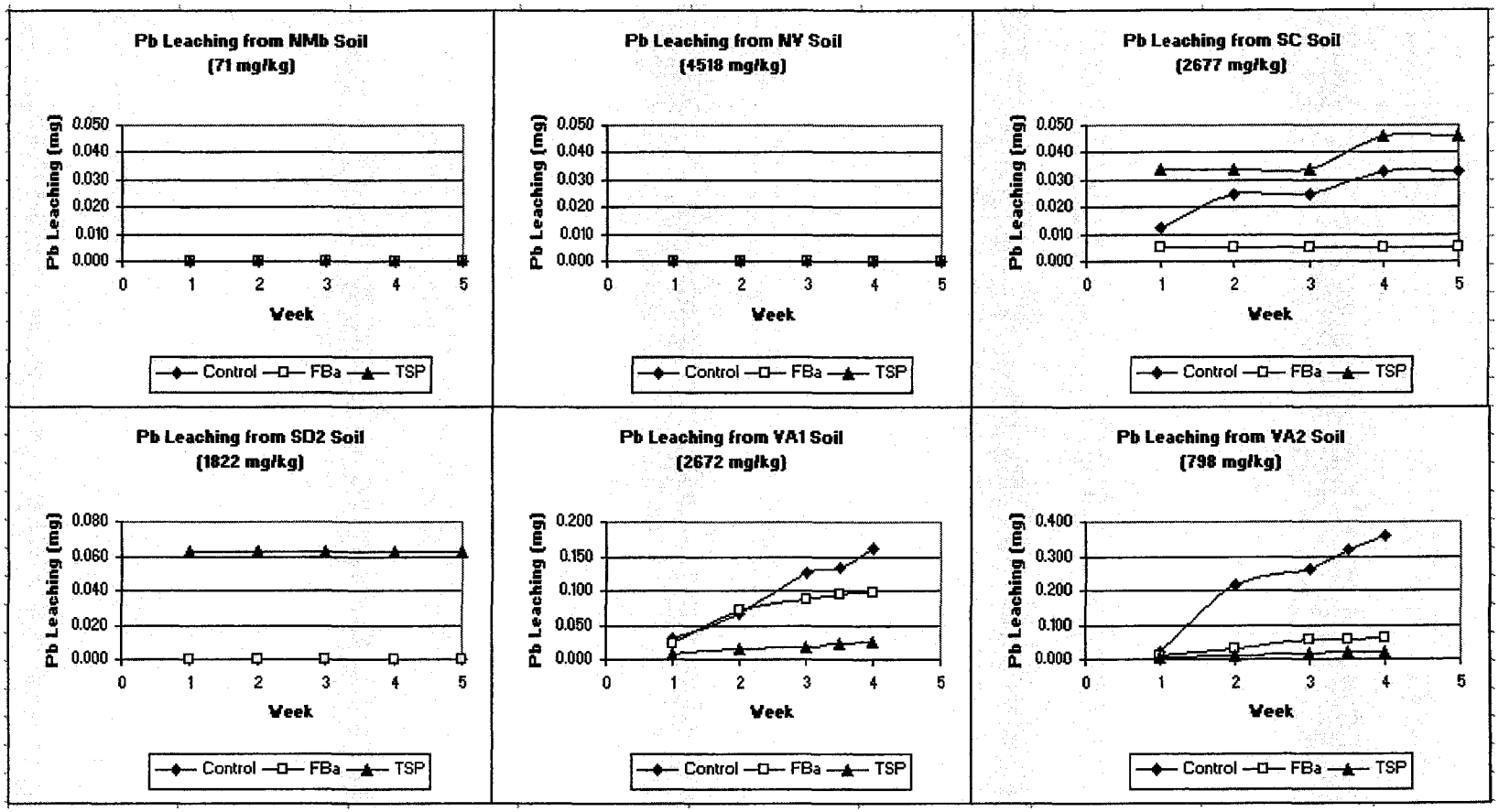

Fig. 45. Continued
Control had no amendments added. Amounts are accumulative over 5 week study period, except VA1 and VA2 study period was 27 days. Original soil lead concentration is shown in parenthesis. Amendment 3% FBa reduced the amount of lead released compared to control for the SC, VA1 and VA2 soils. Amendment 3% TSP reduced the amount of lead released compared to control for VA1 and VA2 soils.

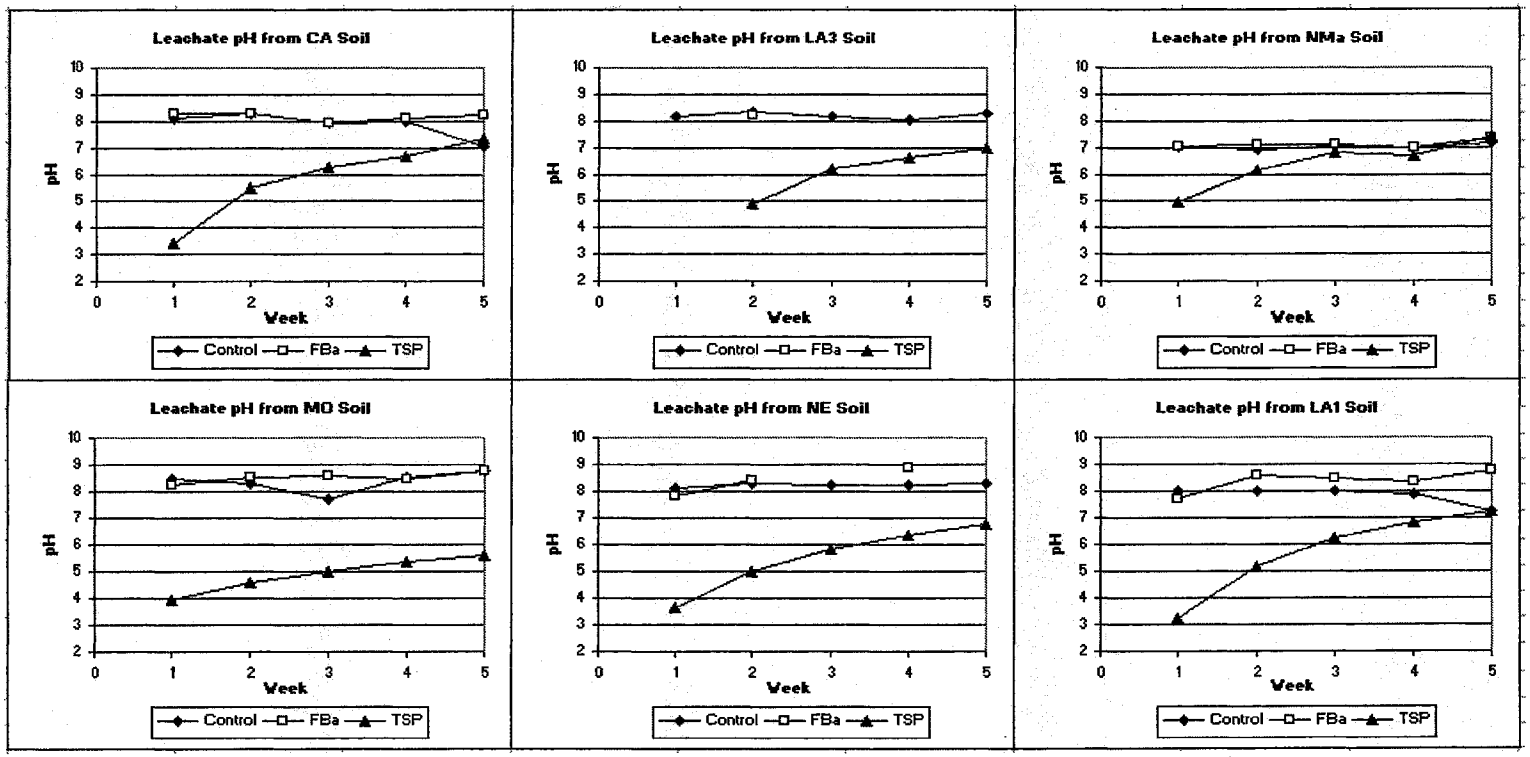

Fig. 46. Column Study Leachate pH
FBa leachate pH was significantly different than control ($F = 9.47$, $P = 0.002$, $n = 119$) and TSP leachate pH was also significantly different than control ($F = 115.5$, $P << 0.001$, $n = 135$). Initial pH drop after TSP treatment was substantial and in most cases never returned to control value. LA3 soil with TSP amendment had no leachate at the end of week 1, and FBa amended soil had no leachate at the end of week 1, 3, 4 and 5. NE soil with FBa amendment had no leachate at the end of weeks 3 and 5.

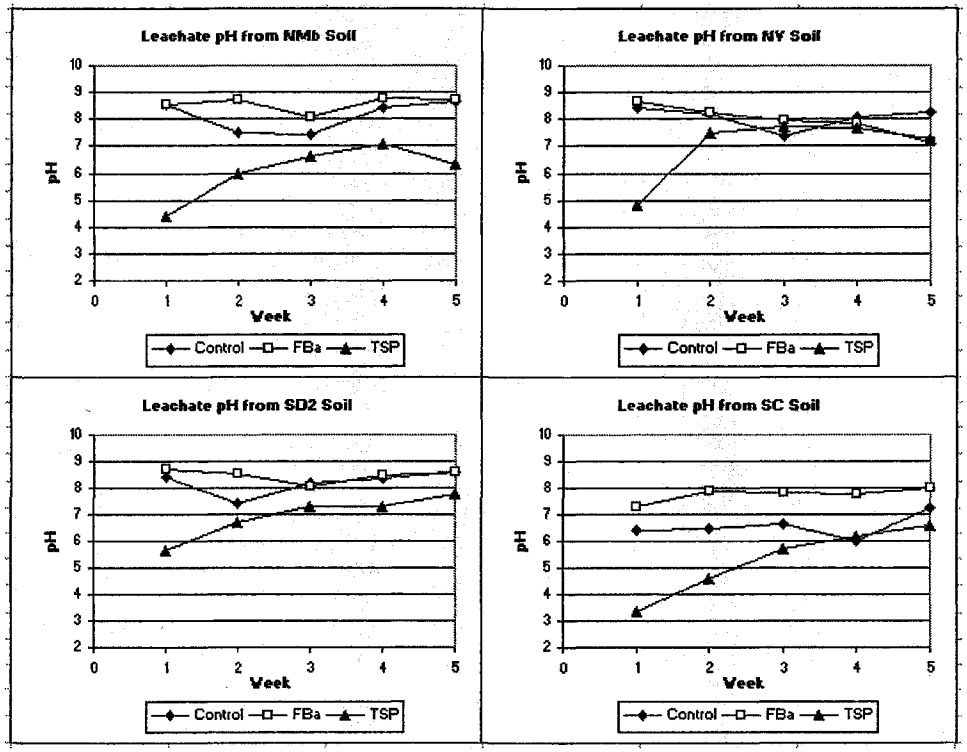

Fig. 46. Continued
FBa and TSP leachate pH were significantly different than control (see Figure 47 note). VA1 and VA2 soils leachate pH were not measured. TSP leachate pH drop was significant in the first week of use, and returned within 1 pH standard unit for NV and SD2 soils by the end of the 5-week study period.

C. FORMATION CONSTANTS

Formation constants are from Puigdomenech, I. (2004), "MEDUSA, Make Equilibrium Diagrams Using Sophisticated Algorithms and HYDRA, Hydro Chemical Equilibrium - Constant Database." Royal Institute of Technology. Downloaded 3 Apr 2006 from http:/www.kemi.kth.se/medusa.

Equilibrium Complexes	Log K	Cation	Soluble or Solid Complexes
34 H+ + 19MoO4 2- = Mo19O59 4-	198	Mo2+	Soluble
3 PO4 3- + Cl- + 5 Pb 2+ = Pb5(PO4)3Cl	84.43	Pb2+	Solid
11 H+ + 7 MoO4 2- = H3Mo7O24 3-	67.92	Mo2+	Soluble
10 H+ + 7MoO4 2- = H2Mo7O24 4-	64.27	Mo2+	Soluble
3 PO4 3- + 5 Pb 2+ = H+ + Pb5(PO4)3OH	62.79	Pb2+	Solid
9H+ + 7 MoO4 2- = HMo7O24 5-	59.44	Mo2+	Soluble
8 H+ + 7 MoO4 2- = Mo7O24 6-	52.99	Mo2+	Soluble
H+ + 4 Ca2+ + 3 PO4 3- = Ca4H(PO4)3	46.9	Ca2+	Solid
2 PO4 3- + 3 Pb 2+ = Pb3(PO4)2	44.362	Pb2+	Solid
5 Ca 2+ + 3 PO4 3- = H+ + Ca5(PO4)3OH	40.459	Ca2+	Solid
4 H+ + 2 PO4 3- + Cu2+ = Cu(H2PO4)2	40.15	Cu2+	Soluble
4 H+ + Ca 2+ +2 PO4 3- = Ca(H2PO4)2	39.05	Ca2+	Soluble
2 PO4 3- + 3 Cu 2+ = Cu3(PO4)2	36.85	Cu2+	Solid
3H+ + 2PO43- + Cu2+ = CuH3(PO4)2	36.41	Cu2+	Soluble
2 PO4 3- + 3 Fe 2+ = Fe3(PO4)2:8H2O	36.0	Fe2+	Solid
2 PO4 3- + 3 Cu 2+ = Cu3(PO4)2:3H2O	35.12	Cu2+	Solid
2 PO4 3- + 3 Zn 2+ = Zn3(PO4)2:4H2O	32.04	Zn2+	Solid
2 H+ + PO4 3- + Cu2+ = CuH2(PO4)2 2-	31.76	Cu2+	Soluble
2 PO4 3- + 3 Ni 2+ = Ni3(PO4)2	31.3	Ni2+	Solid
Ca 2+ + 4 CO3 2- + 3 Mg 2+ = CaMg3(CO3)4	29.968	Ca2+, Mg2+	Solid
3 Ca2 + 2 PO43- = Ca3(PO4)2	28.92	Ca2+	Solid
H+ + PO4 3- + Mn 2+ = MnHPO4	25.293	Mn2+	Solid
2 PO4 3- + 3 Mn 2+ = Mn3(PO4)2	23.827	Mn2+	Solid
H+ + PO4 3- + Pb 2+ = PbHPO4	23.806	Pb2+	Solid
3 Mg 2+ + 2 PO4 3- = Mg3(PO4)2	23.28	Mg2+	Solid
2 H+ + PO4 3- + Fe2+ = FeH2PO4+	22.253	Fe2+	Soluble
3 H+ + PO4 3- = H3PO4	21.702		Soluble
2H+ + PO43- + Cu2+ = CuH2PO4+	21.45	Cu2+	Soluble
2H+ + PO4 3- + Pb 2+ = PbH2PO4+	21.073	Pb2+	Soluble
2 H+ + Mg 2+ + PO4 3- = MgH2PO4+	21.066	Mg2+	Soluble
2H+ + Ca2+ + PO4 3- = CaH2PO4+	20.961	Ca2+	Soluble
CO3 2- + 2 Cl- + 2 Pb 2+ = PbCl2:PbCO3	19.81	Pb2+	Solid
2H+ + PO4 3- = H2PO4-	19.553	Mo2+	Soluble
H+ + Ca 2+ + PO4 3- = CaHPO4 2H2O	18.955	Ca2+	Solid

Equilibrium Complexes	Log K	Cation	Soluble or Solid Complexes
H+ + Mg 2+ + PO4 3- = MgHPO4.3H2O	18.175	Mg2+	Solid
2 CO3 2- + 3 Pb 2+ = 2 H+ + Pb(OH)2:2PbCO3	17.46	Pb2+	Solid
Ca 2+ + 2 CO3 2- + Mg 2+ = CaMg(CO3)2	17.09	Ca2+, Mg2+	Solid
2 CO3 2- + 3 CU 2+ = 2H+ + Cu3(CO3)2(OH)2	16.908	Cu2+	Solid
2 H+ + CO3 2- = H2CO3	16.681		Soluble
H+ + PO4 3- + Cu2+ = CuHPO4	16.45	Cu2+	Soluble
H+ + PO4 3- + Fe 2+ = FeHPO4	15.946	Fe2+	Soluble
MoO4 2- + Pb 2+ = PbMoO4	15.62	Pb2+, Mo2+	Solid
H+ + PO4 3- + Pb2+ = PbHPO4	15.475	Pb2+	Soluble
H+ + Mg2+ + PO4 3- = MgHPO4	15.216	Mg2+	Soluble
H+ + Ca2+ + PO4 3- = CaHPO4	15.085	Ca2+	Soluble
Na+ + 7 Si(OH)4 = H+ + NaSi7O13(OH)3:3H2O	14.3	Na+	Solid
H+ + CO3 2- + Pb 2+ = PbHCO3+	13.229	Pb2+	Soluble
CO3 2- + Pb 2+ = PbCO3	13.13	Pb2+	Solid
H+ + CO3 2- + Cu2+ = CuHCO3+	13.029	Cu2+	Soluble
H + NH3 + PO43- + Fe 2+ = FeNH4PO4	13.0	Fe2+	Solid
H+ + Na+ + PO4 3- = NaHPO4-	12.636	Na+	Soluble
H+ + NH3 + Mg 2+ + PO4 3- = MgNH4PO4	12.6	Mg2+	Solid
4 NH3 + Cu 2+ = Cu(NH3)4+2	12.5	Cu2+	Soluble
H+ + CO3 2- + Ni 2+ = NiHCO3+	12.469	Ni2+	Soluble
H+ + CO3 2- + Zn 2+ = ZnHCO3+	12.429	Zn2+	Soluble
2 Sb(OH)3 = a-Sb2O3	12.365	Sb3+	Soluble
H+ + PO4 3-=HPO4 2-	12.346		Soluble
H+ + CO32- + Fe2+ = FeHCO3+	12.329	Fe2+	Soluble
H+ + CO3 2- + Mn 2+ = MnHCO3+	12.279	Mn2+	Soluble
2H+ + MoO4 2- = H2MoO4	11.67	Mo2+	Solid
H+ + Ca2+ + CO32- = CaHCO3+	11.435	Ca2+	Soluble
H+ CO3 2- + Mg2+ = MgHCO3+	11.399	Mg2+	Soluble
CO3 2- + Mn 2+ = MnCO3	11.13	Mn2+	Solid
H+ + 2 CO3 2- + 3 Na+ = NaHCO3:Na2CO3:2H2O	11.124	Na+	Solid
H+ + CO3 2- + Na+ = NaHCO3	10.877	Na+	Solid
2 CO3 2- + Pb 2+ = Pb(CO3)2 2-	10.64	Pb2+	Soluble
CO3 2- + Fe 2+ = FeCO3	10.45	Fe2+	Solid
H+ + NH3 + SO4 2- = NH4SO4-	10.362		Soluble
H+ + CO3 2- = HCO3-	10.329		Soluble
3 NH3 + Cu2+ = Cu(NH3)3+2	10.3	Cu2+	Soluble
CO3 2- + Zn 2+ = ZnCO3:H2O	10.26	Zn2+	Solid
2 CO3 2- + Ni 2+ = Ni(CO3)2 2-	10.11	Ni2+	Soluble

Equilibrium Complexes	Log K	Cation	Soluble or Solid Complexes
H+ + CO3 2- + Na+ = NaHCO3	10.079	PO4-	Soluble
CO3 2- + Zn 2+ = ZnCO3	10	Zn2+	Solid
2 CO3 2- + Cu2+ = Cu(CO3)2 2-	9.83	Cu2+	Soluble
PO4 3- + Cu 2+ + 2 Pb 2+ = 3 H+ + Pb2CuPO4(OH)3:3H2O	9.79	Pb2+, Cu2+	Solid
2 CO3 2- + Zn 2+ = Zn(CO3)2 2-	9.63	Zn2+	Soluble
CO3 2- = Cu 2+ = CuCO3	9.63	Cu2+	Solid
4 NH3 + Zn 2+ = An(NH3)4 2+	9.3	Zn2+	Soluble
H+ + NH3 = NH4+	9.237001		Soluble
6 NH3 + Ni 2+ = Ni(NH3)6+2	9	Ni2+	Soluble
5 NH3 + Ni 2+ = Ni(NH3)4+2	8.9	Ni2+	Soluble
4 CO3 2- + 5 Mg 2+ = 2 H+ + Mg5(CO3)4(OH)2:4H2O	8.762	Mg2+	Solid
Ca 2+ + CO3 2- = CaCO3	8.48	Ca2+	Solid
2 Sb(OH)3 = Sb2O3	8.48	Sb3+	Solid
2 H+ + MoO4 2- = H2MoO4	8.22	Mo2+	Soluble
CO3 2- + Mg 2+ = MgCO3	8.029	Mg2+	Solid
Ca 2+ + MoO4 2- = CaMoO4	7.95	Ca2+, Mo2+	Solid
4 NH3 + Ni 2+ = Ni(NH3)4+2	7.8	Ni2+	Soluble
SO4 2- + Pb 2+ = PbSO4	7.79	Pb2+	Solid
2 NH3 + Cu2+ = Cu(NH3)2+2	7.45	Cu2+	Soluble
CO3 2- + Pb 2+ = PbCO3	7.24	Pb2+	Soluble
3 NH3 + Zn 2+ = Zn(NH3)3 2+	7.1	Zn2+	Soluble
CO3 2- + Ni 2+ = NiCO3	6.87	Ni2+	Soluble
CO3 2- + Ni 2+ = NiCO3	6.84	Ni2+	Solid
CO3 2- + Cu2+ = CuCo3	6.73	Cu2+	Soluble
3 NH3 + Ni 2+ = Ni(NH3)3+2	6.7	Ni2+	Soluble
Mg2+ + PO4 3- = MgPO4-	6.589	Mg2+	Soluble
4H+ + 2Cl- + MoO4 2- = MoO2Cl2	6.5	Mo2+	Soluble
Ca2+ + PO4 3- = CaPOr-	6.459	Ca2+	Soluble
CO3 2- + Mg 2+ = MgCO3:3H2O	5.621	Mg2+	Solid
CO3 2- + Zn 2+ = ZnCO3	5.3	Zn2+	Soluble
CO3 2- + 2 Cu 2+ = 2 H+ + Cu2CO3(OH)2	5.179	Cu2+	Solid
CO3 2- + Mn 2+ = MnCO3	4.9	Mn2+	Soluble
2 NH3 + Ni 2+ = Ni(NH3)2+2	4.89	Ni2+	Soluble
2 NH3 + Zn 2+ = Zn(NH3)2 2+	4.8	Zn2+	Soluble
2 Cl- + Pb 2+ = PbCl2	4.77	Pb2+	Solid
Ca 2+ + SO4 2- = CaSO4:2H2O	4.58	Ca2+	Solid
CO3 2- + Fe 2+ = FeCO3	4.38	Fe2+	Soluble
Ca 2+ + SO4 2- = CaSO4	4.36	Ca2+	Solid
H+ + MoO4 2- = HMoO4-	4.23	Mo2+	Soluble

Equilibrium Complexes	Log K	Cation	Soluble or Solid Complexes
NH3 + Cu2+ = CuNH3+2	4.05	Cu2+	Soluble
Si(OH)4 = SiO2 (crystalline)	3.98		Solid
2 SO4 2- + Pb 2+ = Pb(SO4)2 2-	3.47	Pb2+	Soluble
2 SO4 2- + Zn 2+ = Zn(SO4)2 2-	3.28	Zn2+	Soluble
Ca 2+ + CO3 2- = CaCO3	3.224	Ca2+	Soluble
4 NH3 + Fe2+ = Fe(NH3)4+2	3.2	Fe2+	Soluble
H+ + Ca2+ + SO4 2- = CaHSO4+	3.068	Ca2+	Soluble
H+ + SO4 2- + Fe2+ = FeHSO4+	3.068	Fe2+	Soluble
3 NH3 + Fe2+ = Fe(NH3)3+2	3.0	Fe2+	Soluble
CO3 2- + Mg 2+ = MgCO3	2.98	Mg2+	Soluble
SO4 2- + Pb 2+ = PbSO4	2.75	Sb3+	Soluble
NH3 + Ni 2+ = NiNH3+2	2.73	Ni2+	Soluble
Si(OH)4 = SiO2 (amorphous)	2.71		Solid
3 H+ + 4 Cl- + Sb(OH)3 = SbCl4-	2.7	Sb3+	Soluble
2 Cl- + Sn 2+ = SnCl2	2.7	Sn2+	Soluble
3 Cl- + Sn 2+ = SnCl3-	2.7	Sn2+	Soluble
SO4 2- + Cu 2+ = CuSO4:5H2O	2.64	Cu2+	Solid
2 NH3 + Fe2+ = Fe(NH3)2+2	2.5	Fe2+	Soluble
Mg2+ + SO4 2- = MgSO4	2.37	Mg2+	Soluble
SO4 2- + Zn 2+ = ZnSO4	2.37	Zn2+	Soluble
SO4 2- + Ni 2+ = NiSO4:7H2O	2.36	Ni2+	Solid
SO42- + Cu2+ = CuSO4	2.31	Cu2+	Soluble
Ca2+ + SO4 2- = CaSO4	2.3	Ca2+	Soluble
NH3 + Zn 2+ = ZnNH3 2+	2.3	Zn2+	Soluble
SO4 2- + Ni 2+ = NiSO4	2.29	Ni2+	Soluble
SO4 2- + Fe 2+ = FeSO4	2.25	Fe2+	Soluble
SO4 2- + Mn 2+ = MnSO4	2.25	Mn2+	Soluble
SO4 2- + Fe 2+ = FeSO4:7H2O	2.209	Mo2+	Solid
Mg 2+ + SO4 2- = MgSO4:7H2O	2.14	Mg2+	Solid
SO4 2- + Ni 2+ = NiSO4:6H2O	2.04	Ni2+	Solid
H+ + SO4 2- = HSO4-	1.98		Soluble
Mg 2+ + MoO4 2- = MgMoO4	1.85	Mg2+, Mo2+	Solid
2 Cl- + Pb 2+ = PbCl2	1.8	Pb2+	Soluble
Cl- + Sn2+ = SnCl+	1.8	Sn2+	Soluble
SO4 2- + Zn 2+ = ZnSO4:6H2O	1.765	Zn2+	Solid
3 Cl- + Pb 2+ = PbCl3-	1.7	Pb2+	Soluble
3 SO4 2- + Zn 2+ = Zn(SO4)3 4-	1.7	Zn2+	Soluble
4 SO4 2- + Zn 2+ = Zn(SO4)4 6-	1.7	Zn2+	Soluble
Cl- + Pb 2+ = PbCl+	1.6	Pb2+	Soluble
3 NH3 + Cu2+ = H+ + Cu(NH3)3OH+	1.55	Cu2+	Soluble

Equilibrium Complexes	Log K	Cation	Soluble or Solid Complexes
3 NH3 + Mn2+ = Mn(NH3)3+2	1.55	Mn2+	Soluble
NH3 + Fe2+ = FeNH3+2	1.5	Fe2+	Soluble
NH3 + Pb2+ = PbNH3 2+	1.5	Pb2+	Soluble
4 NH3 + Mn 2+ = Mn(NH3)4+2	1.45	Mn2+	Soluble
H+ + Sb(OH)3 = Sb(OH)2+	1.41	Sb3+	Soluble
2 NO3- + Pb 2+ = Pb(NO3)2	1.4	Pb2+	Soluble
4 Cl- + Pb 2+ = PbCl4 2-	1.38	Pb2+	Soluble
2 NH3 + Mn 2+ = Mn(NH3)2+2	1.35	Mn2+	Soluble
CO3 2- + 2 Na+ = Na2CO3:10H2O	1.311	Na+	Solid
CO3 2- + Na+ = NaCO3-	1.27		Soluble
NO3- +Pb2+ = PbNO3	1.17	Pb2+	Soluble
2 Na+ + SO4 2- = Na2SO4:10H2O	1.114	Na+	Solid
2 SO4 2- + Ni 2+ = Ni(SO4)2 2-	1.02	Ni2+	Soluble
2 Cl- + Ni 2+ = NiCl2	0.96	Ni2+	Soluble
NH3 + Mn 2+ = MnNH3+2	0.85	Mn2+	Soluble
Na+ + SO4 2- = NaSO4-	0.7	Na+	Soluble
Cl- + Cu 2+ = CuCl+	0.64	Cu2+	Soluble
Cl- + Mn2+ = MnCl+	0.61	Mn2+	Soluble
NH3 + Mg 2+ = MgNH3+2	0.6	Mg2+	Soluble
2 NO3- + Ca 2+ = Ca(NO3)2	0.6	Ca2+	Soluble
3 Cl- + Zn 2+ = ZnCl3-	0.5	Zn2+	Soluble
CO3 2- + 2 Pb2+ = 2 H+ + PbO:PbCO3	0.5	Pb2+	Solid
NO3- + Ca 2+ = CaNO3+	0.5	Ca2+	Soluble
NO3- + Cu 2+ = CuNO3+	0.5	Cu2+	Soluble
2 Cl- + Zn 2+ = ZnCl2	0.45	Zn2+	Soluble
Cl- + Zn 2+ = ZnCl+	0.43	Zn2+	Soluble
Cl- + Ni 2+ = NiCl+	0.4	Ni2+	Soluble
SO4 2- + 2 Pb 2+ = 2 H+ + PbO:PbSO4	0.28	Pb2+	Solid
2 Cl- + Mn 2+ = MnCl2	0.25	Mn2+	Soluble
Ca2+ + NH3 = CaNH3+2	0.2	Ca2+	Soluble
2 Cl- + Cu2+ = CuCl2	0.2	Cu2+	Soluble
2 NH3 + Mg2+ = Mg(NH3)2+2	0.2	Mg2+	Soluble
4 Cl- + Zn 2+ = ZnCl4 2-	0.2	Zn2+	Soluble
2 Na+ + SO4 2- = Na2SO4	0.179	Na+	Solid
Cl- + Fe2+ = FeCl+	0.14	Fe2+	Soluble
2H+ + SO4 2- = H2SO4	0.0	Mo2+	Soluble
CO3 2- + 2 Na+ = Na2CO3.H2O	-0.125	Na+	Solid
Ca2+ + Cl- = CaCl+	-0.14	Ca2+	Soluble
Ca2+ + 2 NH3 = Ca(NH3)2+2	-0.15	Ca2+	Soluble
3 Cl- + Mn 2+ = MnCl3-	-0.31	Mn2+	Soluble
2 NO3- + Cu 2+ = Cu(NO3)2	-0.4	Cu2+	Soluble

Equilibrium Complexes	Log K	Cation	Soluble or Solid Complexes
3 H+ + 3 Cl- + Sb(OH)3 = SbCl3	-0.59	Sb3+	Solid
NO3- + Na+ = NaNO3	-0.6	Na+	Soluble
Cl- + Pb 2+ = H+ + PbOHCl	-0.623	Pb2+	Solid
3 Cl- + Cu2+ =CuCl3-	-1.2	Cu2+	Soluble
H+ + NO3- = HNO3	-1.283		Soluble
Na+ + Cl- = NaCl	-1.582	Na+	Solid
Sn 2+ = 2 H+ + SnO	-1.76	Sn2+	Solid
NH3 = NH3(g)	-1.77		Soluble
SO4 2- + Mn 2+ = Mn SO4	-2.669	Mn2+	Solid
NH3 + Cu2+ = H+ + CuNH3OH+	-2.69	Cu2+	Soluble
2 Cl- + Mn 2+ = MnCl2:4H2O	-2.71	Mn2+	Solid
Si(OH)4 + Zn 2+ = 2 H+ + ZnSiO3	-2.93	Zn2+	Solid
SO4 2- + Cu 2+ = CuSO4	-3.01	Cu2+	Solid
SO4 2- + Zn 2+ = ZnSO4	-3.01	Zn2+	Solid
Sn 2+ = H+ + SnOH+	-3.4	Sn2+	Soluble
2 NO3- + Zn 2+ = Zn(NO3)2:6H2O	-3.44	Zn2+	Solid
4 Cl- + Cu2+ = CuCl4 2-	-3.6	Cu2+	Soluble
2 Cl- + Cu 2+ = CuCl2	-3.73	Cu2+	Solid
2 Sn 2+ = 2 H+ + Sn2(OH)2 2+	-4.77	Sn2+	Soluble
2 Pb2+ = H+ + Pb2OH 3+	-6.36	Pb2+	Soluble
Si(OH)4 + Cu 2+ = 2 H+ + CuSiO3.H2O	-6.5	Cu2+	Solid
2 Cu2+ = H+ + Cu2OH 3+	-6.7	Cu2+	Soluble
3 Sn 2+ = 4 H+ + Sn3(OH)4 2+	-6.88	Sn2+	Soluble
2 Cl- + Zn 2+ = ZnCl2	-7.03	Zn2+	Solid
Sn 2+ = 2 H+ + Sn(OH)2	-7.06	Sn2+	Soluble
Si(OH)4 + Pb 2+ = 2 H+ + PbSiO3	-7.32	Pb2+	Solid
Cl- + Zn 2+ = H+ + ZnClOH	-7.48	Zn2+	Soluble
Zn 2+ = H+ + ZnOH+	-7.5	Zn2+	Soluble
SO4 2- + 2 Zn 2+ = 2 H+ + Zn2(OH)2SO4	-7.5	Zn2+	Solid
Cu 2+ = 2 H+ + CuO	-7.675	Cu2+	Solid
Pb 2+ = H+ + PbOH+	-7.71	Pb2+	Soluble
Cu2+ = H+ + CuOH+	-7.96	Cu2+	Soluble
2 Si(OH)4 = H+ + Si2O2(OH)5-	-8.1	Si4+	Soluble
Pb 2+ = 2 H+ + Pb(OH)2	-8.15	Pb2+	Solid
SO4 2- + 3 Cu 2+ = 4 H+ + Cu3SO4(OH)4	-8.29	Cu2+	Solid
Mg2+ + Si(OH)4 = H+ + MgHSiO3+	-8.56	Mg2+	Soluble
Cu 2+ = 2 H+ + Cu(OH)2	-8.64	Cu2+	Solid
Cl- + 2 Pb 2+ = 3 H+ + Pb2(OH)3Cl	-8.793	Pb2+, Cu2+	Solid
Ca2+ + Si(OH)4 = H+ + CaHSiO3+	-8.81	Ca2+	Soluble
2 Zn 2+ = H+ + Zn2OH 3+	-9.0	Zn2+	Soluble

Equilibrium Complexes	Log K	Cation	Soluble or Solid Complexes
NO3- + 2 Cu 2+ = 3 H+ + Cu2NO3(OH)3	-9.24	Cu2+	Solid
Ni 2+ = H+ + NiOH+	-9.5	Ni2+	Soluble
CO3 2- + 2 Mg 2+ = 2 H+ + MgCO3:Mg(OH)2:3H2O	-9.6	Mg2+	Solid
2 CO3 2- + 5 Zn 2+ = 6 H+ + Zn5(OH)6(CO3)2	-9.69	Zn2+	Solid
2 Ni 2+ = H+ + Ni2OH 3+	-9.8	Ni2+	Soluble
Si(OH)4 = H+ + SiO(OH)3-	-9.83	Si4+	Soluble
Fe2+ = H+ + FeOH+	-10.2	Fe2+	Soluble
2 Cu2+ = 2H+ + Cu2(OH)2 2+	-10.35	Cu2+	Soluble
SO4 2- + 3 Pb 2+ = 4 H+ + PbSO4:2PbO	-10.4	Pb2+	Solid
Ni 2+ = 2 H+ + Ni(OH)2	-10.5	Ni2+	Solid
2Mn2+ = H+ + Mn2OH 3+	-10.56	Mn2+	Soluble
Mn 2+ = H+ + MnOH+	-10.59	Mn2+	Soluble
Cr 2+ = 2 H+ + Cr(OH)2	-10.99	Cr2+	Solid
CO3 2- + 3 Pb 2+ = 4 H+ + PbCO3:2PBO	-11.02	Pb2+	Solid
Zn 2+ = 2 H+ + ZnO	-11.2	Zn2+	Solid
2 NH3 + Cu2+ = 2 H+ + Cu(NH3)2(OH)2	-11.33	Cu2+	Soluble
Mg 2+ + Si(OH)4 = 2HY + MgSiO3	-11.342	Mg2+	Solid
Mg2+ = H+ + MgOH+	-11.44	Mg2+	Soluble
Zn 2+ = 2 H+ + e-Zn(OH)2	-11.5	Zn2+	Solid
SO4 2- + 2 Cu 2+ = 2H+ + CuO.CuSO4	-11.53	Cu2+	Solid
Sb(OH)3 = H+ + Sb(OH)4-	-11.82	Sb3+	Soluble
4 NH3 + Cu2+ = H+ + Cu(NH3)4OH+	-12.42	Cu2+	Soluble
Zn 2+ = 2 H+ + a-Zn(OH)2	-12.45	Zn2+	Soluble
Ni 2+ = 2 H+ + NiO (c)	-12.45	Ni2+	Solid
Ni 2+ = 2 H+ + NiO (cr)	-12.67	Ni2+	Solid
Ca2+ = H+ + CaOH+	-12.78	Ca2+	Soluble
Pb 2+ = 2 H+ + PbO	-12.91	Pb2+	Solid
Fe 2+ = 2 H+ + Fe(OH)2	-12.996	Fe2+	Solid
H2O = H+ + OH-	-14.0	Pb2+	Soluble
Na+ = H+ + NaOH	-14.18	Na+	Soluble
Si(OH)4 + 2 Ni 2+ = 4 H+ + Ni2SiO4	-14.54	Ni2+	Solid
Mg2+ + 2 Si(OH)4 = 2H+ + Mg(HSiO3)2	-14.88	Mg2+	Soluble
2 Cl- + 4 Cu 2+ = 6 H+ + CuCl2:3Cu(OH)2	-14.99	Cu2+	Solid
Mn 2+ = 2 H+ + Mn(OH)2	-15.2	Mn2+	Solid
Cl- + 2 Zn 2+ = 3 H+ + Zn2(OH)3Cl	-15.2	Zn2+	Solid
Si(OH)4 + 2Zn 2+ = 4 H+ + Zn2SiO4	-15.33	Zn2+	Solid
SO4 2- + 4 Cu 2+ = 6 H+ + Cu4SO4(OH)6	-15.34	Cu2+	Solid
2 Mg 2+ + 3 Si(OH)4 = 4 H+ + Mg2Si3O7.5OH:3H2O	-15.76	Mg2+	Solid
Ca2+ + 2 Si(OH)4 = 2H+ + Ca(HSiO3)2	-15.81	Ca2+	Soluble

Equilibrium Complexes	Log K	Cation	Soluble or Solid Complexes
Ca 2+ + Si(OH)4 = 2 H+ + CaSiO3	-15.94	Ca2+	Solid
Cu2+ = 2H+ + Cu(OH)2	-16.24	Cu2+	Soluble
Zn 2+ = 2 H+ + Zn(OH)2	-16.4	Zn2+	Soluble
Sn 2+ = 3 H+ + Sn(OH)3-	-16.61	Sn2+	Soluble
SO4 2- + 4 Cu 2+ = 6 H+ + Cu4SOr(OH)6:H2O	-16.79	Cu2+	Solid
Mg 2+ = 2 H+ + Mg(OH)2	-16.84	Mg2+	Solid
Pb 2+ = 2 H+ + Pb(OH)2	-17.12	Pb2+	Soluble
Mg2+ + Si(OH)4 = 2 H+ + MgSiO3	-17.75	Mg2+	Soluble
2 NO3- + 4 Cu 2+ = 6 H+ + Cu(NO3)2:3Cu(OH)2	-18.48	Cu2+	Solid
Mn2+ = 2H+ + Mn(OH)2	-18.54	Mn2+	Soluble
Ca2+ + Si(OH)4 = 2H+ + CaSiO3	-18.83	Ca2+	Soluble
2 Si(OH)4 = 2H+ + Si2O3(OH)4 2-	-19.0	Si4+	Soluble
2 SO4 2- + 3 Zn 2+ = 2H+ + Zn3O(SO4)2	-19.02	Zn2+	Solid
Si(OH)4 + 2 Pb 2+ = 4 H+ + Pb2SiO4	-19.76	Pb2+	Solid
Ca 2+ + Mg 2+ + 2 Si(OH)4 = 4 H+ + CaMgSi2O6	-19.894	Ca2+, Mg2+	Solid
Ni 2+ = 2 H+ + Ni(OH)2	-20.01	Ni2+	Soluble
Fe2+ = 2 H+ + Fe(OH)2	-20.8	Fe2+	Soluble
2 Si(OH)4 + 3 Fe 2+ = 6 H+ + Fe3Si2O5(OH)4	-20.81	Fe2+	Solid
4 Pb 2+ = 4 H+ + Pb4(OH)4 4+	-20.88	Pb2+	Soluble
3 Cu2+ = 4 H+ + Cu3(OH)4 2+	-21.1	Cu2+	Soluble
SO4 2- + 4 Pb 2+ = 6 H+ + Pb4(OH)6SO4	-21.1	Pb2+	Solid
3 Mg 2+ + 4 Si(OH)4 = 6 H+ + Mg3Si4O10(OH)2	-21.399	Mg2+	Solid
Mg 2+ = 2 H+ + MgO	-21.51	Mg2+	Solid
SO4 2- + 4 Pb 2+ = 6 H+ + PbSO4:3PbO	-22.1	Pb2+	Solid
Ca 2+ = 2 H+ + Ca(OH)2	-22.8	Ca2+	Soluble
Si(OH)4 = 2H+ + SiO2(OH)2 2-	-23.0	Si4+	Soluble
3 Pb 2+ = 4 H+ + Pb3(OH)4 2+	-23.88	Pb2+	Soluble
2Mn2+ = 3H+ + Mn2(OH)3+	-23.9	Mn2+	Soluble
NH3 + Cu2+ = 3 H+ + CuNH3(OH)3-	-24.73	Cu2+	Soluble
4 Si(OH)4 = 3H+ + Si4O7(OH)5 3-	-25.5	Si4+	Soluble
2 Pb 2+ = 4 H+ + PbO:Pb(OH)2	-26.2	Pb2+	Solid
Cu2+ = 3H+ + Cu(OH)3-	-26.7	Cu2+	Soluble
4 Zn 2+ = 4 H+ + Zn4(OH)4 4+	-27.0	Zn2+	Soluble
3 Si(OH)4 = 3 H+ + Si3O8(OH)5 3-	-27.5	Si4+	Soluble
4 Ni 2+ = 4 H+ + Ni4(OH)4 4+	-27.9	Ni2+	Soluble
Pb 2+ = 3 H+ + Pb(OH)3-	-28.06	Pb2+	Soluble
Zn 2+ = 3 H+ + Zn(OH)3-	-28.2	Zn2+	Soluble
2 Mg 2+ + Si(OH)4 = 4 H+ + Mg2SiO4	-28.306	Mg2+	Solid
SO4 2- + 4 Zn 2+ = 6 H+ + Zn4(OH)6SO4	-28.4	Zn2+	Solid

Equilibrium Complexes	Log K	Cation	Soluble or Solid Complexes
3 Si(OH)4 = 3 H+ + Si3O6(OH)3 3-	-28.6	Si4+	Soluble
Ni 2+ = 3H+ + Ni(OH)3-	-29.7	Ni2+	Soluble
Ca 2+ + Mg 2+ + Si(OH)4 = 4 H+ + CaMgSiO4	-30.272	Ca2+, Mg2+	Solid
SO4 2- + 4 Ni 2+ = 6 H+ + Ni4(OH)6SO4	-32	Ni2+	Solid
3 Mg 2+ + 2 Si(OH)4 = 6 H+ + Mg3Si2O5(OH)4	-32.2	Mg2+	Solid
Ca 2+ = 2 H+ + CaO	-32.797	Ca2+	Solid
Fe2+ = 3 H+ + Fe(OH)3-	-33.4	Fe2+	Soluble
Mn2+ = 3H+ + Mn(OH)3-	-34.8	Mn2+	Soluble
4 Si(OH)4 = 4 H+ + Si4O8(OH)4 4-	-36.3	Si4+	Soluble
2 Ca 2+ + Si(OH)4 = 4 H+ + Ca2SiO4	-37.649	Ca2+	Solid
2 Cl- + 5 Zn 2+ = 8 H+ + Zn5(OH)8Cl2	-38.5	Zn2+	Solid
Cu2+ = 4H+ + Cu(OH)4 2-	-39.6	Cu2+	Soluble
Pb 2+ = 4 H+ + Pb(OH)4 2-	-39.7	Pb2+	Soluble
4 Mg2+ = 4 H+ + Mg4(OH) 4+	-39.71	Mg2+	Soluble
Zn 2+ = 4 H+ + Zn(OH)4 2-	-41.3	Zn2+	Soluble
6 Pb 2+ = 8 H+ + Pb6(OH)8 4+	-43.61	Pb2+	Soluble
Ni 2+ = 4H+ + Ni(OH)4 2-	-45.0	Ni2+	Soluble
Fe2+ = r H+ + Fe(OH)4 2-	-46.35	Fe2+	Soluble
2 Ca 2+ + Mg 2+ + 2 Si(OH)4 = 6 H+ + Ca2MgSi2O7	-47.472	Ca2+	Solid
Mn2+ = 4H+ + Mn(OH)4 2-	-48.3	Mn2+	Soluble
2 Zn 2+ = 6 H+ + Zn2(OH)6 20	-54.3	Zn2+	Soluble
2 Ca 2+ + 5 Mg 2+ + 8 Si(OH)4 = 14 H+ +Ca2Mg5Si8O22(OH)2	-56.574	Ca2+, Mg2+	Soluble
3Ca 2+ + Mg 2+ + 2 Si(OH)4 = 8 H+ + Ca3MgSi2O8	-68.543	Ca2+, Mg2+	Solid
3 Ca 2+ + Si(OH)4 = 6 H+ + Ca3SiO5	-73.867	Ca2+	Solid
2 SO4 2- + 8 Cl- + 37 Cu 2+ = 62 H+ + Cu37Cl8(SO4)2(OH)62:8H2O	-238.259	Cu2+	Solid

VITA

LARRY KEITH ISAACS

DEGREES:

Master of Science (Environmental Science), Christopher Newport University, Newport News, VA, May 2003
Bachelor of Science (Electrical Engineering), University of New Mexico, Albuquerque, NM, May 1972

STATES WITHIN WHICH REGISTERED:
Licensed Professional Engineer, New Mexico, 1979, License No. 7083

PROFESSIONAL CHRONOLOGY:

1995 to Present, Chief, Environmental Compliance, Langley AFB, VA
1992 to 1995, Air Toxics Program Manager, Langley AFB, VA
1990 to 1992, Commander, Engineering Squadron, Mt Home AFB, ID
1988 to 1990, Chief Construction Programs Division, Langley AFB, VA
1986 to 1988, Chief Engineering Inspections Division, Langley AFB, VA
1985 to 1986, Base Engineer, Shemya AFB, AK
1979 to 1985, Airborne Weapons Director, Tinker AFB, OK
1977 to 1979, Chief Construction Programs Branch, Cannon AFB, NM
1974 to 1977, Chief Engineer Technical Design, Kadena AB, Japan
1972 to 1974, Electrical Engineer, Webb AFB, TX

SCIENTIFIC AND PROFESSIONAL SOCIETIES MEMBERSHIP:

American Society of Civil Engineers
American Water Works Association
Soil Science Society of America

PUBLICATIONS

Isaacs, L.K. (2007) Lead leaching from soils and in stormwaters at twelve military shooting ranges, *Journal of Hazardous Substance and Research*. VI, 1-30.

Abdel-Fattah, T.M.; Isaacs, L.K.; Payne, K.B. (2003). "Small Arms Range Lead Management Issues: Activated Carbon, Molecular Sieves (5A and 13X), and Naturally Occurring Zeolites as Lead Adsorbents." *Federal Facilities Environmental Journal*. 14(2). 113-126